Study of the factors regulating traction force production by cells

Somanna Kollimada Aiyappa

THÈSE

Pour obtenir le grade de

DOCTEUR DE L'UNIVERSITÉ GRENOBLE ALPES

Spécialité : Physique pour les Sciences du Vivant

Arrêté ministériel : 25 mai 2016

Présentée par

Somanna KOLLIMADA AIYAPPA

Thèse dirigée par **Laurent BLANCHOIN**
et codirigée par **Laëtitia KURZAWA**

préparée au sein du **Laboratoire Laboratoire de Physiologie Cellulaire Végétale**
dans **l'École Doctorale Physique**

Study of the factors regulating traction force production by cells

Thèse soutenue publiquement le **18 décembre 2020**, devant le jury composé de :

Madame Corinne ALBIGES-RIZO
DIRECTEUR DE RECHERCHE, Institute for Advanced Biosciences, Présidente
Madame Cécile SYKES,
DIRECTEUR DE RECHERCHE, Institut Curie/CNRS/PSL/Sorbonne Université, Rapportrice
Monsieur Grégory GIANNONE
DIRECTEUR DE RECHERCHE, CNRS-Université Bordeaux, Interdisciplinary Institute for NeuroScience, Rapporteur
Monsieur Martial BALLAND
MAITRE DE CONFERENCE, Université Grenoble Alpes, Laboratoire Interdisciplinaire de Physique, Examinateur
Monsieur Nils GAUTHIER
PROFESSEUR ASSISTANT, IFOM, Milan and University of Milan, Examinateur

Abstract

Mechanical forces are involved in many physiological processes including morphogenesis, migration, division and differentiation. All these events involve a tight regulation of both the magnitude and spatial distribution of the contractile forces at the cell and tissue-level. Although we know that at the molecular level, the regulation of force production and transmission relies on the complex interplay between a well-conserved set of proteins of the cytoskeleton, we still do not have a comprehensive understanding of the mechanisms supporting force generation at the entire cell level. In addition, the magnitude of the traction forces exerted by cells on their underlying extracellular matrix in culture and as such the cell to cell variation of theses forces remain difficult to predict, largely because of the difficulty to characterize precisely how molecular components forming the actomyosin and adhesion networks, individually or via their specific interplay, are related to the force magnitude exerted by these cells. In this context, the aim of my PhD project was to investigate how key biological parameters are precisely related to force generation and regulation process.

The first part of my study thereby focused on looking into the effect of the progression of the cell cycle on cell to cell heterogeneity in traction forces. I demonstrated that although the cell cycle status of the cells had a major impact on the magnitude of forces exerted by cells, it was not impacting the overall cell to cell variability in the traction force exerted. I also examined next the possibility that some internal/subcellular contractile efforts could be dissipated instead of being transmitted to cell anchorages by looking at the interplay between actin dynamics and traction forces. The analysis of actin turnover in stress fibers showed that although variations in strain energies were associated to variations in actin dynamics, they were not significant enough to explain the large cell to cell heterogeneities measured in traction

force. Finally, I conducted a study dedicated to the characterization of the biochemical composition of the actomyosin network and adhesion pattern of cells in relationship with the force generated and transmitted by cells. To that end, I implemented the standard TFM assay in order to introduce an intermediate labeling step allowing for simultaneous measurement of traction forces and intracellular protein contents. This assay was then used to characterize the content of molecules of the actomyosin cytoskeleton and of the adhesions, either alone or in combination, and force. This work first demonstrated that the vinculin content measured at the level of the entire cell and the area of the focal adhesions, represented good predictors of force. I then showed that actin and myosin displayed broader deviations in their linear relationship to the strain energies, and thus appeared as less reliable predictors of force. Instead, my data suggested that their relative cellular amount plays a key role in setting the magnitude of force exerted by cells. I finally demonstrated that although the alpha-actinin content was not correlated at all with force magnitude, the relative amount of alpha-actinin as compared to actin content was of key importance to regulate force production.

In conclusion, these results identified the biochemical content of focal adhesion and the relative amounts of molecular motors and crosslinkers per actin as key parameters involved in setting the magnitude of force exerted by cells and thereby shed new light on the mechanisms supporting force generation at the entire cell level.

Acknowledgements

First and foremost, I would like to thank my parents and brother without whose constant encouragement and support, it would not have been possible to spend a decade in research culminating in this thesis. I would like to thank Meghana Pemmaiah, who stood by me during the PhD.

To, Laurent Blanchoin and Manuel Théry who gave me the opportunity to be part of the Cytomorpholab and for giving me the chance to learn a lot of knowledge, experience, and their guidance, I give my sincere thanks. The constant encouragement by Laurent gave me the ability to finish this work.

I owe a debt of gratitude to Laëtitia Kurzawa, who helped me every step of the way with patience and kindness. Thank you for your guidance and mentorship.

Fabrice Senger, with whom, many scientific discussions were had, along with random discussions about interesting topics, made me feel welcome and was always ready to help. Thank you.

I would like to thank all the members of the Cytomorpholab for their help and interesting discussions. My thanks to Jérémie Gaillard for his help with all the paperwork and technical support. I would like to thank Sarah Robert for all the help with the French administrative work.

Table of Contents

1 General introduction

Cells are the fundamental units from which multicellular life is built. They organize themselves in a coordinated fashion into complex tissues and organisms to achieve different purposes. How the cells interact with each other to form tissues notably relies on the mechanical properties of their environment. The rigidity of the extracellular matrix that cells are attached to, its geometry at the nano to micrometer scale or the stress that their neighboring cells exert on these cells for example play an important role. Over billions of years that life on earth has existed, cells have evolved methods to sense their surroundings and respond appropriately. These cues have indeed been shown to play important roles in many fundamental biological processes such as differentiation of stem cells (Engler, Sen, Sweeney, & Discher, 2006), cell division (Uroz et al., 2018), polarisation (Pitaval, Tseng, Bornens, & Théry, 2010), apoptosis (Plotkin et al., 2005), individual and collective cell migration (Tambe et al., 2011), morphogenesis (Munjal & Lecuit, 2014), oncogenesis and cancer metastasis (Kraning-Rush, Califano, & Reinhart-King, 2012). To sense and respond to these physical stimuli, cells use a complex regulatory system that is called the mechanotransduction system which transduces the physical signals into biochemical responses. Mechanoresponsive biological pathways integrate the many biochemical signals from the mechanotransduction system as it senses the physical cues from the cell microenvironment. A schematic of the system is given in Figure 1.

One major component of the mechanotransduction system is the cytoskeletal network and its contractile components. Cells use contractile forces generated by the cytoskeletal actomyosin network to drive shape changes and movements at the organelle, cell and tissue-length scales to regulate diverse physiological processes, including intracellular transport and genome replication (Murrell, Oakes, Lenz, & Gardel, 2015). The forces generated by the

contractile systems are transmitted via the cytoskeleton and adhesion molecules to neighboring cells and the matrix shape multicellular systems (Heisenberg & Bellaïche, 2013).

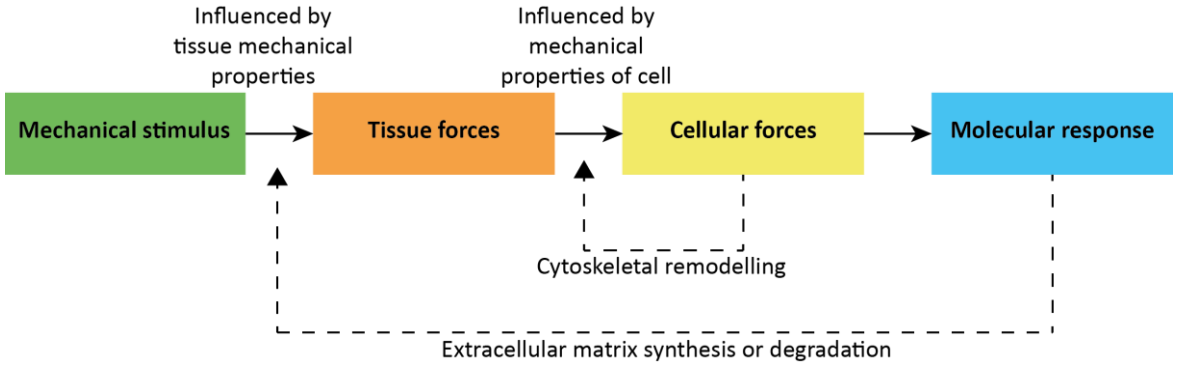

Figure 1: Mechanical forces induce tissue adaptation

Adapted from: (Thompson, Scott, Loghmani, Ward, & Warden, 2016)

Forces generated intrinsically and those applied extrinsically deform tissues. The forces experienced by individual cells in the tissue depends on the mechanical properties of the extra cellular matrix (ECM) and cells themselves. These cells can modify their microenvironment via cytoskeletal rearrangement that in turn alters cellular sensitivity to the forces acting on them. The modification of the microenvironment is initiated by cells through molecular responses to the forces that then leads to synthesis and/or ECM degradation. This in turn can alter mechanical properties of the tissue, which then feeds back to influence tissue forces.

The mechanical cues from these surroundings are converted by cells into chemical signals that are used to modulate cellular response (Bershadsky, Balaban, & Geiger, 2003; Martinac, 2004; Shemesh, Geiger, Bershadsky, & Kozlov, 2005; Silver & Siperko, 2003). Force on peripheral contacts can produce signaling molecules that translocate to the nucleus and induces cell level changes (Dupont et al., 2011; Sansores-Garcia et al., 2011). Continual feedback is obtained by cells through sensing of force, rigidity, cell contractility and biochemical

signals. This feedback is used by cells to regulate cell and tissue shape and ultimately, that of the organism (Vogel & Sheetz, 2006). A schematic of the sensing of mechanical signals from the cell to the tissue level is shown in Figure (1). These signals received from cells by mechanosensing are then used in many important biological processes.

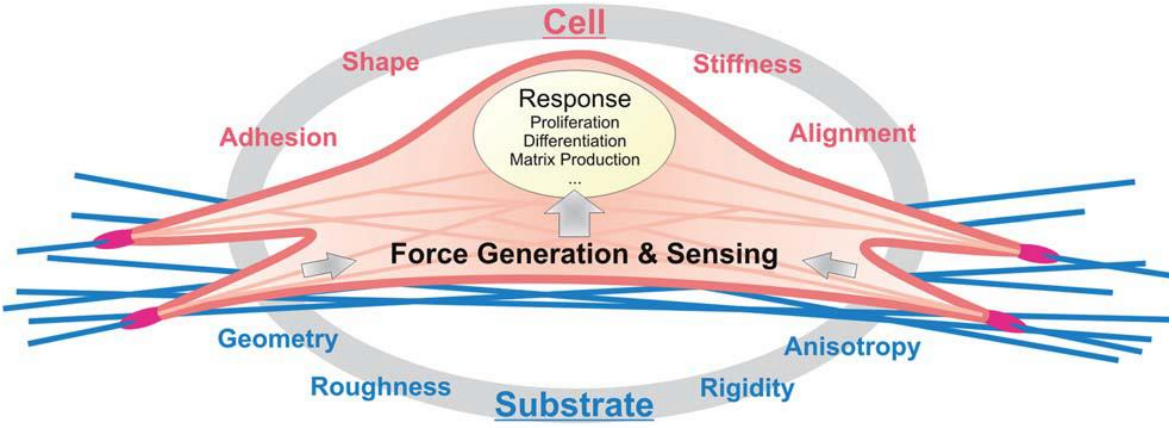

Figure 2: The sense of touch of cells

Adapted from: (Kollmannsberger, Bidan, Dunlop, & Fratzl, 2011)

A cell adhered to the substrate (e.g. the extracellular matrix shown as blue fibers) applies mechanical forces through its focal adhesions. The cell adapts its shape and stiffness to the properties of the substrate by contracting and remodeling the cytoskeleton. Through this interplay of force generation and sensing, cells respond to mechanical stimuli by switching between different biological programs such as cell division, differentiation, or ECM production.

Vital physiological processes such as the differentiation of naïve mesenchymal stem cells depends on the stiffness of the substrate that they grow on (Engler et al., 2006; McBeath, Pirone, Nelson, Bhadriraju, & Chen, 2004). Inhibiting the generation of contractile forces by with the actomyosin network of cell, which is required for mechanistic sensing leads to elimination of these substrate stiffness induced changes to stem cell fate. It was also found that

as the substrate stiffness increased, the forces that cells exert on it increases and their morphology changes from spindle like on soft substrates to more isotropic shapes on stiffer substrates (Califano & Reinhart-King, 2010). The stiffness of the cellular microenvironment has also been found to be altered during cancer progression (Levental et al., 2009; Paszek et al., 2005) and cardiovascular diseases (Huynh et al., 2011). Other physical cues also regulate cell contractility. The geometry of their adhesive area leads to shape dependent reorganization of their actomyosin network (Théry, Pépin, Dressaire, Chen, & Bornens, 2006), and the spread area of cells was found to be a good predictor of the forces that were exerted by them (Califano & Reinhart-King, 2010).

The protrusion-retraction of membranes during cell motility is highly dependent on the forces generated within cells which are transmitted to their substrate (J. Lee, Leonard, Oliver, Ishihara, & Jacobson, 1994; T Oliver, Dembo, & Jacobson, 1999; Tim Oliver, Jacobson, & Dembo, 1995). During collective migration of cellular monolayers, the forces exerted within the system direct the direction of migration within the sheet (Serra-Picamal et al., 2012; Tambe et al., 2011). The stresses applied across the cell-cell junctions in the sheet are used by cells to orient local cellular migration along the direction of local maximal principal stress. On the boundaries of cell clusters, polarizing the tension within the cellular cytoskeleton directs the formation of leader cells which pull the sheet forward (Messi, Bornert, Raynaud, & Verkhovsky, 2020; Rausch et al., 2013). During morphogenesis, coordinated cellular deformations generated by the contractile networks in cells drive tissue movement (Munjal & Lecuit, 2014; Rauzi, Lenne, & Lecuit, 2010).

Understanding the precise regulation of these forces that cells exert is hence important to improve our understanding of how cells regulate their physiological processes. The objective

of the present study was to determine the factors that regulate the variations in forces exerted by cells. In the next section, some of the major factors involved in the contractile machinery are discussed. To understand how contractility in cell populations is modulated by variations in the relative levels of these proteins in individual cells a modification of an existing protocol was developed. The details of the method and the results obtained from this are given.

2 Force production and regulation by the cytoskeleton

2.1 The actin network

At the molecular level, the regulation of force production and transmission relies on the complex interplay between a well-conserved set of proteins of the cytoskeleton (Murrell et al., 2015). As described in the previous section, cells use these contractile forces to drive shape changes and movements at the organelle, cell and tissue length scales to regulate diverse processes (Munjal & Lecuit, 2014; Salbreux, Charras, & Paluch, 2012; Vicente-Manzanares, Ma, Adelstein, & Horwitz, 2009). The cytoskeleton senses, generates and mediates coordinated forces to control the normal cell and tissue functions. The base for the actomyosin system is the protein actin. It is a globular protein that polymerizes into filaments with different types of organization based on different factors controlling the polymerization. The polymers are filamentous structures that have a right-handed helical twist. The two ends of the filament, one called the barbed end and the other the pointed end, differ in their dynamics. The barbed end is more dynamic and elongates 10 times faster than the pointed end at a rate of 11.6 $\mu M^{-1}.s^{-1}$. These filaments can polymerize into cell-length scales in short times due to the high concentration of monomers inside cells (Pollard, Blanchoin, & Mullins, 2000). In-vitro measurements have shown that actin filaments are semi-flexible at the scale of a cell (Harasim, Wunderlich, Peleg, Kröger, & Bausch, 2013). Actin filaments self-assemble into many structures within the cell and this is achieved by cells employing a battery of accessory proteins such as profilin, Arp2/3, WASP/WAVE family of proteins, and formins which help in controlling filament elongation and capping proteins, cofilin, etc. which help in regulating filament length and disassembly (Figure 3). Using these different proteins, cells sculpt the network into many different architectures and control the resulting mechanical properties (Blanchoin, Rajaa,

Sykes, & Plastino, 2014). The different types of structures composed of actin are displayed along with some of the important factors that regulate them.

The actin filament mechanical properties can vary depending on the proteins bound to them (Elam, Kang, & De La Cruz, 2013). The different networks also can have varying mechanical properties depending on their composition (Stacey Lee, Kassianidou, & Kumar, 2018). Crosslinkers such as α-actinin and myosin motors play important roles in the determination of the actin network organization and properties (Bendix et al., 2008; Ennomani et al., 2016). The filaments in the network have a turnover associated with them which is controlled by the pool of monomeric actin available, crosslinkers, motors and nucleation factors, all of which plays important roles in maintaining structural integrity (Chugh et al., 2017; Dehapiot et al., 2020; Smith, Blankman, Gardel, Luettjohann, & Waterman, 2010; Yanshu Zhang et al., 2017). In further sections some of the important factors involved in regulating the architecture, contractility of system and force transmission to the substrate are discussed.

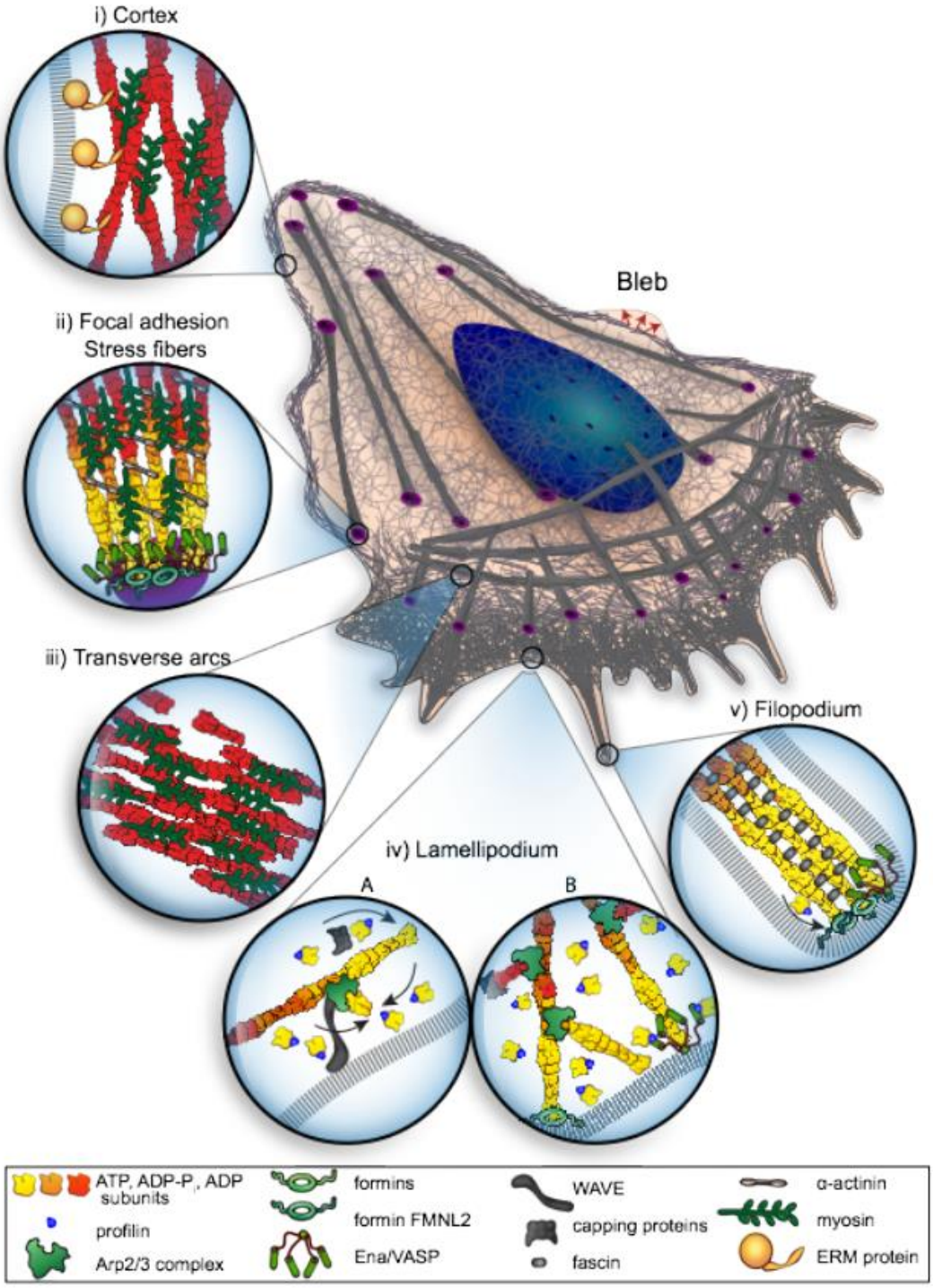

Figure 3: Cells produce varied actin structures in cells using a number of regulatory proteins.

Adapted from: (Blanchoin et al., 2014)

i) Below the membrane is a layer of actin filaments associated with it through ERM proteins. The filaments here are interlinked through myosin motors and helps provide the cell rigidity.

ii) The stress fibers are one category of contractile bundles that span the cell, are attached to focal adhesions directly or indirectly, through other stress fibers and involve factors such as formins, Ena/VASP proteins, alpha actinins and myosins.

iii) Transverse arcs are another class of stress fibers that are found towards the back of the lamellipodium. They have myosin incorporated into them allowing contraction.

iv) The lamellipodium is composed of branched actin filaments that are undergoing rapid, massive and localized polymerization that is driven by Arp2/3 which binds to a preexisting actin filament and then nucleates a new filament. There are interactions in the lamellipodium region with many different proteins such as WAVE family of proteins, profiling/actin complexes which ferry actin monomers to the barbed filament ends close to the plasma membrane, and Ena/VASP proteins, formins which induce linear filament growth and capping proteins which control the elongation of the network. The complex interplay between these different proteins in this region is used by cells in regulation of the dynamics of polymerization and growth of actin filaments.

v) Filopodia are senor organelles filled with parallel actin bundles that are elongated by formin, Ena/VASP and are tightly packed by fascin. Another type of edge protrusions are blebs, which initially form due to internal cellular pressure in cytoskeleton free regions of the membrane.

2.2 Role of molecular motors

The forces produced by cells modulate cell shape (Green, Paluch, & Oegema, 2012), division (Green et al., 2012; Salbreux et al., 2012), migration (Vicente-Manzanares et al., 2009)

and contraction of multicellular populations as in smooth muscle cells and non-muscle tissue (Lecuit, Lenne, & Munro, 2011; Levayer & Lecuit, 2012). There are many mechanoenzymes that act as molecular-scale force generators. Of these, the myosin family of proteins which convert chemical energy into translational or rotational movement act on the filamentous actin (F-Actin) generating forces that are transmitted across diverse length scales. Understanding the interplay between F-actin and myosin is vital to understand how cells use their force generation capabilities which can be used for building quantitative and predictive models of physiological processes.

In the first place, force originates from the interaction between F-actin and non-muscle myosins II (Chrzanowska-Wodnicka & Burridge, 1996; Katoh, Kano, Masuda, Onishi, & Fujiwara, 1998; Koenderink & Paluch, 2018). Actomyosin contractility is predominantly a result of mechanical action of Myosin II motors on actin filaments. The energy for this motor action is obtained from the hydrolysis of ATP and is used to exert forces on actin filaments (Watanabe, Hosoya, & Yonemura, 2007). Myosin II motors have two globular head domains joined by a long tail domain (Figure 4). The head domains bind to actin filaments and selectively move towards the end of the actin filament called the plus end. These head domains have the binding site for ATP (Citi & Kendrick-Jones, 1987; Hu et al., 2017). The tail domain of one myosin II filament attaches to the tail domain of another myosin filament to form bipolar structures with motor heads on either end (Koenderink & Paluch, 2018). The ATPase activity of myosin results in a change in the conformation when it is bound to actin. These interactions lead to the formation of actomyosin bundles called stress fibers in cells (Chrzanowska-Wodnicka & Burridge, 1996).

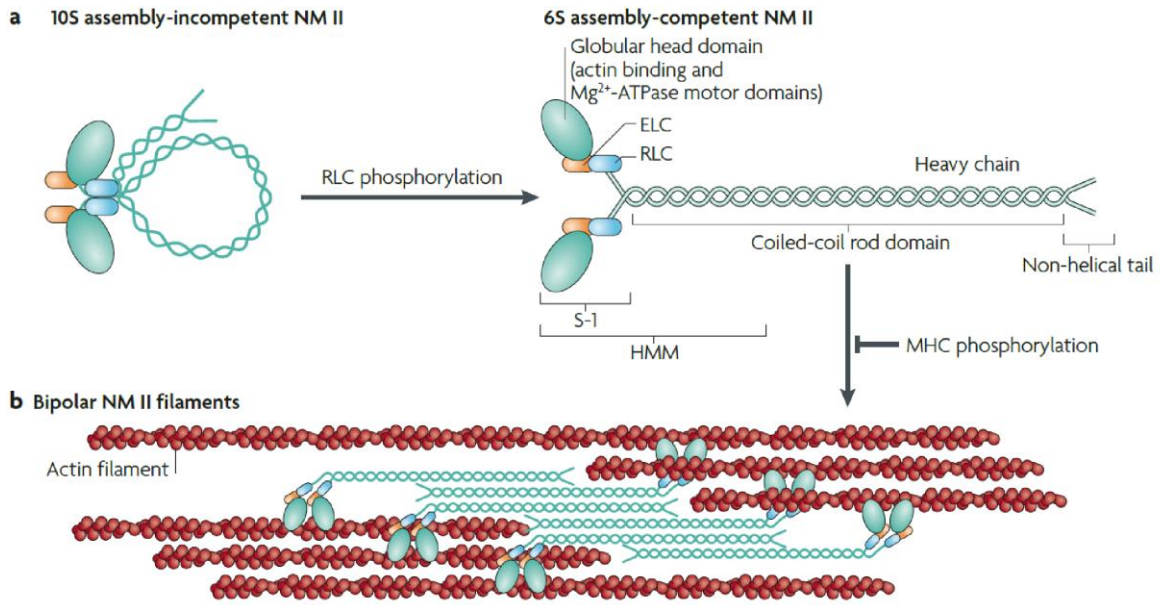

Figure 4: Domain structure of Myosin II

Adapted from : Vicente-Manzanares, et.al., *Nature Reviews Molecular Cell Biology*, 2009

a. The subunit and domain structure of non-muscle myosin II (NM II), which forms a dimer through interactions between the α-helical coiled-coil rod domains. The globular head domain contains the actin-binding regions and the enzymatic Mg2⁺-ATPase motor domains. The essential light chains (ELCs) and the regulatory light chains (RLCs) bind to the heavy chains at the lever arms that link the head and rod domains. In the absence of RLC phosphorylation, NM II forms a compact molecule through a head to tail interaction. This results in an assembly-incompetent form (10S; left) that is unable to associate with other NM II dimers. On RLC phosphorylation, the 10S structure unfolds and becomes an assembly-competent form (6S). S-1 is a fragment of NM II that contains the motor domain and neck but lacks the rod domain and is unable to dimerize. Heavy meromyosin (HMM) is a fragment that contains the motor domain, neck and enough of the rod to effect dimerization.

b. NM II molecules assemble into bipolar filaments through interactions between their rod domains. These filaments bind to actin through their head domains and the ATPase activity of the head enables a conformational change that moves actin filaments in an anti-parallel manner. Bipolar myosin filaments link actin filaments together in thick bundles that form cellular structures such as stress fibres.

There are three isoforms of non-muscle myosin (NMM) II, IIA, IIB and IIC expressed in mammalian cells. NMM IIA and B show the highest prevalence in cells with the isoforms showing specific localization in different tissues and show distinct biophysical properties (Beach et al., 2014; Sandquist & Means, 2008; Sandquist, Swenson, DeMali, Burridge, & Means, 2006). The NMM II isoforms assemble into heterotypic filaments. There is evidence for differential distribution of NMM IIA and IIB in cells. But this differential distribution is less pronounced in freshly spread cells suggesting that sorting mechanisms act over time. Overall, it is suspected that individual NMM II isoforms perform both isoform specific and isoform redundant functions while coassembling with other NMM II isoforms (Beach et al., 2014).

Contractile forces generated within the actomyosin system depend on motor proteins. The concentration of NMM II motors has been shown to effect the contraction speed of actin networks in vitro (Bendix et al., 2008). The study also showed that inhibition (with blebbistatin) or depletion on the motors completely removed contractility and that the contraction saturates when the ratio of myosin/actin exceeds 0.05 in the absence of motor inhibition. Progressively increasing the concentration of blebbistatin which inhibits myosin motor activity (Kovács, Tóth, Hetényi, Málnási-Csizmadia, & Sellers, 2004) has been shown to reduce F-actin anisotropy in cells, a decreases in stress fiber formation, cell stiffness and cellular contractility (Ayala et al., 2017; Lu, Oswald, Ngu, & Yin, 2008). Inhibiting the motors also changes the microstructure of

the actin network, with a change from a mix of bundled actin filaments and an actin mesh in untreated cells to only a mesh being present when treated with blebbistatin (Goeckeler, Bridgman, & Wysolmerski, 2008). Reduction in focal adhesions also suggest that cell contractility is reduced in this condition.

While the reduction in contractility with reduced/inhibited myosin has been shown, it has also been shown that myosin plays a role in the disassembly of actin filaments (Reymann et al., 2012) allowing the network to turnover (Sonal et al., 2019; Wilson et al., 2010). This is important as the turnover rates have been shown to play a role in maintaining cortical tension (Tinevez et al., 2009). While myosin initially lead to formation of actin bundles, at high enough concentration, it was shown that the motors completely disassembled actin filaments in vitro (Haviv, Gillo, Backouche, & Bernheim-Groswasser, 2008).

These results suggest that in the absence of active myosin II, neither actomyosin tension nor the structural integrity of stress fibers can be maintained. However, in the presence of high motor concentration with respect to actin filament density, there can be disassembly of filaments in cells leading to lower contractility. Quantifying myosin density in cell populations and the forces that these cells are capable of exerting should allow us to understand if varying concentrations in the actomyosin system plays a role in the variation of traction force in cell populations.

2.3 α-actinin

While interaction between actin and NMM has been shown to generate contraction in in vitro systems, it has also been shown in these systems, that crosslinkers such as α-actinin play a role by changing the mechanical properties of the network (Xu, Wirtz, & Pollard, 1998). Changes in α-actinin expression have been shown to be a feature of many different malignant

tumors and overexpression of actinin-4 protein and ACTN4 gene amplification is suggested as a biomarker for evaluating the potential metastatic ability of tumors in patients (Honda, 2015). These studies highlight the importance of the role of α-actinin in biological processes.

Changing the crosslinking density of the actomyosin network in vitro or changing the expression levels of α-actinin in cells changed the characteristics of the contractility of both systems(Bendix et al., 2008; Ennomani et al., 2016; Hu et al., 2019). Changing α-actinin density has also been seen to effect bundling of actin filaments in vitro which was found to effect the polymerization of actin filaments (Falzone, Lenz, Kovar, & Gardel, 2012). These studies show that the role of the density of α-actinin in cells with respect to the actin filament density can have consequences on the ability of cells to generate contractile forces. If the levels of crosslinkers vary significantly in cells, these studies implicate that there will be large variations in the force production capability of the cells. Quantifying the variation of these factors in cell populations should provide us insight into variations in the magnitude of traction forces exerted in cell populations.

α-actinin is a ubiquitously conserved protein that both bundles and crosslinks actin filaments. It belongs to the spectrin superfamily (Blanchard, Ohanian, & Critchley, 1989). There are four main isoforms of α-actinin, smooth muscle isoforms (ACTN2 and ACTN3) and non-muscle isoforms (ACTN1 and ACTN4), with the non-muscle variants only found in non-muscle cells (Carol A. Otey & Carpen, 2004). The difference between the muscle and non-muscle variants being that the binding of the non-muscle variants is calcium sensitive while that of the muscle variants being calcium insensitive (Burridge & Feramisco, 1981). ACTN1 and ACTN4, the non-muscle isoforms are found in focal contacts and in stress fibers (Blanchard et al., 1989; Carol A. Otey & Carpen, 2004; Pavalko & Burridge, 1991). The basic structure of α-actinin is

described below (Figure 5). It has a actin binding domain composed of two calponin homology domains. Attached to this actin binding domain are four spectrin repeats flowed by Calmodulin like domain. Together they form a rod like structure which. Two actinin molecules forms dimers with the actin binding domains on either side which helps in the crosslinking of actin filaments.

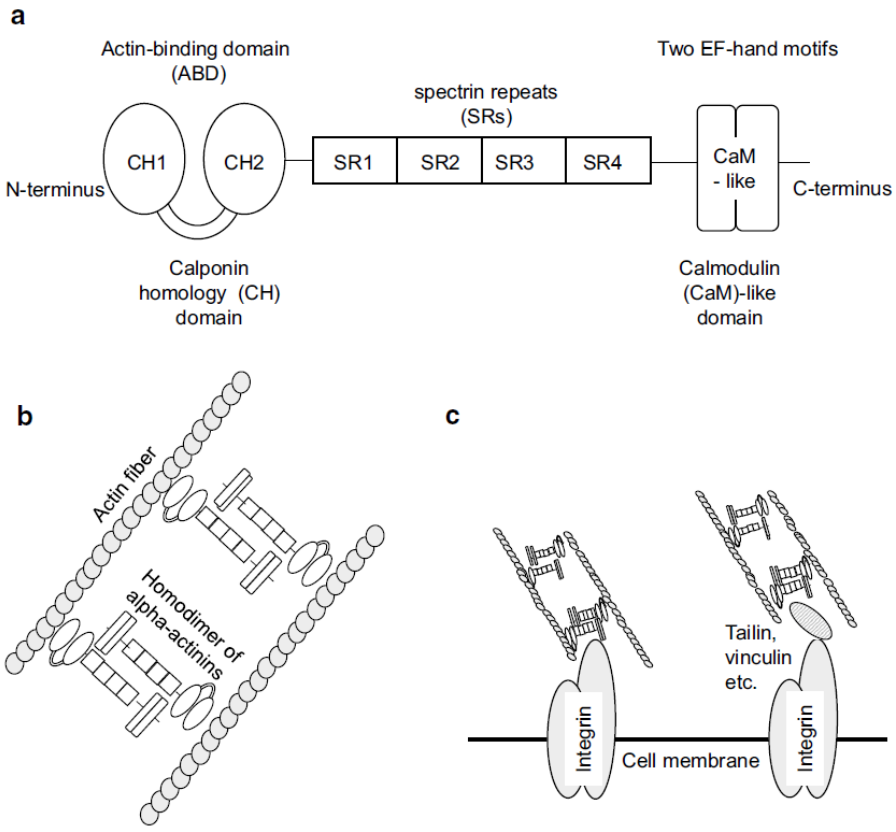

Figure 5: Domain structure of α-actinins and mode of action in cells

Adapted from (Honda, 2015)

(a). Schematic of the domain structure of alpha-actinins: Alpha-actinins are composed of an actin-binding domain (ABD), four spectrin repeats (SRs), and a calmodulin (CaM)-like domain. ABDs are composed of two calponin homology (CHs) domains (CH1 and CH2). CaM-like domains are composed of two EF-hand motifs.

Schematic of actin bundling with alpha-actinins (b). Actinins form an anti-parallel dimer, and homodimers of actinins bundle actin fibers by interacting with the ABD. Schematic of interactions between actin fibers and cell membranes

(c). Actin fibers bundled with actinins directly or indirectly interact with the cell membrane through integrins

α-actinin is known to localized to many of the actin structures in cells including stress fibers, the cell cortex, cell adhesions, and lamellipodium (Craig & Pardo, 1979; Benjamin Geiger & Singer, 1979; Lazarides & Burridge, 1975). Non-muscle α-actinin1 associates with cell adhesion molecules, such as integrin ß1 and alpha-catenin, allowing actin filaments to link to the membrane in some locations (C. A. Otey, Vasquez, Burridge, & Erickson, 1993; C A Otey, Pavalko, & Burridge, 1990). It also has an important role in cell adhesion stabilization and cell shape and cell motility regulation (Glück & Ben-Ze'ev, 1994; Gluck, Kwiatkowski, & Ben-Ze'ev, 1993; Knudsen, Soler, Johnson, & Wheelock, 1995). The role of α-actinin in the lamellipodium is not yet clearly understood and it is possible that it simply follows a redistribution of actin to the lamellipodium. As mentioned earlier, α-actinin has two actions on actin filament, crosslinking and bundling. In crosslinking, actinin links two randomly oriented filaments and when more actinin is present, they align the filaments to form F-actin bundles. In vitro, this can be controlled by altering the rate of actin polymerization or the temperature in which actinin is interacts with filamentous actin (Falzone et al., 2012; Jockusch & Isenberg, 1981; Wachsstock, Schwartz, & Pollard, 1993). In the past, this change from a meshwork of cross-linked filaments or bundles was termed gelation or solation respectively.

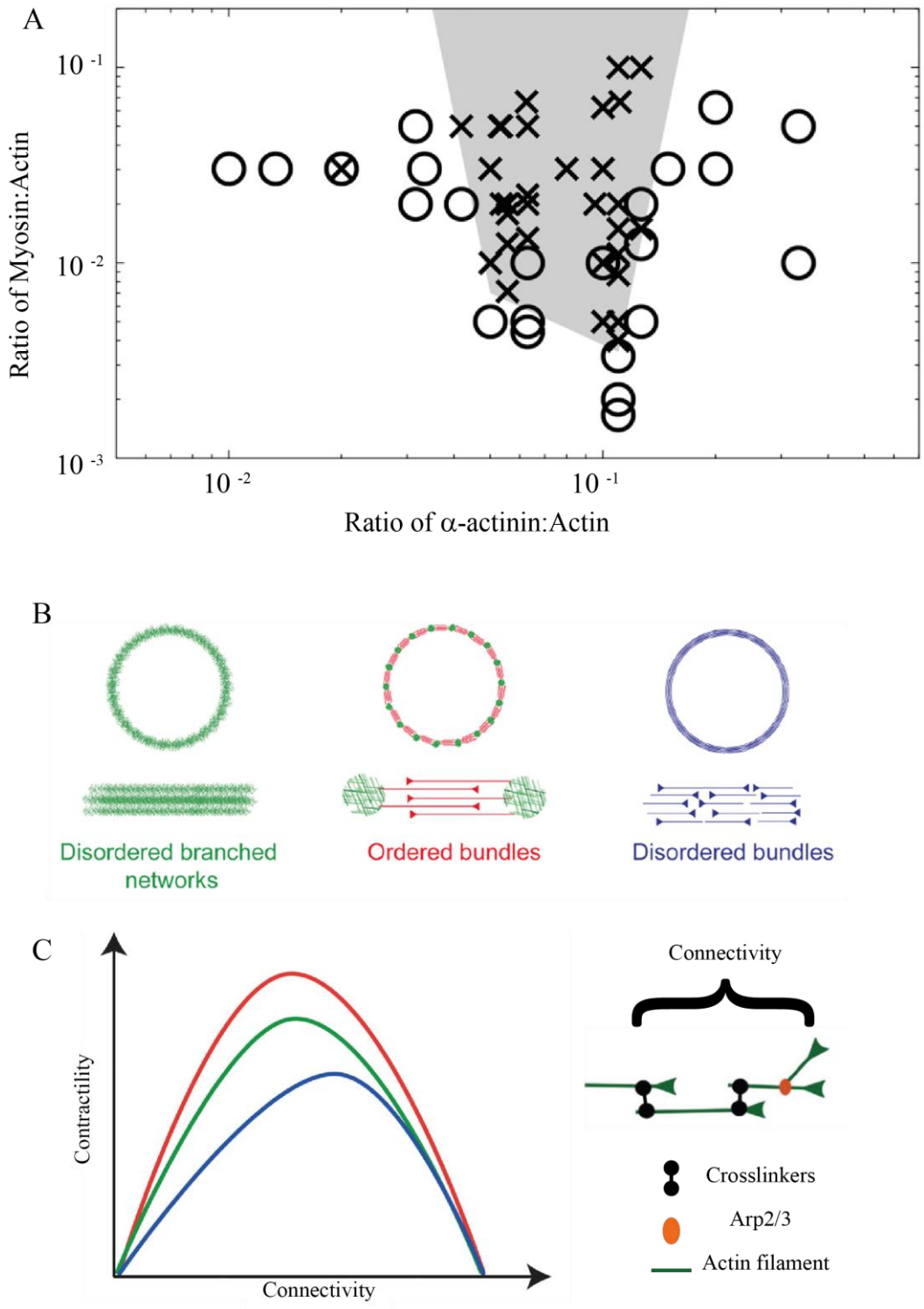

Figure 6: Actin network connectivity and architecture play a role in contractility

A: Adapted from (Bendix et al., 2008)

Actin network contractility is only present at a certain motor concentration and connectivity. The state diagram shows the dependence of macroscopic contractility on the molar ratios of a-actinin cross-linkers and myosin II motors to a fixed actin concentration and filament length. The crosses in the figure are the only networks that contract. All the circles are non-contracting networks. Outside the shaded region, at low myosin and a-actinin concentrations (RM:A , 0.003, Ra:A , 0.04) and at high a-actinin concentrations, there is no macroscopic contraction.

B & C: Adapted from (Ennomani et al., 2016)

In panel B, the different types of architectures generated are shown. The green network is composed of a branched actin network. The red network has regularly spaced branched networks bridged by an linear actin filaments that are in an anti-parallel configuration. The blue network is composed of linear actin filament bundles. The three networks are denoted by the same colors in the plot on panel C.

In panel C, on the left, a schematic of the role of connectivity and network architecture on contraction is shown. The connectivity of the system varies depending on the architecture of the network and this affects the contractility. The contraction of all three network architectures are described by a curve of the same shape. On the right of panel C, a schematic representation of connectivity shows the two types of connections in the networks, one being actin filaments crosslinked by α-actinin and the other being branches of actin nucleated on pre-existing filaments by Arp2/3.

In vitro studies have clearly shown that the lack of sufficient number of crosslinks hinders contractility of the actomyosin network (Bendix et al., 2008). Bendix et al., showed that in the absence of α-actinin, a mix of actin filaments and myosin never contract even at the highest myosin concentration they used (Figure 6A). Indeed, the actin-myosin II network

without α-actinin was indistinguishable from the actin alone network. This suggests that in the absence of crosslinking to hold the actin filaments together, the myosins just slide the actin filaments next to each other leading to the lack of net contraction in the system. They also showed that in such systems, contraction is only possible when the ratio of actin-myosin and actin-α-actinin is within a specific range (Figure 6A). The absence of α-actinin has also been shown to cause asymmetric contraction of actomyosin rings in vitro instead of symmetric contractions (Figure 7) suggesting an important role for the protein in maintaining balance in force distribution within these networks (Senger et al., 2019). These results suggest that a randomly ordered filament network cannot contract without a certain number of crosslinks that can transmit the myosin generated contractile forces through the network. Their results also show that if the proportion of α-actinin to the given amount of actin is too high, then there is no contraction even at high motor concentration suggesting that the system is too rigid and deformation resistant.

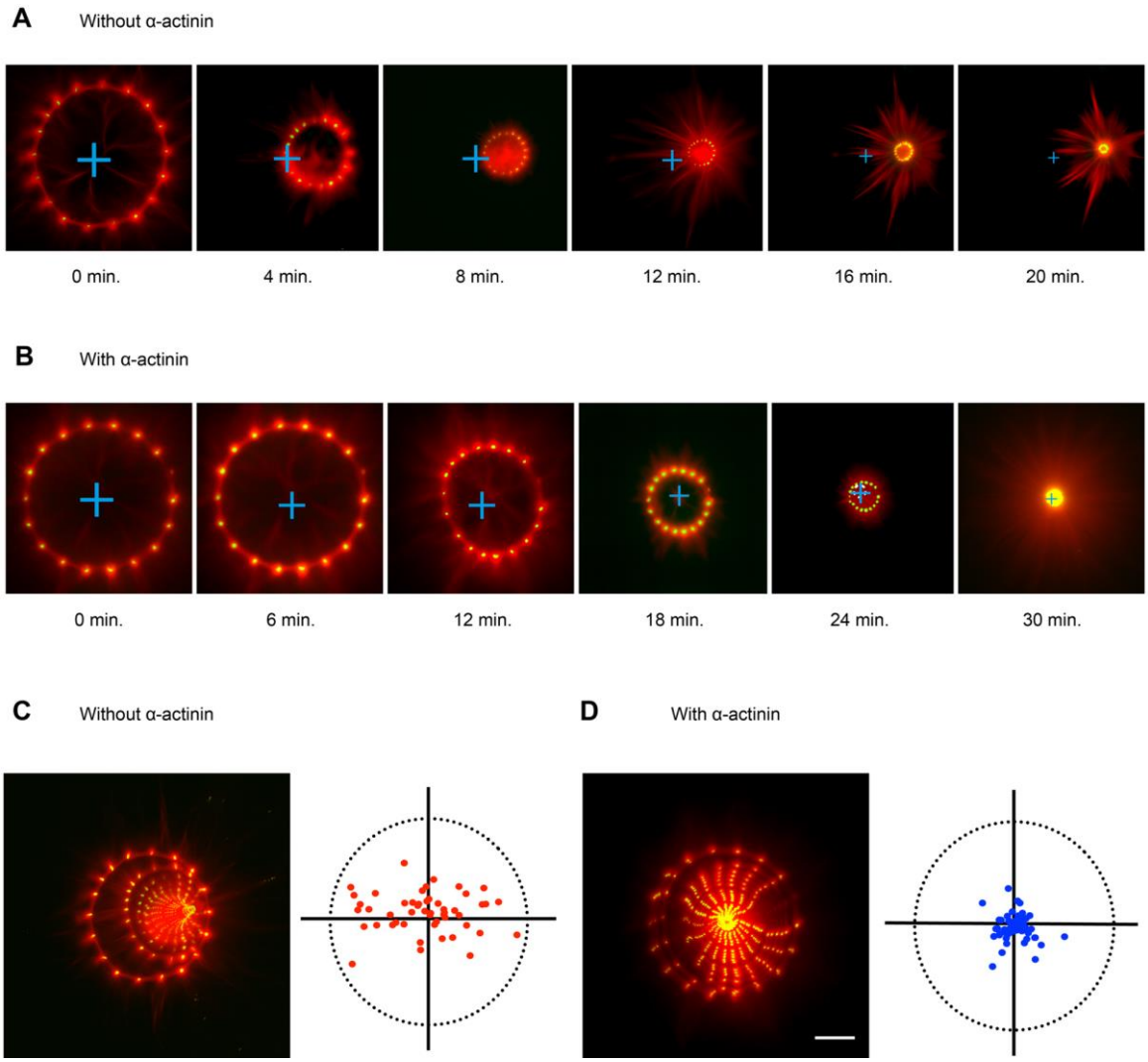

Figure 7: α-Actinin modulates the symmetry of actin network contractility in vitro.

Adapted from: (Senger et al., 2019)

Actin ring assembly was initiated from the polymerization of actin filaments from micropatterned dots coated with actin nucleation-promoting factors. (A,B) Contraction of the actin rings upon addition of myosin motors in the absence (A) or presence (B) of α-actinin. Time is indicated in minutes. t=0 corresponds to the onset of contraction. The blue cross highlights the geometrical center of the initial actin structure at time, t=0. (C,D) Images show the maximum projection of pictures shown in A and B, respectively. The plots represent the

coordinates of the centre of the contractile ring after full contraction (C, n=73; D, n=50). Scale bar: 20 µm

However Ennomani et al., showed that the architecture and connectivity of the actin network also plays a role in the contraction of the system (Ennomani et al., 2016) (Figure 6B&C). They showed that even in the absence of crosslinkers, if the network architecture has interconnections in the system through a branched actin filaments (Disordered branched network in Figure 6B), then, myosin based contraction is possible. A network architecture that had a mixture of branched actin and antiparallel bundles also showed contraction in the absence of α-actinin suggesting that it is the connectivity in the network that allow myosins to transmit forces through it. In ring shaped networks composed of linear filaments lacking connections to each other (disordered bundles), no contraction was observed. But the addition of α-actinin to this same linear filament system allowed contraction, again highlighting the role of network connectivity that allows force transmission through the network. Interestingly, they observed that the three different network architectures showed a relation between contractility and network connectivity that had the same shape even though the amplitudes of the curves were different (Figure 6C).

In cells, actinin is involved in the organization of actin filament bundles and is present in the stress fibers (discussed in the next section) of cells where it alternates with myosin bands (Langanger et al., 1986; Lazarides & Burridge, 1975). α-actinin is now known to be involved in the turnover of stress fibers and its reduction/absence leads to much thicker stress fibers and increase in the traction forces exerted by cells (Hu et al., 2017; Kemp & Brieher, 2018) while injecting α-actinin into cells was shown to be able to disrupt stress fiber formation (Pavalko & Burridge, 1991). Changing actinin expression in cells led to marked changes in substrate

stiffness dependent cell polarization suggesting that the ability of cells to control the mechanical properties of the cytoskeleton is vital for cells to adapt to its substrate (Doss et al., 2020). α-actinin knockdown in cells also leads to the development of an asymmetric actomyosin network, changes in the organization of the stress fiber positioning, and altered traction force dipole orientations in cells on micropatterns compared to control cells (Senger et al., 2019). The knockdown of α-also leads to increase in the traction forces exerted by cells (Hu et al., 2019) whereas the overexpression of α-actinin can lead to decrease in the traction forces (Doss et al., 2020). Transfecting a mutant version of α-actinin (K255E), which has an increased binding affinity to actin leading to its binding kinetics to be insensitive to tension (Chaubet, Khadivi Heris, Ehrlicher, & Hendricks, 2020) has been shown to increase turnover and suppress stress fibers (Kemp & Brieher, 2018). The mutant also leads to an increase in traction force produced by cells (Ehrlicher et al., 2015). These studies prompt the question of how variations in the cellular levels of actin:myosin and actin:actinin could change actomyosin contractility, the associated cellular contractility and the resulting traction forces exerted by cells. That all adherent cells are able to exert contractile forces suggest that cells maintain a minimum level of actinin in cells required for maintaining connectivity sufficient for transmitting forces.

2.4 Focal adhesions

Focal adhesions are the connection between the extra cellular matrix and the internal contractile machinery of cells. They are involved in many biological processes such as wound healing, angiogenesis and morphogenesis (Burridge & Chrzanowska-Wodnicka, 1996; Gunawan et al., 2019; J. T. Yang, Rayburn, & Hynes, 1995). These complexes are multifunctional organelles and they mediate cell-ECM adhesion, force transmission, cytoskeletal regulation and signaling (Bershadsky et al., 2003; Burridge & Chrzanowska-Wodnicka, 1996; Benjamin Geiger,

Bershadsky, Pankov, & Yamada, 2001). They have a complex architecture composed of many proteins as seen below (Figure 8).

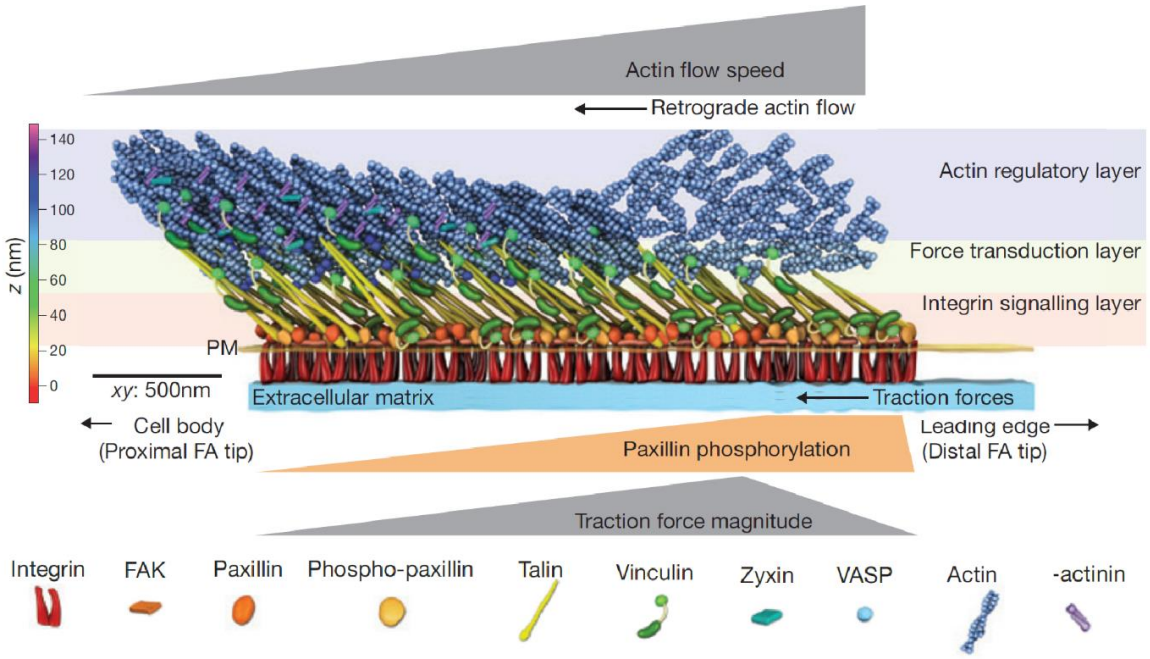

Figure 8: Nanoscale architecture of focal adhesions

Adapted from: (Case & Waterman, 2015)

Schematic model of focal adhesion molecular architecture, depicting experimentally determined protein positions and mechanical signatures. The distal tip is where the lamellipodial branched actin interacts with the adhesion. The integrin signaling layer is directly above the plasma membrane, attached to transmembrane integrins and is composed of Focal Adhesion Kinase (FAK) and paxillin and talin head domains. Following this signaling layer, a force transduction layer composed of Talin and vinculin is present where actin interacts with the focal adhesion. An actin regulatory layer composed of VASP, zyxin and actin filament ends is found above the force transduction layer. α-actinin is found attached to the actin filaments above the focal adhesion.

Being the link of the cytoskeleton to the extracellular matrix, focal adhesions are the sites at which contractile actomyosin forces are transmitted to the surface (B. Geiger, Yehuda-Levenberg, & Bershadsky, 1995; Yamada & Geiger, 1997). It has been known for some time that tension is capable of reinforcing focal adhesions (Choquet, Felsenfeld, Sheetz, & Carolina, 1997) and allowing them to grow (Riveline et al., 2001). Integrin binding to fibronectin and actin binding proteins has been shown to reduce their diffusion in the plasma membrane. Nascent focal adhesion containing β1-integrin and paxillin form at, and near the leading cell edge, within the lamellipodium and they either disassemble or mature through growth and elongation (Choi et al., 2008). The actin flow in the region local to these new adhesions decreases suggesting engagement of the focal adhesions with actin (Alexandrova et al., 2008). As some of the nascent adhesions mature, new, small and linear actin filaments grow from them in a VASP and formin dependent fashion (Chrzanowska-Wodnicka & Burridge, 1996; B. D. Hoffman, Grashoff, & Schwartz, 2011; Hotulainen & Lappalainen, 2006; Oakes, Beckham, Stricker, & Gardel, 2012; Riveline et al., 2001; S. Tojkander, Gateva, Husain, Krishnan, & Lappalainen, 2015). FAK and vinculin in nascent adhesions are also known to interact with the ARP2/3 complex which nucleates branched actin using a preexisting filament as a base (DeMali, Barlow, & Burridge, 2002). A study has shown that preexisting actin filaments at focal adhesions might recruit talin which then binds to free, diffusing integrins inducing fast activation and subsequent binding to fibronectin (Rossier et al., 2012). These could be mechanisms that increases the coupling of actin with that of maturing focal adhesions (Choi et al., 2008). Incorporation of α-actinin, which bundles the actin filaments is followed by increasing paxillin, talin and vinculin recruitment (Choi et al., 2008; Serrels et al., 2007; Weed et al., 2000) leading to maturation of the adhesion.

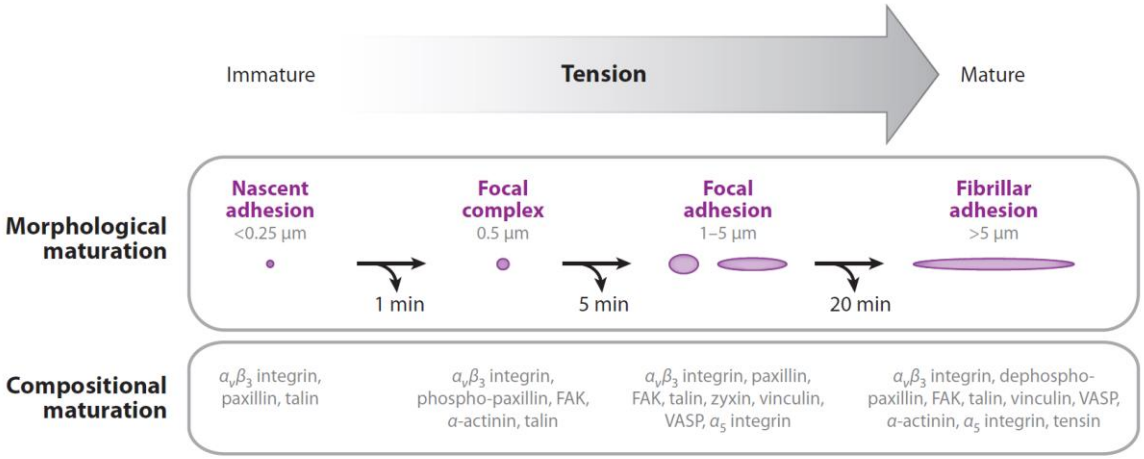

Figure 9: Morphological phases of focal adhesion maturation

Adapted from: (Gardel, Schneider, Aratyn-Schaus, & Waterman, 2010)

A schematic representation of the phases of focal adhesion maturation (the adhesions are represented by purple ovals; length scales indicated by focal adhesion lengths) and the composition of the adhesions at each phase are given below. The curved black arrows at each step denote the possibility of adhesion turnover, which can happen after a certain time (timescale given below each arrow). FAK - Focal Adhesion Kinase; VASP – Vasodilator-stimulated phosphoprotein.

The linkage of the focal adhesion to the cytoskeleton is mediated by the protein talin which is recruited directly from the cytosol (Rossier et al., 2012) and binds to the integrin receptors via its head domain and transmits information directly to the cytoskeleton through its rod domain (Critchley, 2009; Kanchanawong et al., 2010). This is achieved through vinculin, which binds to the talin protein molecule when it is stretched by Pico newton level of forces (Austen et al., 2015; Del Rio et al., 2009; J. Liu et al., 2015). While the talin molecule is still able to experience smaller forces by engaging directly with F-actin in the absence of vinculin (J. Liu

et al., 2015), it is only when vinculin binds to the molecule that talin experiences higher tension (Austen et al., 2015).

The vinculin protein has a head and tail domain linked by a short proline rich linker (Bakolitsa, de Pereda, Bagshaw, Critchley, & Liddington, 1999; Borgon, Vonrhein, Bricogne, Bois, & Izard, 2004). When the molecule is in its 'closed' conformation, the vinculin head interacts with its tail and on the head domain binding to other proteins, the tail domain is released and the molecule takes an open conformation in which, the vinculin tail binds to actin (Johnson & Craig, 1995). Vinculin is suspected to first bind to paxillin rich (Case et al., 2015), proximal regions of a focal adhesion, and as it treadmills to the distal part (Sarangi et al., 2017), vinculin can bind to existing actin bundles, modify them and stimulate the formation of new actin bundles (Wen, Rubenstein, & DeMali, 2009). Mutations of the tail domain can impair F-actin binding, stimulate actin polymerization and bundle F-actin in vitro (Jannie et al., 2015). Vinculin is thought to act as a molecular clutch in these conditions by engaging the retrograde actin flow (Renkawitz et al., 2009; Thievessen et al., 2013). While studies have shown that cell contractility, focal adhesion turnover (Stutchbury, Atherton, Tsang, Wang, & Ballestrem, 2017) and focal adhesion size are affected by the substrate stiffness (Engler et al., 2006; Mitrossilis et al., 2010), the relation between the tension generated on the vinculin molecules themselves is substrate stiffness independent (Sarangi et al., 2017). These results taken together show that, when in the focal adhesion, vinculin, in a substrate stiffness dependent manner, can establish new actin assemblies allowing new links from the substrate to the existing cytoskeleton.

The incorporation of different proteins, maturation of the focal adhesion and increase in tension occurs along with the assembly of actin-myosin-actinin bundles. As these adhesions bear forces, the protein zyxin is recruited which in turn recruits VASP to the site allowing for

further elongation of actin filaments (Uemura, Nguyen, Steele, & Yamada, 2011). Myosin II based tension was found to allow maturation of focal adhesions, promoting the focal adhesions to change their morphology and composition, to modulate adhesion dynamics, the forces they are capable of exerting on the ECM and to modulate the ECM (Gardel et al., 2010; Benjamin Geiger & Yamada, 2011; Vogel & Sheetz, 2006; Webb et al., 2004). External mechanical stress on the cells also leads to mobilization of zyxin from the focal adhesions to the actin filaments and a zyxin dependent mobilization of VASP to these same sites, thickening the stress fibers (L. M. Hoffman, Jensen, Chaturvedi, Yoshigi, & Beckerle, 2012; Yoshigi, Hoffman, Jensen, Yost, & Beckerle, 2005). However, tension alone is not sufficient for focal adhesion maturation. It was shown that without a stress fiber template attached to the focal adhesion, it would not mature even though there was significant tension generated by the contractile lamella (Oakes et al., 2012). Tojkander et al., showed that high tension by myosin II generated contraction in ventral stress fibers inhibits actin polymerization at their focal adhesions through inhibition of VASP (S. Tojkander et al., 2015). This inhibition of VSAP was through AMPK mediated phosphorylation (Blume et al., 2007; Butt et al., 1994) at focal adhesions under high tension (S. Tojkander et al., 2015). This could lead to stabilization of tension within the stress fibers and through this mechanism, inhibit the growth of focal adhesions.

The forces exerted on the substrate by cells via mature focal adhesions is along the direction of their long axis (Balaban et al., 2001). In non-motile cells, a close relation was found between the local force at the adhesion and adhesion size (Balaban et al., 2001). Other studies have also found correlations between forces exerted at focal adhesions and their size (Goffin et al., 2006; Tan et al., 2003). However, it was later shown that a strong correlation between adhesion size and traction force exists only in the initial stages of adhesion maturation and growth (Stricker, Aratyn-Schaus, Oakes, & Gardel, 2011). In this study, no correlation was

observed between tractions and size of adhesions after maturation. It was also shown in the study that mature focal adhesions could withstand six-fold increase in tension without any change in their size and that when the cells are rapidly protruding, the traction stresses decrease in large adhesions. Another study showed that without a stress fiber template attached to the focal adhesion, it would not mature even though there was significant tension generated by the contractile lamella and that focal adhesion size and composition was not correlated with the force exerted through them (Oakes et al., 2012). It is possible that connections between stress fibers can lead to redistribution of the contractile forces leading to variations in forces via adhesions (C. W. Chang & Kumar, 2013; S. Kumar et al., 2006; Tanner, Boudreau, Bissell, & Kumar, 2010). The above-mentioned studies indicate some of the reasons as to why determining a relation between focal adhesion size and traction forces are difficult.

The magnitude of the forces transmitted to the substrate varies significantly depending of the migratory state of the cell. Stationary cells have been found to generate stronger, less dynamic and more peripherally located traction stresses than migrating cells (S. S. Chang, Rape, Wong, Guo, & Wang, 2019). The study also found that these changes were accompanied by reduced focal adhesion turnover and enhanced paxillin phosphorylation. In migrating cells, they found that a new adhesion forming in front of an older one leads to reduction in the mechanical output of the older adhesion. This cross talk between the newly formed and preexisting adhesions might play a role in inhibiting traction forces in migrating cells, limit focal adhesion size and increase variation in forces exerted via mature focal adhesions. This also provides a possible answer as to why an earlier study found that nascent focal adhesions in the leading edge of cells exert higher forces compared to mature focal adhesions more towards the interior of the cell (Beningo, Dembo, Kaverina, Small, & Wang, 2001). The lack of new adhesions ahead of the older ones in migration-restricted cells is suspected to lead to decreased assembly of

new focal adhesions and increase in tractions on the pre-existing ones. This is supported by a study where traction forces peaked at a distance from the leading edge in rapidly protruding regions, but localized close to non-protruding edges (Stricker et al., 2011). The action of Kank proteins which are found on the boundary of mature and longer focal adhesions and absent in the nascent and small adhesions can also play a role in force transmission as they diminishes the talin-actin linkage and reduce force transmission (Sun et al., 2016).

Another factor to remember with focal adhesions is that they are not rigid anchors that transmit all the forces that are exerted on them to the substrate (Elosegui-Artola et al., 2014). Focal adhesion composition is a key factor in determining the forces that are transmitted through them. Reduction of forces transmitted to the substrate occurs on removal of any of the key elements such as paxillin, vinculin (Plotnikov, Pasapera, Sabass, & Waterman, 2012), and talin (Austen et al., 2015), or by preventing the recruitment and clustering of integrins (Y. Liu et al., 2014). The exact integrin composition of the focal adhesions also finely modulates signaling pathways found downstream and the traction forces magnitude (Bharadwaj et al., 2017; Milloud et al., 2017; Schiller & Fässler, 2013).

The dynamics of the focal adhesion also plays a role in force transmission. As mentioned earlier, the maturation process is controlled by positive feedback loops related to the traction and promotion of adhesion growth via the recruitment of new molecules (Kuo, Han, Hsiao, Yates III, & Waterman, 2011; Schiller & Fässler, 2013; Ye et al., 2014). Integrin β1 engagement activates myosin II and integrin αV activates contractile bundles enlargement. The rates of binding/unbinding of integrins to focal adhesions control the magnitude of the forces exerted on the ECM (Elosegui-Artola et al., 2014). These help the traction force adapt to the substrate stiffness (Schiller & Fässler, 2013). This positive feedback also involves the removal of factors

that inactivate force generation such as betaPix and the Rac pathway (Kuo et al., 2011). The forces applied on the adhesions promote formin mediated actin filament nucleation (Courtemanche, Pollard, & Chen, 2016; Jégou, Carlier, & Romet-Lemonne, 2013), which reduces the tension on the adhesions. It has been shown that interference of filament nucleation leads to strong increase in traction forces (Elkhatib et al., 2014). This reduction in tension with increasing actin filament nucleation acts as a negative feedback loop. This interplay between the negative and positive feedback loops can generate oscillating forces that are important in substrate stiffness sensing (Plotnikov et al., 2012; Z. Wu, Plotnikov, Moalim, Waterman, & Liu, 2017). These oscillations again make it difficult to quantify a relation between single focal adhesions and traction forces. Another issue that leads to difficulty in relating forces to focal adhesion size is that sometimes, the contacts that focal adhesions have with the ECM can rupture leading to frictional slippage which occurs at low ECM stiffness and low forces (Aratyn-Schaus & Gardel, 2010).

There can also be rupture between the actin network and the focal adhesions similar to engagement and disengagement of a clutch. This can prevent the transmission of actomyosin contractility to the ECM and hence a reduction in measured tractions. The engagement of the focal adhesion "clutch" to the contractile machinery can be measured by the retrograde actin flow in the vicinity of the adhesion and show a relation to the traction force (Sabass, Gardel, Waterman, & Schwarz, 2008). Similarly, the inward translocation of actin filament bundles at contractile fiber ends also gives a measure of the tractions forces (Elkhatib et al., 2014; Russell et al., 2011). Weakness in the connections between focal adhesions and the actin network can, in the presence of high actin retrograde flow or high ECM stiffness lead to forces on the clutch mechanism that is too high to maintain. Kank2 protein can induce integrin-ligand slippage which leads to sliding of the focal adhesion and hence reduction of the traction forces (Sun et

al., 2016). This leads to disengagement of the connections between the adhesions and the actomyosin network leading to reduction in measured forces. This disengagement can in some cases be overridden by the unfolding of talin which would then mediate the recruitment of vinculin allowing the increased transmission of traction forces (Elosegui-Artola et al., 2016).

These studies suggest that there is a bi-directional relation between actin and cell-ECM adhesions. Signals originating from the focal adhesions have been shown to regulate the polymerization and organization of actin (Riveline et al., 2001; Vicente-Manzanares, Newell-Litwa, Bachir, Whitmore, & Horwitz, 2011). They also showed that focal adhesions allow for actin assembly, while the dynamics of the actomyosin system allows for focal adhesion maturation and disassembly. The coupled input and output of mechanical forces involved in these processes could play important roles in regulating signals for cell growth and differentiation. Understanding how the forces are transmitted from the actomyosin network via the focal adhesions to the ECM and the role of proteins involved in this force transfer is hence important. However, as discussed above, the relation between individual focal adhesions and traction forces can be difficult to quantify as there are many factors that affect the force transmission at each adhesion. This is possibly the reason for the existence of a debate on the role of focal adhesion size and traction forces.

2.5 Stress fibers formation and dynamics

One of the major contractile elements in cells are the stress fibers (Kassianidou & Kumar, 2015; Pellegrin & Mellor, 2007; Vallenius, 2013). They were observed decades ago as bundles of microfilaments that crossed the cell body (Abercrombie, Heaysman, & Pegrum, 1971), terminating in dense plaques at the base of the cell and classified as contractile structures (Isenberg, Bielser, Meier-Ruge, & Remy, 1976; Kreis & Birchmeier, 1980). They were found to

be actomyosin bundles crosslinked by α-actinin, with the actin in bi-polar arrangement (Lazarides & Burridge, 1975; Mitchison & Cramer, 1996). These contractile structures are often anchored to focal adhesions, connecting the cytoskeleton to the ECM (Mitchison & Cramer, 1996; Naumanen, Lappalainen, & Hotulainen, 2008; Pellegrin & Mellor, 2007).

The mechanical and biochemical interactions between the ECM and cells modulates stress fiber abundance, structure and organization. Hence, stress fibers are important features of cells that encounter mechanical resistance (S. Tojkander, Gateva, & Lappalainen, 2012). Fibroblasts develop prominent stress fibers during wound closure through generation of tension and ECM remodeling (Sandbo & Dulin, 2011). Epithelial cells involved in wound closure also display stress fibers and then differentiate into myoepithelial cells (Pellegrin & Mellor, 2007). During embryogenesis, stress fiber like cables that span multiple cells are present in epithelial cells during dorsal closure (Jacinto et al., 2002). The endothelial cells which experience mechanical strain due to the hydrostatic pressure caused by blood flow also display prominent stress fibers (Wong, Pollard, & Herman, 1983). The presence of these structures in such varied cell types that experience mechanical stimuli shows their importance in regulating the mechanical signals that cells receive. Understanding the factors involved in generation and maintenance of these stress fibers is hence important in building models that are physiologically relevant.

Myosins were found to be part of the stress fiber of non-muscle cells along with actin a few decades ago and it was also found that myosin II forms periodic striations along these stress fibers (Weber & Groeschel Stewart, 1974). Electron microscopy studies of platinum replicas showed without a doubt that myosin II filaments are present in these cells (Svitkina, Verkhovsky, McQuade, & Borisy, 1997; Verkhovsky, Svitkina, & Borisy, 1995). These early

studies showed that, in fibroblasts, myosin II filaments have uniform length and form super-structures where multiple parallel filaments are organized in registry forming filament stacks. Such structures were also found later in the interphase state of other non-muscle cells and contractile rings of dividing cells (Fenix et al., 2016; Goeckeler et al., 2008). In more recent studies, utilizing techniques such as TIRF (Total Internal Reflection Microscopy) and SIM (Structured Illumination Microscopy) (Gustafsson, 2000; Kner, Chhun, Griffis, Winoto, & Gustafsson, 2009), the visualization of the individual bipolar filaments in non-muscle cells has improved significantly (Beach et al., 2014; Burnette et al., 2014; Shutova, Spessott, Giraudo, & Svitkina, 2014). The filaments have been found not only in the ventral stress fibers, but also in the transverse arcs (these structures to be discussed later) and it was observed that they are present at the cell periphery (Burnette et al., 2011, 2014), sometimes near focal adhesions (Pasapera et al., 2015). The stacks that Myosin II filaments form are perpendicular to the actin filament orientations and the myosin II stacks are spaced regularly, with the regions in between the stacks being taken by α-actinins (Gordon, 1978; Langanger et al., 1986; Lazarides & Burridge, 1975). The organization of NMM's in cells has been shown to effect traction forces exerted by cells and the contractility of the actin network (Dasbiswas, Hu, Bershadsky, & Safran, 2019; Hu et al., 2017, 2019). Over time, these structures were classified into different types of stress fibers, each with specific roles that they undertake (Naumanen et al., 2008; S. Tojkander et al., 2012). The four main classes of stress fibers are called the dorsal stress fibers, the transverse arcs, the ventral stress fibers and the perinuclear actin cap (Figure 10).

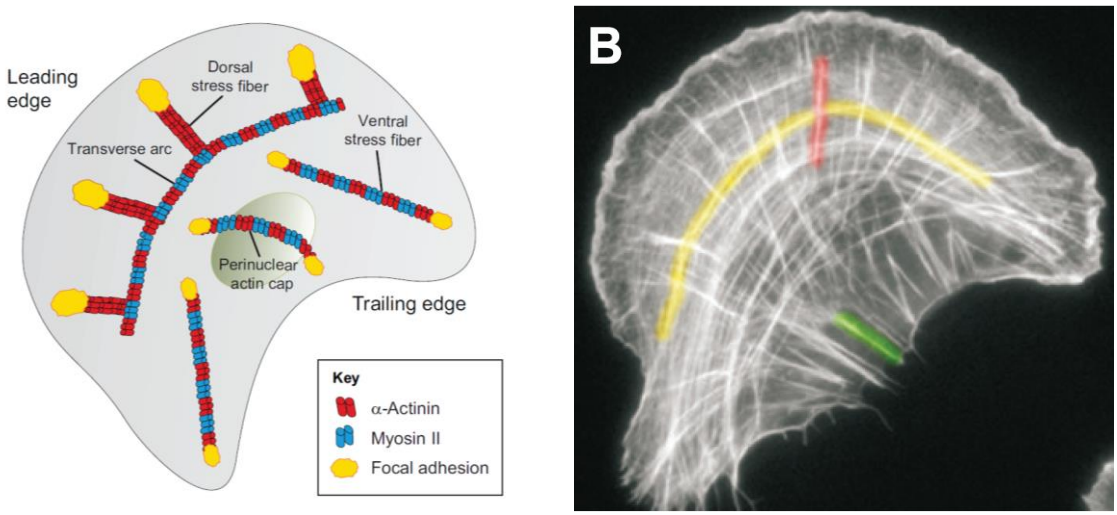

Figure 10: Different types of stress fibers

Adapted from: (S. Tojkander et al., 2012)

On the left, we see a schematic presentation of the stress fiber network of motile mesenchymal cells. There can be four discrete categories of stress fibers. The dorsal fibers are anchored to focal adhesions at their distal ends. The transverse arcs present as curved, contractile actomyosin bundles that move from the cell periphery to the cell center over time. The ventral stress fibers are actomyosin bundles anchored on both ends to the substrate via focal adhesions. The perinuclear actin cap goes over the nucleus at its center, but is anchored on both ends via focal adhesions.

On the right, the stress fiber network of a motile U2OS cells is shown. Examples of dorsal stress fibers, arcs and ventral stress fibers, indicated with red (dorsal), yellow (arcs) and green (ventral) lines, are marked.

Dorsal stress fibers are α-actinin containing filaments composed of parallel bundles of actin attached to focal adhesions on their distal end that only rarely contain myosin II (Hotulainen & Lappalainen, 2006; Sari Tojkander et al., 2011). No phosphorylated Myosin Light Chain has been found on them (Stacey Lee et al., 2018). Hence, they are not able to contract. But they are mechanically coupled to the transverse arcs and hence under some tension (Stacey Lee et al., 2018). They elongate from the focal adhesions and mDia1/DRF1 formin based actin polymerization has been shown to play a role in their formation and elongation (Hotulainen & Lappalainen, 2006). Their distal ends are composed of unipolar actin filaments and the barbed ends there rapidly grow facing the cell periphery while their proximal parts are composed of actin filaments of mixed polarity (Cramer, Siebert, & Mitchison, 1997; Pellegrin & Mellor, 2007). They also contain the crosslinker palladin and the VASP complex (Burnette et al., 2014; Gateva, Tojkander, Koho, Carpen, & Lappalainen, 2014). The VASP complex and formins are thought to help them extend from the focal adhesions to the cell center (Hotulainen & Lappalainen, 2006; S. Tojkander et al., 2015). They are thought to be a platform for the assembly of other types of stress fibers and to link them to focal adhesions (Hotulainen & Lappalainen, 2006; Sari Tojkander et al., 2011). The dorsal fibers have been observed to serve as tracks that transverse arcs use to slide centripetally (Hotulainen & Lappalainen, 2006; Tee et al., 2015).

Transverse arcs are long, curved actin structures that display repetitive bands of myosin and α-actinin that form near and in the lamellipodium from Arp2/3 and formin nucleated actin fibers from (Burnette et al., 2011; Hotulainen & Lappalainen, 2006; Sari Tojkander et al., 2011; X. F. Zhang, Schaefer, Burnette, Schoonderwoert, & Forscher, 2003). Formin nucleated filaments have been shown to be especially important, with these linear filaments being organized by myosin II into antiparallel concentric arcs (Murugesan et al., 2016). These arcs have been shown to contain actin filaments of mixed polarity some time ago (Svitkina et al.,

1997), and are contractile structures not connected to any focal adhesions, and centripetally slide along the dorsal fibers in a myosin II dependent fashion (Tee et al., 2015; X. F. Zhang et al., 2003). They are known to be mechanically coupled to the dorsal stress fibers close to their distal ends to which they are connected, but not those near their center (S. Tojkander et al., 2015). This connection between the dorsal and transversal stress fibers is mediated by α-actinin (Figure 11) which plays a role in maintaining symmetry of the network as a whole and in the formation of the transverse arcs (Senger et al., 2019). Tojkander et al., showed that the focal adhesion attached to these distal dorsal stress fibers enlarge and align along the direction of the contractile actomyosin bundle. Towards the cell center they fuse to form thick, contractile actomyosin bundles. At their terminal parts, they contain more filaments with barbed ends facing the nearest cell edge (Svitkina et al., 1997).

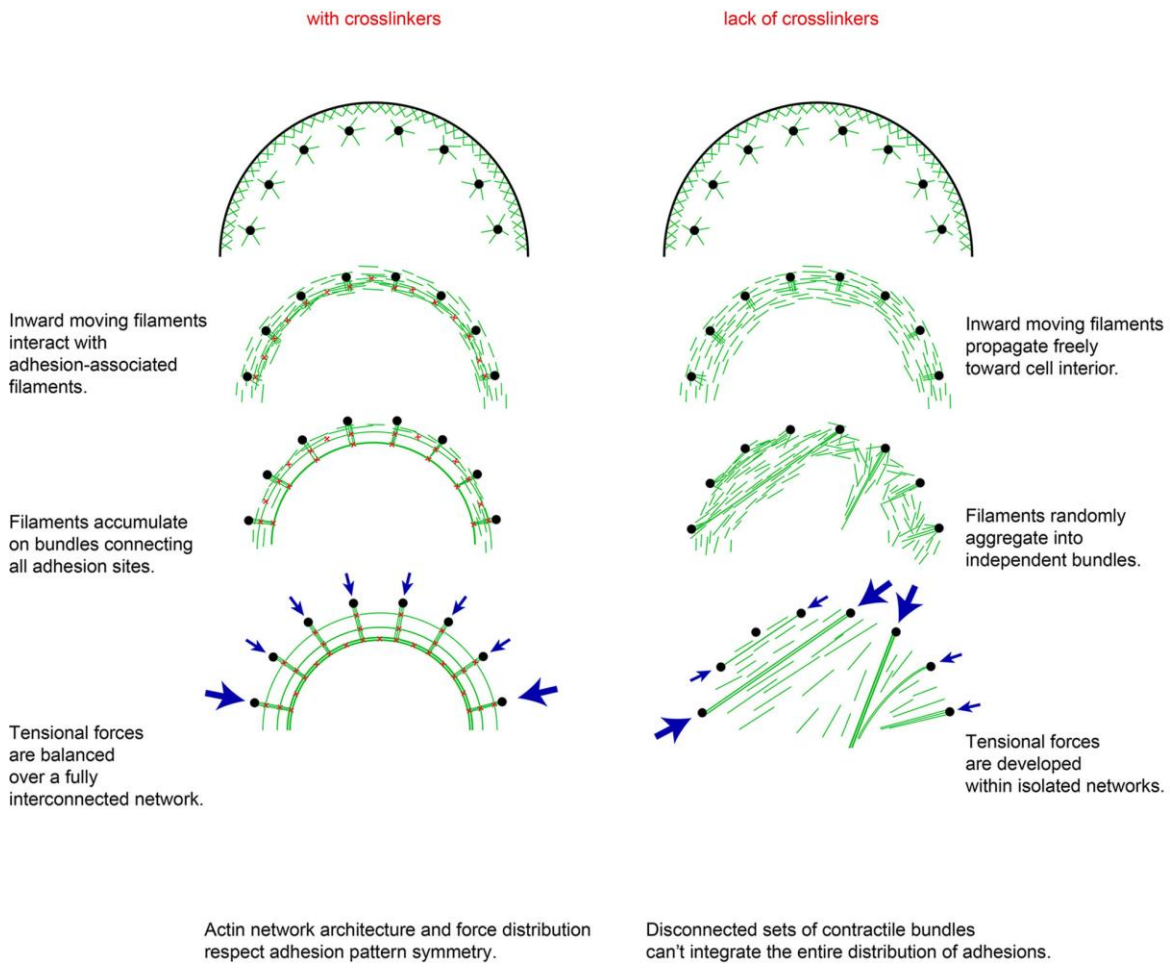

Figure 11: Actin network dynamics in the cell above the curved adhesive edge in presence (left column) or absence (right column) of α-actinin.

Adapted from: (Senger et al., 2019)

The schemes show the speculative journey of actin filaments (green) from their nucleation at the membrane (top) to their incorporation into contractile networks (bottom) in control (left) and α-actinin-depleted cells (right). α–actinin is shown as red crosses and the focal adhesions as small black circles. The blue arrows denote the forces exerted by cells. In the right column, without α-actinin to bundle and crosslink the filaments generated in the lamellipodium, the transverse arcs do not form.

Ventral stress fibers have characteristics of both dorsal stress fibers and transverse arcs in that they are contractile and attached to focal adhesions on both ends (Livne & Geiger, 2016; S. Tojkander et al., 2012). They are the major contractile machinery of many interphase cells (Small, Rottner, Kaverina, & Anderson, 1998). Near their center, they are composed of alternating bands of α-actinin and myosin II of non-uniform lengths. One of the mechanism for the formation of ventral stress fibers is the merger of a transverse arc with two dorsal stress fibers close to their distal ends in a tension dependent manner (Hotulainen & Lappalainen, 2006; S. Tojkander et al., 2015). Tojkander et al., showed that these distal dorsal stress fibers provide newly forming ventral stress fibers the link to the substrate via focal adhesions on either side of the cell (Figure 12) called terminal dorsal fiber. Tension provided by the contraction of the transverse arcs that are connected to these dorsal stress fibers leads to enlargement of their focal adhesions and VASP based elongation of the actin filaments at these adhesions cease due to the myosin II contraction, allowing further increase in tension. The transverse arcs attached to these fibers fuse to thicken the emerging ventral stress fiber. Disassembly of non-contractile dorsal fibers found in between the distal dorsal stress fibers is mediated by cofilin1 and they do not participate in the formation of the ventral stress fiber. The terminal dorsal fibers are under tension, which protects them from the tension sensitive cofilin1 (S. Tojkander et al., 2015). Another method that ventral stress fibers can form is the annealing of short actomyosin fragments (Hotulainen & Lappalainen, 2006; Kovac, Teo, Mäkelä, & Vallenius, 2013; Machesky & Hall, 1997; S. Tojkander et al., 2015). Ventral stress fibers are not isolated structures that exist independent of the cortex. Recent work has shown that these structures are embedded into the cortical network (Vignaud et al., 2020) suggesting that further study is required to understand the role of actin dynamics in stress fiber formation.

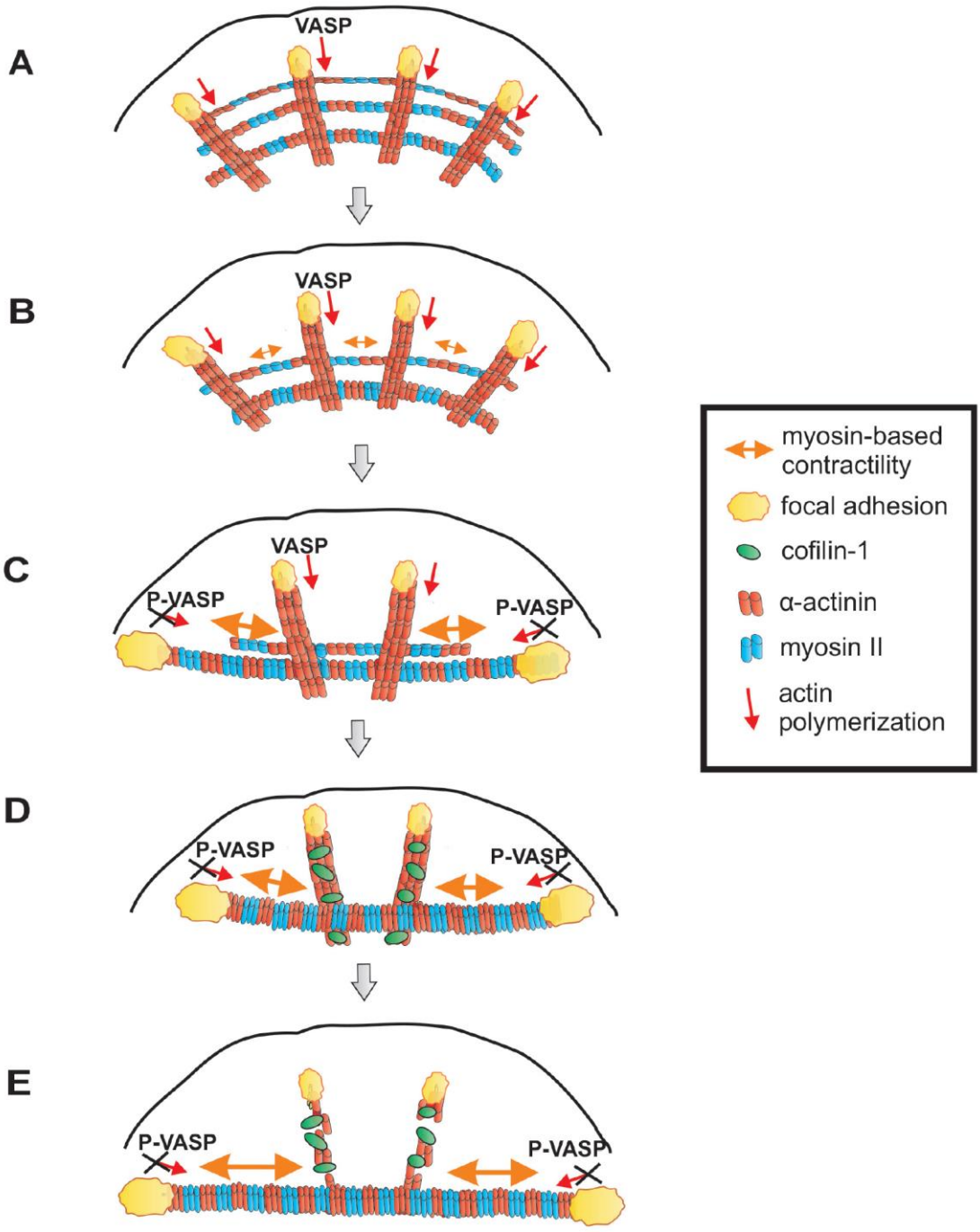

Figure 12: Ventral stress fiber formation model

Adapted from (S. Tojkander et al., 2015)

(A) Dorsal stress fibers elongate through vectorial actin polymerization from focal adhesions located at the leading edge of the cell, and form a spider net -like structure with multiple transverse arcs. At least Dia1 formin and VASP are involved in vectorial actin polymerization and consequent dorsal stress fiber elongation from focal adhesions.

(B) Arcs flow along the elongating dorsal stress fibers towards the cell center, and fuse with each other to form thicker and more contractile actomyosin bundles.

(C) Tension provided by the contraction of arcs is mediated through dorsal stress fibers to those focal adhesions that are linked to the end of the arc. This leads to enlargement of 'terminal' adhesions and their alignment along the direction of the contractile arc bundle. Tension provided by myosin II –driven contractility of the arc inhibits vectorial actin polymerization in 'terminal' focal adhesions, and this is at least partially mediated by VASP phosphorylation. Consequently, elongation of the actomyosin bundle ceases, thus allowing its efficient contractility. Please note that focal adhesions are likely to be composed of many actin filament populations, and for simplicity only the one undergoing vectorial actin polymerization and thus promoting stress fiber elongation is shown in the model.

(D) Cofilin-1 specifically binds to and promotes the disassembly of non-contractile dorsal stress fibers, which are connected to the central regions of the arc and thus do not participate in the formation of the ventral stress fiber.

(E) Whereas non-contractile stress fibers are disassembled by cofilin-1, contractile stress fibers are protected from tension-sensitive cofilin-1–induced severing. Eventually, this leads to the formation of a contractile ventral stress fiber, which is connected to one large focal adhesion at its each end and aligned perpendicularly to the direction of lamellipodium extension.

The organization of myosin motors on the stress fibers also plays a role in force generation. Muscle cells have a sarcomeric organization, where there are aligned bands of myosin filaments that alternate with relatively thin bands of α-actinin (M. A. Bray, Sheehy, & Parker, 2008). This organization of sarcomeres has been shown to produce and transmit forces that are independent of the length of the myosin bands (D. E. Rassier, MacIntosh, & Herzog, 1999; Dilson E. Rassier & Pavlov, 2010). In non-muscle cells, the contractile units display alternating bands of myosin and α-actinin, but the banding is not regular like present in muscle cells. The relation between the banding length and contraction is not linear in these cells. In some non-muscle cells, the tension increases with increasing band length (Aratyn-Schaus, Oakes, & Gardel, 2011), but in others when some band lengths decrease, other bands elongate (Chapin, Blankman, Smith, Shiu, & Beckerle, 2012; Peterson et al., 2004), making the net effect difficult to predict. The myosin bands generate forces while the α-actinin bands would bundle and link the actin filaments allowing the forces to be transmitted over longer lengths. The variation in the band length of myosin stacks in non-muscle cells may allow higher force generation in the wider bands, but the forces might be dissipated due to the noneffective filament translocation (Kurzawa et al., 2017). Dynamic reorganization of the actomyosin bundles can also lead to modulation of force generation. Actin filament nucleation at the contractile stress fiber ends (Russell et al., 2011; Skau & Waterman, 2015; Tee et al., 2015) opposes the transmission of tension to the ECM by elongation of the filaments (S. Tojkander et al., 2015). As the newly formed filaments move towards the stress fiber center, they are subject to local variations in internal tension. The stretched sarcomeric like structures can elongate and new sarcomeres are generated (Chapin et al., 2012). These length fluctuations have been proposed to be a method used by cells for maintaining a constant tension on the anchoring points (Chapin et al., 2012; Russell et al., 2011). While there can be elastic deformations of

these actomyosin structures when cells undergo small mechanical loads, at high loads, they may undergo plastic deformations (Bonakdar et al., 2016) which would lead to dissipation of the contractile forces within the system rather than transfer them to the focal adhesions. These plastic deformations are likely associated with the breaks in the actin filament crosslinks and the disengagement of myosin from actin filaments.

To get a better sense of the dynamics of actin filaments, I take a small step back to look at actin filament nucleation and turnover. An actin filament has a barbed and pointed end. The barbed end has a higher affinity for actin monomer incorporation. For filament elongation here, the end has to be free, i.e. it should not be capped. Free barbed ends are generated at the membrane through three mechanisms. Uncapping of pre-existing barbed ends capped by capping protein, or gelsolin related proteins (Hartwig et al., 1995), severing of F-actin by the actin –binding cofilin/ADF (Chan, Bailly, Zebda, Segall, & Condeelis, 2000) and the de novo nucleation of filaments involving the Arp2/3 complex or formins (Pollard et al., 2000). Of these, cofilin mediated disassembly has emerged as one of the important factors regulating actin dynamics (Ono, 2003; Pollard & Borisy, 2003). Cofilins bind cooperatively to actin filaments, change the twist of the filament and severs the filament at the boundary between the cofilin decorated and bare regions (Huehn et al., 2018). This is achieved by changing the actin filament bending mechanics on binding, leading to differences in mechanics of the filament at the boundary of cofilin bound and unbound regions (Elam et al., 2013). Cofilin has also been implicated in fluidization of the cytoskeleton through severing of F-actin when cells are stretched (Lan et al., 2018) and in attaching to stress fibers whose tension is suddenly reduced (Hayakawa, Tatsumi, & Sokabe, 2011). These studies show the importance of cofilin in controlling actin architecture in cells by promoting filament severing leading to recycling of existing filaments and generation of new structures.

Each F-actin filaments in stress fibers also associate with two strands of tropomyosin molecules assembled head-to-tail along two helices of the actin filament (J. R. Moore, Campbell, & Lehman, 2016; Squire, Paul, & Morris, 2017). Tropomyosin has been shown in vitro, to protect actin filaments from disassembly (Bernstein & Bamburg, 1982; Ono & Ono, 2002), prevent Arp2/3 from binding to actin filaments to initiate branches (Blanchoin, Pollard, & Hitchcock-DeGregori, 2001), interfere with actinin assembly in cells and change the ordering of myosin mini-filaments (Hu et al., 2019; Kemp & Brieher, 2018). It has been shown in these studies that this change in the ordering of myosin is achieved by competition between tropomyosin and α-actinin (Figure 13). When tropomyosins are knocked out in cells, it leads to higher actinin4 association in cells that leads to a more crosslinked network and highly ordered myosin stack formation. This highly ordered Myosin II structure surprisingly leads to lower force transmission.

A

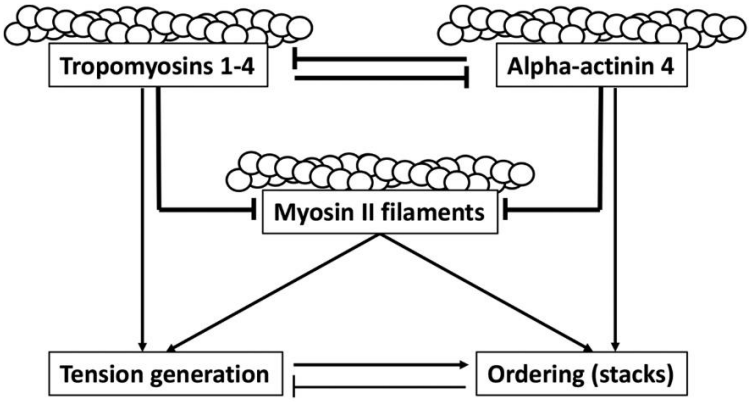

B

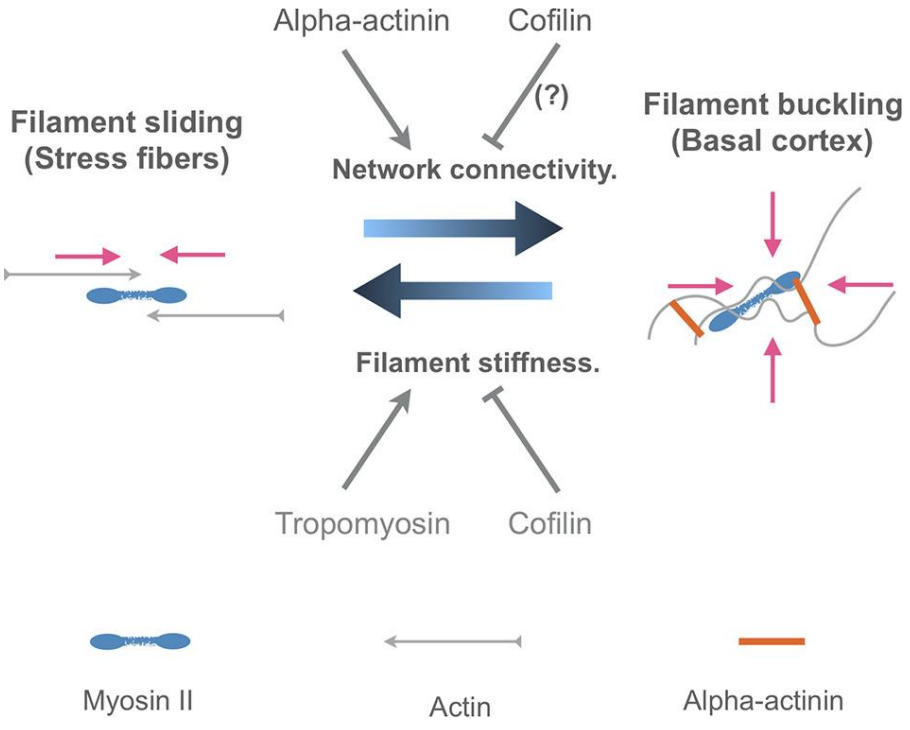

Figure 13: Actinin competes with tropomyosin, which protects actins from cofilin mediated severing

A: Adapted from (Hu et al., 2019)

Schematic model of the reciprocal regulation of actomyosin structure and contractility by alpha-actinin-4 and tropomyosins. Tropomyosin 1-4, alpha-actinin 4, and myosin II filaments all compete for binding along F-actin. The balance between the levels of these proteins dictates the degree of order found in myosin stacks and the corresponding tension generated by the actomyosin network. α-actinin4 promotes less tension and more order, whereas tropomyosin promotes less order and higher tension. The drawn lines do not imply direct interaction, but reflect the phenotypic observations in the study.

B: Adapted from: (Kemp & Brieher, 2018)

Model depicting one way in which α-actinin-4 might suppress stress fiber formation. In the presence of α-actinin, due to restriction of filament sliding by crosslinking, a highly interconnected network of disordered actin filaments forms at the basal surface of cells that undergoes myosin mediated biaxial contraction through filament buckling. In the absence of α-actinin, network connectivity is lost, favoring stress fiber formation by filament condensation. Loss of α-actinin also allows tropomyosin to bind to F-actin, which stiffens the filaments to further inhibit buckling and favors stress fiber formation. Pink arrows show the directions of contractile forces.

These results suggests that high actinin crosslinking of stress fibers leads to a jammed system where forces are dissipated within the actin-myosin-actinin network, rather than the forces being to the substrate. While the relative levels of proteins such as tropomyosin and cofilin can be quantified, actinin and myosin interact with them and compete for actin binding. As such, quantifying force transmission to the substrate and comparing the values to the relative ratios of actin-myosin, myosin-actinin and actinin-actin should shed light on the role of these different interactions between proteins and traction force variations in cell populations.

Along with actin filament nucleation at the focal adhesions, there will be an equivalent disassembly of filaments in the existing fiber. In the absence of this disassembly, the fibers should keep getting thicker. Studies that analyzed the turnover rates along the length of the stress fibers show that filaments turnover with a characteristic lifetime of 1 minute compared to the lifetime of the stress fiber which is around 1 hour (Hu et al., 2017). The myosin and actinin turnover is faster near the center of the fiber compared to the ends (Peterson et al., 2004). These dynamics, which can lead to reorganization of the stress fibers, make it difficult to relate the forces exerted by them to their observed composition. The protein zyxin has been shown to be recruited to damaged regions of stress fibers and help in the recovery process by recruiting VSAP, α-actinin and inducing filament formation and bundling (Smith et al., 2010). This might be a method through which new actin filaments that are more aligned to the stress fiber are generated around it. Conclusively identifying the parameters regulating this dynamic exchange of filaments and the sharing of the available actin monomer pool between these contractile structures should help elucidate the link between force production at the cellular level and actin network remodeling.

Stress fibers are not isolated structures within cells (Kassianidou, Brand, Schwarz, & Kumar, 2017; Marek, Kelley, & Perdue, 1982; Vignaud et al., 2020). While the connection of dorsal to transverse stress fibers has already been discussed, ventral stress fibers are also not isolated structures. Laser ablation of single stress fibers have been shown to compromise the entire traction force field (S. Kumar et al., 2006; Tanner et al., 2010) and lead to changes in the tension at focal adhesions not connected to these fibers (C. W. Chang & Kumar, 2013). These studies show that contractile forces generated in one stress fiber can propagate to other stress fibers through the connections between them (Kassianidou et al., 2017). Kurzawa et al., showed that contractile bundles not only possess interconnections to other stress fibers by are also

embedded in a continuous meshwork of cortical filaments along their entire length (Figure 14). The cortical actin filaments close to the stress fiber were more aligned to it compared to those further away from them, which suggests that randomly oriented filaments were being realigned and incorporated into the stress fiber. They showed that this cortical network has myosin motors attached to it and is also contractile. These results are in agreement with previous studies that showed cortical actin connections to stress fiber (A. Kumar et al., 2019; Marek et al., 1982; Svitkina, 2018). It is possible that the interconversion of filaments between the cortical structure and the stress fiber is essential for the modulation of the production of traction forces.

A

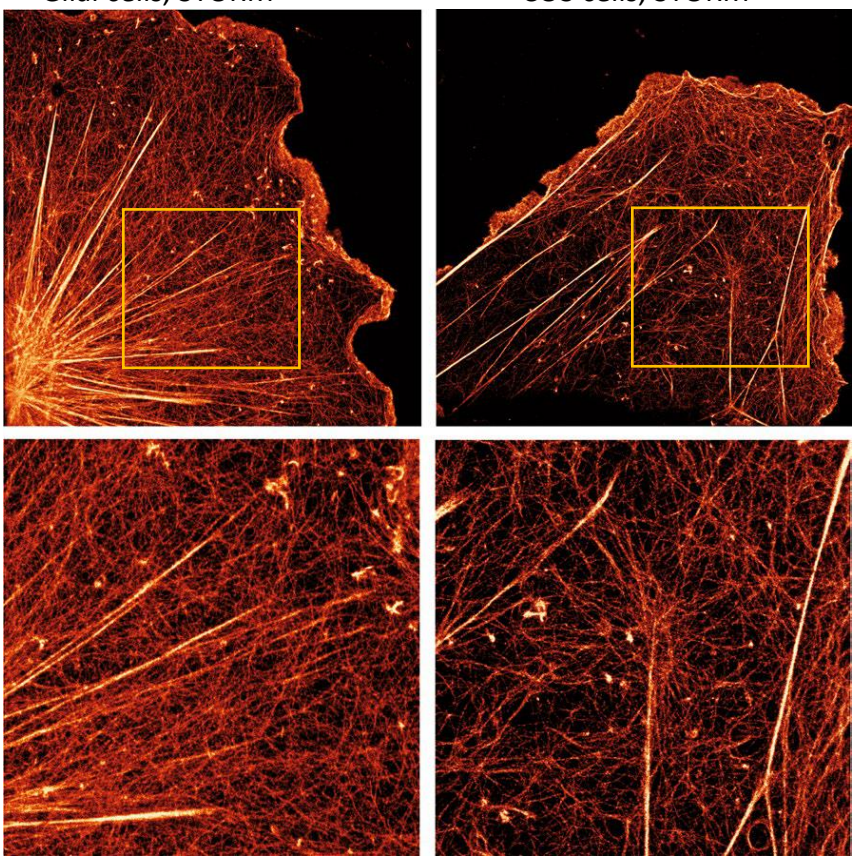

B

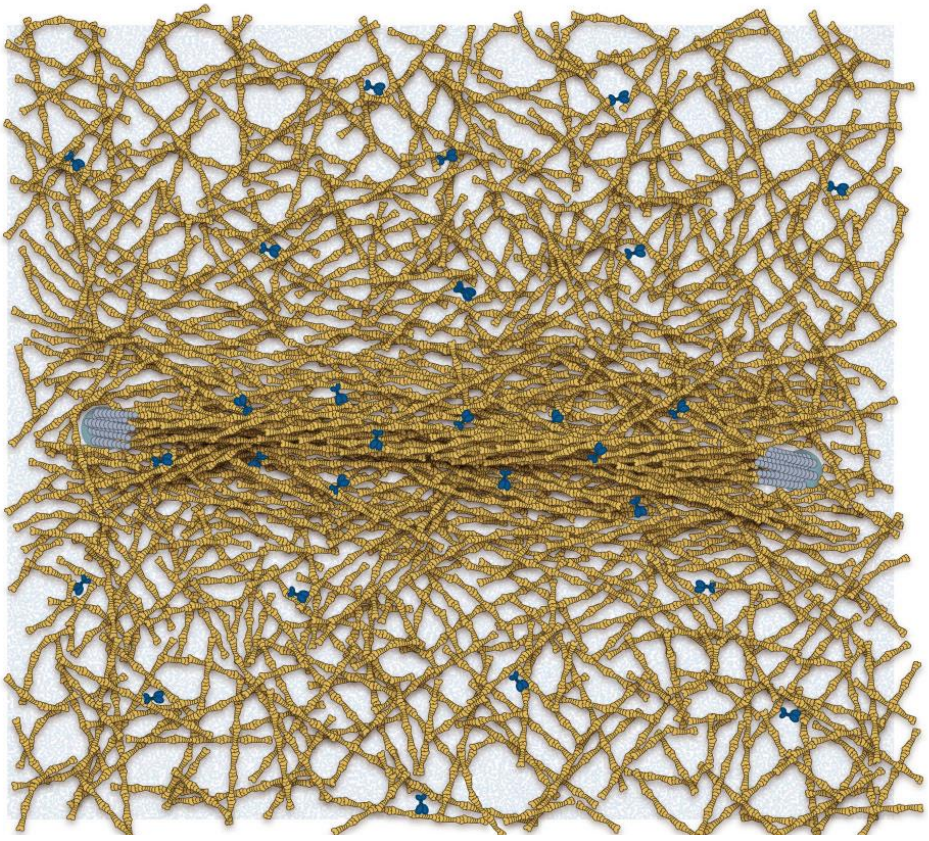

Figure 14: Stress fibers are embedded in a cortical network.

Adapted from: (Vignaud et al., 2020)

A: STORM reconstructed image of the actin network of a rat astrocyte and a COS-7 cell and associated zoomed-in images of the yellow insets below. Scale bars, top panel-5 µm. Zoomed-in scale bars, 1 µm.

B: Schematic representation of the stress fiber anchored at its two edges on the substrate via focal adhesions (blue disks) as a fully embedded structure within the surrounding contractile actin cortex (myosins are represented by blue bow-ties)

2.6 Actomyosin cortex

The animal cell shape is controlled primarily by the cell cortex (Salbreux et al., 2012). This is a thin network of actin filaments, myosin proteins and actin –binding proteins that are situated immediately below the plasma membrane of most eukaryotic cells that lack a cell wall. It is the main determinant of the stiffness of cellular surface and it resists external mechanical stress (D. Bray & White, 1988). It is thought to oppose intracellular osmotic pressure (Stewart et al., 2011). Local changes in the mechanical properties of the cortex drives many cellular deformations, like those occurring during mitotic cell rounding, cytokinesis, cell migration and morphogenesis (Bergert et al., 2015; D. Bray & White, 1988; Heisenberg & Bellaïche, 2013; Levayer & Lecuit, 2012; Maddox & Burridge, 2003; Sedzinski et al., 2011).

Quantifying the ultrastructure of the cortex has been difficult in part due to its location below the plasma membrane which makes it difficult to image using electron microscopy compared to flat actin structures such as lamellipodial and Filopodia (Svitkina et al., 2003). However, using fast scanning AFM and super resolution microscopy has provided important details of the apical and basal cortex architecture and composition in recent years (Xia et al.,

2019; Yanshu Zhang et al., 2017). They have shown that the cortical mesh size and orientation of actin filaments diverge significantly depending on cell type and the various actin binding proteins involved in the maintenance suggesting the cells tune their cortex based on their function.

Cortical tension is regulated by myosin II motors as they create contractile forces by pulling actin filaments with respect to one another (Clark, Wartlick, Salbreux, & Paluch, 2014; Vicente-Manzanares et al., 2009). It has been shown that inhibition of myosin contraction reduces bleb growth while increase in myosin activity through RhoA transfection resulted in increased bleb size (Tinevez et al., 2009). In mitotic cells, increased recruitment of myosin II to the cortex has been shown to correlate with increasing intracellular pressure (Ramanathan et al., 2015). Tinevez et al., also showed that by impairing actin turnover is leads to changes in the cortical tension. Depletion of ADF/cofilin and the barbed end capping protein CAPZB leads to increases in the tension and cortical thickness increases(Chugh et al., 2017), whereas cytochalasinD treatment resulted in ten-fold decrease in the tension compared to control cells. Chemical inhibition of Arp2/3, formins and myosin also lead to changes in cortical filament length, architecture (Shirai et al., 2017; Xia et al., 2019) and tension (Chugh et al., 2017). These studies suggest that the type of actin network, the length of actin filaments, actin dynamics and myosin activity plays important roles in maintaining cortical architecture. Reduction in α-actinin has also been shown to reduce mitotic cell tension suggesting that crosslinks in the cortex helps maintain its strength. As it has been discussed earlier, α-actinin crosslinking has been demonstrated to coordinate long range contraction of actomyosin systems. The protein helps to maintain connections between all the filaments in a mesh, allowing the contractile stresses to propagate. However, a high concentration of actinin inhibits contraction, suggesting that the

excessive crosslinks can jam the system, preventing forces from being transmitted across the system (Bendix et al., 2008; Chugh et al., 2017; Ennomani et al., 2016).

3 Traction force measurement methods:

The technique of traction force microscopy (TFM), provides a powerful tool that can be used to measure the forces exerted by cells on their substrate. In the last few decades, different methods have been created to measure the forces generated by cells. Each method comes with positives and negatives that are discussed below in brief.

3.1 Substrate deformation based:

One of the earliest methods used to measure forces generated by individual cells was using wrinkles generated on a silicone layer(Harris, Wild, & Stopak, 1980). However, getting quantitative information regarding cellular forces was difficult as the wrinkles were nonlinear and irregularly shaped. In later work, beads were introduced onto a non-wrinkling elastic film made of silicone and the deformation of the layer observed through the displacement of the beads (J. Lee et al., 1994; Tim Oliver et al., 1995). However, these substrates were nonporous, poorly adhesive and their mechanical properties could not be tuned easily to match the force generation capacity of many mammalian cells (Dembo & Wang, 1999). These limitations were overcome by using polyacrylamide (PA) hydrogels as the substrate to plate cells. These substrates are non-toxic, optically transparent, elastic, can be embedded with fluorescent beads, the protein density can be independently controlled and the stiffness can be tuned to the physiological range of many cell types (Wang & Pelham, 1998). They can also be micropatterned with proteins with micrometer precision allowing for control of cellular morphology and actomyosin architecture (Thery, 2010; Tseng et al., 2011; Vignaud, Ennomani, & Théry, 2014). The calculations to obtain the forces from the deformation of these substrates

has been well characterized (Figure 15) and optimized (Dembo & Wang, 1999; Stricker, Sabass, Schwarz, & Gardel, 2010; Tambe et al., 2011; Tseng et al., 2011). However, careful application of the regularization procedure used to add additional constraints to the force estimation or filter the image data is required to avoid error in measurement (Kulkarni, Ghosh, Seetharaman, Kondaiah, & Gundiah, 2018; Martiel et al., 2015).

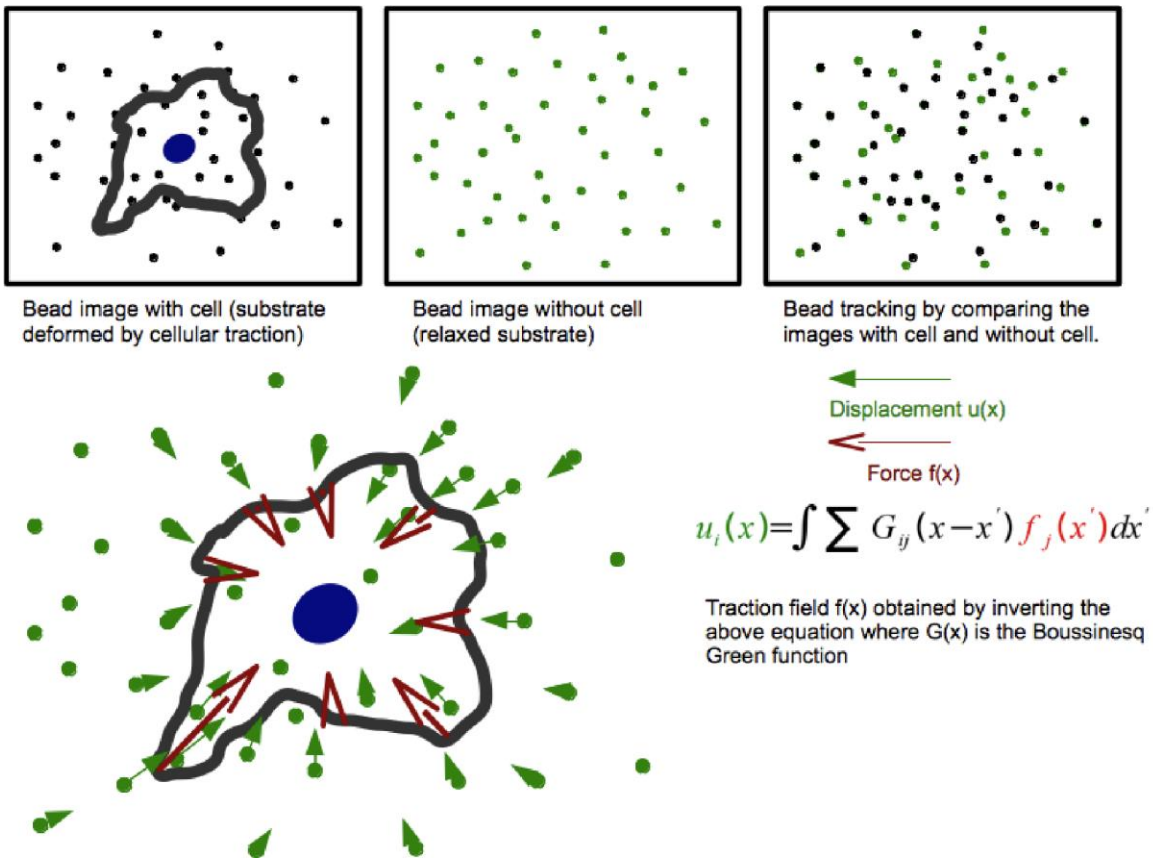

Figure 15 : Traction force microscopy on soft substrates

Adapted from: Production de forces par le cytosquelette d'actine : mécanismes et régulation par le micro-environnement, 2013

The deformation of the soft substrate is tracked using the beads embedded in them. First, an image of the deformed substrate with a cell growing on it is taken. Then the cell is detached to allow the substrate to relax and another image obtained. Using these two images, the displacements of the gel is calculated. Using the displacements, and the material properties of the substrate, the forces exerted by the cell is calculated using the inverse of the equation given.

Living cells exert forces that deform the gel. However, measuring the forces exerted by these cells requires detaching them from that region or allowing them to migrate away to obtain the relaxed reference configuration of the gels which is required to calculate the forces. This eliminates the ability to fix and fluorescently label the cells to determine their internal cytoskeletal organization and protein content to compare with the traction forces. There have been studies where fluorescent markers with regular spacing have been printed on the gel surface to avoid the need for the reference images (Bergert et al., 2016; Polio et al., 2014). Berger et al., achieved this by printing 200 nm disks composed of quantum dots with submicron accuracy onto silicone substrates in a regular array and allowing cell attachment by functionalizing the silicone surface with fibronectin (Figure 16). Polio et al., achieved printing of a regular array of fluorescent proteins on glass which was then transferred to acrylamide hydrogels. This allowed cells to spread on the gel using the protein array as attachment points. In both methods, the array spacing of the patterns in the absence of cells is known. These pre-stress array spacing can be compared to the array spacing of patterns on regions where cells deform the substrate to calculate forces without detaching the cells. However, the method by Bergert et al., requires the ability to both synthesize and print the quantum dots with submicron precision or purchase these printed arrays. The method by Polio et al., could have trouble in restricting cells in regions unless only part of the region (of the dimension of a cell) has protein patterns. Their method also has the issue of allowing cell attachment only in isolated dots

where the protein is present. The rest of the surface is non cell-adhesive. Which might lead to changes in focal adhesion attachment, morphology and dynamics.

In both these methods, unless a reference array to detect position accurately is introduced during the patterning, re-finding a cell after removal of the sample from the microscope can be cumbersome. This can be overcome by performing the labelling on the microscope. However, this requires either microfluidics or significant dexterity and cumbersome maneuvering to prevent displacing the sample on the stage while changing reagents, washing the sample, which can lead to losing the position.

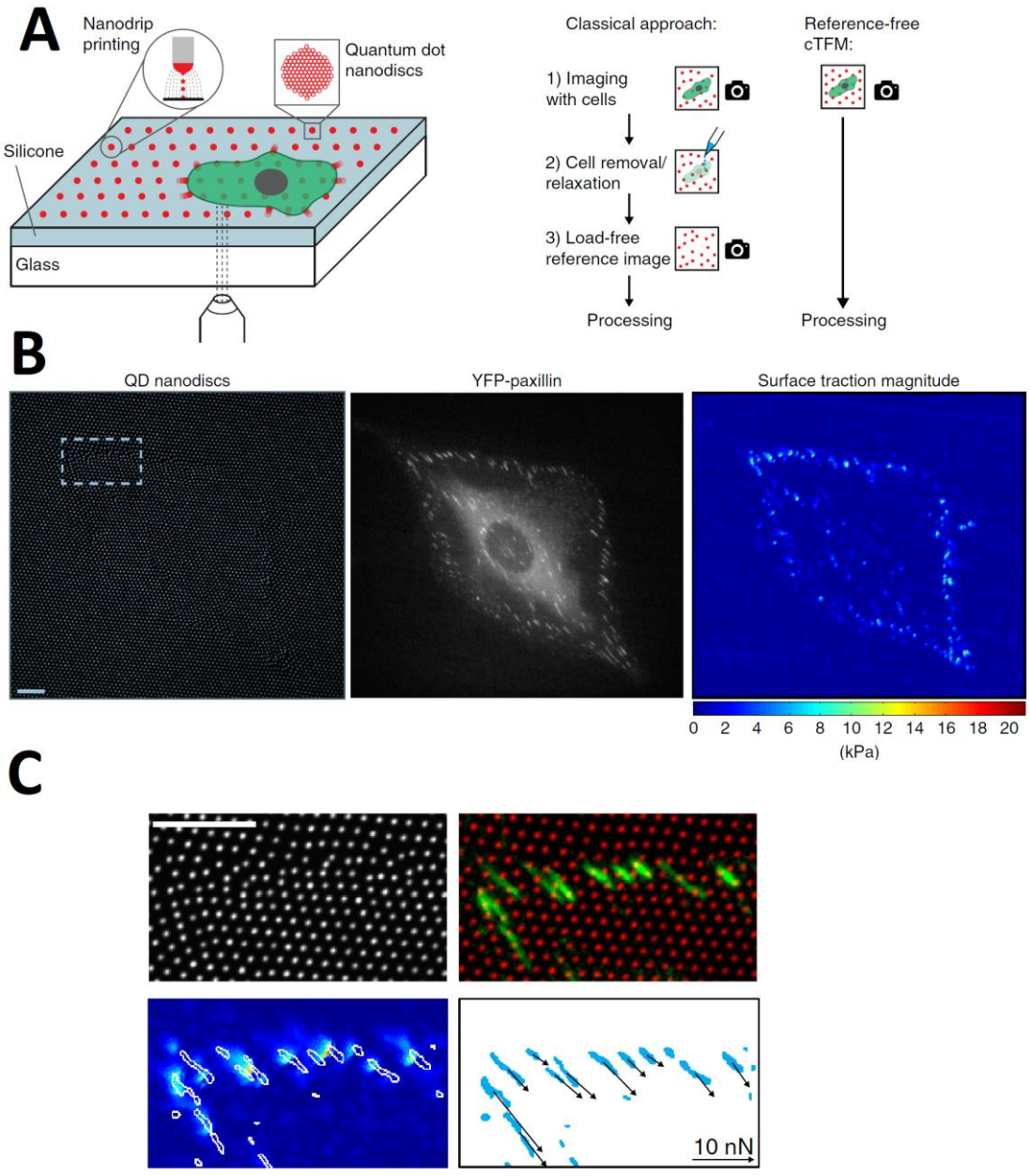

Figure 16: Reference free traction force microscopy method

A. Schematic of the cTFM set-up and involved techniques and Workflow of the classical continuum approach versus the one-step cTFM process

B. High-resolution detection of forces exerted at focal adhesions. From left to right, cTFM substrate with red quantum dot nanodisks (spacing: 1.5 mm), REF-paxillin expressing cell

showing focal adhesion (Scale bar, 10 µm) and reconstructed surface tractions peaks are located at the cell circumference

C. Top panel: Quantum dots and focal adhesions from the inset in nanodisk image from B. Bottom panel: Reconstructed tractions and direction of forces from individual focal adhesions. The surface traction peaks and focal adhesions can be seen to colocalize. Scale bar, 10 µm.

3.2 Cantilever based methods

Micropillar based traction force detection is another useful method in which, microfabricated arrays of polydimethylsiloxane (PDMS) (du Roure et al., 2005; Tan et al., 2003) or acrylamide (S. W. Moore, Biais, & Sheetz, 2009) serve as substrates and force sensors. As the micropillars are made out of elastic material attached to a stiff substrate, a force exerted on the free end causes the pillar to bend (Figure 17). If this force is sufficiently small compared to the pillar height, the force is proportional to the displacement allowing simple calculation of traction forces exerted by cells. The spring constant of these pillars can be quantified using elastic theory and the dimensions of the pillar or by quantifying thermal fluctuations of the pillar (Hutter & Bechhoefer, 1993). If the pillars are closely spaced and only their top surfaces are selectively coated with proteins, cells attach and exert forces only on the tips of the pillars. This method has a few advantages. Displacements can be calculated without a reference image. The displacement of a pillar depends only on the force applied on it and not on the other pillars. The stiffness of the pillar can be modulated by changing the geometry of the pillars allowing generation of steep and heterogeneous mechanical environments without altering material properties (Sujin Lee, Hong, & Lee, 2016; Saez, Ghibaudo, Buguin, Silberzan, & Ladoux, 2007). The disadvantages include having cells attach to discrete regions and topology, instead of a uniform adhesive surface which influences the morphology of cell-ECM adhesions. As the

topography of the substrate has been shown to affect biological behavior of cells such as differentiation (Trappmann et al., 2012) and focal adhesion formation (Huang et al., 2009; Malmström et al., 2010), the availability of discrete regions of adhesion in micropillar assays is a concern. Focal adhesions attached to one pillar can extend beyond the adhesive area (Sarangi et al., 2017). Fabrication technology restricts the stiffness range to approximately one order of magnitude compared to continuous substrates where the stiffness range is around two orders of magnitude (Roca-Cusachs, Conte, & Trepat, 2017).

A

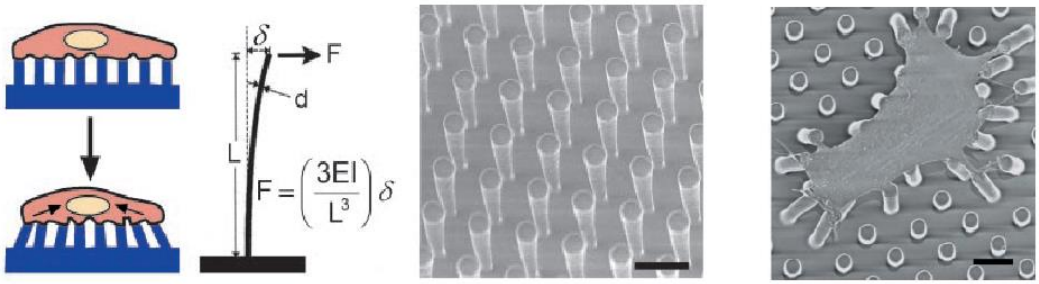

B

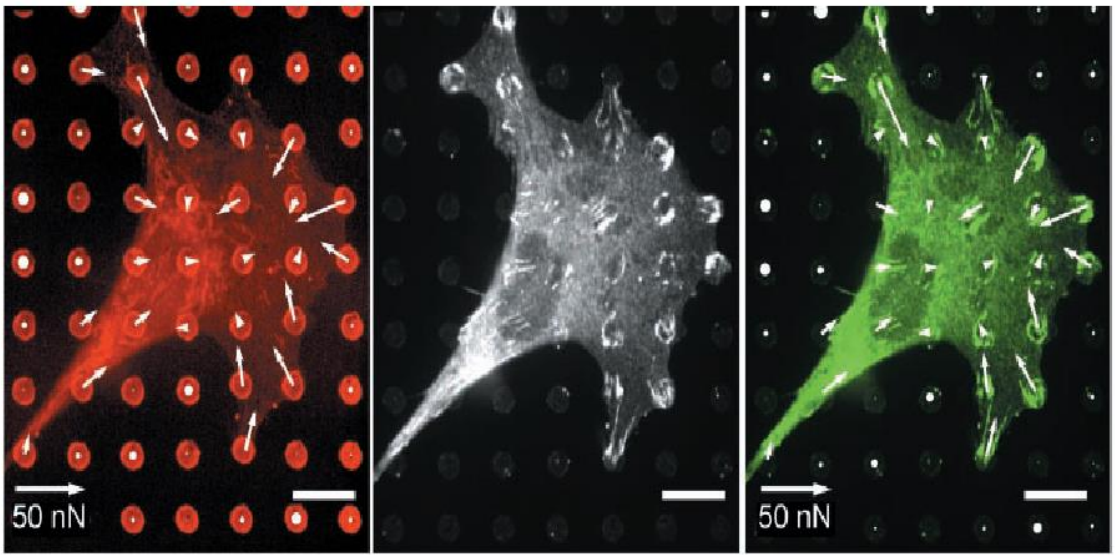

Figure 17: Micropillar based traction force microscopy

Adapted from: (Tan et al., 2003)

A. From left to right: Schematic of cells exerting traction forces and deflecting pillar. Schematic of values used for force calculation (E denotes the Young's modulus of the material). Scanning electron microscopy image of fabricated micropillars. Scanning electron microscopy image of cell on micropillars deflecting them.

B. Confocal images of immunofluorescence staining of a smooth muscle cell on posts. From left to right: Position of fibronectin on the tips of the posts was used to calculate force exerted by cells (white arrows). The force map was spatially correlated to immunofluorescence localization of the focal adhesion protein vinculin (white) and overlay of the vinculin labelling and forces exerted. The lengths of arrows indicate the magnitude of the calculated force (Length for 50 nN force shown in left image). White circles on undeflected posts depict the background error in the force measurement, where the diameter of the circle (same length scale as the arrows) indicates the magnitude of calculated force on each post not attached to a cell. (Scale bars indicate 10 µm)

Other method which use cantilevers are atomic force microscopy (Taubenberger, Hutmacher, & Muller, 2014), microelectromechanical systems (MEMS) (Rajagopalan & Saif, 2011) or micromechanical devices (Kollimada et al., 2017) to measure forces exerted by cells. These devices have the advantage of precise, real-time force measurement using cantilever displacement, which can be used to implement force feedback systems. The range of force measurement in these systems varies from 10 pN – 100 µN and can be chosen based on the type of study (Roca-Cusachs et al., 2017). However, these methods have relatively low throughput as the properties of each cell has to be individually measured which makes getting sufficient numbers for analysis time consuming.

3.3 Molecular sensors

Genetically encoded molecular sensors are another method being used to measure forces on individual molecules within cells (Figure 18). These are molecules that change their fluorescent state based on tensile forces applied on them and are capable of resolving forces in the 1- 10 pN range. They have provided valuable information on the dynamics of tension in

focal adhesions and consequently the distribution of tension across the cytoskeleton (Jurchenko & Salaita, 2015; A. Kumar et al., 2019; Sarangi et al., 2017). In these methods, by measuring the intensity of the FRET and non-FRET signal in regions, a qualitative measure of the active levels of the protein can be obtained. However, these sensors need to be expressed in cells at levels that do not lead to changes in interactions with other components, do not provide directional information, can be difficult to calibrate and have low signal-to-noise ratios. DNA origami based tension sensors, synthetic molecules that can be tagged to the substrate and fluoresce on the application of tensile forces at focal adhesions have been developed and used to show heterogeneous force profiles across focal adhesions (Blakely et al., 2014; Yun Zhang, Ge, Zhu, & Salaita, 2014). They have also been used to show that the force thresholds controlling adhesion and spreading transitions in cells depend on substrate stiffness (Rahil et al., 2016). Another synthetic molecule, a titin based nanoparticle tension sensor has also been developed and used to show that integrins apply up to 110 pN within focal adhesions while other sensors have only suggested forces between the range of 1 to 50 pN (Galior, Liu, Yehl, Vivek, & Salaita, 2016). These types of molecular sensors have better signal-to-noise ratio compared to genetically encoded sensors, but are so far, only available for extracellular ligands. This reduces their utility for measuring forces within cells.

A

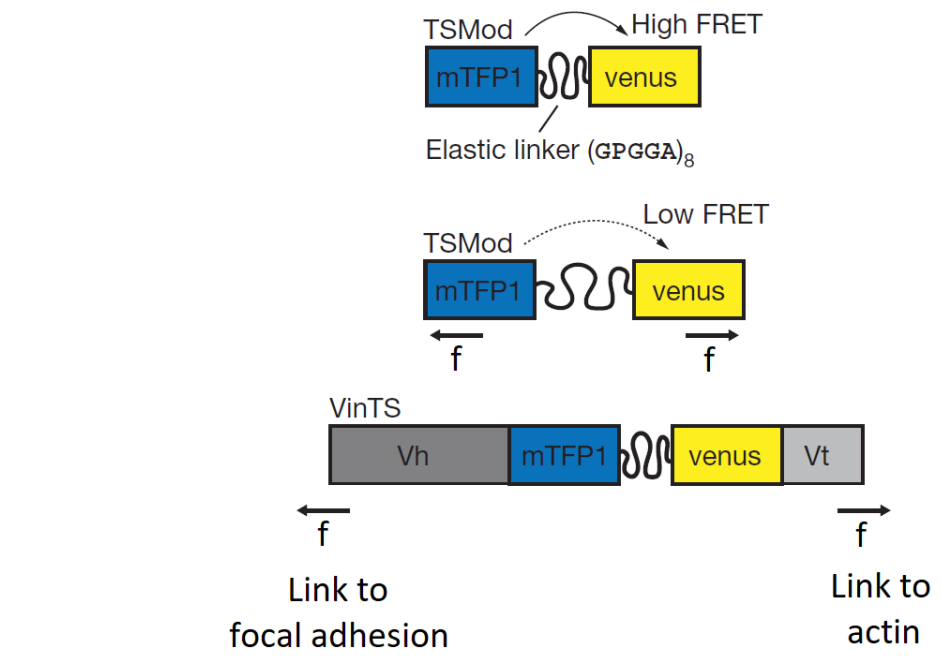

B

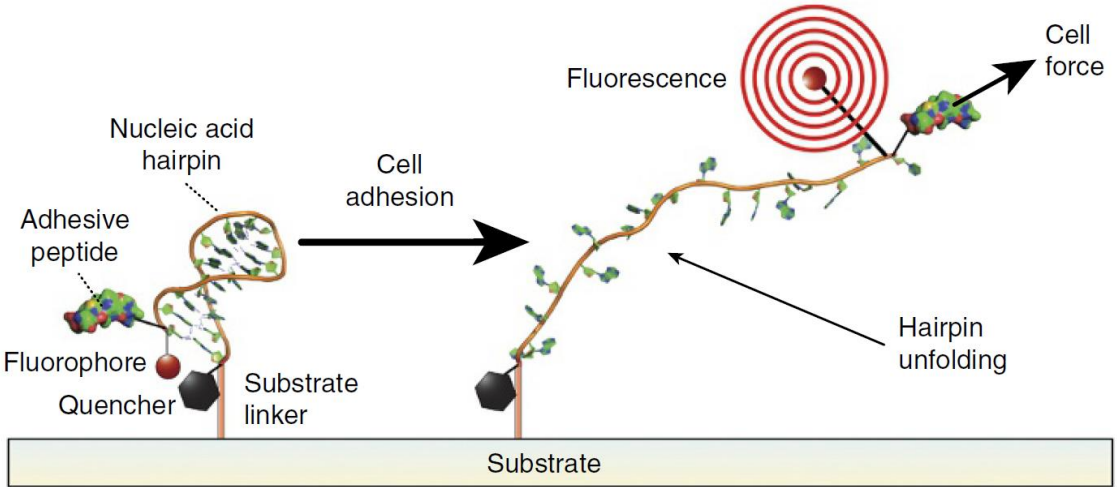

Figure 18: Principles of molecular force sensing

A. Adapted from: (Grashoff et al., 2010)

Vinculin tension sensor (TS) construct. The tension sensor module (TSMod) consists of two fluorophores separated by an elastic linker sequence $(GPGGA)_8$. In the absence of force, the two fluorophores are close enough for efficient FRET. When force (f) across the TSMod extends the linker and increases the spaces between the two fluorophores, FRET efficiency decreases. The

vinculin tension sensor (VinTS) has the TSMod inserted between the head (Vh) and tail (VT) domains of the vinculin molecule. The head binds to focal adhesion and the tail to actin. Tensile forces applied by actin stretch the molecule and decreases FRET efficiency leading to changes in the fluorescence, which can be quantified.

B. Adapted from (Blakely et al., 2014)

Schematic depiction of the Tension Probe. A DNA hairpin is functionalized with a fluorophore-quencher pair, covalently conjugated by the 3' end of the DNA hairpin to a solid substrate and conjugated at its 5' end, via a PEG spacer, to the integrin-binding peptide RGD. Cells can attach to the RGD peptide and upon the application of sufficient force, unfold the hairpin. Upon unfolding, the fluorophore separates from the quencher and fluoresces.

4 Positioning of the study

Mechanical forces are key to many physiological processes. As such, the mechanisms by which the forces are generated and transmitted have been extensively studied. However, and despite years of investigation, we still do not have a comprehensive understanding of the mechanisms supporting force generation at the entire cell level. More importantly, the magnitude of the traction forces exerted by cells on their underlying extracellular matrix in culture remains difficult to predict. Part of the problem comes from the difficulty to characterize precisely how molecular components forming the actomyosin and adhesion networks, individually or via their specific interplay, are related to the force magnitude exerted by these cells. Indeed, although the role of these proteins in force regulation appears to be well established (Murrell et al., 2015), understanding how their relative amount and their structural organization impacts cellular force production remains challenging. Both local variations of these proteins content and/or dynamic assembly into structural networks within a cell and

more globally between different cells is indeed leading to significant variations in cellular traction force (Kurzawa et al., 2017). In this context, the aim of my PhD project was to investigate how different biological parameters could relate to force generation and regulation process and how they could impact cell to cell traction force variability.

To address this question, the first part of my study focused on looking into the effect of two parameters on the regulation of force magnitude: the progression of the cell cycle and the actin dynamics. In the second part of my PhD, I conducted a study dedicated to characterize the biochemical composition of the actomyosin network and adhesion pattern of cells in relationship with the force generation and transmission process.

Part 1: Role of the cell cycle and actin dynamics on force generation

As mentioned earlier, cells exhibit large intercellular variability of the magnitude of forces exerted, and this variability has considerably hindered identifying the mechanisms regulating force generation. In order to identify key parameters involved in force generation process, we designed dumbbell-shaped micropatterns on which epithelial cells were shown to display essentially two peripheral SF, thereby mimicking the minimal system required for contractility establishment (Vianay et al., 2018; Vignaud et al., 2020). While measuring associated traction forces, we surprisingly observed large variations in contractile energies among the cell population, although the apparent actin architecture remained quite conserved. This intriguing finding indicated that a key feature of the production and transmission of forces was missing in our description of contractile networks.

We first studied the possibility that the progression through the cell cycle could affect the cell contractility status and lead to the significant heterogeneity observed in our assay between cells. Previous work from the lab (Figure 19) indeed demonstrated that there is a

statistically significant difference in the traction forces exerted by cells as they progress through different stages of the cell cycle and that the highest strain energy is found in cells that are in the S phase of the cell cycle (Vianay et al., 2018). Similar results were also found in human epithelial cancer cells, in which forces were invariably higher in the G1 and early S phases than in the ensuing late S/G2 (Panagiotakopoulou et al., 2018). In order to test whether the high cell-to-cell variability could emanate from differences in cell cycle status between different cells, different synchronization strategies were used in combination to the use of RPE1 FUCCI cells, which express cell cycle stage specific fluorescence.

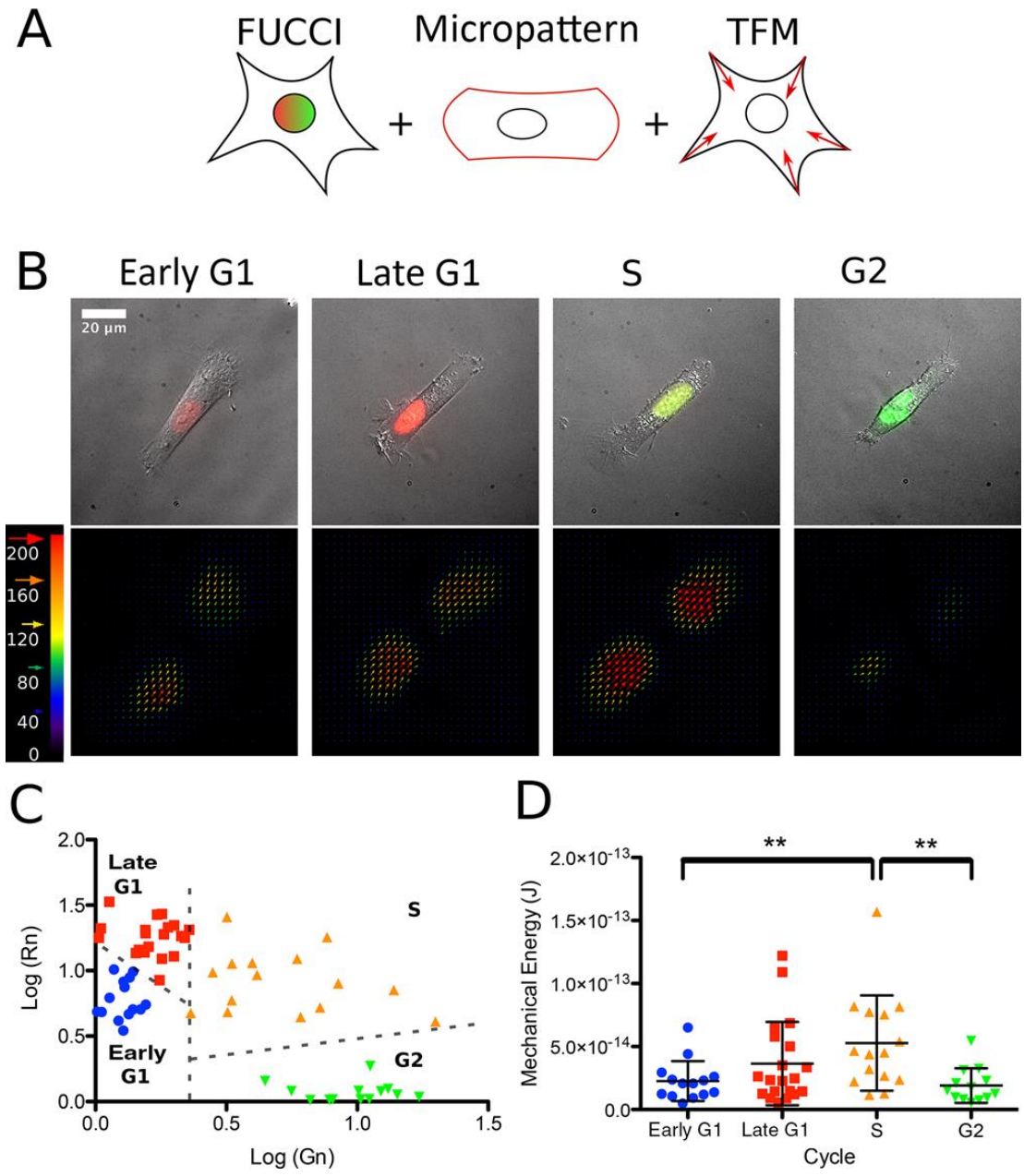

Figure 19: Variation in traction forces with cell cycle stage

Adapted from: (Vianay et al., 2018)

(A) Experimental set up to determine traction force variation with cells cycle. RPE1-FUCCI cells were seeded on micropatterned (59 µm dumbbell) gels and their traction forces quantified along with the cell cycle state.

(B) Micropatterned RPE1 cells expressing FUCCI construct. Both phase contrast, and red and green fluorescent images that show the cell cycle reporters were acquired and the overlay is shown (top row). Examples show cells in the distinct stages of the cell cycle. From left to right, early G1, late G1, S and G2 with their corresponding traction force fields (bottom row). Arrows represent the local force magnitude and orientation. Force scale bar is in Pascal.

(C) Log–log diagram of the nuclear FUCCI fluorescence. The graph shows normalised red fluorescence in function of the normalised green fluorescence. Each point represents a cell. The dashed lines separate cycle phases.

*(D) Comparison of the mechanical traction energies produced by cells in early G1, late G1, S and G2. Groups were classified as defined in panel B. Bars represent mean values and error bars the standard deviations (**P < 0.01).*

Cells were treated with the drugs aphidicolin (Hammond, 2003; Poxleitner, Dawson, & Cande, 2008) and thymidine (Thomas & Lingwood, 1975), which have been shown to arrest cells in the G1/S transition of the cell cycle. However, it was found that the RPE1 FUCCI cells still showed significant numbers in the G1 and G2 stages while they should mainly be in the G1/S transition.

The RPE1 wild type cells were also subjected to the same treatment and checked with FACS sorting to determine if the cells had been arrested in the G1/S transition. However, while we noticed an enrichment of the cells in the G1/S transition, there were still a significant number of cells present in the G1 and G2 stages of the cell cycle. Along with this, we also found that both drugs led to an increase in the strain energy of the cell population. As such, cell cycle synchronization was eliminated as a method to reduce traction force variations in the cell population.

We therefore next examined the possibility that some internal/subcellular contractile efforts could be dissipated instead of being transmitted to cell anchorages by looking at the interplay between actin dynamics and traction forces in these cells. Indeed, various structures—meshwork and fibers—can exert forces with distinct force/dynamics relationships (Aratyn-Schaus et al., 2011). As discussed in the section on stress fibers, these structures are undergoing permanent reorganization that include splitting and fusion events. Recent works also showed that they are fully embedded in a contractile cortical mesh and that they form from the alignment and contraction of smaller filaments from the actomyosin cortex (Vignaud et al., 2020). The dynamics between these structures and tension were shown to induce plastic deformations associated with disengagement of myosins and α-actinin from the F-actin and could lead to dissipation of contractile energy within the system (Bonakdar et al., 2016). In addition, SF can also be disassembled in a tension-dependent manner which leads to a complex force-producing network (S. Tojkander et al., 2015). They can also be damaged and repaired over time, leading to changes in the forces transmitted at their ends (Smith et al., 2010). In summary, SF possess a high turnover rate that varies along the length of the stress fibers (Hu et al., 2017; Peterson et al., 2004) and all these dynamic event make the relationship between the simple structural organization of the fibers and the force transmitted to the substrate very complex. To investigate whether variations in the traction forces produced by cells could originate from stress fiber dynamics, we decided to measure different parameters associated with SF dynamics. To that end, we photoconverted regularly spaced spots along the SF length to measure their velocity as an indication of fiber growth and filament sliding which would lead to movement of the spot. We then also measured the fluorescence turnover in these spots after photoconversion to assess the turnover of actin in these structures. This part of the work demonstrated that cells with strain energies separated by an order of magnitude had similar

values in the spot turnover and movement. Hence, the stress fiber dynamics is not the major cause for large variations in traction forces.

Part 2: Role of the biochemical composition of actomyosin network on force generation and transmission

We finally decided to characterize the biochemical composition of the network responsible for force production together with the mechanical state of the cells. In particular, we focused our study on measuring actin, myosin, alpha-actinin and focal adhesions contents in cells and to study how their levels could relate to forces exerted by the same cells.

The method:

As standard TFM requires detachment of the cells to get the undeformed configuration of the soft substrates, it eliminates the ability to fix and label cells, a necessary step to explore further the molecular composition of the SF and the surrounding network. Other methods allow for combination of TFM and labelling but suffer from intrinsic limitations. In reference free traction force methods, it is possible to fix and fluorescently label the components of interest, however, these methods either rely on analysing forces after fixation, which is known to impact the mechanical status of the gel, or involve ectopic expression of fluorescently tagged proteins. As the quantity of protein expressed by these cells is difficult to control, it is difficult to know at which extend the use of such genetic constructs perturb the biological system. Different cells additionally turn out to have different levels of the introduced fluorescent protein depending on the amount of the genetic material taken up by the cells, making the comparison between different cells difficult. In the case of actin, fusions with fluorescently labelled proteins have been demonstrated to be functionally impaired. For example, GFP-actin, when expressed at low quantities has been shown to incorporate to Arp2/3 generated

branches, but not to formin mediated linear filaments (Q. Chen, Nag, & Pollard, 2012; Doyle & Botstein, 1996). GFP-actin also does not incorporate into contractile rings in fission yeast (Q. Chen et al., 2012; J.-Q. Wu, 2005) or in many other cells (Gerisch & Weber, 2000). In this context, a big part of my PhD study was to set up a method in which both the traction forces and the levels of the different molecular components of the contractile system could be compared.

Hence, I first established a new protocol that combines micropatterning and TFM with fluorescent labelling of the molecular components. An alignment grid with numbering patterned along with the dumbbells allow for finding cells of interest and aligning the images. This unique procedure allowed us to access simultaneously to the forces exerted by cells and the associated molecular state of its network.

The adhesion network

Since focal adhesions transmit force internally generated by the cytoskeletal network to the ECM (Riveline et al., 2001), we first decided to use our assay to investigate the controversial relationship between one of their component, vinculin, and cell strain energy. As discussed in the section on focal adhesions, there is a debate on the relationship between focal adhesions size and the traction forces exerted through them. While some studies have shown that a close relation exists between focal adhesion size and the local force (Balaban et al., 2001; Goffin et al., 2006; Tan et al., 2003), others have found such a relation only exists in the initial stages of adhesion maturation (Stricker et al., 2011). Part of this debate probably originates from discrepancies between the different studies that measured the forces locally exerted at the focal adhesions, at different stages of their maturation, and in different migratory states of the cells. In order to investigate this controversial relationship between one of the FA

components, vinculin, and cell strain energy, we used our TFM assay. In this experimental set up, we took advantage of the use of micropatterns to constrain the cell shape and size and perform our measurements in stationary cells in order to study the FA composition independently of their turnover associated to the migration process. As previous work from our lab demonstrated that the peripheral stress fibers and internal mesh represent a mechanical continuum pulling on the substrate at various focal adhesions simultaneously, we hence decided to perform characterization of vinculin at the entire cell-level.

This work shows that vinculin signal intensity at the focal adhesions and the total focal adhesion area of the cell increases with increasing strain energy suggesting the existence of a regulation mechanism at the entire cell level.

The actomyosin network

Stress fibers represent structural templates essential for FA maturation (Oakes et al., 2012) and as such they play a key role in regulating both the assembly and size of FA and force transmission at these anchorage points (Burridge & Wittchen, 2013; Chrzanowska-Wodnicka & Burridge, 1996). We thus investigated next how the actomyosin content could impact the magnitude of traction forces. As shown in vitro (Bendix et al., 2008; Ennomani et al., 2016) in an myosin-actinin system, only an optimal range of concentrations of these components leads to actin network contractility. The bell-shaped curve described in Ennomani et al. indicates the existence of a non-linear relationship between the levels of crosslinkers per F-actin and the contractility of biological systems. Similarly, Bendix et al. showed that an optimum level of crosslinker was required for their actin-myosin-actinin system to contract. As for myosin, Bendix et al., showed that a minimum motor concentration is required for contractility of a crosslinked actin filament network. But, myosin has also been shown to disassemble actin

networks and induce turnover of the network (Haviv et al., 2008; Reymann et al., 2012; Sonal et al., 2019; Wilson et al., 2010). As these results suggest that at the level of the entire cell, the relative proportion of molecular motors as compared to the total F-actin plays a key role in regulating the forces produced by cells, we decided to quantify this value as well.

In cells, the effects obtained following the modification of the level of crosslinkers suggest that this optimum also exist and set the magnitude of forces exerted by cells. Indeed, overexpression of alpha-actinin or its knockdown have been shown respectively to decrease and increase the traction forces exerted by populations of cells (Doss et al., 2020; Hu et al., 2019). However, the direct incidence of the relative cellular amount of either molecular motors or crosslinkers per F-actin on force generation and transmission to the substrate has never been clearly established. To address this point, we used the develop TFM assay together with immunolabelling of myosin and alpha-actinin alone, or in combination with actin staining. As to study the contribution of peripheral SF composition, we first measured actin content in these structures. In order to take into account the role of the actomyosin cortex in the mechanical properties of cells, we then performed the quantifications for actin and the other components at the level of the entire cell. This work shows that strain energy increases with increasing cellular F-actin, the F-actin present in the stress fibers and total phosphorylated myosin content of cells. It is also shown that, a high myosin:F-actin ratio leads to low strain energy. α-actinin alone shows no relation with strain energy, but strain energy decays exponentially with an increasing ratio of α-actinin:actin.

5 Methods

5.1 Pattern design

The dumbbell pattern was designed as described in (Vignaud et.al 2020) and a schematic of the pattern is shown in Figure 20. The pattern consists of two solid disks of diameter 12 µm separated by a center to center distance of 47 µm. The disks are connected by line of width 1 µm. The length was set as 59 um along the long axis as it was shown in earlier work to be the average length of the cell population on a plain substrate (Vignaud. T. (2018) *Production de forces par le cytosquelette d'actine : mécanismes et régulation par le micro-environnement*, Université Joseph Fourier).

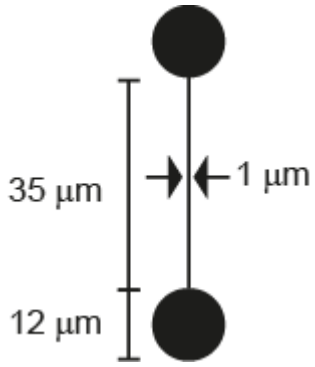

Figure 20: Dumbbell micropattern design

The two disks allow cell attachment. The line between the disks allows the cell to grow between the disks.

5.2 Mask design

The photomask (TOPPAN) with the dumbbell patterns was designed with markers and numbers to facilitate finding specific patterns after the gel is removed from the microscope and placed back. The mask was designed in CLEWIN software. The design was based on simplifying

finding specific reference locations on the pattern field. Relative to these reference positions, other positions where cell attach could be located.

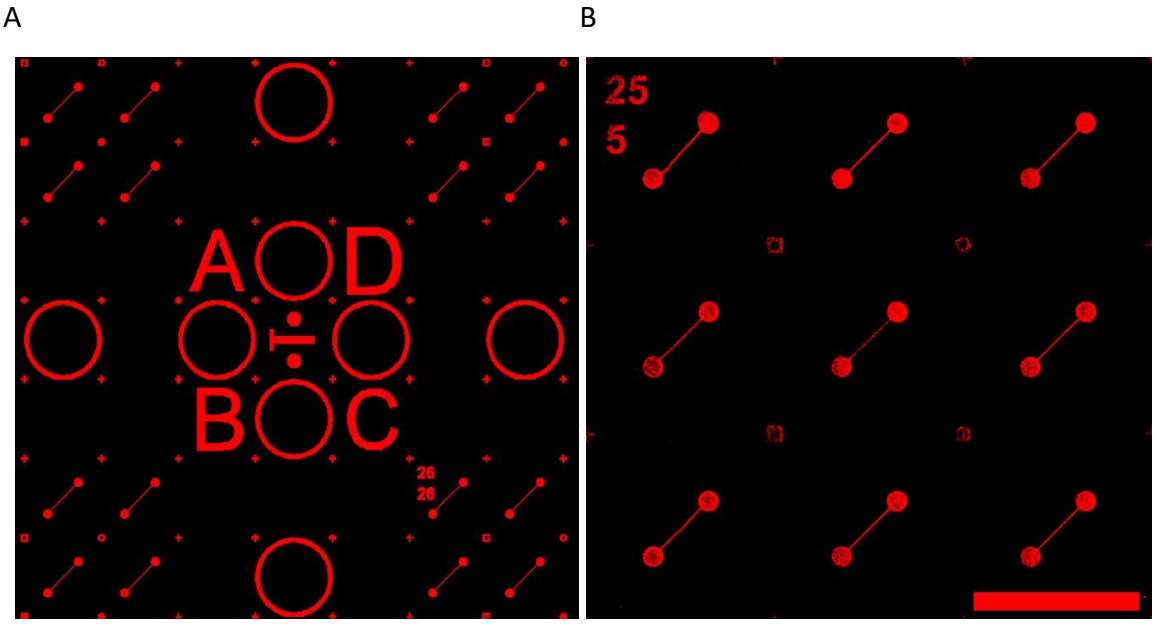

Figure 21: Design of mask for rotation and translation correction.

A: The letters (A, B, C and D) at the center of the array allows for centering of the coverslip and to determine the orientation of the array.

*B: A 3*3 array of patterns imaged with a 20X objective are shown with the alignment marks next to them. A 3*3 array of patterns fits perfectly within the imaging window when using this objective. Scale bar 100 µm*

For identification of the reference position and translation and rotation correction, specific designs are placed on the patterns (Figure 21). The camera field of view when using a 60X objective is 113.6 µm * 113.6 µm. A single, vertical and horizontal array of circles (diameter 113.6 µm, center-center distance 227.2 µm), intersecting at the center of the pattern field divide the gel into four quadrants. At the center of the pattern field, where the arrays of circles intersect, the letters A, B, C, D were placed as shown in Figure 21.

The arrays of circles divide the gel into four quadrants. The dumbbell micropatterns were separated by 113.6 µm center-center distance and a 78*78 array of dumbbells was placed in each quadrant. The dumbbells were placed at a 45º degree angle to the horizontal providing the greatest separation between patterns (Figure 21B). Every third dumbbell pattern was numbered (Figure1 C) in both horizontal and vertical directions for redundancy in finding cells.

The arrays of circles and the letters are used for preliminary translation and rotation alignment on the microscope. On the four vertices of each 113.6*113.6 µm region, with the letters, circles and dumbbell patterns in the center, a set of small symbols (**+, o, □**) of 10 um width and height and 2 µm line thickness are present. These were used for the final manual rotation correction. When these are present at the vertices of the camera field of view at 60X magnification, the gel was aligned. With this method it was possible to manually correct for rotation error of less than 1°.

5.3 Silanized coverslip preparation

For attachment of the gels to the coverslips, the glass coverslips were treated with plasma to activate the surface followed by immersing them in 2% (v/v) of 3-(trimethoxysilyl)propyl methacrylate (#M6514 Sigma) in ethanol, containing 1% (v/v) acetic acid for 20 minutes. The coverslips were rinsed in ethanol twice to remove silane residue, dried with compressed air and baked at 120° C for 1 hour. The coverslips can be stored at 4° C for at least 4 months and used for gel fabrication.

5.4 Passivation of fluorescent beads

Carboxylate modified 200 nm polystyrene fluorescent beads (FluoSpheres (365/415) blue, Invitrogen, F8805) were passivated according to two distinct methods, either by covalent

or non-covalent linkage of PLL-PEG (JenKem Technology, ZL187P072). The details for the covalent linking of PLL-PEG to the beads is as follows. All solutions detailed below were kept on ice unless otherwise mentioned. After vortexing the stock to disperse the beads, 20 µl of the bead suspension was diluted in 80 µl of MES buffer (10mM pH 5.5) - Solution1. 500 µl of 1 mg/ml PLL-PEG in HEPES buffer (10mM, pH 8.5) – Solution2. 200 µl of 8 mg/ml EDC (1-ethyl-3-[3-dimethylaminopropyl]carbodiimide hydrochloride ; Pierce) in MES buffer (10mM pH 5.5) – Solution3. 200µl of 16mg/ml 1 N-hydroxysuccinimide (NHS; Fluka) in MES buffer (10mM pH 5.5) – Solution4. Solutions, 1 and 2 are mixed, the beads dispersed with ultrasonic agitation for 30 seconds. Solutions 3 and 4 are mixed and immediately added to the mix containing beads and PLL-PEG. This final mixture is vortexed for 20 seconds, covered in aluminum foil and placed on a rotary shaker for 1 hour at room temperature allowing the covalent linking to complete. To recover the beads and eliminate the EDC/NHS and PLL-PEG solution, the suspension is spun down at 15000 rpm (Biofuge, Pico) for 15 minutes, the supernatant is discarded, and the beads are re-suspended in 2 ml of 10mM HEPES, pH 7.4. This is repeated twice. After in the final spin, the beads are re-suspended in 40 µl of 10 mM HEPES, pH 7.4 and stored at 4° C. The beads are used in gel fabrication on the same day. For non-covalent linking of the PLL-PEG to the beads, 50 µl of the bead suspension stock was added to 1 ml of 10 mM PLL-PEG solution in HEPES pH 7.4 and mixed on a rotary shaker for 1 hour at 4 C.

5.5 Polyacrylamide micropatterning

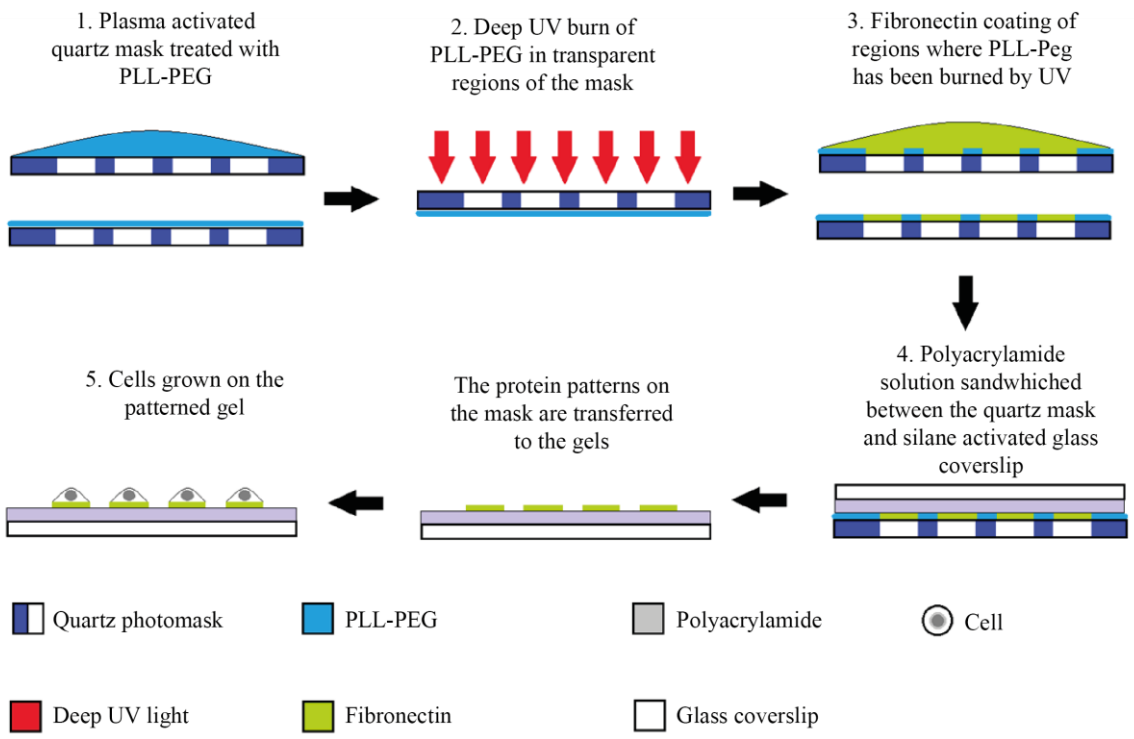

Figure 22: Polyacrylamide micropatterning schematic

Schematic representation of the micropatterning protocol

The preparation of patterned polyacrylamide hydrogels was performed according to the "Mask method" previously described in(Vignaud et al., 2014). A schematic of the process is given in Figure 22. The photomask was first cleaned with soap and water, thoroughly rinsed with water to remove traces of soap and dried with compressed air. Next, it is cleaned with acetone followed by iso-propyl alcohol, drying with compressed nitrogen after each rinse. The mask surface is activated using oxygen-plasma (AST product, 300 W) for 3.5 min at 200 W and the regions with patterns of choice are incubated for 30 minutes with 35 µl of 0.1 mg/ml PLL-PEG (JenKem Technology ZL187P072) in HEPES buffer (10mM, pH 7.4), sandwiched between the mask surface and another plasma activated coverslip. Then the coverslip is gently lifted and

kept aside for use during the protein coating, and excess PLL-PEG is washed off with Millipore water and the mask allowed to dry in air. The mask is exposed to deep-UV (UVO cleaner, Jelight) with the non-chrome side facing the lamp for 5 minutes to burn the PLL-PEG in the transparent pattern region. The mask is incubated with 35 µl of solution containing 40 µg/ml of fibronectin (Sigma) and 40 ug/ml fibrinogen-Alexa-Fluor-647 (#F35200, Invitrogen) in 100 mM bicarbonate buffer for 30 minutes. The solution is sandwiched between the mask and the coverslip used earlier during the passivation of the mask surface. Excess protein solution is removed after gently lifting the coverslip and rinsing the mask with Bicarbonate buffer (100 mM, pH 8.4). The mask is placed in a vertical position and the buffer in the patterned regions should dewet due to the PLL-PEG. The buffer outside the patterned regions can be wiped off gently with a Kimwipe tissue to hasten the drying process. A mix of 8% acrylamide and 0.264% bis-acrylamide solution (Sigma) corresponding to an experimental Young modulus of 35 kPa was degassed during the protein coating, mixed with the 200 nm fluorescent beads colvalently linked to PLL-PEG and sonicated before addition of APS and TEMED. 25 µl of that solution was added on the region of the photomask where protein is adsorbed to the patterns, covered with a silanized coverslip (Silane, #M6514, Sigma) and allowed to polymerize for 25 min. The sandwiched gels are covered with the sodium bicarbonate buffer (100 mM, pH 8.5) for 10 minutes before they are gently detached from the mask. Micropatterns were stored overnight in sodium bicarbonate buffer at 4°C in 35 mm petri dishes. Prior to plating cells, the bicarbonate buffer is removed and the gels washed twice with PBS buffer (Gibco, 14190-094) and then left in culture media for 15 minutes.

5.6 Cell culture

REP1 wild type cells were cultured in DMEM/F12 (Gibco,31331-028) with 10% fetal bovine serum (Gibco) and 1% penicillin/streptomycin (GIBCO/Life Technologies) at 37° C and 5% CO^2. 250,000 cells were seeded on each gel and allowed to attach for 40 minutes before gently pipetting on the gel to wash off non-attached cells. The cells were allowed to spread for 4 hours before imaging was started.

5.7 Imaging

All images were acquired using a Nikon spinning-disk confocal microscope (EclipseTi-E Nikon inverted microscope equipped with a CSUX1-A1 Yokogawa confocal head, an Evolve EMCCD camera from Roper Scientific, Princeton Instruments) using a 60X Nikon Plan Apo 1.4 NA oil immersion objective. The microscope was driven using Metamorph software (Molecular Devices). Temperature was maintained in a Stage-top incubator system at 37° C and CO2 at 5% using with a Live Cell Instrument CU-109 and FC-5 respectively. The micropatterned gel was placed in the Stage-top microscope incubator using a Chamlide 35mm dish type magnetic chamber for square coverslip (CM-S20-1) which allows high magnification imaging with an oil immersion objective.

5.8 Protocol for fixed cell assay

The stage is moved to its central position and the gel mounted in the Chamlide magnetic holder is placed in the Stage-top incubator system and fixed in place with springs. These springs allow the sample to be moved by hand, but otherwise remain in place when the imaging chamber is moved. A 20X objective was used for initial alignment (PlanAPO 20X/0.75). At this magnification, a 3x3 array of the patterns fit within the imaging window. The sample is manually

rotated to the correct orientation using the alignment marks next to the patterns. It is then manually translated using the numbering next to the patterns to get to the center of the pattern field which contains the patterned letters A, B, C and D (Figure1 C). The objective is changed to the 60X oil objective, focus reacquired and minor rotation and translation adjustments done manually to get one of the letters within the field of view with the alignment marks appearing at the four corners of the imaging window. The stage position of the chosen letter is recorded and will be used as reference when realigning the system for imaging the labelled cells and the gel after detachment of the cells.

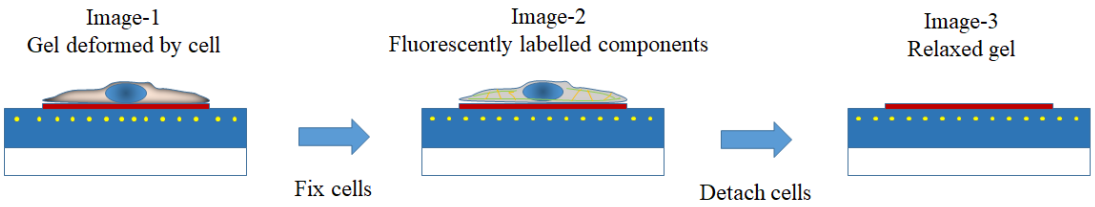

Figure 23: Schematic of imaging used in the assay

The experimental protocol for the assay is shown in the figure. Starting from left, cells seeded on gels are imaged when live to acquire the deformed configuration of the gels. Then, the cells are fixed, labelled and imaged to acquired the biochemical composition of the cells. Then the cells are detached using a sequential treatment of TGS buffer and Trypsin.

Well spread individual cells on the micropattern array are located by manually scanning the gel and the position of each cell is recorded along with the reference position. After the stage positions of sufficient cells are recorded, the image of the live cells, the patterns and the beads in the deformed gels are recorded.

The cells are then pre-permeabilized, fixed and labelled for the proteins of choice. The pre-permeabilization was done to reduce cytosolic components and get improved clarity of the actomyosin structure. For imaging, the gel is re-mounted on the Stage-Top incubator, in the

Chamlide magnetic holder with PBS to prevent drying. The microscope stage is moved to the reference position recorded earlier and the gel re-aligned to the reference letter chosen earlier at 20X for and then again for minor corrections at 60X. The temperature is maintained at 37°C to avoid any changes in the relative positions due to contraction of the gel. The cells are re imaged for the fluorescent components (10 z slices, 0.75 µm spacing), the beads in the gel and the patterns.

To detach cells and measure the relaxed configuration of the gel, the samples are first left overnight in 10X TGS buffer (BIO-RAD,161-0772), washed four times with PBS and then treated with TryplE reagent (Gibco, 12605-010) for 1 hour at 37° C. The cells detach on pipetting onto the surface of the gel vigorously. After cell detachment, the gels are mounted in the Chamlide magnetic holders, placed on the Stage-top incubator, realigned and the positions are reimaged for the beads, patterns and to confirm that the cells have detached.

5.9 Fluorescent labelling of cells

For labelling p-MLC, alpha-actinin and Vinculin, cells were pre-permeabilized in 0.5% Triton X-100 in Cytoskeleton buffer for 10 seconds and then immediately fixed in 4% paraformaldehyde in Cytoskeleton buffer with 10% sucrose, pH 6.1 for 20 minutes at room temperature. The cells were washed twice in cytoskeletal buffer to get rid of excess paraformaldehyde and then quenched in 0.1 M ammonium chloride for 10 minutes then washed thrice in PBS, 10 minutes/wash. Blocking nonspecific binding was done with 1% BSA and 10% FBS in PBS for 1 hour at room temperature before being incubated with appropriate dilutions of primary antibodies in PBS containing 1% BSA and 0.1% Tween overnight at 4° C in a humid chamber.

The primary antibodies used were, anti-phospho-myosin light chain 2 (#3671, CST), anti-alpha actinin (#05-384, Millipore), anti-alpha actinin4 (19096-1-AP, Protein tech) and Anti vinculin-clone hVIN-1(V9131, Sigma). The secondaries used are anti-rabbit Alexa Fluor-488 (A21441, Molecular Probes) and anti-mouse Alexa Fluor-546 (A11003, Invitrogen). For the data set where actin alone was imaged, pre-permeabilization was not done. The cells were fixed, washed thrice in PBS, and labelled for F-actin using Phalloidin-FITC (#P5282, Sigma).

Fluorescent Tetraspeck microspheres of 0.2 or 0.5 µm diameter (#T7281, Life Technologies) were in some cases added to the PBS when imaging the labelled cells as an internal fluorescence intensity reference.

5.10 Image processing of fluorescent images

A maximum intensity projection of the z-stacks of each fluorescently labelled cells are created in MATLAB for analysis. The images are rotated by 45 degrees to have the long axis of the cell horizontal in the image, cropped to 300*300 pixel dimension with the cells in the center. The average signal intensity in a 50*50 pixel region at the top of the cropped image is calculated for noise subtraction. The sum of the signal in all the pixels after subtracting the noise provides the relative measure of the total protein content in each cell.

Vinculin quantification has been performed using the "Focal Adhesion Analysis" server (https://faas.bme.unc.edu/) with default settings. This is a freely available online tool which uses computer vision algorithms to process fluorescence images of labelled focal adhesion proteins(Berginski, Vitriol, Hahn, & Gomez, 2011). We used two global parameters for the quantification, i.e., the total adhesion area per cell and the total adhesion signal, respectively the sum of the area and the signal of the detected adhesion structures.

5.11 Translation and rotation correction functions

The translation and rotation correction algorithm uses the normxcorr2 function in the MATLAB image processing toolbox. The function computes the normalized cross-correlation between the reference image and the image to be corrected. The resulting matrix C contains the correlation coefficients. The bead images from the experiment are used to detect the translation and rotation errors and is then propagated to the other images from the same position.

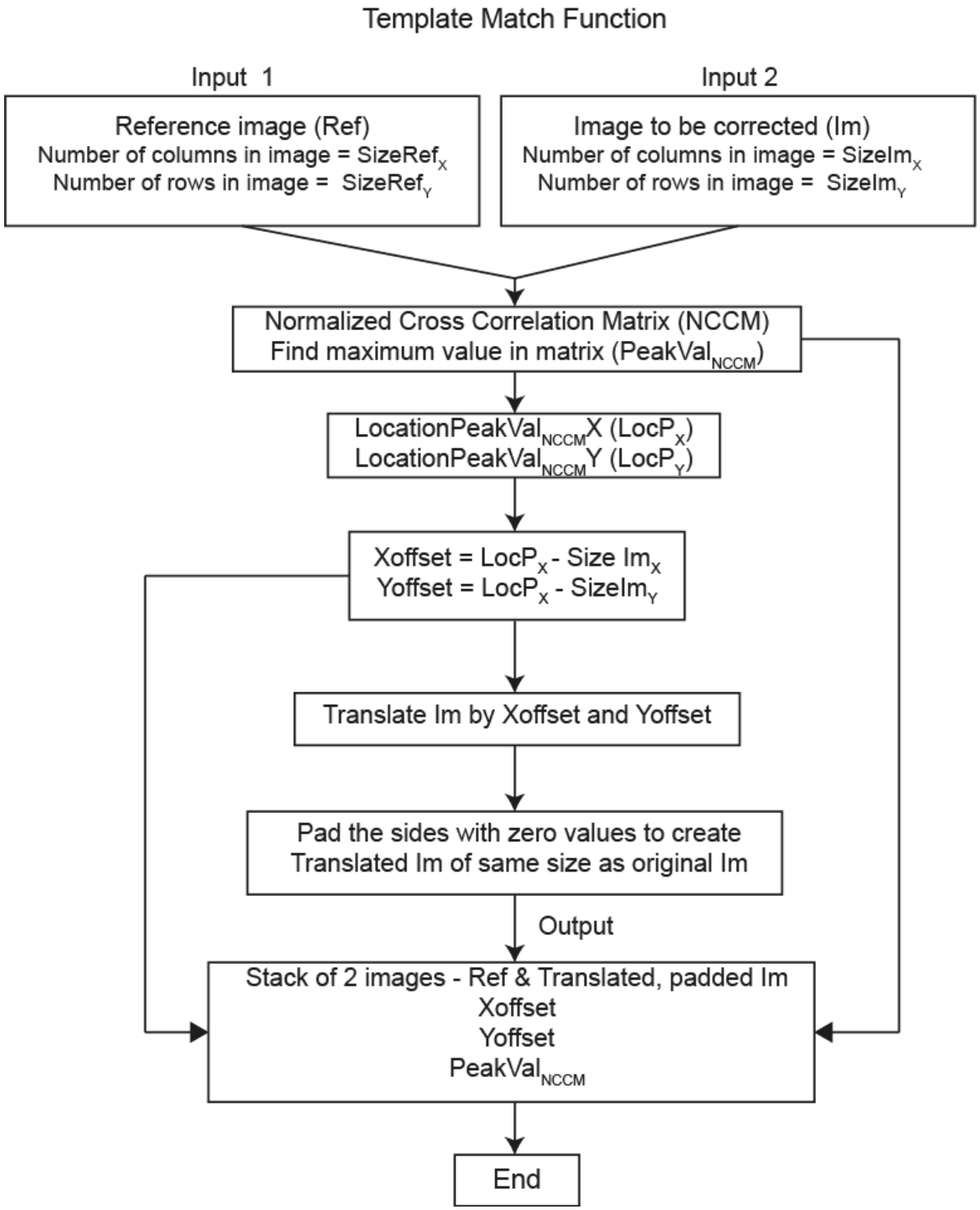

Figure 24: Translation correction algorithm

The algorithm used for template matching the images is described.

Translation correction module (Figure 24): To start, a function - TemplateMatch was created. The first step in this function is to calculate the normalized cross-correlation matrix **C**, using the normxcorr2 function between the reference image **Ref** (bead image obtained when the cell is alive on the gel), and the image to be corrected **Im** (bead image obtained when the cell is detached from gel), for translation and rotation. The location of the maximum value in **C** and the size of the image is used to calculate the x and y offsets needed to align the two images and correct for translation giving us **Im'**. The edges of the image are padded with 0 values to give **Im'** the same size as **Ref**. The function gives the **Ref**, **Im'**, a tiff stack of these two images, the x and y offsets used for the translation and the highest value in **C** as the outputs.

Rotation Correction module (Figure 25): The rotation correction is performed by a function – RotateTranslate, which uses the TemplateMatch function. Following the translation correction described previously, **C** is calculated with respect to **Ref** for **Im'** rotated by 0.1° to the left (**Im-**) and the right (**Im+**). The image with the highest value in **C** with respect to **Ref** (PeakValNCCM) gives the direction of rotation. This rotated image is corrected for translation using the TemplateMatch function before iteratively rotating by 0.1° (in the direction which gives the highest **C)**, computing **C** again with respect to **Ref** and correcting for translation, until the first iteration where the value of **C** decreases compared to the preceding iteration. This gives the corrected image.

The outputs of the RotateTranslate function are the images **Ref**, **Tryp-rotated-translated**, a tiff stack of the two images, the x and y offset and the final angle of rotation. These translation and rotation correction values are then propagated to the images of the pattern and the maximum z projection images of the labelling.

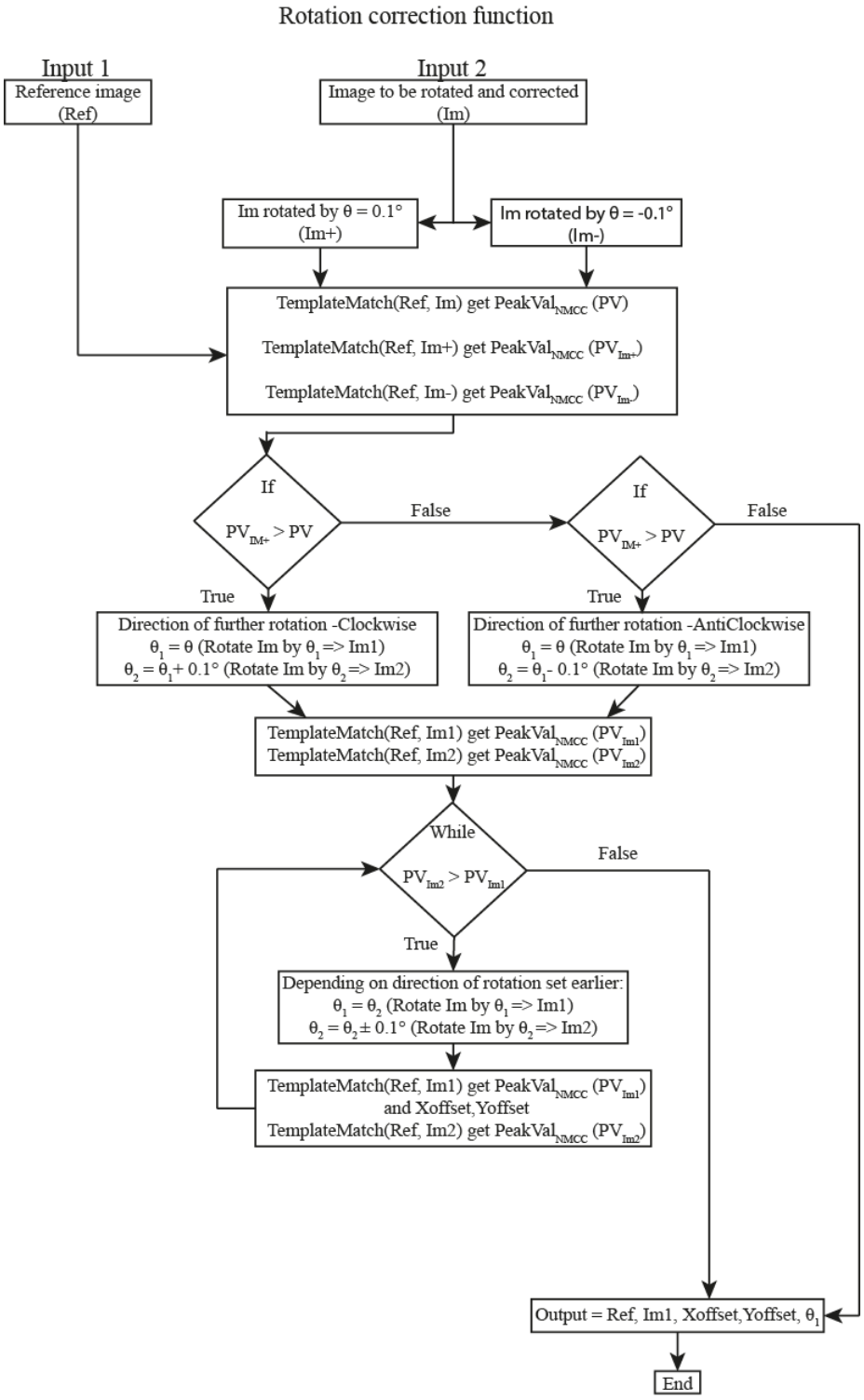

Figure 25: Rotation correction using the template match function

The rotation correction algorithm details are given in the figure. It uses the TemplateMatch function to generate the normalized cross-correlation matrix and rotates the image to be corrected iteratively until the maximum value is obtained.

5.12 Traction force microscopy analysis

Data were analysed with a set of macros in Fiji using the method previously described in (Martiel et al., 2015). Displacement fields were obtained from fluorescent bead images before and after removal of cells by trypsin treatment. Bead images that were already corrected for rotation and translation as described earlier were again paired and re-aligned with a macro that corrected with subpixel accuracy. Displacement fields were calculated by particle imaging velocimetry (PIV) which uses a normalized cross-correlation based method with an iterative scheme. Final vector-grid size ranged from 1.55 µm X 1.55 µm. Erroneous vectors where discarded owing to their low correlation value and replaced by the mean value of the neighboring vectors. Fourier-transform traction cytometry was used to compute the Traction-force field, with a regularization parameter set to 3.2×10^{-10}. Force vectors located outside of the micropattern area were discarded for calculation of strain energy.

5.13 Automated acquisition

Automated acquisition with Metamorph (Figure 26): As the original goal for the fixed cell assay was to image a large array of patterns without cells, to get the reference configuration of the gels, we designed first an automated method. A large array of patterns without gels would be imaged, cells seeded, allowed to spread, fix, label and image for the deformed configuration and labelled components. Journals were written using Metamorph software in order to automate the acquisition process.

One of the issues encountered with imaging when using gels is that the top of the gel is beyond the range of the Perfect Focus System which can be used to maintain focus lock on the coverslip. The gel height is maintained at 100 µm to prevent the cells from feeling the glass at the bottom of the gel which can raise the apparent stiffness of the system (REFERENCE). As this height is beyond the range of the Perfect Focus system, a different method had to be used to detect the gel top during automated acquisition. The pattern channel was used for this purpose. A journal was implemented in the software and it worked as follows: After manually finding the top of the gel and centering a dumbbell pattern within the field of view, a z stack of 10 slices, 1 µm spacing, centered on the manually located focus of the pattern was scanned. The variance in the intensity for all the 5 slices of the stack was calculated. The slice with the pattern in sharp focus has the highest variance. The z motor position corresponding to this slice is used to set the z position for acquisition.

After the sample is placed on the stage and aligned, regions with high number of cells is located by manually scanning. To provide the system information of pattern spacing for stage movement, the position of a pattern is recorded after aligning the rotation-translation alignment reference marks to the vertices of the camera field of view. Following this, the stage is moved by 20 patterns to the right, aligned again to have the reference and the position recorded again. By comparing these two stage positions, the x and y movement required for by the stage to image patterns in an array are calculated. Every third pattern in the horizontal and vertical direction is numbered by row and column. The acquisition is started on a pattern with the identifying numbers. The pattern is brought into focus and aligned so that the vertices of the field of view align with the reference markers.

On starting the acquisition with the journal it prompts the user to input the number of columns to be imaged. Each column is set to be 3 Columns*15 rows of dumbbell patterns. Next, the focus for the pattern is found by the journal described above and an image of the patterns, the cell (in brightfield) and a z-stack (5 slices, 0.5µm separation centered around the pattern focus position) of the beads is obtained before sequentially moving to the next two patterns on the right and acquiring the same set of images. Focus detection is not done for these two patterns. The journal then moves the stage to the starting of the next row and finds the focus automatically before imaging the three patterns and corresponding cell and bead images. This is repeated for 15 rows and then the stage is moved to the next column top. To make sure that focus is not lost when moving up 15 rows, the focus for every third row is automatically found until the top of the column is reached.

The journal allows for imaging one column (15 rows and 3 columns in each column), containing 45 patterns in around 7 minutes (the timing can vary depending on the acquisition time for each channel). This allows for imaging 225 patterns in around 35 minutes. If imaging a region with many cells on patterns, this provides a method of obtaining large data sets to quantify traction forces and biochemical composition of cells.

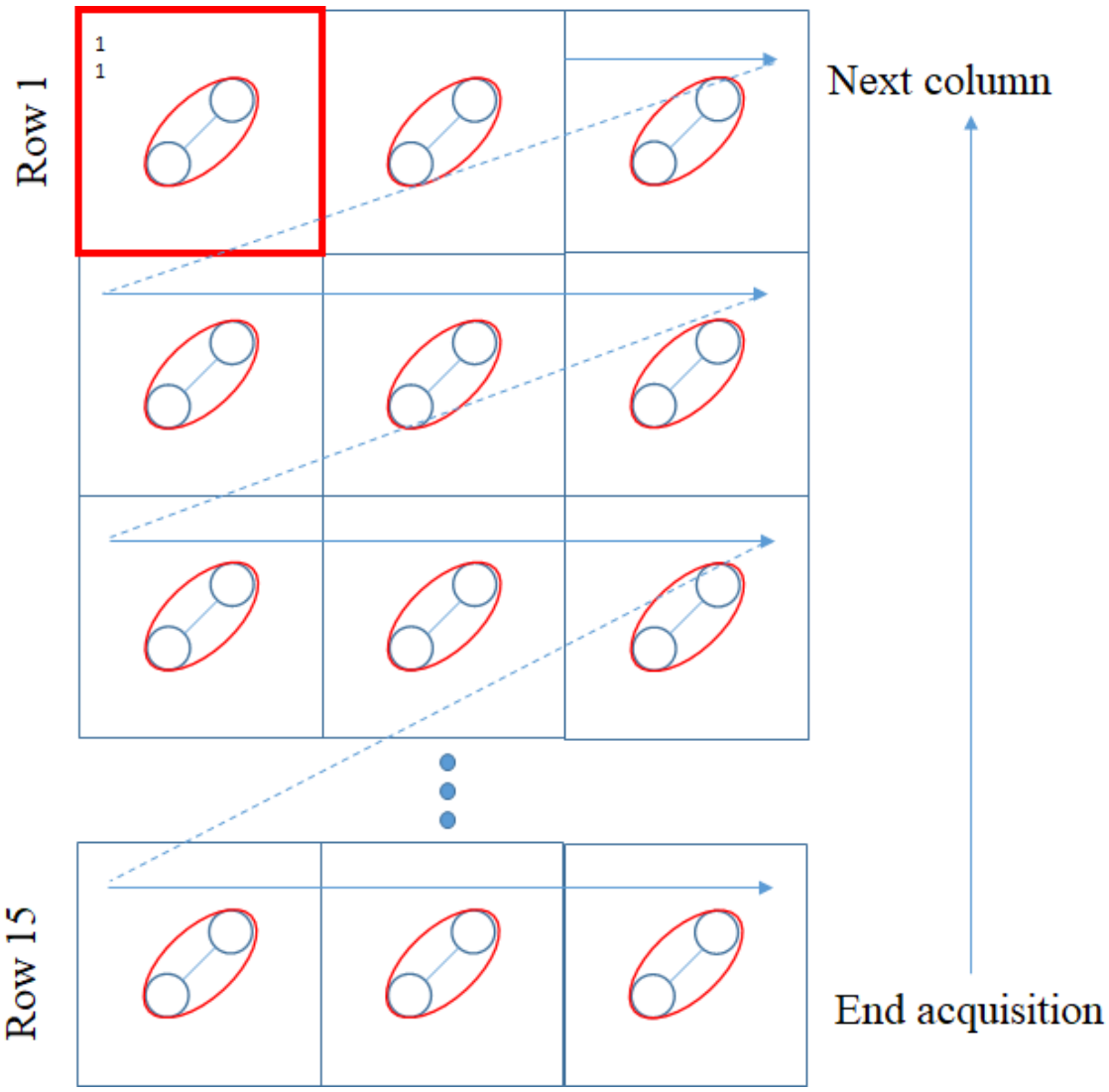

Figure 26: Automated acquisition of the cells on the micropattern array.

*The journal finds the focus of the pattern by using the variance of the image. At best focus, the image has the highest variance. This focus is set, the pattern and cell imaged, then the stage is moved right by 113.6 µm and the next pattern, cell imaged. This is done for 3 patterns, then moved to the next row and the imaging continued for 15 rows. Then, the next column composing 3*15 patterns is imaged. The journal can acquire 45 patterns in around 7 minutes.*

5.14 Transfection protocol

Transfection of Actin mEOS3.2 plasmid (mEos3.2-Actin-C-18, Addgene, plasmid # 57443) to RPE1 WT cells was done using X-treme GENE transfection reagent (Merck, 6366244001). 250,000 cells/well are seeded in a 6-well dish and allowed to attach and grow for 24 hours. The transfection mix was prepared as follows: For a single well, 1.5 µg of plasmid was mixed with 200 µl of Opti-MEM media (Thermofisher scientific, 31985062) and gently agitated with a pipette to disperse the plasmid. To this mixture, 3 µl of X-Treme GENE reagent was added, gently pipetted 5-6 times to uniformly disperse the reagent and incubated to room temperature for 15 minutes. The full volume of mixture was added dropwise throughout the well (of a 6 well petri dish) with cells (in full media) and the dish gently shaken, not stirred to evenly distribute the vesicles containing the plasmid. The petri dishes were incubated in an incubator for 4 hours allowing the plasmid to be internalized by the cell before washing off with full media and allowing cell growth for two days before using the cells for photoconversion experiments. At this stage it is possible to have close to 50% of cells in the well showing green fluorescence.

5.15 Photoconversion experiment protocol

The transfected cells (300,000/petri) are seeded onto fibronectin patterned gels with far red 0.2 µm fluorescent beads, excess non-attached cells washed off after 45 minutes and those adhered to patterns allowed to spread for 4 hours. The gel is loaded onto a chamlide chamber and mounted on the Stage Top incubation system onto the microscope.

The iLas2 device (Gataca Systems) controlling a 405 nm diode laser is used to photoconvert the mEos 3.2 system. Imaging was done with the 60X oil immersion objective.

The laser power was set by picking a test cell and photoconverting on different 8*8 pixel region on the stress fiber until the converted signal was clearly visible. The power was not so high as to cause observable bleaching on the green channel. A total of 10 spots on each cell, i.e 5 on each stress fiber were photoconverted (Figure 27A). Each region was provided to the iLas2 software as a region of 8*8 pixels (1.7µm * 1.7 µm), with center to center separation of 25 pixels (5.5 µm).

Images were acquired every 1 minute for 15 minutes in the GFP, TxRed and Cy5 channels to image the non-photoconverted, photoconverted and bead signals.

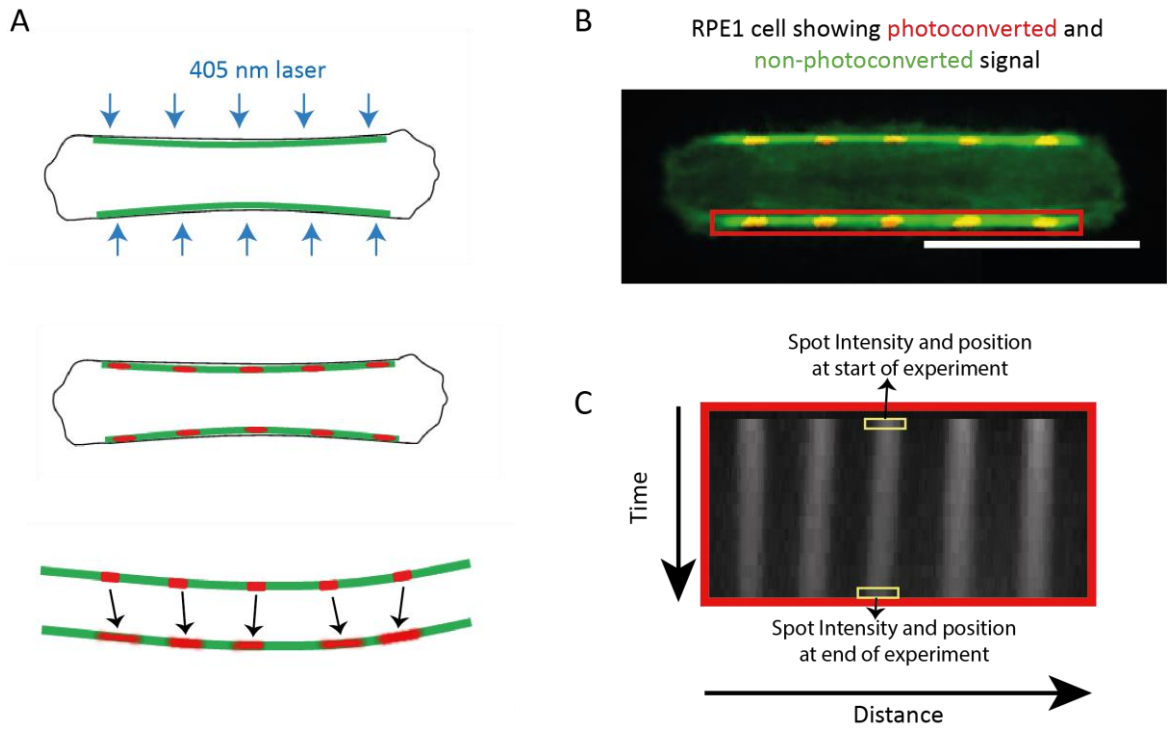

Figure 27: Photoconversion experiment

A: Schematic of the photoconversion on stress fibers in a cell. From top to bottom- The stress fibers (green) of a cell transfected with actin-mEos3.2 being photoconverted with a 405 nm laser (blue). The photoconverted signal of the stress fiber is shown in red (5 points spaced 5.5 um

along the stress fiber are photoconverted). A schematic of the dispersion of the signal and the movement of the spots in a single stress fiber is shown. The position and intensity of the spots are tracked over time.

B: Image of RPE1 cell growing on the dumbbell pattern showing the mEos3.2 signal. The green in the non-photoconverted signal and the red is the photoconverted signal. Scale bar 25 um. The contrast has been enhanced to show the photoconverted signal clearly.

C:.A kymograph of the photoconverted signal from a single stress fiber marked by a red box in B is shown. The boxes on the kymograph show the regions used to measure the photoconverted signal and position of a single spot at the start and end of the experiment.

5.16 Quantification of photoconverted signal in cells

Quantification of the signal was done manually using ImageJ for the highest and lowest strain energy exerting cells. The images of the photoconverted signal were loaded as a stack and a segmented line along the entire length of the stress fibers was drawn with a line width of 5 pixels. A kymograph was generated using this line for the photoconversion channel. The speed of each spot was quantified by manually recording the location of the centers of each spot at the start (Immediately after photoconversion) and end of the experiment (After 15 minutes), finding the displacement of the spot and dividing by the time. The relative change in intensity of each spot was quantified by obtaining the signal of the spots over the duration of the experiment and dividing the final intensity by the intensity of the spot immediately after photoconversion.

5.17 Data plotting and statistical analysis

For multiparametric representation graphs have been produced using R (https://www.r-project.org/) and RStudio (https://rstudio.com/) relying on the use of the "plot3D" package (Karline Soetaert. plot3D: Tools for plotting 3-D and 2-D data. http://cran.r-project.org/web/packages/plot3D/vignettes/plot3D.pdf). Statistical analysis and chart design was performed using Graphpad Prism 6 (www.graphpad.com) and R version 3.4.0 together with RStudio version 1.0.143.

6 Results

6.1 Cell cycle analysis

The transition of cells to different stages of the cell cycle has been shown to depend on the forces exerted on cells (Uroz et al., 2018). It was shown in Uroz et al., that cells in a monolayer subject to higher intercellular tension exhibited a higher probability to transition to the S phase from G1 as well as shorter G1 and S-G2-M phases. However, it has also been shown that the cell cycle is one of the reasons for variations in traction forces. It has been shown in previous work that strain energy varies with cell cycle stage (Panagiotakopoulou et al., 2018; Vianay et al., 2018). Traction forces show a biphasic behavior with cell cycle. Strain energy is highest in the S phase of the cell cycle and lower in the G1 and G2 phases. However, even after classifying cells based on different phases of the cell cycle, large variations in traction forces are found (Vianay et al., 2018). These studies suggest that while the forces exerted by cells change with the cell cycle and that the cell cycle is effected by the tension applied on cells, this is not the main cause for variations in intracellular traction forces.

Still, if we were to understand traction force variation, it made sense to reduce the variation present in the cell population as much as possible. It made more sense to try quantifying the traction force variation in cells that are all in the same stage of the cell cycle. This should reduce cell cycle induced variations in cellular components. So, an attempt was made to synchronize the cells in the G1/S transition using the drugs thymidine and Aphidicolin (Figure 28).

A: Untreated cells

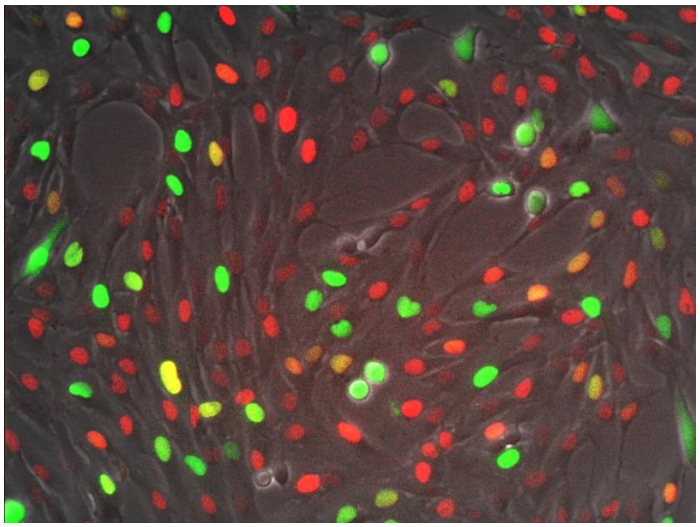

B: Thymidine double block (5 mM)

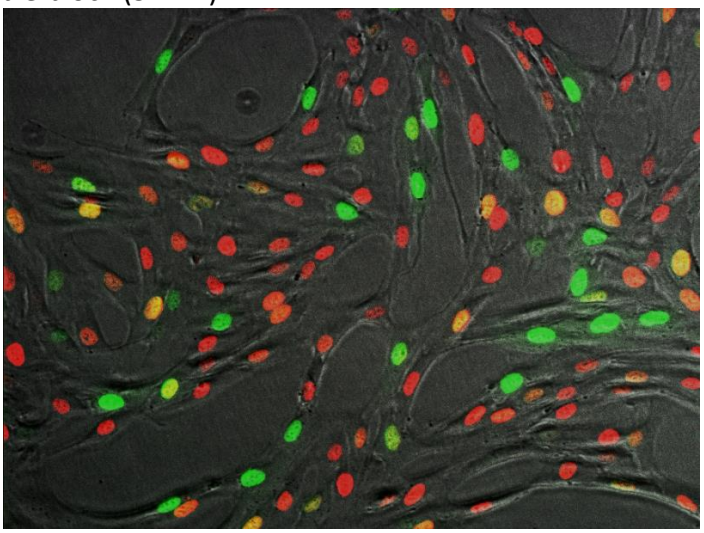

C: Aphidicolin treated cell

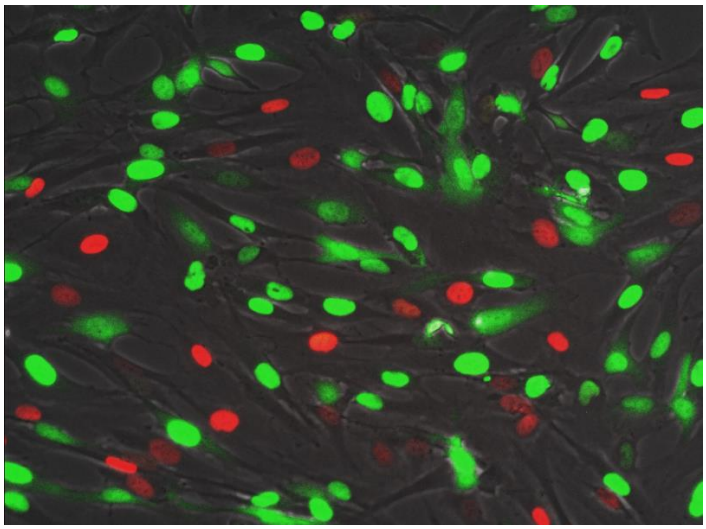

Figure 28: Control and drug treated of RPE1 FUCCI cells for cell cycle synchronization.

A: Untreated RPE1 FUCCI cells showing that cells are in G1 (red nuclei), S (orange and yellow nuclei) and G2 (green nuclei) stages of the cell cycle.

B: RPE1 FUCCI cells treated with a 5 mM thymidine double block protocol. Cells still present in G1 (red) and G2 (green) phases of cell cycle.

C: RPE1 FUCCI cells treated for 48 hours with 14 mM Aphidicolin. More cells found in G2 stage of the cell cycle ().

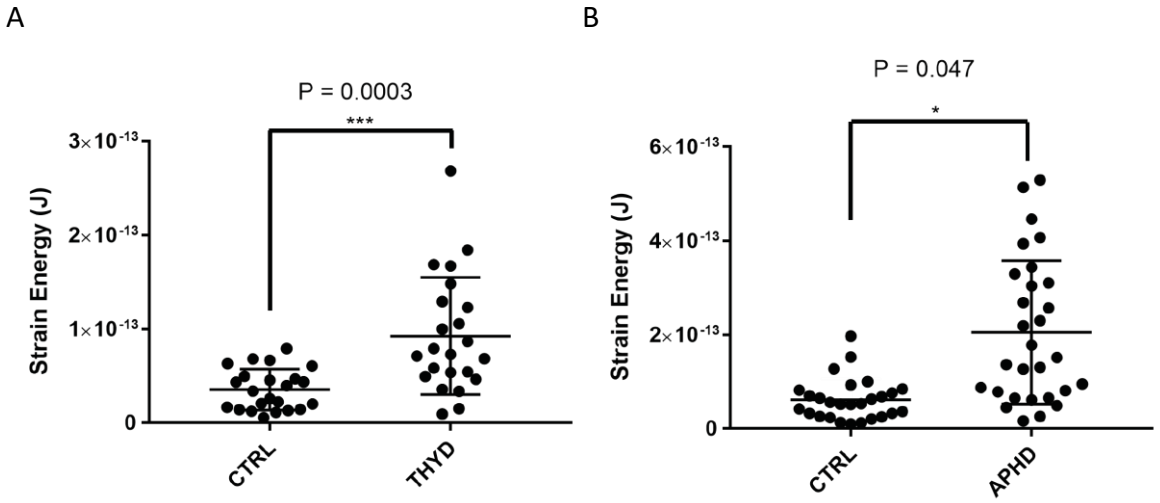

Figure 29: Attempt to control traction force variation by synchronizing the cells into the G1/S transition resulted in cells increasing the traction forces that they generated.

A. Comparison between the strain energy of control (CTRL) and 5 mM thymidine treated (THYD) cells seeded on the 59 µm dumbbells. The drug treatment increases the strain energy. (N = 23 cells for CTRL and THYD)

B. Comparison between the strain energy of DMSO (CTRL) and 14 mM Aphidicolin treated (APHD) cells. This treatment also increases the strain energy exerted by cells. (N = 27 cells for CTRL and 29 cells for APHD).

*The bars represent mean and error bars. (*** P<0.0005)*

On using the drugs on RPE1 FUCCI cells plated on petri dishes, we found that there were still cells in the G1 and G2 phases. If cells from these drug treated populations were used, we would have variations in traction forces due to the presence of cells in different stages of the cell cycle. Along with this issue, it was found that the use of either of the drugs increased the average strain energy exerted by wild type cells without in any way reducing the variability (Figure 29). As the cause of the drug treatment leading to increase in traction forces is not known, this method was discarded as not very useful to the study.

6.2 Actin dynamics results

To check if there were significant variations in the actin dynamics of the stress fibers in relation to traction forces, RPE1 wild type cells were transfected using the X-treme GENE transfection reagent (Merck, 6366244001) with the photoconvertible actin-mEos3.2 construct (mEos3.2-Actin-C-18). This construct fluoresces on excitation with blue excitation, to give green emission. On illuminating the construct with 405 nm, the construct converts to excite with green emission to give red fluorescence. To confirm that the transfection did not significantly modify the traction forces exerted by cells, we compared the strain energy exerted by wild type RPE1 and the transfected cells using traction force microscopy. It was found that there were no statistically significant differences between the two groups. As such, we used the transfected cells for measuring the dynamics of actin in the stress fibers (Figure 30).

A

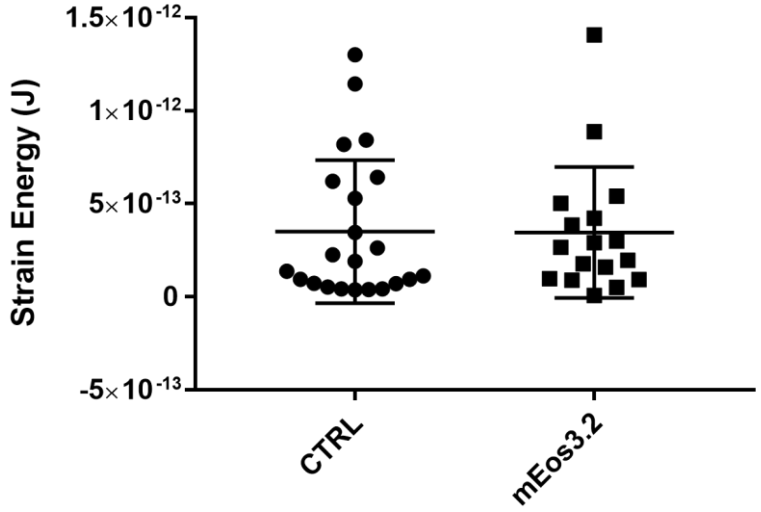

Figure 30: Traction force of RPE1 wildtype and RPE1 wildtype transfected with actin-mEos3.2

No statistically significant differences in strain energy could be observed between the two populations. N = 22 wild type cells and 17 transfected cells from 1 experiment. Statistical significance ($p < 0.05$) was determined by the Students' t-test.

There is a large range in the strain energy produced by cells. To determine if there was a relation between traction forces and the actin dynamics of stress fibers, we decided to compare the cells at the extreme ends of the strain energy range. Cells with strain energy above 1 pJ were classified as High SE cells and those below 0.1 pJ were classified as Low SE cells (Figure 31). The actin dynamics data from the two groups of cells is given below. To check the actin dynamics between the cells, 5 regions were photoconverted along the length of the two stress fibers and the movement of the spots and the change in the fluorescence intensity with time was quantified.

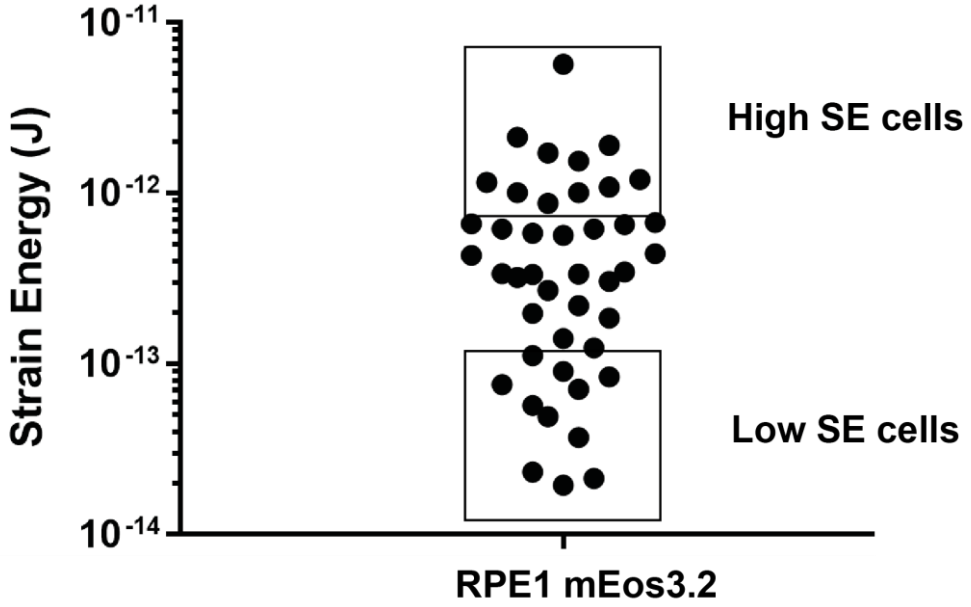

Figure 31: Strain energy variation in RPE1 cells transfected with actin-mEos3.2

To determine if actin dynamics varied between the cells that had high and low strain energies, the 11 cells with the highest and 12 cells with the lowest strain energies were selected and analyzed. N= 43 cells from four different experiments.

The strain energy of the cells during the course of the experiment was measured along with the actin dynamics. We see that there are no major fluctuations in the traction forces produced by the cells during the 15 minutes when the photoconversion is done and observed (Figure 32). The changes in strain energy seen are exaggerated due to the log representation of the Y axis, especially for the Low SE cells.

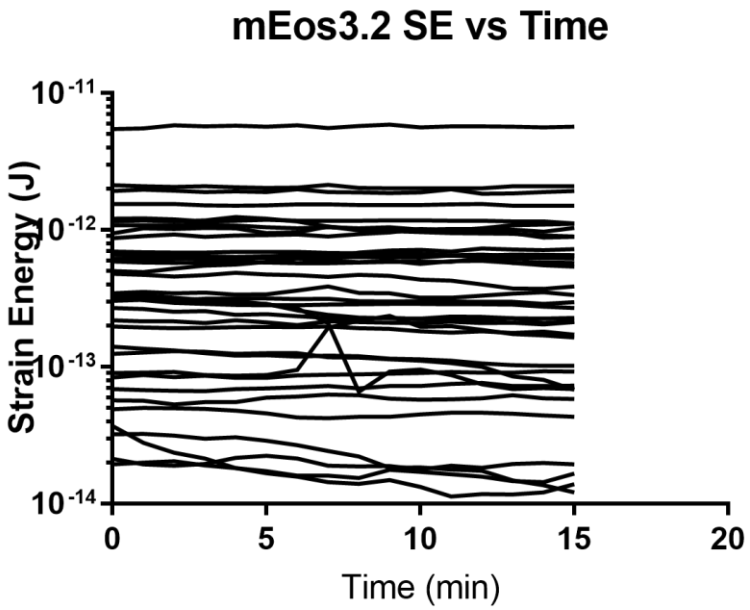

Figure 32: Strain energy variation of actin-mEos3.2 transfected cells

The variation of strain energy with time shows no significant variations. Note that the y-axis is a log scale to better show the variation. Except in a rare case, the cells maintain similar levels of strain energy throughout the duration of the experiment with only minor variations.

First, the speed of movement of the spots on the stress fibers of the two classes of cells mentioned were found. The speeds of all the spots in all the cells belonging to the two classes of cells are shown below (Figure 33). There are differences between the speeds of the spots from the two classes. There is however significant overlap between the values from the two classes.

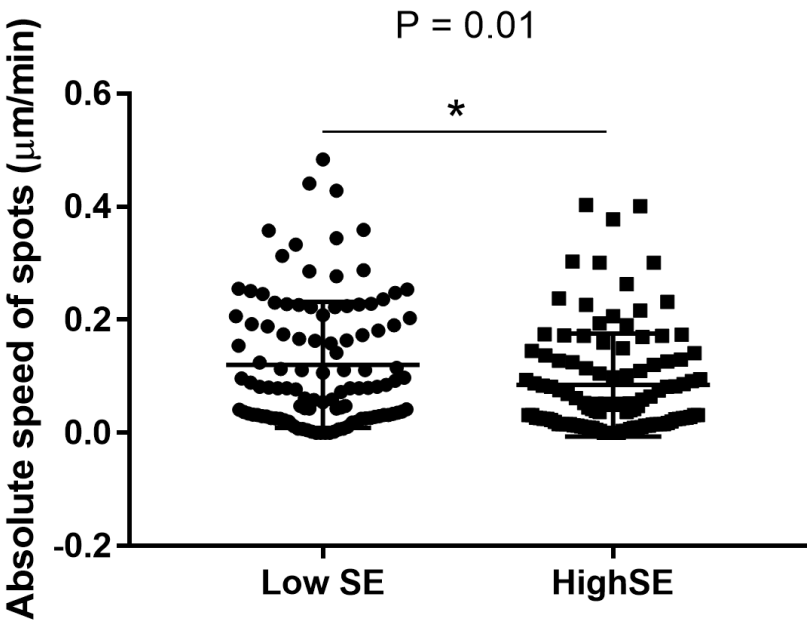

Figure 33: The absolute speed of all the spots in the low and high strain energy cells.

Quantification of the absolute speeds of the photoconverted spots on stress fibers. Comparison between the speeds on Low and High strain energy exerting cells show differences between them, but there is still significant overlap between them. Statistical analysis done using Students T test. N = 120 spots (12 cells, 10 spots on each cell, 5 spots on each of the two stress fibers) for Low SE cells and 110 spots (11 cells) for High SE cells. Cells from four different experiments were included. Statistical significance ($p < 0.05$) was determined by the Students' t-test

To check if we could obtain a clearer trend in the spot speeds, the speed of the fastest moving spots on each stress fiber were taken. The data again shows statistically significant differences between the two groups, but with significant overlap between the two groups (Figure 34). These results suggest that while there are differences between the movement of filaments within the stress fibers of High and Low strain energy cells, the overlap suggests that this is unlikely to be the main reason for differences in traction forces between the groups. Hence, we next looked at the dynamic turnover of the spots during the experiment

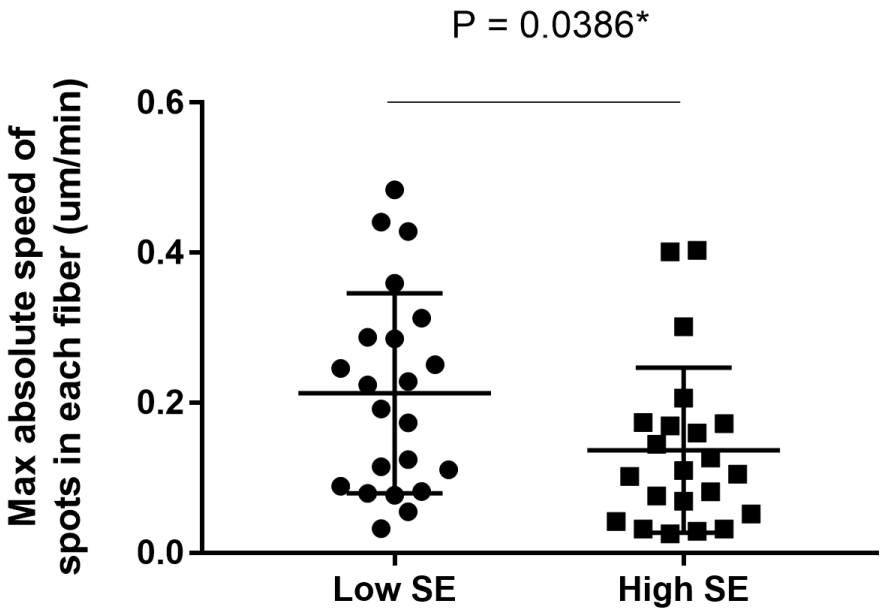

Figure 34: Maximum speed of spot in each stress fiber of the low and high strain energy cells

The speed of the fastest moving spot on each stress fiber in the low and high strain energy exerting cells are shown. There is a statistically significant difference between the speeds of the fastest moving spots in each cell between the low and high strain energy cells. Statistical significance ($p < 0.05$) was determined by the Students' t-test. (N = 22 spots. The spot on each stress fiber from 11 cells of each group with the highest change absolute speed is shown)

The turnover of the spots was characterized by measuring the intensity of the spots immediately after the photoconversion and then again at the end of 15 minutes. The change in the fluorescence signal was normalized with respect to the fluorescence immediately after photoconversion. The data from all the spots on the Low and High strain energy cells are shown below (Figure 35). There was no statistically significant difference between the values from the two groups. Again, there were large variations in the change in intensities in both groups. The Low strain energy cells had spots that hardly lost any intensity and some that had lost around

70% of the signal. The variations in the change in normalized intensity for the high strain energy cells was comparatively lower.

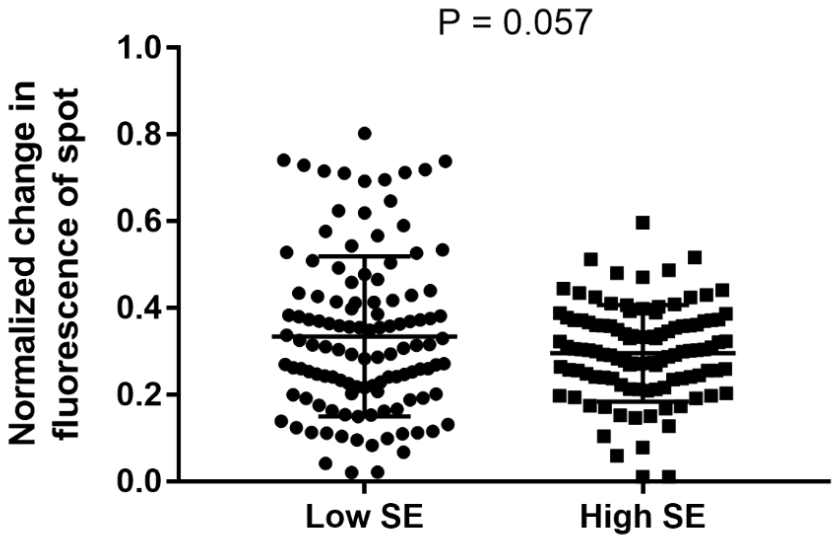

Figure 35: Normalized change in intensity of all 10 photoconverted spots in each of the highest and lowest strain energy cells.

The data shows that there are no statistically significant differences between the two groups of cells on using a Students T test. (N = 120 and 110 spots for Low and High strain energy cells respectively. The normalized change in intensity of 5 spots on each of the two stress fiber in each cell are shown)

To check if there were differences that could be observed between the two groups when taking the maximum change in normalized intensity on each stress fiber, the spots with the highest change in each stress fiber were taken and are shown below (Figure 36). While there were no statistically significant differences between the two groups, again we see that the Low strain energy cells have higher variations compared to the High strain energy cells.

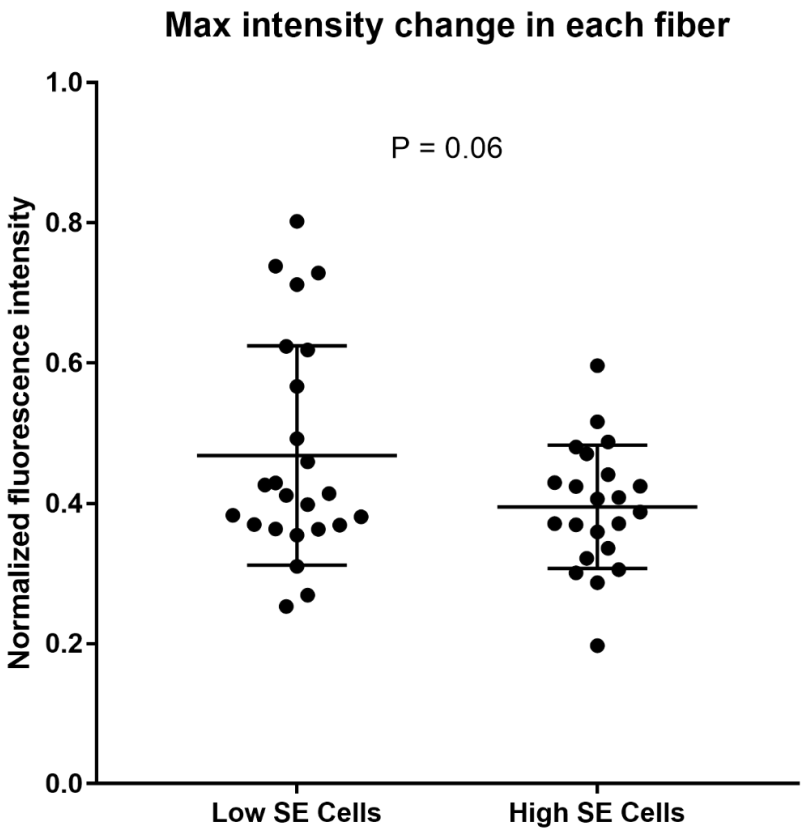

Figure 36: Maximum normalized change in intensity value on each stress fiber of the highest and lowest strain energy cells.

The data shows that there are no statistically significant differences between the two groups of cells on using a Students T test. (N = 24 and 22 spots for Low and High strain energy cells respectively. The spot with the maximum normalized change in intensity amongst all 5 spots on each of the two stress fiber in each cell are shown)

To understand why such large variations exist in the change in fluorescence, the values of all the spots on the two stress fibers from two cells belonging to each strain energy group were plotted (Figure 37). We see that there are significant variations in the values within each stress fiber and the values between stress fibers in the same cell.

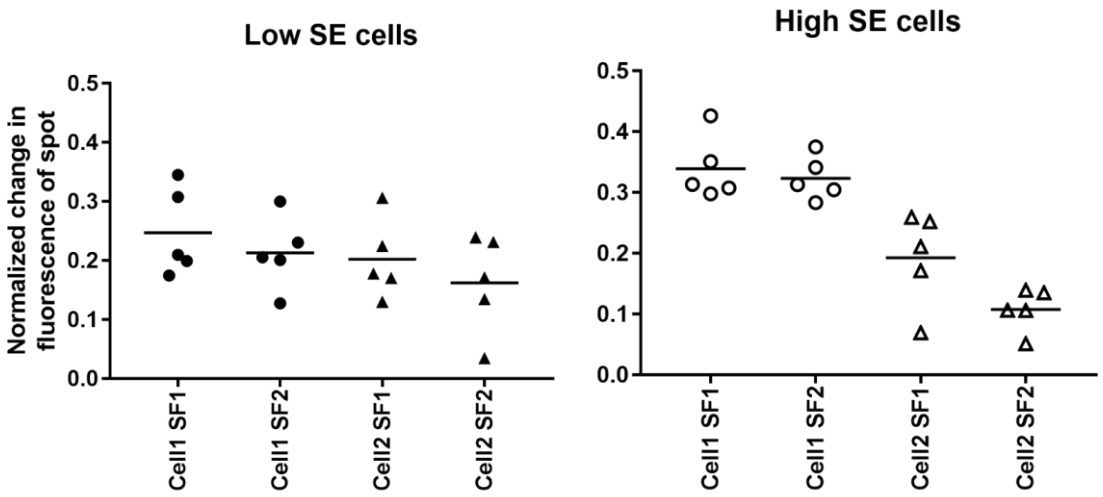

Figure 37: Normalized change in intensity value of all 5 spots on each stress fiber of two cells

The values of the normalized change in intensity of two of the lowest (filled circle and triangle) and highest (empty circle and triangle) strain energy cells. The data shows that there are significant differences in the turnover of spots on each stress fiber (labelled SF1 and SF2), those between stress fibers in individual cells, and between turnover in individual cells. The mean value for each stress fiber is shown.

These heterogeneities within a cell and between cells belonging to the same group lead to large variations within the data from each group. This makes it difficult to determine if variations in actin dynamics between the two groups play a role in strain energy variations. It was however interesting to note that the values of both the absolute spot speed and the normalized change in intensity had larger variations with the Low strain energy cells compared to the High strain energy cells.

6.3 Biochemical characterization (Paper draft)

The combination of immuno-stainings and traction force microscopy revealed an optimal composition of the actomyosin network to produce mechanical forces.

Somanna Kollimada[1], Fabrice Senger[1], Timothée Vignaud[2], Manuel Théry[3], Laurent Blanchoin[1], Laëtitia Kurzawa[1]

1 Université Grenoble Alpes, CEA, INRA, CNRS, UMR5168, lnstitut de recherche interdisciplinaire de Grenoble, Département de Biologie Structurale et Cellulaire Intégrée, CytoMorpho Lab, F-38000, Grenoble, France.
2 Clinique de chirurgie digestive et endocrinienne, Hôtel Dieu, Nantes, 44093, France.
3 Université de Paris, CEA, INSERM, UMRS1160, Hopital Saint Louis, Institut Universitaire d'Hematologie, CytoMorpho Lab, F-75475, Paris, France.

ABSTRACT

Mechanical forces are essential for different physiological processes that require a tight regulation of both the magnitude and spatial distribution of the contractile forces at the cell and tissue-level. Although at the molecular level, the regulation of force production and transmission relies on the complex interplay between a well-conserved set of proteins of the cytoskeleton, we still do not have a comprehensive understanding of the mechanisms supporting force generation at the entire cell level. In particular, the magnitude of the traction forces exerted by cells on their underlying extracellular matrix in culture remains difficult to predict. In this study, we explored how the biochemical composition of the actomyosin and adhesion networks is related to the force magnitude exerted by cells. By implementing a novel TFM assay including an intermediate labeling step, we could quantify the endogenous contents of intracellular F-actin, myosin, alpha-actinin and vinculin and relate them directly to the traction forces exerted by these cells. Our experimental results first demonstrated that the vinculin content measured at the level of the entire cell and the area of the focal adhesions represented good predictors of force. Actin and myosin, when analyzed individually, displayed broader deviations in their linear relationship to the strain energies, and thus appeared as less direct predictors of force. Instead, the analyzes suggested that their relative cellular amount plays a key role in setting the magnitude of force exerted by cells. Finally, our study revealed that although the alpha-actinin content was not correlated at all with force magnitude, its relative amount as compared to actin content was of key importance to regulate force production. In conclusion, this work identified the biochemical content of focal adhesion and the relative amounts of molecular motors and crosslinkers per actin filament as key parameters for setting the magnitude of force exerted by cells.

INTRODUCTION

Mechanical forces are central to many physiological processes including morphogenesis (Heisenberg & Bellaïche, 2013; Murrell, Oakes, Lenz, & Gardel, 2015), migration (Leal-Egaña et al., 2017; Maiuri et al., 2015), division (Sedzinski et al., 2011) and differentiation (Kilian, Bugarija, Lahn, & Mrksich, 2010; McBeath, Pirone, Nelson, Bhadriraju, & Chen, 2004). All these events involve a tight regulation of both the magnitude and spatial distribution of the contractile forces at the cell and tissue-level (Agarwal & Zaidel-Bar, 2019; Murrell et al., 2015).

At the macroscopic scale, such an accurate control of cellular force depends on key parameters including substrate stiffness (Lo, Wang, Dembo, & Wang, 2000), adhesive ligand density (Reinhart-King, Dembo, & Hammer, 2003), cell area (Califano & Reinhart-King, 2010) and shape (Rape, Guo, & Wang, 2011). At the molecular level, the regulation of force production and transmission relies on the complex interplay between a well-conserved set of proteins of the cytoskeleton. In the first place, force essentially originates from the interactions between F-actin and non-muscle myosins II (Chrzanowska-Wodnicka & Burridge, 1996; Katoh, Kano, Masuda, Onishi, & Fujiwara, 1998; Koenderink & Paluch, 2018). The early and elementary step of traction force production by these actomyosin structures is indeed determined by the amount of active myosin and the local alignment and connectivity of actin filaments (Ennomani et al., 2016; Linsmeier et al., 2016; Luo et al., 2013; Reymann et al., 2012; Thoresen, Lenz, & Gardel, 2011). The remodeling of these actin filaments by the action of crosslinkers, in particular alpha-actinins, also plays a key role in regulating the mechanical properties of the network (Xu, Wirtz, & Pollard, 1998) and additionally participates to the formation of stress fibers (Langanger et al., 1986; Lazarides & Burridge, 1975). These structures are in turn essential for tension generation against the extracellular matrix (ECM) and propagate contractile forces throughout the cell (Chang & Kumar, 2013; Deguchi, Ohashi, & Sato, 2005; Naumanen, Lappalainen, & Hotulainen, 2008). The proportion of contractile energy transmitted to the cell surroundings finally depends on focal adhesion (FA) complexes, themselves experiencing variations in their composition, size and dynamics (Elosegui-Artola et al., 2016).

Despite years of investigations, which led to great levels of structural and molecular descriptions of these actomyosin networks and cell adhesion complexes, understanding precisely of how each of these molecular players individually or via their specific interplay, is related to force magnitude in the cells remains challenging. Although the role of this set of proteins in force regulation appears to be well-conserved (Murrell et al., 2015), both their relative amount, state and structural organization can indeed vary locally within a cell and more globally between cells, leading to various effects on cellular traction force (Kurzawa et al., 2017). For example, the relationship between force and focal adhesion features is controversial, as observations made in migrating cells or when overexpressing adhesion proteins were found to be questioned in other cellular contexts. Hence, it was shown that the linear relationship described between the size of individual adhesions above 1 µm2 and the amount of local force (Balaban et al., 2001) does not hold anymore when considering supermature FA above 8 µm (Goffin et al., 2006) or smaller adhesions for which the stress is highly variable (Tan et al., 2003). Additionally, a complex relationship was described in migrating cells, for which adhesions at the front and at the trailing edge turned out to behave differently with force (Beningo, Dembo, Kaverina, Small, & Wang, 2001). An inverse correlation was indeed observed in this case at the front of the cells, where small adhesions could transmit strong forces whereas larger ones were associated to weaker forces. Finally, more recent work demonstrated that the history of focal adhesion assembly also plays a crucial role in this relationship, as FA size and force were shown to be correlated only during the initial steps of the FA maturation process (Stricker, Aratyn-Schaus, Oakes, & Gardel, 2011).

The early development of Traction Force Microscopy (TFM) methods that map the force at the cell surface by measuring deformations of the underlying substrate greatly helped identifying the molecular components involved in force production and regulation (Dembo & Wang, 1999; Kraning-rush, Carey, Califano, Smith, & Reinhart-king, 2011). However, despite its

broad use, this easy and straightforward technique includes a disruptive step of cell removal, precluding the possibility to further characterize the biochemical composition of the cellular network responsible for the production of traction force. In the case of focal adhesions in particular, the characterization of their molecular morphometry has been limited to live observations of fluorescent proteins fused to paxillin or vinculin, thereby preventing the access to endogenous levels of these proteins (Balaban et al., 2001; Mohl, Kirchgessner, Schafer, Hoffmann, & Merkel, 2012; Plotnikov, Pasapera, Sabass, & Waterman, 2012). ¬¬¬¬¬ Other methods including 2D micropillars (Tan et al., 2003), DNA-based sensors (Grashoff et al., 2010) or reference-free techniques (Banda, Sabanayagam, & Slater, 2019; Bergert et al., 2016) provide alternative ways to measure intracellular forces without requiring cell detachment and therefore allow for further cell characterization, but also suffer from intrinsic limitations (Roca-Cusachs, Conte, & Trepat, 2017). Micropillars interfere with cell behavior due to the non-continuous nature of the pillars, their topography, and the fact that cell adhesions are geometrically constrained (Malinverno et al., 2017; Trichet et al., 2012). DNA force-based sensors can measure precisely the maximal force produced by cells but not the lower values and in addition do not provide information about their directionality (Ma, Bai, & Wang, 2013). Global or local deformations of micropatterned cells are not precise enough to investigate fine regulations of force production (Ghagre et al., 2020; Pushkarsky et al., 2018; Tseng et al., 2011).

In this context, alternative methods are required to conduct a concomitant study of traction force and biochemical composition of the cellular network, and achieve a comprehensive understanding of this relationship. To address this need, we modified the standard TFM assay by adding fixation and immuno-labeling steps to access simultaneously traction forces exerted by cells and characterize the endogenous molecular composition of their cytoskeleton network. By combining this method with micropatterning to normalize cell shape and size, we were able to study the relationship between vinculin, actin, myosin, and alpha-actinin composition of cells and their strain energy. Our results identified both the total vinculin area and its intensity, measured at the level of the entire cell, as the most reliable predictors of cellular force. We then showed that actin and myosin, displayed broader deviations in their linear relationship to the strain energies, and thus appeared as less direct predictors of force. Instead, our data suggested that their relative cellular amount plays a key role in setting the magnitude of force exerted by cells. We finally demonstrated that although the alpha-actinin content was not correlated at all with force magnitude, the relative amount of alpha-actinin as compared to actin content was of key importance to regulate force production.

RESULTS

Figure 1: Development of a modified TFM assay----------

A key set of molecular players is responsible for the force generated by cells. This diversity and interplay between the components lead to a non-trivial relationship between individual actors involved in intracellular contractility generation and the actual force transmitted by these cells. In this work, we asked how the biochemical composition of the cytoskeleton network and the interplay between its molecular components relates to the traction force exerted by cells on their substrate. To address this question, we first adapted the classical TFM assay to study the intrinsic composition of the cytoskeletal network for a panel of

molecular components involved in intracellular force generation: vinculin, actin, myosin, alpha-actinin, and study how their content relates to the mechanical work done by these cells.

In a classical TFM assay, fluorescent beads embedded in the gel are imaged first in the presence of cells exerting traction forces on the substrate to obtain the deformed configuration of the gel (Figure 1a step 1), then cells are removed following trypsin treatment to access to the relaxed configuration of the gel upon force release (Figure 1a step 2). This experimental procedure thus provides a direct measurement of traction forces exerted by the cells but prevents further intracellular characterization such as immunolabelling. To overcome this limitation and allow simultaneous intracellular characterization, we adapted the standard assay by adding an intermediate labeling step of the cells (Figure 1b step 2). In this modified assay, beads were as for the standard assay imaged at step 1 and 3 to determine traction forces exerted by the cells (Figure 1b steps 1 and 3). An intermediate imaging step (Figure 1b step 2) was additionally performed after cells were being fixed and stained with fluorescently-labelled antibodies, allowing for the immunolabelling and study of any cellular molecular component. As in the case of a standard assay, forces were computed between steps 1 and 3 after total cell removal as we noticed that fixation led to a significant but not full relaxation of the gel (Figure supp1a).

The cytoskeleton molecular composition and organization can vary drastically from one cell to another, and as both parameters are intimately linked to the force generation process, studying how they relate to each other turns out to be challenging in an heterogeneous cell population. We therefore took advantage of the use of micropatterned substrates to overcome this limitation and minimize the inherent variability experienced by non-confined cells. To that end, an array of dumbbell-shaped micropatterns of 60 µm total length was designed on top of photochrome masks (Figure 1c). We specifically selected this micropattern size as it represents the average length of RPE-1 cells grown on plain substrates (Vignaud et al., 2020). Fiduciary marks were also included next to the micropatterns in order to appear on each field of view during the imaging process (Figure 1c). As the sample was imaged multiple times after being removed from the microscope stage, the presence of reference marks indeed allowed us to retrieve the same region of the sample between steps 1, 2 and 3 and to correct manually for the drift in the sample position (Figure 1b). Traction forces were then computed using the method previously described in Martiel JL. et al. (Martiel et al., 2015). On top of the regular bead images processing including a correction for experimental drift, a computational rotation correction step was additionally performed to fine tune the alignment of the beads using a cross-correlative approach (Figure supp1b).

In order to validate our experimental approach, RPE-1 cells were first plated and allowed to spread on top of 20 kPa polyacrylamide gels for 4 hours before proceeding to the traction force measurement and immunostainings. As previously described (Vignaud et al., 2020), most cells were able to attach and fully spread on top of the micropatterns coated with fibronectin within this time frame (Figure supp 2a). Cells that were not fully spread or that were spreading outside of the adhesive area of the micropatterns were manually discarded from our analysis (Figure supp 2b). As to validate our approach for studying the relationship between molecular composition of the cells and their strain energy, we then immuno-stained the cells for vinculin, actin, myosin, alpha-actinin, and measured the associated forces (Figure 1d). In agreement with our previous observations (Vignaud et al., 2020), cells displayed mainly focal

adhesion protein vinculin above the two main adhesive area of the micropattern. Additionally, mainly two peripheral prominent stress fibers containing actin, myosin and alpha-actinin were formed and spanned the non-adhesive area in between these adhesion points (Figure 1d). As for the strain energies, they were successfully measured and distributed as previously described in a range comprised between 0pJ and 2,5pJ.

These data show that, despite some technical hurdles, including the partial relaxation of the gel during fixation and the manual repositioning of the sample after the immuno-labelling, we managed to combine IF and TFM in order to analyze both the molecular composition and the strain energy in the same individual cells.

Figure 2: Correlation between FA area, vinculin content and force at the entire cell level-------

Since focal adhesions transmit force internally generated by the cytoskeletal network to the ECM (Balaban et al., 2001), we first decided to use our assay to investigate the controversial relationship between one of their component, vinculin, and cell strain energy. We specifically selected vinculin as a readout of the focal adhesion content for our analysis because it represents a marker of choice of both focal complexes (DePasquale & Izzard, 1987) and larger and more stable focal adhesions (Geiger, Bershadsky, Pankov, & Yamada, 2001). We also took advantage of the use of micropatterns to constrain the cell shape and size and perform our measurements in stationary cells in order to study the FA composition independently of their turnover associated to the migration process. We used Focal Adhesion Server (FAS) to extract key focal adhesion parameters including vinculin signal and area (see material and methods). Previous work from our laboratory demonstrated that tractions forces were not only applied on the ECM by anchorage points located at the periphery of prominent stress fibers but were instead produced equally and transmitted by the actin mesh embedding these structures (Vignaud et al., 2020). As the peripheral stress fibers and internal mesh represent a mechanical continuum pulling on the substrate at various focal adhesions simultaneously, we hence decided to perform quantifications of vinculin signal and area at the entire cell-level as they represent more appropriate measurements than local ones (Figure 2a).

Interestingly, we first observed that although cell shapes were normalized, the total area and protein content of FA displayed large variations (Figure 2 a and 2b). The associated traction forces were also highly variable from one cell to the other. We took advantage of this intrinsic variability to assess first the relationship between FA total area and force (Figure 2 b left panel). We noticed that vinculin area, integrated over the whole cell, scaled non-linearly with strain energy, displaying an exponential increase (Figure 2a and 2b upper panel; R2=0.51). In addition, the relationship between strain energy and whole cell vinculin intensity was characterized by a linear increase (Figure 2a and b bottom panel; Pearson=0,71; R2=0,51). Finally, we noticed that the FA signal was not located all over the adhesive area of the micropattern but was instead mainly confined to the periphery of the cell in an area corresponding to the lamellum region (Figure 2c). Interestingly, we found out that this adhesion pattern ended up forming a continuous belt of increasing length along the rim of the cell as the strain energy increased, but that its thickness remained rather constant with increasing force.

As previously established, the existence of a shared regulation mechanism between local FA composition and size, and the overall force transmitted to the substrate was also

confirmed in our data at the entire cell-level. These measurements in addition suggested that even when not submitted to massive FA reorganizations due to migratory processes, cells can still undergo significant variations in their actomyosin content associated with changes in their focal adhesion assembly and force production, as previously demonstrated in moving cells (Chrzanowska-Wodnicka & Burridge, 1996; Oakes, Beckham, Stricker, & Gardel, 2012).

Figure 3: Correlation between SE and total or stress-fiber related F-actin content ----------

Stress fibers represent structural templates essential for FA maturation (Oakes et al., 2012) and as such they play a key role in regulating both the assembly and size of FA and force transmission at these anchorage points (Burridge & Wittchen, 2013; Chrzanowska-Wodnicka & Burridge, 1996). We thus tested next whether the heterogeneity in the magnitude of traction forces observed could be associated with actin filament contents. To test this hypothesis, we used our modified TFM assay to measure traction force in cells plated on dumbbell-shaped micropatterns that were stained for actin filament using Phalloidin (Figure 3a and b). The FITC-phalloidin fluorescence signal was first used as a measure of total actin filament content over the whole cell (yellow box) and compared to the strain energies measured in the same cells (Figure 3a). As expected, we noticed large variations in total F-actin contents and associated forces within the cell population analyzed, recapitulating our FA observations. This result showed that despite being standardized in their shape and actin architectures in terms of size and number of prominent stress fibers, traction force fields were still displaying large cell-to-cell differences.

We next decided to take advantage of these variations in actin content and strain energies over the cell population to study the relationship between these two parameters. By plotting individual data of actin filament content versus strain energy, we first observed that strain energy displayed a significant correlation with total actin filament content of cells (Pearson=0.57, R2=0.32), following a linear increase trend (pink dots and box in Figure 3a and c respectively). We next decided to assess more accurately the relationship between actin content of the two prominent stress fibers formed in between the adhesive area of the micropatterns and the cells strain energies to test whether the actin content of these bundles would represent a better predictor of force than total actin due to their fundamental role in force generation and transmission (Figure 3b). To test this hypothesis, actin filament signal was quantified as the sum of the signal measured in the two prominent peripheral SF (Figure 3b top panel). In agreement with the case of total actin filament, strain energy increased linearly with the signal integrated over the two peripheral stress fibers (Figure 3b bottom panel). Unexpectedly, the correlation coefficients measured for total and stress fibers related actin filament were almost identical, showing that actin in stress fibers, even if measured in structures dedicated to force production, did not represent a better predictor of force than total cellular actin (Pearson r=0.57 and 0.55, with R2=0.32 and 0.3 respectively).

Even if correlated with force, measurements of both total and SF related F-actin contents were displaying large dispersion around the linear trend (Figure 3a, b and c). For example, cells displaying the same amount of actin were able to exert a wide range of strain energies going from 0.2 to 1.4 pJ (green dots and box in Figure 3a and c respectively). Reversely, cells transmitting the same amount of force to the substrate displayed a wide range of amounts of actin (orange dots and box in Figure 3a and c respectively). Altogether, these results revealed

an interdependence between total actin filament content and strain energy. However, despite significant, the correlation was rather weak and data were quite dispersed around the main linear trend, suggesting that additional relevant and uncharacterized players were involved in that content-force relationship.

Figure 4: Correlation between SE, myosin and actomyosin content----------

The contractility of actin networks has been shown to derive from the motor activity of myosins (Bendix et al., 2008; Thoresen et al., 2011). We thus investigated next how endogenous myosin content was related to strain energy by measuring traction force in cells labelled for phospho-myosin light chain (Figure 4a). As our previous results demonstrated that total cellular actin filament was an equivalent predictor of force than actin filament contained in SF, we focused our analysis on total phospho-myosin signal (Figure 4a left panel, yellow box). We observed that phospho-myosin signal increased in a linear fashion with strain energies (pink dots and box in Figure 4a and b respectively). Interestingly, myosin overall signal displayed a better coefficient than total F-actin with strain energy (Myosin Pearson=0.67, R2=0.32; F-actin Pearson=0.57, R2=0.45), indicating that phospho-myosin represents a better force predictor than actin filament. However, we still observed a noticeable variability between these parameters (Figure 4a and b). Indeed, we noticed that cells having the same amount of myosin could exert a wide range of forces and reversely that cells displaying the same contractile energy could have a high dispersion in their myosin content (green and orange dots and boxes in Figure 4 a and b respectively). This result indicated that as in the case of actin filament, myosin content alone cannot solely account for the magnitude of forces exerted by cells.

We next hypothesized that the variations of strain energy experienced by some cells sharing the same amount of myosin could be due to intrinsic variations in their actin content. We thus postulated that traction forces might scale linearly with myosin and actin content as more myosin in the actin network should increase the contractility. To test this idea, we took advantage of our experimental design to conduct a TFM assay in dual-labeled cells to access both their actin filament and phosphorylated myosin content in relationship with force. We first noticed that myosin signal increased linearly with the signal corresponding to total actin filament content (Pearson=0.71, R2=0.5 in Figure 4c left panel), showing that the levels of these proteins are correlated. As expected, the linear increase in actin and myosin content were also associated with a linear increase of force, as illustrated by the color-coded representation of the strain energy in between the two dashed-lines on both plots (Figure 4c left panel). Unexpectedly, we also observed that outside of this linear regime corresponding to a concomitant increase in both actin filament and myosin, forces were found to drop drastically (below 0.5 pJ) despite the presence of high amount of either actin filament or myosin. This suggested that the value of the actomyosin was key to set the magnitude of traction forces exerted by cells, so we next decided to plot the ratio of myosin/F-actin versus strain energy (Figure 4c right panel). We first observed that the ratio correlated rather poorly with strain energy (Pearson =-0.006, R2=3.38.10-5). More interestingly, we noticed the presence of an optimum ratio (in between the two dashed lines), for which only cells could produce high forces (defined as above 1pJ). When the actomyosin ratio deviated from this optimal range, strain energies dropped down significantly. For low myosin/actin filament ratios, corresponding to the case where the proportion of actin filament to myosin was higher than the averaged trend, the force measured were below 0.5 pJ. The opposite trend appeared deleterious as well: when

myosin/actin filament ratio was higher than the average, cells were limited to the same range of force. These results showed that, although when considered individually, higher amounts of actin or myosin correspond to higher force, an optimal balance between total amount of myosin and actin filament exists and leads to maximize the production and transmission of traction forces.

Figure 5: Correlation between SE, alpha-actinin content and actinin/actin ratio----------

Crosslinkers such as α-actinins constitute key regulators of the actomyosin network contractility as they affect the connectivity of the network and are required for local contraction to be transmitted throughout the network (Bendix et al., 2008; Ennomani et al., 2016; Jensen, Morris, & Weitz, 2015; Senger et al., 2019). Additionally, α-actinins localize to cell adhesions where they promote their maturation (Edlund, Lotano, & Otey, 2001; Oakes et al., 2012; Ye et al., 2014). In vitro, the contribution of crosslinkers to force production is biphasic: a minimum amount is required to ensure the connectivity of the network and the transmission of forces but an excess can stall the system by preventing filament sliding and force production (Bendix et al., 2008; Ennomani et al., 2016). By contrast, in cells, alpha-actinin knock down specifically increases traction forces and its overexpression suppresses them (Doss et al., 2020), suggesting that the cellular amount of alpha-actinin sets the cells close to the optimum ratio of crosslinker per actin (Oakes et al., 2012). However, how endogenous α-actinin levels affect the overall mechanical work in cells is remains unknown.
In order to study the relationship between endogenous alpha-actinin content of cells and strain energy, traction force was measured in cells immuno-labelled for alpha-actinin (Figure 5a left panel, yellow box). Surprisingly, we found no correlation between alpha-actinin content and strain energy (Figure 5a right panel; Pearson r=0.08, R2=0.007). These results showed that the total amount of alpha-actinin alone was a poor predictor of force production and suggested that the relative proportion of this crosslinker compared to the actin filament may be more meaningful.

We thus decided to assess how the relative amount of actin and alpha-actinin were related to strain energy in cells (figure 5b left panel). We first noticed that alpha-actinin signal increased linearly with the signal corresponding to total actin filament content (Pearson r=0.59, R2=0.35 in Figure 5b left panel), showing that the levels of these proteins are correlated. However, by opposition to what we observed in the case of the myosin-F-actin relationship, forces appeared to be maximal when alpha-actinin levels were in the low range for a given amount of F-actin. This result appeared to be conflicting the hypothesis of the existence of an optimum ratio of crosslinker per actin filament. To explore further the relationship between alpha-actinin and F-actin, we next decided to plot the ratio of these protein contents as a function of the strain energy (Figure 5b right). We observed that the actinin to F-actin ratio was following an exponential decay trend (R2=0.48). This result indicated that for high actinin/F-actin ratios, meaning when alpha-actinin levels were high for a given amount of F-actin, the production of force was limited to a low range of force found below 0.4 pJ (Figure 5b right panel and c). On the contrary, high force production was limited to cells displaying low alpha-actinin per F-actin ratios, showing that in cells, a low amount of crosslinker per F-actin is required to generate high forces and thereby contradicting previous in vitro observations.

DISCUSSION

The implementation of an intermediate immuno-labelling step in the standard TFM assay allowed us to successfully measure traction force exerted by cells onto their underlying substrate and concomitantly access the biochemical composition of their actomyosin network and adhesion. By first applying this method to the study of the actomyosin network, we highlighted a complex relationship between its biochemical composition and the force generation and transmission at the level of the entire cell (Figures 3 and 4). By opposition, the FA area and composition appeared as a more straightforward readout of the force produced (Figure 2), which is consistent with the structural role of FA as the convergence point of all the forces produced in cells (Chang & Kumar, 2013). Indeed, the concomitant linear increase in vinculin signal and exponential increase in area with force, observed in a standardized ECM context and at a global cellular scale, corroborate previous work in which measurements were performed locally on mature adhesions and in migrating cells (Balaban et al., 2001; Goffin et al., 2006) and stem from the increase in the tension generated by the associated contractile machinery (Chrzanowska-Wodnicka & Burridge, 1996; Grashoff et al., 2010; Verma, Meng, Sachs, & Hua, 2015). Interestingly, we observed that the overall FA pattern organized into a peripheral belt whose length increased with strain energy (Figure 2c), as previously described in migrating cells (Mohl et al., 2012). We also noticed that while the length of this belt was constantly increasing with force up to forming a continuous structure along the rim of the cell, vinculin localization remained limited to a narrow band and did not progress above the more internal part of the adhesive micropattern. Previous study reported on the existence of a threshold spreading area for which both adhesion strength and focal adhesion assembly reached a saturation limit (Gallant, Michael, & Garcı, 2005) that could be at the origin of the phenotype observed in our cells. Altogether, these data suggest that the existence of an intrinsic limitation in the expansion of the adhesion pattern at the cell front may regulate the maximal force produced by the cells and transmitted to their surrounding substrate.

When analyzed at their individual level, both F-actin and phospho-myosin contents increase were correlated with increased strain energies (Figure 3a and 4a), in good agreement with the main role endorsed by myosin on actin filaments reorganization and pulling to generate intracellular contractility (Reymann et al., 2012; Stachowiak et al., 2012; Thoresen et al., 2011). However, their concomitant analysis in cells revealed a biphasic relationship of their ratio with force production as a minimum amount of total myosin per actin was required to produce force on one side, and on the opposite side, too much motor per F-actin turned out to impair force production (Figure 4c). These data highlighted the existence of an optimal ratio of molecular motor per F-actin setting the maximum of the force exerted by cells. These results are in good agreement with the complex role of myosin motors on both actin network reorganization, contraction and disassembly. Indeed, previous works reported that in addition to its role in generating force, myosin can disassemble actin filaments (Haviv, Gillo, Backouche, & Bernheim-Groswasser, 2008; Matsuda, Kobayashi, Sugawa, Koiso, & Yoko, 2018; Reymann et al., 2012; Wilson et al., 2010), which could account for the production of low traction forces in cells with high amount of myosins per actin filaments. These results suggested that at the level of the entire cell, the relative proportion of molecular motor per F-actin is key for regulating the amount of force produced by the cell.

By opposition to the relationship established between actin, myosin and force, the alpha-actinin content alone was identified as a very poor predictor of force (Figure 5a). The

ratio of crosslinker per actin filament as for it turned out to be in good correlation with cell strain energy (Figure 4b). In particular, we observed that the production of force required a low to intermediate amount of crosslinker per actin filament to produce high forces and that too much crosslinker per F-actin led to a drastic drop of the cell mechanical energy. Intriguingly, we did not observe the bell-shape contractile response curve previously described for both disorganized and structured actin networks in vitro (Alvarado, Sheinman, Sharma, MacKintosh, & Koenderink, 2013; Bendix et al., 2008; Ennomani et al., 2016) as we did not register any force drop corresponding to low actinin/F-actin ratios. As the present study was focusing on alpha-actinin analysis, we therefore cannot exclude that other crosslinkers such as paladin or filamin A, known to play a key role in force generation (Azatov, Goicoechea, Otey, & Upadhyaya, 2016; Kumar et al., 2019), were ensuring the network connectivity required for force production when alpha-actinin levels were low. We could also imagine that cells displaying very low amount of alpha-actinin per F-actin and corresponding to cells exerting low amount of force were not able to spread entirely on the micropattern and were thereby discarded from our analysis.

Our results further indicated that the total F-actin content was an equivalent predictor of force than the F-actin solely contained in stress fibers (Figure 3a and b). As actin filament in the SF represents in average only 50% +/-7 of the total F-actin, this result further indicated that actin filaments located in the SF were not the only contributors to force transmission to the substrate. Instead, these data supported the conclusions of previous works on the role of the cortical meshwork of F-actin in overall cell contractility (Kumar et al., 2019; Vignaud et al., 2020). In good agreement with this hypothesis, we noticed that the FA were not only found at the anchorage points of prominent peripheral fibers but also all around the adhesive edge of the micropattern (Figure 2a), indicating that the cortical mesh of actin is actively pulling on the substrate via these anchorage points.

We finally observed that despite sharing the same biochemical content, some cells still experienced significant variations in their strain energies. Regarding vinculin, these variations represent hallmarks of FA turnover, characterized by the assembly, maturation and disassembly events occurring during the migration process and leading to local changes in FA size and force (Ridley et al., 2003). However, as our measurements were performed at the level of the entire cell and in stationary cells, FA turnover in the context of migration cannot account for the cell to cell strain energy variations registered. Instead, these inter-cellular heterogeneities most likely result from the differences in the engagement of actomyosin bundles from focal adhesions (molecular clutch), thereby affecting the amount of force transmitted to the ECM. In addition, cell cycle status differences between cells could impact both the biochemical composition of the cells, as the cellular mass was shown to double during G1 phase (Son et al., 2012), and the force as significant variations can be registered during cell cycle progression (Vianay et al., 2018). We finally cannot exclude that this cell to cell heterogeneity could arise from subtle variations in actomyosin architectures or content not captured by our analysis. In support to this hypothesis, previous work demonstrated that the SF network architecture formed by cells spread on the same rectangular micropatterns could vary depending on the initial cell position (Kassianidou et al., 2019).

In conclusion, our method, in addition of being precise and unbiased by the topography of the substrate, offers a unique opportunity to study the relationship between any cellular

protein alone or in combination with its partners and force generated by the cells. Although the use of standard fluorophores for both protein labels, beads and micropatterns appeared as a limitation to the characterization of more than two proteins at a time in the present study, future work combining this method with spectral multiplexed imaging by DNA-PAINT technique (Jungmann et al., 2014; Wade et al., 2019), could theoretically extend the spectrum of analyzed proteins to virtually any protein of interest.

FIGURE LEGENDS

Figure 1: Development of a modified TFM assay including a fixation and labeling step enabling the concomitant traction force measurement and intracellular composition analysis.

a. Scheme displaying the two steps of a standard Traction Force Microscopy (TFM) assay.
b. Scheme of the modified TFM assay including an intermediate fixation and immunolabeling step of the cells.
c. Left panel: scheme of the dumbbell-shaped micropattern and its associated dimensions. Middle panel: representation of the micropattern in a field of view used for imaging and of the fiduciary marks in the corners used for rotation correction. Right panels: representative low magnification images of the dumbbell shaped micropatterns and fiduciary marks (Fibrinogen-cy3) used for retrieving the exact sample position between the different steps of the TFM process. Image scale bars = 100 µm.
d. Selected images of RPE-1 cells immunostained for vinculin, F-actin (phalloidin-ATTO488), p-MLC, alpha-actinin 4 and the associated traction stress maps computed in the same cells. Image scale bar = 10 µm. Force scale colour bar in Pa.

Figure supp 1

a. Left panel: overlay of an RPE-1 cell imaged in phase transmission and the adhesion micropattern (in red, fibrinogen-cy3); associated traction stress maps computed after cell removal and full gel relaxation. Force scale colour bar in Pa. Image scale bar = 10 µm. Right panel: overlay of the same RPE-1 cell fixed and labelled for actin (phalloidin-ATO-488) and the adhesion micropattern (in red, fibrinogen-cy3); associated traction stress maps computed after fixation and labeling. Force scale colour bar in Pa.
b. Schematic pipeline of the rotation correction steps. A first normalized cross-correlation step allows for translation in X and Y of the bead images. Then iterative rotation by 0.1° is performed until maximum normalized cross-correlation coefficient is obtained.

Figure supp 2

a. Phase transmission image of RPE-1 cells acquired at low magnification and overlaid with their micropattern image (in red: fibrinogen-cy3); Image scale bar = 50 µm.
b. Images of RPE-1 cells acquired at low magnification (phase transmission overlaid with fibrinogen-cy3 signal in red) displaying examples of cells discarded from the analyses. Left panel image displays a cell not fully spread on the micropattern; Middle and right panels point at cells “escaping” the micropattern; Image scale bar = 20 µm.

Figure 2: Total cellular vinculin content and area represent good predictors of cell strain energy

a. From top to bottom: Images of RPE-1 cells labelled for vinculin; corresponding binary images obtained following image thresholding by intensity; associated traction stress maps. Image scale bar = 10 µm. Force scale colour bar in Pa.
b. Upper panel: scatter plot of the strain energy (pJ) as a function of total vinculin area (µm2). The data were pooled from two independent experiments. Color-coded points following the trend of an exponential regression were selected and the corresponding cells and traction stress maps highlighted above in a with the same colors. The corresponding R square is indicated on top of the plot.
   Bottom panel: scatter plot of the strain energy (pJ) as a function of total vinculin signal intensity (au). The Pearson correlation coefficients and corresponding R square are indicated on top of the plot.
c. From top to bottom: representation of averaged intensity projections of vinculin stainings from cells displaying increasing strain energy (n=33 cells for each image). Averaged strain energy values for each group is indicated at the bottom left of the image. Image scale bar = 10 µm.

Figure 3: Total F-actin and F-actin content of the SF increase linearly with force and exhibit broad variations to this linear relationship.

a. Top panel: image of an RPE-1 cell depicting the area used for measurement of total F-actin signal (yellow box). Image scale bar = 10 µm
   Bottom panel: scatter plot of the strain energy (pJ) as a function of total actin signal (au). Different color-coded points were selected on the plot and the corresponding cells and traction stress maps are highlighted in the images below in c. Pink indicate cells following a linear regression; orange: cells exerting the same level of strain energy but displaying a high variability in their actin content; green: cells displaying the same actin content but a high variability in strain energies.
b. Top panel: image of an RPE-1 cell depicting the area used for measurement of total actin signal (yellow box) or actin signal in stress fibers (red lines). Image scale bar = 10 µm
   Bottom panel: scatter plot of the strain energy (pJ) as a function of F-actin signal in peripheral stress fibers (au). The Pearson correlation coefficients and corresponding R square are indicated on top of the plots.
c. Top panels: images of RPE-1 cells labelled for actin (phalloidin-ATO-488); Bottom panels: corresponding traction stress maps. Image scale bar = 10 µm. Force scale in Pa. The color-code refers to the points highlighted in the above scatter plot in b.

Figure 4: The actomyosin ratio displays an optimal range allowing for the production of high forces

a. Left panel: image of an RPE-1 cell depicting the area used for measurement of total myosin signal (yellow box). Image scale bar = 10 µm. Right panel: scatter plot of the strain energy (pJ) as a function of total actin signal (au). Different color-coded points were selected on the plot and the corresponding cells and traction stress maps are highlighted in the images below in b. Pink indicate cells following a linear regression; orange: cells sharing the same level of strain energy but displaying a high variability in

their myosin content; green: cells displaying the same myosin content but a high variability in strain energies. The Pearson correlation coefficient and corresponding R square is indicated on top of the plot.

b. Top panels: images of RPE-1 cells labelled for myosin (p-MLC-488); Bottom panels: corresponding traction stress maps. Image scale bar = 10 µm. Force scale in Pa.
The color-code refers to the points highlighted in the above scatter plot in a.

c. Left panel: scatter plot of total myosin signal as a function of total F-actin signal in dual labelled cells. Dots were color-coded according to the strain energy scale measured for individual cells. Right panel: scatter plot of the strain energy (pJ) as a function of total myosin/F-actin signal (au) in dual labelled cells. The same color-code as displayed in the left panel was used to highlight strain energy values of each individual cell. The Pearson correlation coefficient and corresponding R squares are indicated on the plots.

Figure 5: The relative amount of alpha-actinin per total F-actin controls the magnitude of force production

a. Left panel: image of an RPE-1 cell depicting the area used for measurement of total alpha-actinin signal (yellow box). Image scale bar = 10 µm. Right panel: scatter plot of the strain energy (pJ) as a function of total alpha-actinin signal (au) in dual labelled cells. The Pearson correlation coefficient and corresponding R square are indicated on top of the plot.

b. Left panel: scatter plot of the total alpha-actinin signal as a function of total F-actin signal (au). The Pearson correlation coefficient and corresponding R square are indicated on top of the plot. Dots were color-coded according to the strain energy values measured for each individual cell.
Right panel: scatter plot of the strain energy (pJ) as a function of total actinin/F-actin ratio (au). The R square corresponding to an exponential decay fit is indicated on top of the plot. The same color-code as displayed in the left panel was used to highlight strain energy values of each individual cell.

c. Top panels: selected images of RPE-1 cells labelled for alpha-actinin (alpha-actinin4-488) displaying an increase in their alpha-actinin total content and corresponding traction stress maps. Image scale bar = 10 µm. Force scale in Pa.
Bottom panels: zoom in images corresponding to yellow insets above displaying actin, alpha-actinin and overlays of both labels in the same cells. Image scale bar = 10 µm.

MATERIAL AND METHODS

Photomask design

The photomask was designed using CleWin software and then provided by TOPPAN Photomasks Inc. company. The dumbbell-shaped micropattern (Figure 1c) was designed as previously described in (Vignaud et.al, Nat. Mat., 2020). The micropattern consisted of two disks of 12 µm diameter separated by a center to center distance of 47 µm. The disks were connected by a 1 µm width line guiding the cell spreading between them. The micropattern was oriented at 45 degrees angle to the horizontal, thereby providing the greatest separation between adjacent micropatterns and avoiding the beads displacement from adjacent cells to

be detected in the imaging field of view. Every third dumbbell micropattern was numbered (Figure1c) in both horizontal and vertical directions for redundancy in finding cells.
Fiduciary marks were designed in addition to the dumbbells in order to retrieve the exact sample location during the different steps of the process including sample removal from the microscope stage. The camera field of view when using a 60X objective was 113.6 µm * 113.6 µm. A single, vertical and horizontal array of circles (diameter 113.6 µm, center-center distance 227.2 µm), intersecting at the center of the pattern field divided the sample into four quadrants. At the center of the pattern field, where the arrays of circles intersect, the letters A, B, C, D were placed as shown in Figure1c. These arrays of circles and the letters were used for preliminary translation and rotation alignment on the microscope performed manually. On the four vertices of each region, with the letter/circle patterns in the center, a set of small symbols (+, o, □) of 10 um width and height and 2 µm line thickness were used for the final manual rotation correction. When these were present at the vertices of the camera field of view, the gel was considered to be aligned, achieving a rotation error of less than 1°.

Preparation of micropatterned polyacrylamide gels

Patterned polyacrylamide hydrogels were prepared following the guidelines previously described in (Vignaud, Ennomani, & Théry, 2014). A quartz photomask was first cleaned through oxygenplasma (AST product, 300 W) for 3.5 min at 200 W. Micropatterns are were then incubated with 0.1 mg/ml PLL-g-PEG (JenKem Technology ZL187P072) in 10mM HEPES pH 7.4, for 30 min. After de-wetting, the mask was exposed under deep-UV for 5 min. Next, patterns on the mask were incubated with a mix of 10 µg/ml fibronectin (#F1141, Sigma) and 20 µg/ml fibrinogen-Alexa-Fluor-647 conjugate (#F35200, Invitrogen) in 100mM sodium bicarbonate buffer pH=8.4 for 30 min. A mix of acrylamide (8%) and bis-acrylamide solution (0.264%) (Sigma) corresponding to a theoritical Young modulus of 19.66 kPa was degassed for approximately 30 min, mixed with 0.2 µm PLL-PEG covalently coated fluorescent beads (Fluorosphere #F8810, Life Technologies) and sonicated before addition of APS and TEMED. 25 µl of that solution was added on the micropatterned photomask, covered with a silanized coverslip (Silane, #M6514, Sigma) and allowed to polymerize for 25 min before being gently detached in the presence of sodium bicarbonate buffer. Micropatterns were stored overnight in sodium bicarbonate buffer at 4°C before plating cells.

Cell culture

Human telomerase-immortalized retinal-pigmented epithelial cells (hTERT RPE-1 from ATCC® CRL-4000™) were grown in a humidified incubator at 37°C and 5% CO2 in DMEM/F12 medium supplemented with 10% fetal bovine serum and 1% Antibiotic-Antimycotic (Thermo Fisher Scientific). Cells were plated at approximately 15000 cells/ml on patterned polyacrylamide gels and left to spread for 3 to 4 hours before imaging.

Imaging process for traction force microscopy assay

Traction force mapping and immunostainings were performed and imaged on a Nikon confocal spinning-disc system (EclipseTi-E) equipped with a CSUX1-A1 Yokogawa confocal head and an Evolve EMCCD camera from Roper Scientific, Princeton Instruments). A 20X objective was used for initial placement of the sample on the field of view (PlanAPO 20X/0.75). At this

magnification, a 3x3 array of the patterns fit within the imaging window. The sample was manually rotated to the correct orientation using the alignment marks next to the micropatterns. It was then manually translated using the numbering next to the patterns as reference to get to the center of the pattern field which contains the patterned letters A,B,C and D (Figure1 c). The 60X oil objective was then used for acquisition following minor rotation and translation adjustments done manually to get one of the letters within the field of view with the alignment marks appearing at the four corners of the imaging window. The stage position of the chosen letter was recorded to be used as reference when realigning the system for imaging the sample at the different steps of the process.

Well spread individual cells on the micropatterns were selected by manually scanning the gel and their position was recorded along with the fiduciary marks. Live cells together with their micropatterns and the beads corresponding to the deformed gel configuration were first imaged. Following sample removal from the stage-top, cells were then pre-permeabilized, fixed and labelled using the antibodies of interest. The sample was then placed back on the Stage-Top and moved to the reference position recorded earlier. A re-alignment to the reference letter chosen earlier at 20X and minor corrections were then performed at 60X. The cells were next imaged for the fluorescent components (10 z slices, 0.75 µm spacing), the beads and the micropatterns. During the whole process, the temperature was maintained at 37° C and the gels were kept in a wet environment to avoid any changes in the gel mechanical properties.

To detach cells, the samples were left overnight in 10X TGS buffer (BIO-RAD, 161-0772), washed four times with PBS and then treated with TryplE reagent (Gibco, 12605-010) for 1 hour at 37° C. The cells detached on pipetting onto the surface of the gel vigorously. After cell detachment, the gels were placed back onto the Stage-top incubator, realigned and the positions were reimaged for the beads, micropatterns.

Fixation and labelling

For labelling p-MLC, alpha-actinin and Vinculin, cells were pre-permeabilized in 0.5% Triton X-100 in Cytoskeleton buffer for 10 seconds and then immediately fixed in 4% paraformaldehyde in Cytoskeleton buffer with 10% sucrose, pH 6.1 for 20 minutes at room temperature. The cells were washed twice in cytoskeletal buffer to be rid of excess paraformaldehyde and then quenched in 0.1 M ammonium chloride for 10 minutes then washed thrice in PBS, 10 minutes/wash. A solution of 1% BSA and 10% FBS in PBS was used or blocking, for 1 hour at room temperature before being incubated with appropriate dilutions of primary antibodies in PBS containing 1% BSA and 0.1% Tween overnight at 4° C in a humid chamber.

The primary antibodies used were, anti-phospho-myosin light chain 2 (#3671, CST), anti-alpha actinin (#05-384, Millipore), anti-alpha actinin4 (19096-1-AP, Protein tech) and Anti vinculin-clone hVIN-1(V9131, Sigma). The secondaries used are anti-rabbit Alexa Fluor-488 (A21441, Molecular Probes) and anti-mouse Alexa Fluor-546 (A11003, Invitrogen). For the data set where actin alone was imaged, pre-permeabilization was not performed. The cells were fixed, washed thrice in PBS, and labelled for F-actin using Phalloidin-FITC (#P5282, Sigma).

Image Processing

Analyses were performed using Matlab software. A maximum intensity projection of the z-stacks of each fluorescently labelled cells was first created. The images were rotated by 45 degrees to have the long axis of the cell horizontal in the image, cropped to 300*300 pixel dimension with the cells in the center. The average signal intensity in a 50*50 pixel region at the top of the cropped image was calculated for noise subtraction. The sum of the signal in all the pixels after subtracting the noise provided the relative measure of the total protein content in each cell. From all the cells imaged, only those with two well established stress fibers, one on either side of the long axis of the cell were chosen for quantification of the fluorescent signal and TFM analysis.

Translation and rotation correction was performed using the normxcorr2 function in custom written functions that work as described below. Translation correction done using the peak in the normalized cross-correlation matrix (C) between the reference bead image (With force, Figure 1a) and for the bead image to be corrected (Relaxed configuration, Figure 1a). The normalized cross-correlation between the With force image and Translation corrected, image (Translation corrected') rotated by 0.1° in both clockwise and anti clockwise directions is calculated. The direction with the highest value of C is chosen to be the direction of rotation (b). The rotation and calculation of C, correcting for translation at each step is iteratively done, comparing the C for the nth iteration with the (n-1)th iteration until the first iteration where C decreases compared to the previous iteration. The angle of rotation is given by (n-1)*0.1°. The final translation and rotation correction values are then propagated to the pattern and cell images. Similarly, translation and rotation correction is done for the image of the Partially relaxed gel (Figure 1b), with respect to the With force image and the correction propagated to the images of the pattern and fluorescently labelled components. The functions are available provided in supplementary information.

Measurement of cell traction forces with ImageJ

Data were analyzed with a set of macros in Fiji using the method previously described in (Martiel et al., 2015). Displacement fields were obtained from fluorescent bead images before and after removal of cells by trypsin treatment. Bead images that were already corrected for rotation and translation as described earlier were again paired and re-aligned with a macro that corrected with subpixel accuracy. Displacement fields were calculated by particle imaging velocimetry (PIV) which uses a normalized cross-correlation based method with an iterative scheme. Final vector-grid size ranged from 1.55 µm X 1.55 µm. Erroneous vectors where discarded owing to their low correlation value and replaced by the mean value of the neighboring vectors. Fourier-transform traction cytometry was used to compute the Traction-force field, with a regularization parameter set to 3.2 x 10-10. Force vectors located outside of the micropattern area were discarded for calculation of strain energy.

Data analysis

Vinculin quantification has been performed using the "Focal Adhesion Analysis" server (https://faas.bme.unc.edu/) (Berginski, Vitriol, Hahn, & Gomez, 2011) https://doi.org/10.1371/journal.pone.0022025

+ https://doi.org/10.1016/j.cell.2011.12.034) with default settings. We used two global parameters for the quantification, i.e., the total adhesion area per cell and the total adhesion signal, respectively the sum of the area and the signal of the detected adhesion structures.

Data plotting

For multiparametric representation graphs have been produced using R (https://www.r-project.org/) and RStudio (https://rstudio.com/) relying on the use of the "plot3D" package (Karline Soetaert. plot3D: Tools for plotting 3-D and 2-D data. http://cran.r-project.org/web/packages/plot3D/vignettes/plot3D.pdf).

Statistical analysis

Statistical analysis and chart design was performed using Graphpad Prism 6 (www.graphpad.com) and R version 3.4.0 together with RStudio version 1.0.143.

FUNDING

This work was supported by grants from European Research Council (741773, AAA) awarded to LB, (771599, ICEBERG) awarded to MT, from Agence Nationale de la recherche ANR (ANR-14-CE11-0003-01, MaxForce) awarded to LB and MT.

ACKNOWLEDGEMENTS

We thank the live microscopy facility MuLife of IRIG/DBSCI, funded by CEA Nanobio and labex Gral for equipment access and use.

COMPETING INTERESTS

The authors declare no competing or financial interests.

REFERENCES

- Agarwal, P., & Zaidel-Bar, R. (2019). Principles of Actomyosin Regulation In Vivo. Trends in Cell Biology, 29(2), 150–163. https://doi.org/10.1016/j.tcb.2018.09.006

- Alvarado, J., Sheinman, M., Sharma, A., MacKintosh, F. C., & Koenderink, G. H. (2013). Molecular motors robustly drive active gels to a critically connected state. Nature Physics, 9(September). https://doi.org/10.1038/nphys2715

- Azatov, M., Goicoechea, S. M., Otey, C. A., & Upadhyaya, A. (2016). The actin crosslinking protein palladin modulates force generation and mechanosensitivity of tumor associated fibroblasts. Scientific Reports, 6(June), 1–12. https://doi.org/10.1038/srep28805

- Balaban, N. Q., Schwarz, U. S., Riveline, D., Goichberg, P., Tzur, G., Sabanay, I., … Geiger, B. (2001). Force and focal adhesion assembly: a close relationship studied using elastic micropatterned substrates. Nature Cell Biology, 3(5), 466–472. https://doi.org/10.1038/35074532

- Banda, O. A., Sabanayagam, C. R., & Slater, J. H. (2019). Reference-Free Traction Force Microscopy Platform Fabricated via Two-Photon Laser Scanning Lithography Enables Facile Measurement of Cell-Generated Forces. ACS Applied Materials & Interfaces, 11(20), 18233–18241. https://doi.org/10.1021/acsami.9b04362

- Bendix, P. M., Koenderink, G. H., Cuvelier, D., Dogic, Z., Koeleman, B. N., Brieher, W. M., … Weitz, D. A. (2008). A Quantitative Analysis of Contractility in Active Cytoskeletal Protein Networks. Biophysical Journal, 94(8), 3126–3136. https://doi.org/10.1529/biophysj.107.117960

- Beningo, K. A., Dembo, M., Kaverina, I., Small, J. V., & Wang, Y. (2001). Nascent Focal Adhesions Are Responsible for the Generation of Strong Propulsive Forces in Migrating Fibroblasts. The Journal of Cell Biology, 153(4), 881–888. https://doi.org/10.1083/jcb.153.4.881

- Bergert, M., Lendenmann, T., Zündel, M., Ehret, A. E., Panozzo, D., Richner, P., … Ferrari, A. (2016). Confocal reference free traction force microscopy. Nature Communications, 7. https://doi.org/10.1038/ncomms12814

- Berginski, M. E., Vitriol, E. A., Hahn, K. M., & Gomez, S. M. (2011). High-Resolution Quantification of Focal Adhesion Spatiotemporal Dynamics in Living Cells. PLoS ONE, 6(7), e22025. https://doi.org/10.1371/journal.pone.0022025

- Burridge, K., & Wittchen, E. S. (2013). The tension mounts: Stress fibers as force-generating mechanotransducers. Journal of Cell Biology, 200(1), 9–19. https://doi.org/10.1083/jcb.201210090

- Califano, J. P., & Reinhart-King, C. a. (2010). Substrate Stiffness and Cell Area Predict Cellular Traction Stresses in Single Cells and Cells in Contact. Cellular and Molecular Bioengineering, 3(1), 68–75. https://doi.org/10.1007/s12195-010-0102-6

- Chang, C. W., & Kumar, S. (2013). Vinculin tension distributions of individual stress fibers within cell-matrix adhesions. Journal of Cell Science, 126(14), 3021–3030. https://doi.org/10.1242/jcs.119032

- Chrzanowska-Wodnicka, M., & Burridge, K. (1996). Rho-stimulated contractility drives the formation of stress fibers and focal adhesions. Journal of Cell Biology, 133(6), 1403–1415. https://doi.org/10.1083/jcb.133.6.1403

- Deguchi, S., Ohashi, T., & Sato, M. (2005). Evaluation of tension in actin bundle of endothelial cells based on preexisting strain and tensile properties measurements. Molecular and Cellular Biomechanics, 2(3), 125–133. https://doi.org/10.3970/mcb.2005.002.125

- Dembo, M., & Wang, Y.-L. (1999). Stresses at the Cell-to-Substrate Interface during Locomotion of Fibroblasts. Biophysical Journal, 76(4), 2307–2316. https://doi.org/10.1016/S0006-3495(99)77386-8

- DePasquale, J. A., & Izzard, C. S. (1987). Evidence for an Actin-containing Cytoplasmic Precursor of the Focal Contact and the Timing of Incorporation of Vinculin at the Focal Contact. Journal of Cell Biology, 105(6), 2803–2809. https://doi.org/10.1083/jcb.105.6.2803

- Doss, B. L., Pan, M., Gupta, M., Grenci, G., Mège, R.-M., Lim, C. T., … Ladoux, B. (2020). Cell response to substrate rigidity is regulated by active and passive cytoskeletal stress. Proceedings of the National Academy of Sciences, 117(23), 12817–12825. https://doi.org/10.1073/pnas.1917555117

- Edlund, M., Lotano, M. A., & Otey, C. A. (2001). Dynamics of α-actinin in focal adhesions and stress fibers visualized with α-actinin-green fluorescent protein. Cell Motility and the Cytoskeleton, 48(3), 190–200. https://doi.org/10.1002/1097-0169(200103)48:3<190::AID-CM1008>3.0.CO;2-C

- Elosegui-Artola, A., Oria, R., Chen, Y., Kosmalska, A., Pérez-González, C., Castro, N., … Roca-Cusachs, P. (2016). Mechanical regulation of a molecular clutch defines force transmission and transduction in response to matrix rigidity. Nature Cell Biology, 18(5), 540–548. https://doi.org/10.1038/ncb3336

- Ennomani, H., Letort, G., Guérin, C., Martiel, J.-L., Cao, W., Nédélec, F., … Blanchoin, L. (2016). Architecture and Connectivity Govern Actin Network Contractility. Current Biology, 25(4), 368–379. https://doi.org/10.1016/j.cogdev.2010.08.003.Personal

- Gallant, N. D., Michael, K. E., & Garcı, J. (2005). Cell Adhesion Strengthening : Contributions of Adhesive Area , Integrin Binding , and Focal Adhesion Assembly. Molecular Biology of the Cell, 16(September), 4329–4340. https://doi.org/10.1091/mbc.E05

- Geiger, B., Bershadsky, A., Pankov, R., & Yamada, K. M. (2001). Transmembrane crosstalk between the extracellular matrix and the cytoskeleton. Nature Reviews Molecular Cell Biology, 2(11), 793–805. https://doi.org/10.1038/35099066

- Ghagre, A., Amini, A., Srivastava, L. K., Tirgar, P., Khavari, A., Koushki, N., & Ehrlicher, A. (2020). Pattern-based Contractility Screening (PaCS), a reference-free traction force microscopy methodology, reveals contractile differences in breast cancer cells. BioRxiv. https://doi.org/10.1101/2020.05.14.097006

- Goffin, J. M., Pittet, P., Csucs, G., Lussi, J. W., Meister, J., & Hinz, B. (2006). Focal adhesion size controls tension-dependent recruitment of α-smooth muscle actin to stress fibers. Journal of Cell Biology, 172(2), 259–268. https://doi.org/10.1083/jcb.200506179

- Grashoff, C., Hoffman, B. D., Brenner, M. D., Zhou, R., Parsons, M., Yang, M. T., … Schwartz, M. A. (2010). Measuring mechanical tension across vinculin reveals regulation of focal adhesion dynamics. Nature, 466(7303), 263–266. https://doi.org/10.1038/nature09198

- Haviv, L., Gillo, D., Backouche, F., & Bernheim-Groswasser, A. (2008). A Cytoskeletal Demolition Worker: Myosin II Acts as an Actin Depolymerization Agent. Journal of Molecular Biology, 375(2), 325–330. https://doi.org/10.1016/j.jmb.2007.09.066

- Heisenberg, C. P., & Bellaïche, Y. (2013). Forces in tissue morphogenesis and patterning. Cell, 153(5). https://doi.org/10.1016/j.cell.2013.05.008

- Jensen, M. H., Morris, E. J., & Weitz, D. A. (2015). Mechanics and dynamics of reconstituted cytoskeletal systems. Biochimica et Biophysica Acta (BBA) - Molecular Cell Research, 1853(11), 3038–3042. https://doi.org/10.1016/j.bbamcr.2015.06.013

- Jungmann, R., Avendaño, M. S., Woehrstein, J. B., Dai, M., Shih, W. M., & Yin, P. (2014). Multiplexed 3D cellular super-resolution imaging with DNA-PAINT and Exchange-PAINT. Nature Methods, 11(3), 313–318. https://doi.org/10.1038/nmeth.2835

- Kassianidou, E., Probst, D., Jäger, J., Lee, S., Roguet, A.-L., Schwarz, U. S., & Kumar, S. (2019). Extracellular Matrix Geometry and Initial Adhesive Position Determine Stress Fiber Network Organization during Cell Spreading. Cell Reports, 27(6), 1897-1909.e4. https://doi.org/10.1016/j.celrep.2019.04.035

- Katoh, K., Kano, Y., Masuda, M., Onishi, H., & Fujiwara, K. (1998). Isolation and contraction of the stress fiber. Molecular Biology of the Cell, 9(7), 1919–1938. https://doi.org/10.1091/mbc.9.7.1919

- Kilian, K. A., Bugarija, B., Lahn, B. T., & Mrksich, M. (2010). Geometric cues for directing the differentiation of mesenchymal stem cells. Proceedings of the National Academy of Sciences of the United States of America, 107(11), 4872–4877. https://doi.org/10.1073/pnas.0903269107

- Koenderink, G. H., & Paluch, E. K. (2018). Architecture shapes contractility in actomyosin networks. Current Opinion in Cell Biology, 50, 79–85. https://doi.org/10.1016/j.ceb.2018.01.015

- Kraning-rush, C. M., Carey, S. P., Califano, J. P., Smith, B. N., & Reinhart-king, C. A. (2011). The role of the cytoskeleton in cellular force generation in 2D and 3D environments. Physical Biology, 8(1), 1–19. https://doi.org/10.1088/1478-3975/8/1/015009.

- Kumar, A., Shutova, M. S., Tanaka, K., Iwamoto, D. V., Calderwood, D. A., Svitkina, T. M., & Schwartz, M. A. (2019). Filamin A mediates isotropic distribution of applied force across the actin network. Journal of Cell Biology, 218(8), 2481–2491. https://doi.org/10.1083/jcb.201901086

- Kurzawa, L., Vianay, B., Senger, F., Vignaud, T., Blanchoin, L., & Théry, M. (2017). Dissipation of contractile forces: the missing piece in cell mechanics. Molecular Biology of the Cell, 28(14), 1825–1832. https://doi.org/10.1091/mbc.E16-09-0672

- Langanger, G., Moeremans, M., Daneels, G., Sobieszek, A., De Brabander, M., & De Mey, J. (1986). The molecular organization of myosin in stress fibers of cultured cells. Journal of Cell Biology, 102(1), 200–209. https://doi.org/10.1083/jcb.102.1.200

- Lazarides, E., & Burridge, K. (1975). α-Actinin: Immunofluorescent localization of a muscle structural protein in nonmuscle cells. Cell, 6(3), 289–298. https://doi.org/10.1016/0092-8674(75)90180-4

- Leal-Egaña, A., Letort, G., Martiel, J.-L., Christ, A., Vignaud, T., Roelants, C., … Théry, M. (2017). The size-speed-force relationship governs migratory cell response to tumorigenic factors. Molecular Biology of the Cell, 28(12), 1612–1621. https://doi.org/10.1091/mbc.e16-10-0694

- Linsmeier, I., Banerjee, S., Oakes, P. W., Jung, W., Kim, T., & Murrell, M. P. (2016). Disordered actomyosin networks are sufficient to produce cooperative and telescopic contractility. Nature Communications, 7(1), 12615. https://doi.org/10.1038/ncomms12615

- Lo, C., Wang, H.-B., Dembo, M., & Wang, Y. (2000). Cell Movement Is Guided by the Rigidity of the Substrate. Biophysical Journal, 79(1), 144–152. https://doi.org/10.1016/S0006-3495(00)76279-5

- Luo, W., Yu, C., Lieu, Z. Z., Allard, J., Mogilner, A., Sheetz, M. P., & Bershadsky, A. D. (2013). Analysis of the local organization and dynamics of cellular actin networks. The Journal of Cell Biology, 202(7), 1057–1073. https://doi.org/10.1083/jcb.201210123

- Ma, J., Bai, L., & Wang, M. D. (2013). Transcription Under Torsion. Science, 340(6140), 1580–1583. https://doi.org/10.1126/science.1235441

- Maiuri, P., Rupprecht, J. F., Wieser, S., Ruprecht, V., Bénichou, O., Carpi, N., … Voituriez, R. (2015). Actin flows mediate a universal coupling between cell speed and cell persistence. Cell, 161(2), 374–386. https://doi.org/10.1016/j.cell.2015.01.056

- Malinverno, C., Corallino, S., Giavazzi, F., Bergert, M., Li, Q., Leoni, M., … Scita, G. (2017). Endocytic reawakening of motility in jammed epithelia. Nature Materials, 16(5), 587–596. https://doi.org/10.1038/nmat4848

- Martiel, J.-L., Leal, A., Kurzawa, L., Balland, M., Wang, I., Vignaud, T., … Théry, M. (2015). Measurement of cell traction forces with ImageJ. In Methods in Cell Biology (Vol. 125, pp. 269–287). https://doi.org/10.1016/bs.mcb.2014.10.008

- Matsuda, K., Kobayashi, T., Sugawa, M., Koiso, Y., & Yoko, Y. (2018). Myosin-driven fragmentation of actin filaments triggers contraction of a disordered actin network. BioRxiv.

- McBeath, R., Pirone, D. M., Nelson, C. M., Bhadriraju, K., & Chen, C. S. (2004). Cell Shape, Cytoskeletal Tension, and RhoA Regulate Stem Cell Lineage Commitment. Developmental Cell, 6(1), 483–495. https://doi.org/10.1016/S1534-5807(04)00075-9

- Mohl, C., Kirchgessner, N., Schafer, C., Hoffmann, B., & Merkel, R. (2012). Quantitative mapping of averaged focal adhesion dynamics in migrating cells by shape normalization. Journal of Cell Science, 125(1), 155–165. https://doi.org/10.1242/jcs.090746

- Murrell, M., Oakes, P. W., Lenz, M., & Gardel, M. L. (2015). Forcing cells into shape: the mechanics of actomyosin contractility. Nature Reviews Molecular Cell Biology, 16(8), 486–498. https://doi.org/10.1038/nrm4012

- Naumanen, P., Lappalainen, P., & Hotulainen, P. (2008). Mechanisms of actin stress fibre assembly. In Journal of Microscopy (Vol. 231, pp. 446–454). https://doi.org/10.1111/j.1365-2818.2008.02057.x

- Oakes, P. W., Beckham, Y., Stricker, J., & Gardel, M. L. (2012). Tension is required but not sufficient for focal adhesion maturation without a stress fiber template. The Journal of Cell Biology, 196(3), 363–374. https://doi.org/10.1083/jcb.201107042

- Plotnikov, S. V., Pasapera, A. M., Sabass, B., & Waterman, C. M. (2012). Force Fluctuations within Focal Adhesions Mediate ECM-Rigidity Sensing to Guide Directed Cell Migration. Cell, 151(7), 1513–1527. https://doi.org/10.1016/j.cell.2012.11.034

- Pushkarsky, I., Tseng, P., Black, D., France, B., Warfe, L., Koziol-White, C. J., … Di Carlo, D. (2018). Elastomeric sensor surfaces for high-throughput single-cell force cytometry. Nature Biomedical Engineering, 2(2), 124–137. https://doi.org/10.1038/s41551-018-0193-2

- Rape, A. D., Guo, W., & Wang, Y.-L. (2011). The regulation of traction force in relation to cell shape and focal adhesions. Biomaterials, 32(8), 2043–2051. https://doi.org/10.1016/j.biomaterials.2010.11.044

- Reinhart-King, C. A., Dembo, M., & Hammer, D. A. (2003). Endothelial Cell Traction Forces on RGD-Derivatized Polyacrylamide Substrata †. Langmuir, 19(5), 1573–1579. https://doi.org/10.1021/la026142j

- Reymann, A.-C. A., Boujemaa-paterski, R., Martiel, J.-L. J., Guerin, C., Cao, W., Chin, H. F., … Blanchoin, L. (2012). Actin Network Architecture Can Determine Myosin Motor Activity. Science, 336(6086), 1310–1314. https://doi.org/10.1126/science.1221708.

- Ridley, A. J., Schwartz, M. A., Burridge, K., Firtel, R. A., Ginsberg, M. H., Borisy, G., … Horwitz, A. R. (2003). Cell Migration: Integrating Signals from Front to Back. Science, 302(5651), 1704–1709. https://doi.org/10.1126/science.1092053

- Roca-Cusachs, P., Conte, V., & Trepat, X. (2017). Quantifying forces in cell biology. Nature Cell Biology, 19(7), 742–751. https://doi.org/10.1038/ncb3564

- Sedzinski, J., Biro, M., Oswald, A., Tinevez, J.-Y., Salbreux, G., & Paluch, E. (2011). Polar actomyosin contractility destabilizes the position of the cytokinetic furrow. Nature, 476(7361), 462–466. https://doi.org/10.1038/nature10286

- Senger, F., Pitaval, A., Ennomani, H., Kurzawa, L., Blanchoin, L., & Théry, M. (2019). Spatial integration of mechanical forces by α-actinin establishes actin network symmetry. Journal of Cell Science, 132(22), jcs236604. https://doi.org/10.1242/jcs.236604

- Son, S., Tzur, A., Weng, Y., Jorgensen, P., Kim, J., Kirschner, M. W., & Manalis, S. R. (2012). Direct observation of mammalian cell growth and size regulation. Nature Methods, 9(9), 910–912. https://doi.org/10.1038/nmeth.2133

- Stachowiak, M. R., McCall, P. M., Thoresen, T., Balcioglu, H. E., Kasiewicz, L., Gardel, M. L., & O'Shaughnessy, B. (2012). Self-Organization of Myosin II in Reconstituted Actomyosin Bundles. Biophysical Journal, 103(6), 1265–1274. https://doi.org/10.1016/j.bpj.2012.08.028

- Stricker, J., Aratyn-Schaus, Y., Oakes, P. W., & Gardel, M. L. (2011). Spatiotemporal Constraints on the Force-Dependent Growth of Focal Adhesions. Biophysical Journal, 100(12), 2883–2893. https://doi.org/10.1016/j.bpj.2011.05.023

- Tan, J. L., Tien, J., Pirone, D. M., Gray, D. S., Bhadriraju, K., & Chen, C. S. (2003). Cells lying on a bed of microneedles: An approach to isolate mechanical force. Proceedings of the National Academy of Sciences, 100(4), 1484–1489. https://doi.org/10.1073/pnas.0235407100

- Thoresen, T., Lenz, M., & Gardel, M. L. (2011). Reconstitution of Contractile Actomyosin Bundles. Biophysical Journal, 100(11), 2698–2705. https://doi.org/10.1016/j.bpj.2011.04.031

- Trichet, L., Le Digabel, J., Hawkins, R. J., Vedula, S. R. K., Gupta, M., Ribrault, C., … Ladoux, B. (2012). Evidence of a large-scale mechanosensing mechanism for cellular adaptation to substrate stiffness. Proceedings of the National Academy of Sciences, 109(18), 6933–6938. https://doi.org/10.1073/pnas.1117810109

- Tseng, Q., Wang, I., Duchemin-Pelletier, E., Azioune, A., Carpi, N., Gao, J., … Balland, M. (2011). A new micropatterning method of soft substrates reveals that different tumorigenic signals can promote or reduce cell contraction levels. Lab on a Chip, 11(13), 2231. https://doi.org/10.1039/c0lc00641f

- Verma, D., Meng, F., Sachs, F., & Hua, S. Z. (2015). Flow-induced focal adhesion remodeling mediated by local cytoskeletal stresses and reorganization. Cell Adhesion & Migration, 9(6), 432–440. https://doi.org/10.1080/19336918.2015.1089379

- Vianay, B., Senger, F., Alamos, S., Anjur-Dietrich, M., Bearce, E., Cheeseman, B., … Thery, M. (2018). Variation in traction forces during cell cycle progression. Biology of the Cell, 110(4), 91–96. https://doi.org/10.1111/boc.201800006

- Vignaud, T., Copos, C., Leterrier, C., Toro-Nahuelpan, M., Tseng, Q., Mahamid, J., … Kurzawa, L. (2020). Stress fibres are embedded in a contractile cortical network. Nature Materials. https://doi.org/10.1038/s41563-020-00825-z

- Vignaud, T., Ennomani, H., & Théry, M. (2014). Polyacrylamide Hydrogel Micropatterning. Methods in Cell Biology, 120, 93–116. https://doi.org/10.1016/B978-0-12-417136-7.00006-9

- Wade, O. K., Woehrstein, J. B., Nickels, P. C., Strauss, S., Stehr, F., Stein, J., … Jungmann, R. (2019). 124-Color Super-resolution Imaging by Engineering DNA-PAINT Blinking Kinetics. Nano Letters, 19(4), 2641–2646. https://doi.org/10.1021/acs.nanolett.9b00508

- Ma, J., Bai, L., & Wang, M. D. (2013). Transcription Under Torsion. Science, 340(6140), 1580–1583.https://doi.org/10.1126/science.1235441

- Wilson, C. A., Tsuchida, M. A., Allen, G. M., Barnhart, E. L., Applegate, K. T., Yam, P. T., … Theriot, J. A. (2010). Myosin II contributes to cell-scale actin network treadmilling through network disassembly. Nature, 465(7296), 373–377. https://doi.org/10.1038/nature08994

- Xu, J., Wirtz, D., & Pollard, T. D. (1998). Dynamic cross-linking by α-actinin determines the mechanical properties of actin filament networks. Journal of Biological Chemistry, 273(16), 9570–9576. https://doi.org/10.1074/jbc.273.16.9570

- Ye, N., Verma, D., Meng, F., Davidson, M. W., Suffoletto, K., & Hua, S. Z. (2014). Direct observation of α-actinin tension and recruitment at focal adhesions during contact growth. Experimental Cell Research, 327(1), 57–67. https://doi.org/10.1016/j.yexcr.2014.07.026

Figure 1

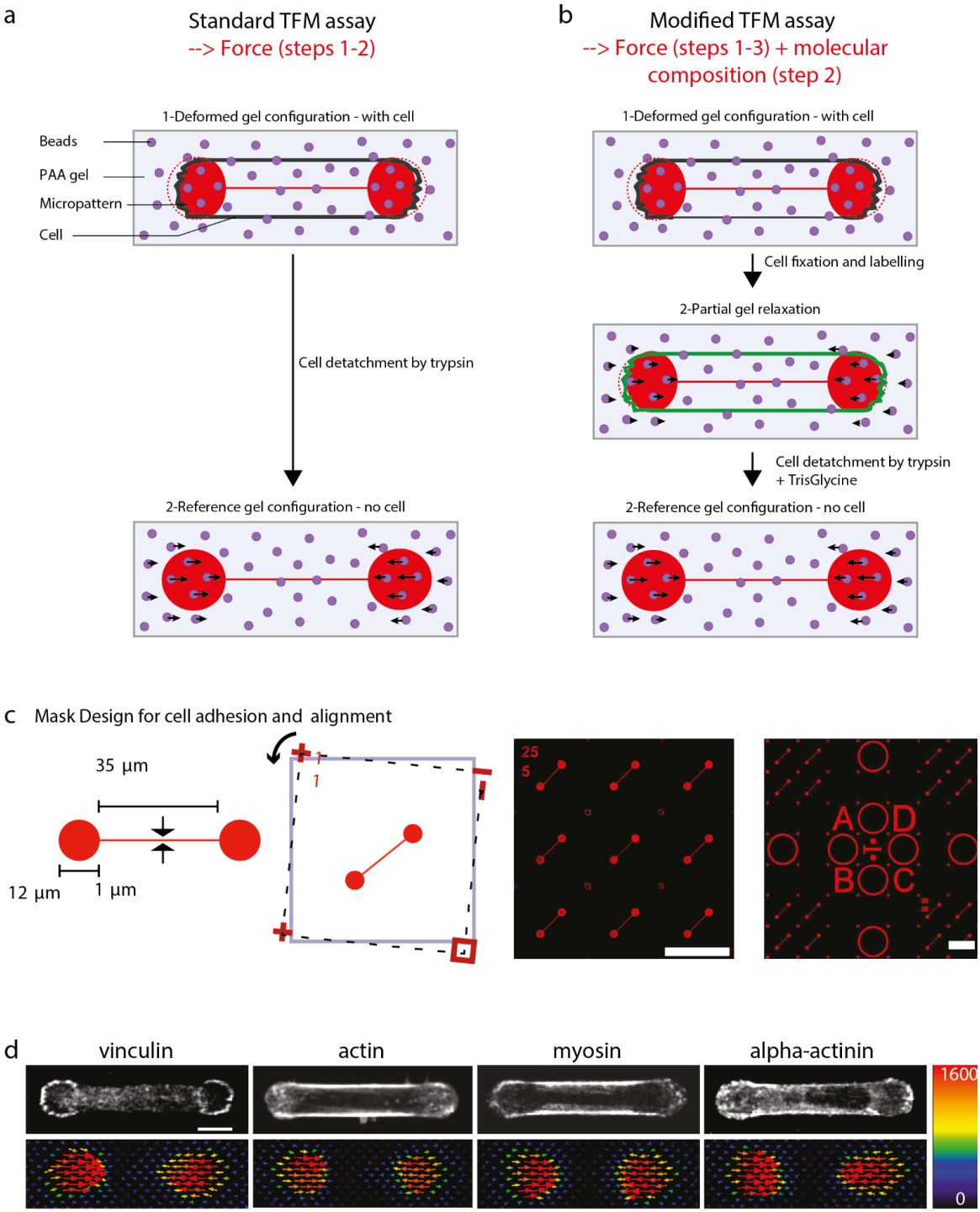
a
Standard TFM assay
--> Force (steps 1-2)
1-Deformed gel configuration - with cell
Beads
PAA gel
Micropattern
Cell
Cell detatchment by trypsin
2-Reference gel configuration - no cell
b
Modified TFM assay
--> Force (steps 1-3) + molecular composition (step 2)
1-Deformed gel configuration - with cell
Cell fixation and labelling
2-Partial gel relaxation
Cell detatchment by trypsin + TrisGlycine
2-Reference gel configuration - no cell
c
Mask Design for cell adhesion and alignment
35 µm
12 µm
1 µm
A
D
B
C
d
vinculin
actin
myosin
alpha-actinin
1600
0

Figure 2

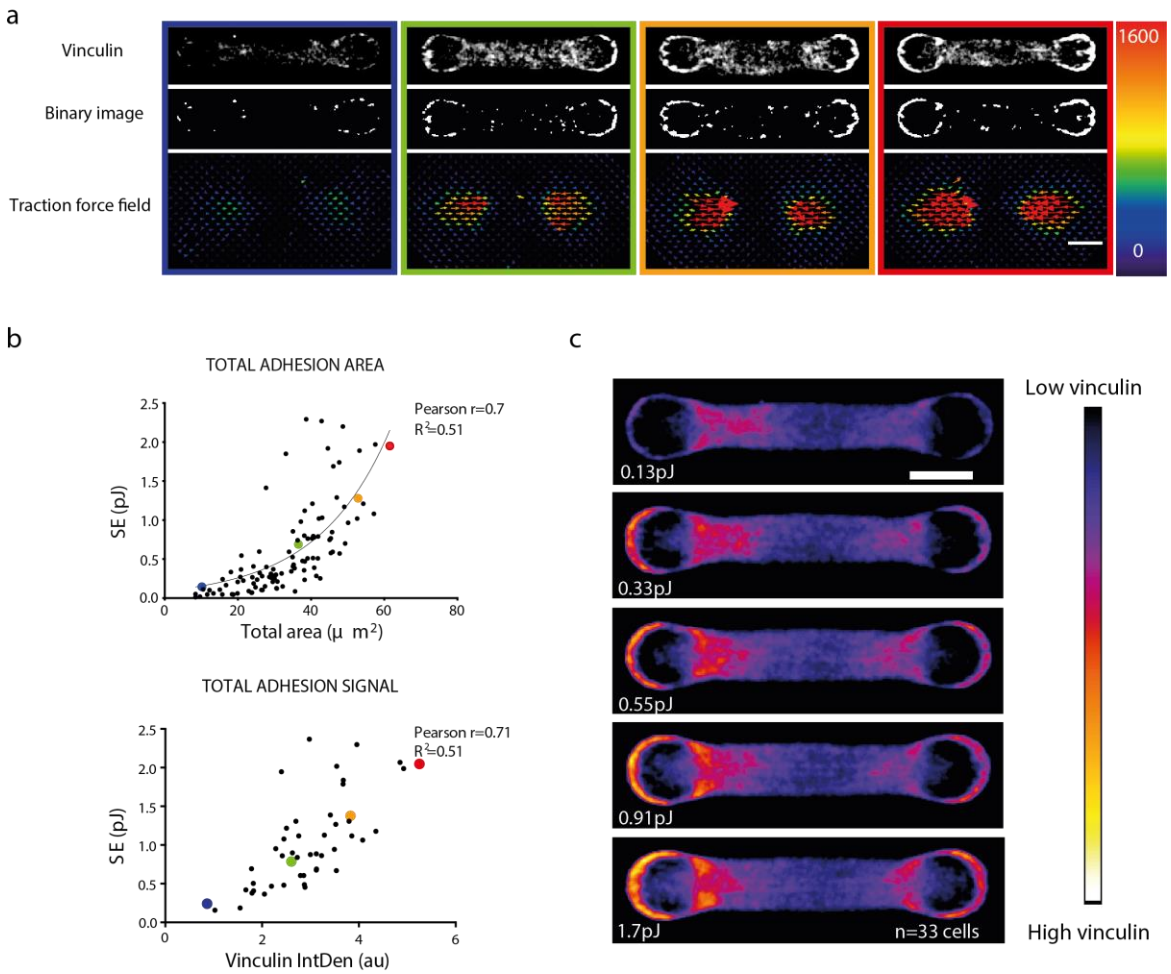
a
Vinculin
Binary image
Traction force field
1600
0
b
TOTAL ADHESION AREA
Pearson r=0.7
R2=0.51
SE (pJ)
Total area (μ m2)
TOTAL ADHESION SIGNAL
Pearson r=0.71
R2=0.51
SE (pJ)
Vinculin IntDen (au)
c
0.13pJ
0.33pJ
0.55pJ
0.91pJ
1.7pJ
n=33 cells
Low vinculin
High vinculin

Figure 3

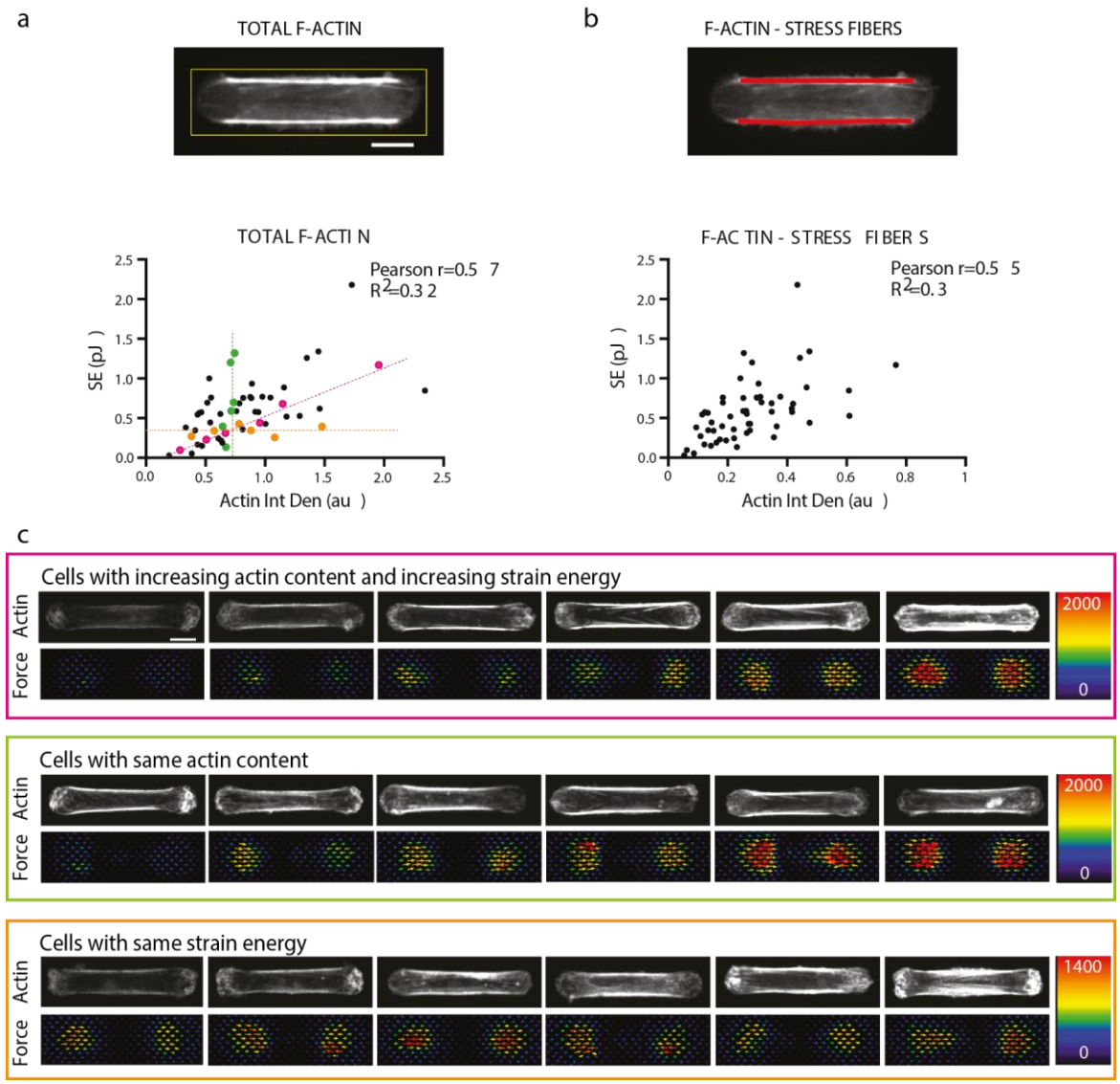
a
TOTAL F-ACTIN
b
F-ACTIN - STRESS FIBERS
TOTAL F-ACTI N
Pearson r=0.5 7
R2=0.3 2
SE (pJ)
Actin Int Den (au)
F-AC TIN - STRESS FI BER S
Pearson r=0.5 5
R2=0. 3
SE (pJ)
Actin Int Den (au)
c
Cells with increasing actin content and increasing strain energy
Actin
Force
2000
0
Cells with same actin content
Actin
Force
2000
0
Cells with same strain energy
Actin
Force
1400
0

Figure 4

a

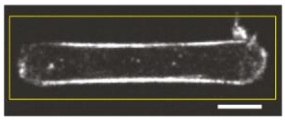

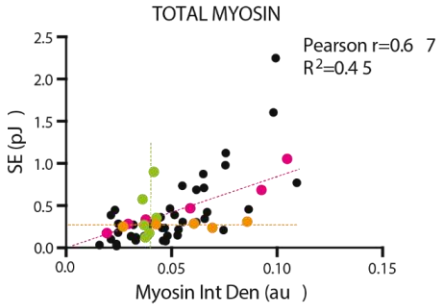
TOTAL MYOSIN
Pearson r=0.6 7
R2=0.4 5
SE (pJ)
Myosin Int Den (au)

b

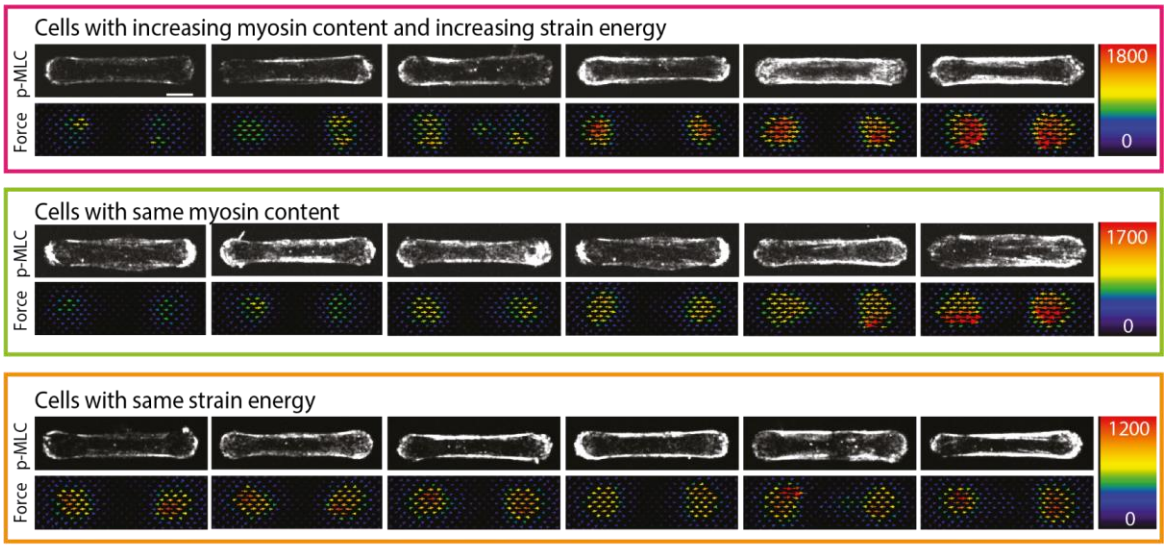
Cells with increasing myosin content and increasing strain energy
p-MLC
Force
1800
0
Cells with same myosin content
1700
Cells with same strain energy
1200

c

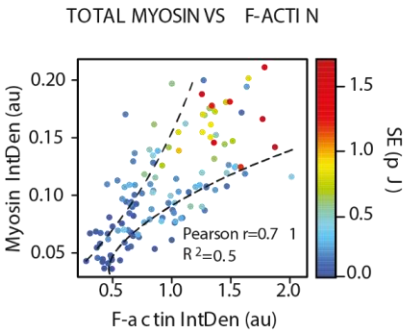
TOTAL MYOSIN VS F-ACTI N
Myosin IntDen (au)
Pearson r=0.7 1
R 2=0.5
F-a c tin IntDen (au)
SE (p J)

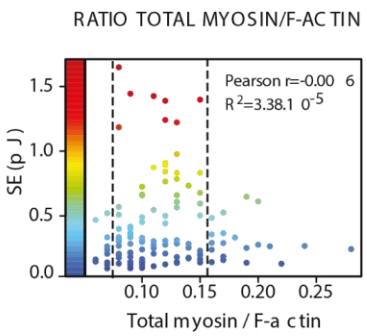
RATIO TOTAL MYOSIN/F-AC TIN
Pearson r=-0.00 6
R 2=3.38.1 0-5
SE (p J)
Total myosin / F-a c tin

Figure 5

a

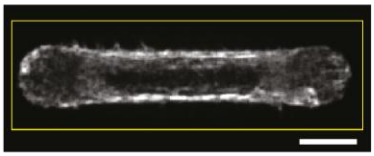

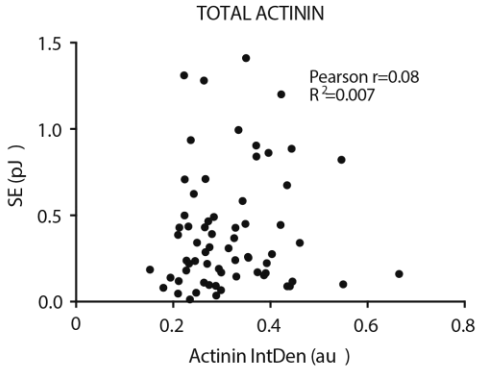
TOTAL ACTININ
Pearson r=0.08
R 2=0.007
SE (pJ)
Actinin IntDen (au)
0.0
0.5
1.0
1.5
0
0.2
0.4
0.6
0.8

b

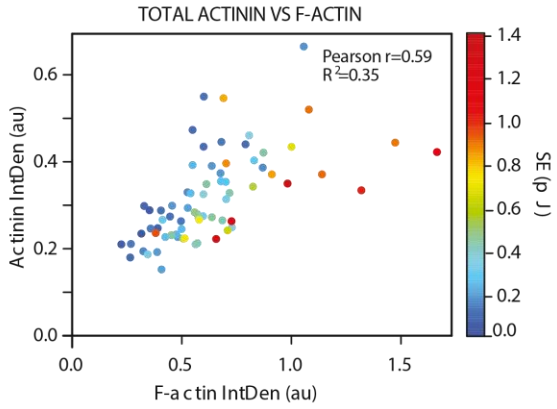
TOTAL ACTININ VS F-ACTIN
Pearson r=0.59
R 2=0.35
Actinin IntDen (au)
F-actin IntDen (au)
SE (p J)
0.0
0.2
0.4
0.6
0.5
1.0
1.5
1.4
1.2
0.8

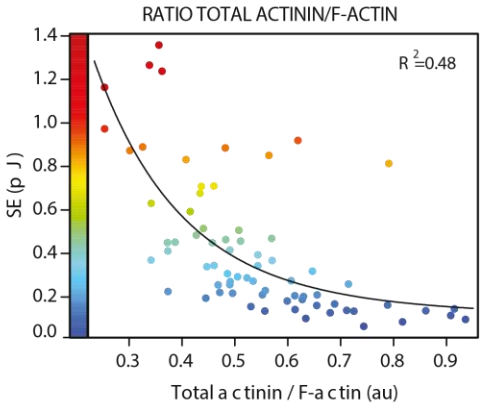
RATIO TOTAL ACTININ/F-ACTIN
R 2=0.48
SE (p J)
Total actinin / F-actin (au)
0.0
0.2
0.4
0.6
0.8
1.0
1.2
1.4
0.3
0.5
0.7
0.9

c

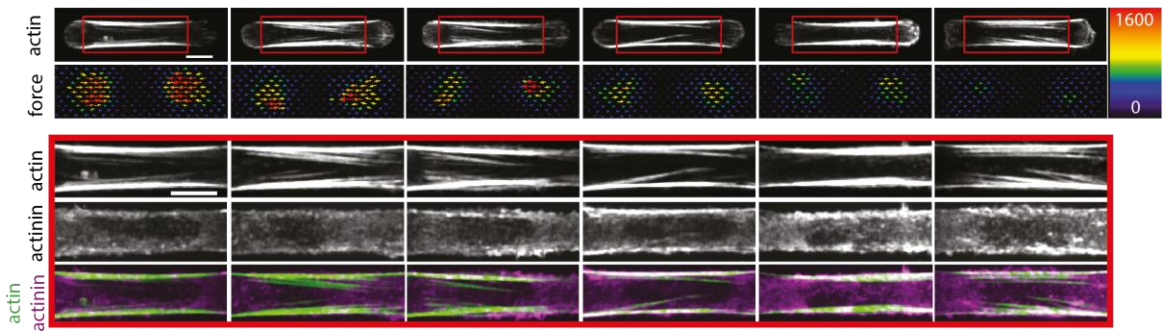
actin
force
1600
0
actin
actinin
actin
actinin

Figure 1 supp

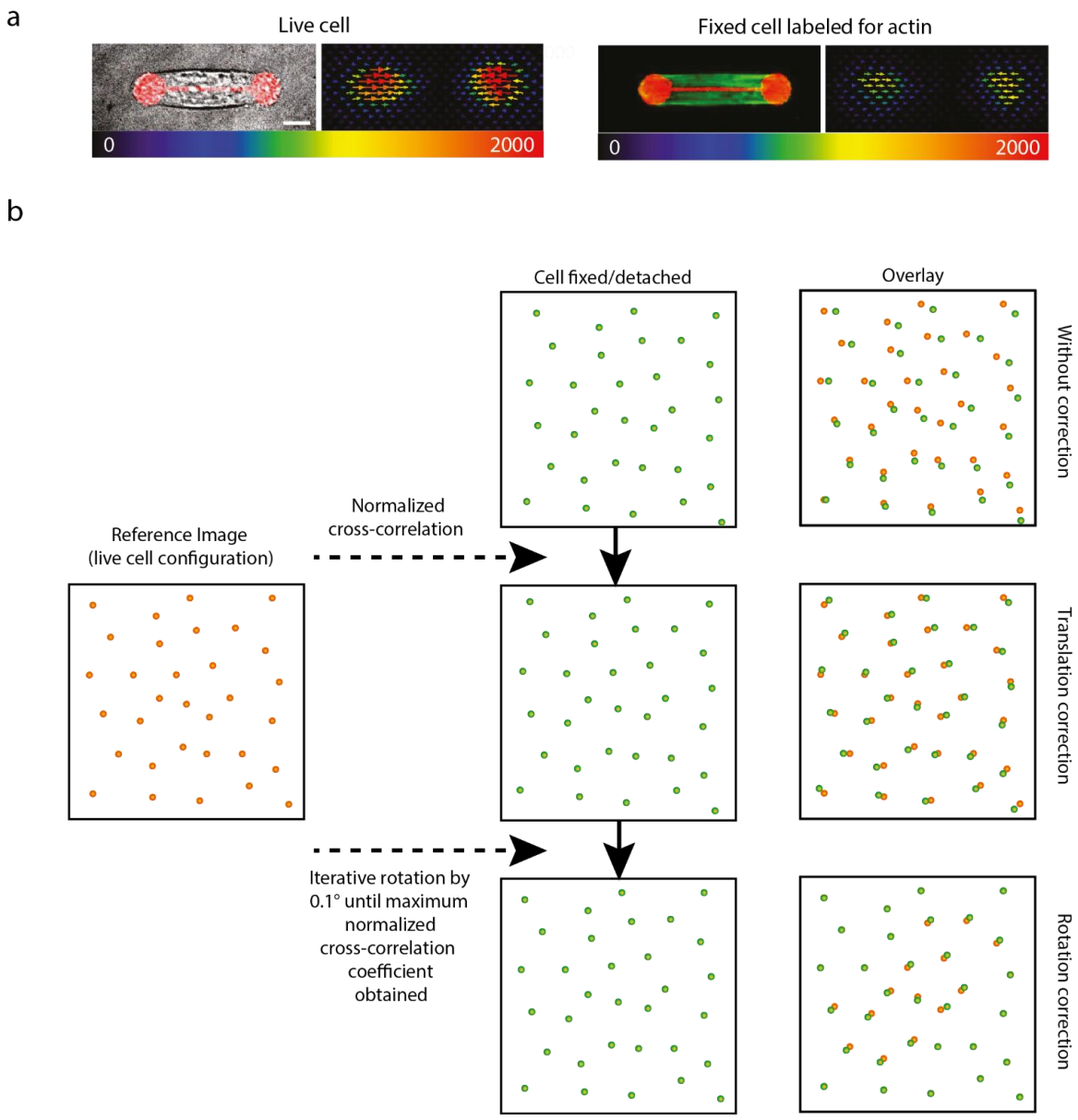

Figure 2 supp

a

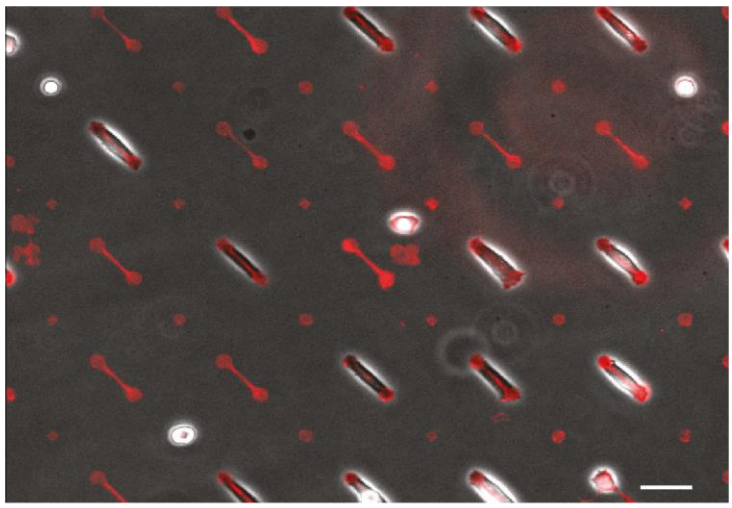

b

Examples of cells discarded from the analysis

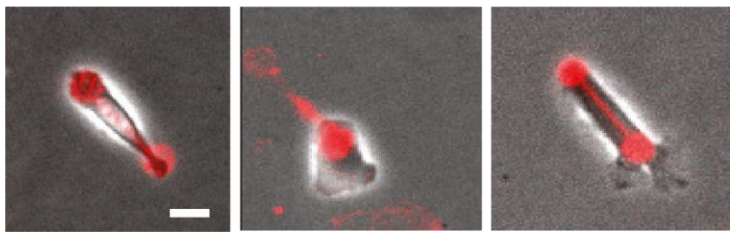

6.4 Extra Biochemical Characterization data

To determine if recruitment of actin and myosin to the stress fiber region varied with the level of expression in each cell, we checked the relative proportion of the proteins that were being recruited to the stress fiber region. We found that the relative proportion of F-actin that was recruited to a 2.2 μm wide region that encompassed the stress fiber was constant with varying expression level in cells. However, the relative level of myosin recruited to similar regions (cells from a different experiment where myosin alone was labelled) showed an increasing trend with increase in expression levels. As the ratio of the total α-actinin:F-actin was found to be lower in the cells exerting higher strain energies, this suggests that myosin is being recruited to those regions to make up for the space not occupied by actinin.

A

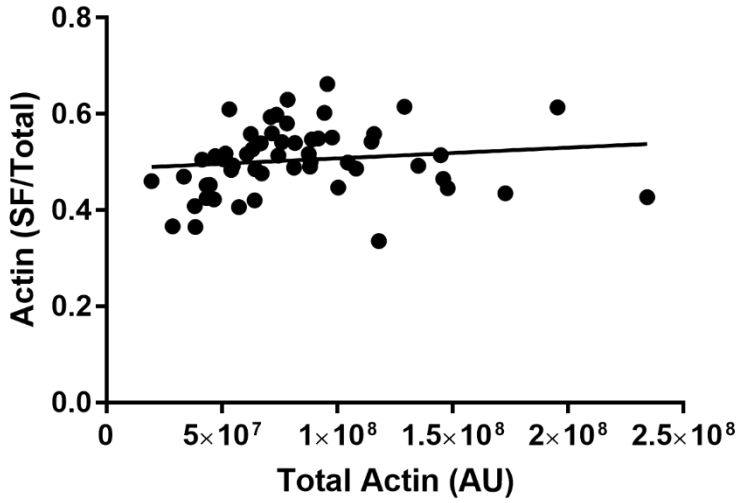

B

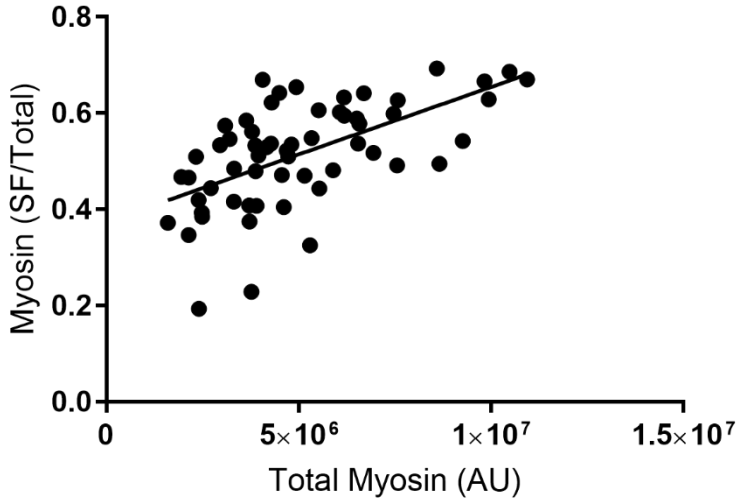

Figure 38: Relative level of actin and myosin incorporated into stress fiber region

A: The proportion of the total actin that is recruited into a 2.2 µm wide region along the stress fiber is shown. There is no variation in the level of actin recruited into this region with increasing actin.

B: The proportion of the total myosin that is recruited into a 2.2 µm wide region along the stress fiber is shown. There is an increase in the level of actin recruited into this region with increasing total myosin.

7 General conclusions and perspectives about the work presented in this thesis manuscript.

7.1 The modified TFM assay:

We demonstrated that the modified traction force protocol implemented during my PhD provides the unique opportunity to assess simultaneously the biochemical composition of the cell and measure the associated traction forces exerted by cells onto their substrate. We can look at endogenous levels of proteins in cells rather than having to transfect a fluorescent reporter that could modify the dynamics of the proteins. The method also saves us from the trouble of establishing a stably transfected cell line, which might also lead to selection of specific cells and bias the results. This allows for the use of wild type cells, which provides access to the entire range of variations, in cellular biochemistry and the resulting force production by these cells. The only bias that can originate is selection of cells that are capable of spreading fully on the patterns that are used. In addition, due to imaging through the gel embedded with beads throughout it, the resolution in the images acquired is not very high. While the intensity of the signal from regions could be measured, finer details such as individual focal adhesions and banding of actinin and myosin on stress fibers could not be determined. In spite of that, as was seen in the results section, it was possible to quantify that variations in the levels of different proteins expressed by cells exist. These variations were linked to the forces exerted by cells. The variation in localization of proteins to different regions could be quantified.

The time between imaging the live cells and fixation was between 20 and 30 minutes. This could lead to some reorganization of the cytoskeleton, but not to significant changes in the protein levels in the cells. As such, this assay is useful to study the relationship between cellular protein content, localization to specific regions and the resulting traction forces.

Some of the issues with the assay can lead to it being tricky to implement at present. But these issues can be dealt with. To start with, the method developed in this assay involves several steps of manual intervention on the microscope to reposition the sample on top of the stage and retrieve the positions imaged. As such, this technique requires some practice and accuracy and can lead to errors at different steps of the process. Experimentally, the most challenging part of the assay was to be manually translate and rotate the sample to near micron and a degree of accuracy. This level of accuracy in rotation is required as a small difference in the rotational orientation of the sample can still lead to significant translation at a distance from the error origin. This can lead to losing the position that was marked earlier. While the lost position can be found using the row and column numbers, an easier method would be to align the sample well at the start. While the alignment markings allows this rotation and translation to be done, it takes significant dexterity and time while actually doing it on the microscope without losing the position from the field of view.

Having a mechanism that allows the sample to be easily rotated without any translation can simplify the experiment significantly along with the ability to move the sample for labelling and cell detachment without losing the position on the stage. Keeping the sample position fixed with respect to the stage can be achieved by a sample holder which does not allow the coverslip to move while also being detachable from the stage (see Figure 30). After imaging the live cells, the holder could be detached from the stage, the cells fixed, labeled, reimaged, detached and the reference configuration of the gel imaged, all while the coverslips are still within the holders. Using the recorded stage positions, the cells imaged in the first instance would be recoverable. Only minor translations could arise and could be easily fixed by using the row and column numbers present next to the micropatterns. Designing a holder that can first allow

rotation of the coverslip and to then fix it would be of great use and make this method very easily useable.

A

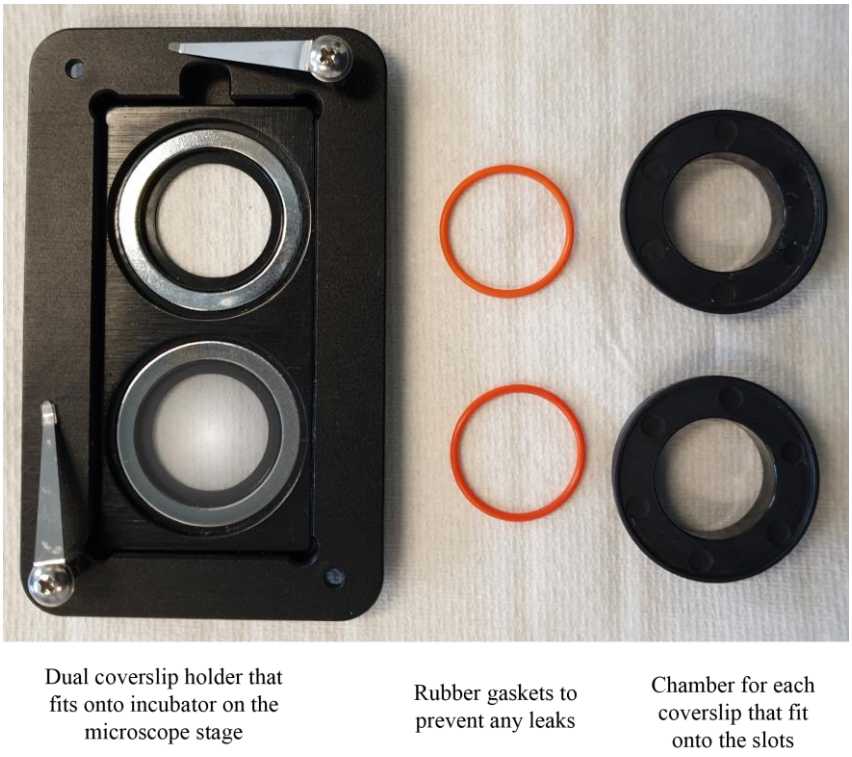

Figure 39: Coverslip holder that can be used to prevent translation and rotation of sample.

A: The commercially available coverslip holder can be used to prevent any translation or rotation errors during the labelling. (Chamlide dual magnetic type coverslip holder)

Because of the current method employing a manual alignment of the sample and leading to a lack of accuracy in rotational alignment, a dedicated computational correction based on iterative rotation and cross correlation had to be implemented. Although simple, this method is an extra step and using a sample holder like mentioned above can eliminate it.

The use of fluorescent beads for tracking the gel deformation, fluorescently labelled micropatterns and fluorescently tagged proteins in the present study limited our analysis to examine the content of two proteins at a time only. Indeed, our imaging system, a confocal

spinning disk, was equipped for the detection of only four dyes at a time. To overcome this limitation and keep the whole assay simple, we could extend the spectrum of the fluorescent probes used for the beads and micropatterns in the far-red spectrum together with using a scanning confocal microscope equipped with detectors allowing for further tuning of the wavelengths collected. Finally, using transient binding probes such as those available with the DNA-PAINT technique (Jungmann et al., 2014) could be a way to get over this limitation by sequentially labelling and imaging proteins of interest.

Another issue is that this assay relied on the quantification of the arbitrary signal intensity obtained from fluorescently labelled antibodies targeting our protein of interest. Although this method proved to be useful to assess the global and relative amount of intracellular protein analyzed, it was not sufficient to determine the actual quantitative protein levels in cells as a direct correlation between the signal and the number of fluorescent molecules and/or antibodies recognizing the proteins is difficult to establish. To achieve a quantitative measurement of the protein levels in cells, fluorescent standards displaying a known and tunable number of fluorophores should be used (Hsia et al., 2016). This method would in addition provide the advantage to allow the comparison of datasets obtained from different samples on different days as it would provide an internal reference.

7.2 Biochemical composition study

The study of the biochemical composition of cells and its relation to traction force first suggested that the individual levels of F-actin and myosin in cells were related to the strain energy that cells are capable of exerting. This result appeared to be in good agreement with previous work demonstrating that increasing myosin content is related to increased contractility (Bendix et al., 2008). However, the large spread in the data suggested that the

content of individual proteins alone was not enough to account for the magnitude of traction forces exerted by the cells. Indeed, cells exhibiting similar levels of actin or myosin could display large variations in their traction forces. Interestingly, on looking at the levels of actin and myosin together in cells, a trend of increasing strain energy when the levels of both proteins rose was found which is in good agreement with the role of motor proteins on contractility of the system.

However, when looking at the actomyosin ratio, an optimal range was found to be necessary for cells to exert high traction forces onto their underlying substrate. Outside of this range, the forces were found to drop drastically. Indeed, on one hand we observed that for low myosin/actin ratio forces remained low which suggested that a minimal amount of motor was required to exert forces on the actin filaments. On the other hand, the same level of force was measured when the ratio of myosin/F-actin was high. As previous studies have shown that myosin is capable of disassembling F-actin and inducing treadmilling of the network (Haviv et al., 2008; Sonal et al., 2019; Wilson et al., 2010), our results suggest that high myosin/F-actin ratio in cells could lead to increased actin network disassembly instead of force production.

Regarding the alpha-actinin, the analysis of the protein level alone revealed an unexpected absence of correlation between alpha-actinin content and force. Previous *in vitro* data showed that there is an optimum amount of crosslinker at which contractility is highest (Bendix et al., 2008; Ennomani et al., 2016). As the levels of actin vary in cells but variations in the level of actinin is low, it was decided that looking at the ratio of crosslinkers per F-actin would be more meaningful. In this work, the ratio of α-actinin:F-actin displayed an exponential decrease in the strain energy as the ratio increased. This only shows a partial agreement with the *in vitro* studies. Indeed, the results do demonstrate the existence of a non-linear relationship between the level of motor or crosslinker as compared to F-actin and contractility as previously

described. However, they did not reveal the existence of a bell-shape curve between connectivity and contractility as demonstrated by Ennomani et al. *in vitro* (Ennomani et al., 2016). This suggests, that similar to what was demonstrated in vitro, excessive crosslinking of the actin cellular network impaired the filaments sliding by rigidifying the network and thereby reduced contractility. It is possible that the left part of the bell-shaped curve seen in Ennomani et al., has a ratio of actinin:F-actin that is too low compared to that seen in cells and that we are only able to see the right side of the curve in cells.

Along with alpha-actinin, other crosslinkers such as paladin and fascin, (Elkhatib et al., 2014; Gateva et al., 2014) are present in cells and were not analyzed in that study. These crosslinkers have been shown to play a key role in force generation as they increase VASP recruitment and prevent myosin binding to the stress fibers. Knockdown of both these crosslinking proteins was also shown to increase the traction forces produced by cells (Azatov, Goicoechea, Otey, & Upadhyaya, 2016; Elkhatib et al., 2014). Azatov et al. also predicted a bell-shape relationship between palladin levels and the forces exerted by cells and also suggested that wild type cells were, in their culture conditions, found in the right part of the bell-shape curve, supporting our conclusions. We cannot exclude that in our cells, the interaction between these other crosslinkers and actin could maintain the connectivity in the presence of low alpha-actinin levels. Altogether, these results suggest that it is not the level of individual proteins alone that plays a role in setting the magnitude of forces exerted by cells. Instead, the relative levels between different components also plays an important role.

The data on focal adhesions is different from those in literature where individual focal adhesion size is usually measured. Earlier studies have shown an increase in traction force with focal adhesion size (Balaban et al., 2001), and others that show no relation (Oakes et al., 2012). Oakes

et al., also shown that mature focal adhesions can take a six-fold increase in tension without any change in their size. However, in this study, it is difficult to measure the individual focal adhesions due to the pattern shape. The adhesive region is small and does not allow large spacing between the focal adhesions which were mainly found in a belt like region on the longitudinal ends of the patterns. The thickness of the belt increases with increasing strain energy. This, along with imaging the fluorescence signal through a gel which has beads embedded in it, lowers the resolution compared to optimal. The sum of the size of the focal adhesions, and the intensity of the vinculin signal was measured. This total area of focal adhesions in cells increases with strain energy. The increase in the integrated vinculin signal from the cells with increasing strain energy suggests that more tension is present in these regions as vinculin is recruited due to unfolding of talin due to tension (Austen et al., 2015; Del Rio et al., 2009). These results show that there is a shared regulation mechanism between the focal adhesion composition, size and the overall force transmitted to the substrate at the cell level. It would be interesting to look at the levels of proteins that compose individual focal adhesions and compare them to the forces exerted at those adhesions.

7.3 Actin dynamics results cannot explain difference in cell forces.

The actin dynamics study of the stress fiber showed some differences between the highest and lowest strain energy exerting cells. The average speed of movement of all the photoconverted spots is a measure of stress fiber elongation. This measure shows differences between the Low and High strain energy exerting cells, with the higher strain energy cells showing lower speeds. However, there is significant overlap (Figure 33) between the High and Low strain energy cells. The decrease in average spot speed in high strain energy cells is in agreement with previous work demonstrating that high myosin induced tension can inhibit actin polymerization at their

focal adhesions through inhibition of VASP, leading to reduction in elongation of stress fibers to maintain contractility (S. Tojkander et al., 2015).

The average actin dynamic turnover of all the spots were not significantly different between the two classes of cells. This measure could not explain the large heterogeneity of traction forces measured within each group. These results together suggested that the actin filament turnover in stress fiber was not having a major effect on the magnitude of the traction forces exerted by cells on their substrate. However, it was difficult to conclude from the present data as the number of cells analyzed remained rather low due to the experimental difficulty to perform photoconversion on top of polyacrylamide gels embedded with fluorescent beads. Additionally, we observed an important turnover variability within individual stress fibers and stress fibers from the same cells, that, when combined to the variability between different cells, led to a very heterogeneous dataset. Actual differences between high strain energy group and low strain energy group may therefore be masked by this important intrinsic variability. Earlier studies have shown that there are variations in dynamics in different parts of the stress fibers (Peterson et al., 2004). Peterson et al., also found that there were variations in the band width of myosin and α-actinin in different regions of the stress fibers. Damage to the stress fibers is also repaired by induction of filament nucleation (Smith et al., 2010). With the stress fiber being embedded into the cortex (Vignaud et al., 2020), different parts might experience varying stress depending on the cortical tension at those regions which could also lead to changes in dynamics. These factors suggest that there can be variations in the dynamics of the stress fibers along its length depending on the composition and stress that is experienced by the different regions.

7.4 Perspectives

The study of the biochemical composition of the network in relationship to intracellular force production and transmission raised two interesting questions that would require more exploration in future work.

First, the quantification of individual actin levels in both the SF and whole cells revealed that the content of this protein measured at the entire cell level was an equivalent predictor of force than when measured in the SF. We also measured that the sum of the F-actin signal from the two ventral stress fibers accounted for 50% of the total F-actin present in cells. We additionally observed that this ratio held true for cells throughout the entire range of strain energies. This suggested first that cells constrained to a specific adhesion surface were able to recruit a fixed amount of the total actin into stress fibers. More interestingly, it also meant that compared to the high levels of actin found locally in the stress fibers, the cortex might display much lower densities of F-actin. Previous work from our lab, performed in the same experimental setup in live cells showed that an individual SF was storing about 25% of the contractile energy of the cell and the cortex about 20% of that energy (Vignaud et al., 2020). Taken together, these results suggested that two very different local concentrations of F-actin, respectively low and high, in the cortex and in the SF, could lead to an equivalent production of force in the cells. However, we noticed that the balance of myosin to actin content was rather low in the SF as compared to the cortex for low strain energy cells whereas it was higher cells producing high forces. This inverted balance in the ratio of molecular motor and F-actin content between the two networks could explain why different densities of F-actin lead to produce an equivalent tension in both networks. In future work, we could take advantage of the modified TFM assay developed to explore further the importance of the balance between local actomyosin network

composition and force by designing new micropatterns shapes that would allow a progressive modification of the relative importance between the SF and the cortical network.

The present study identified the biochemical composition of the actomyosin network as a key parameter setting the magnitude of forces generated by cells. Earlier studies from the lab using the same micropattern design, but changing the length between the disks have shown that there is a biphasic behavior of the force upon stress fiber length increase (Vignaud, 2013). This result appears to be in apparent contradiction with the current dogma in the field, stating that increasing the projected area increases traction forces exerted by cells (Califano & Reinhart-King, 2010; Rape, Guo, & Wang, 2011). Endogenous proteins content analyses of SF were performed in fixed cells for alpha-actinin, actin and phospho-myosin. They showed that while increasing the length of the fiber, the myosin content remained constant while the actin and alpha-actinin levels decreased, suggesting that the myosin/F-actin ratio decreases whereas the actinin/F-actin ratio remains constant. Although this result could account for both the force increase and drop, we could not directly correlate the biochemical content of these cells with their strain energy. The development of the new TFM assay thereby opens a new avenue to study the force scaling in relationship with the molecular composition of the SF and the cortical network. In addition, for a constant cell area, it will be interesting to study how cell shape may affect the protein quantitative distribution within the different actin structures and may therefore induce different traction force. We have focused our quantitative analysis on actin, myosin, alpha-actinin and vinculin, but other actin-binding proteins involved on actin turnover (ADF/cofilin) or in the identity of actin filament (tropomyosins) could be of a great interest to study using this new approach. We have in hand a method to establish a general cartography of actin binding proteins in cells in relation with force. Finally, how the principles that we have

established during my thesis could be extended to other cell types will be also a logic perspective of this work.

A

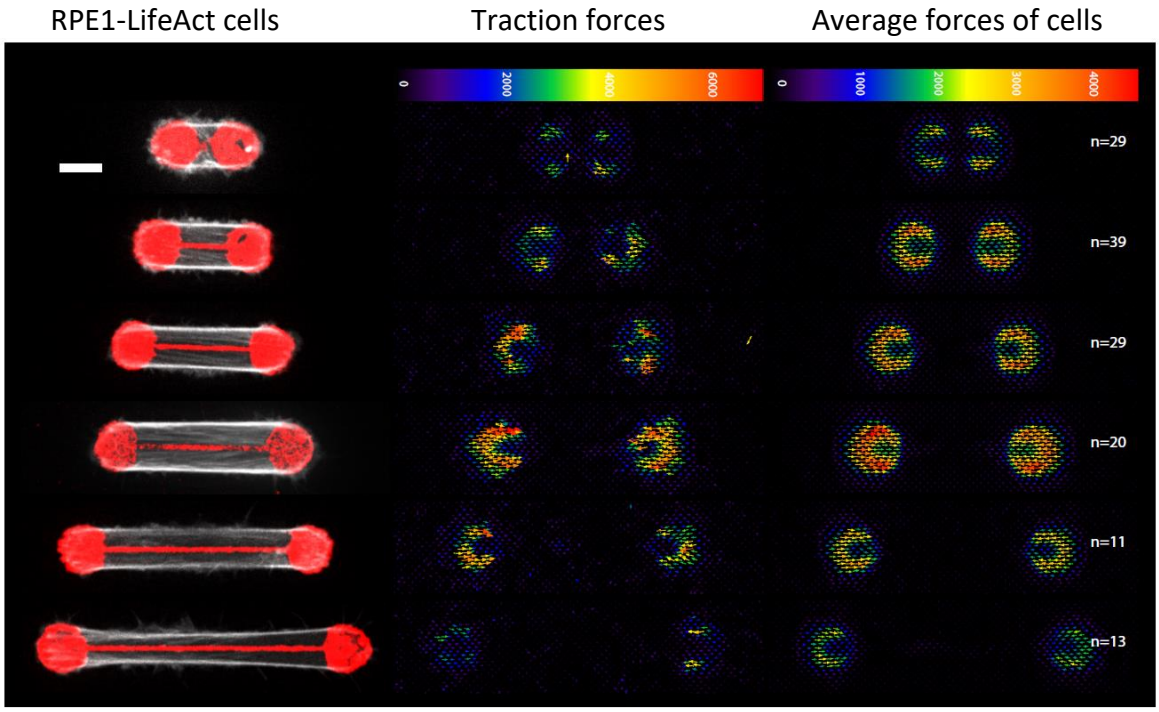

B

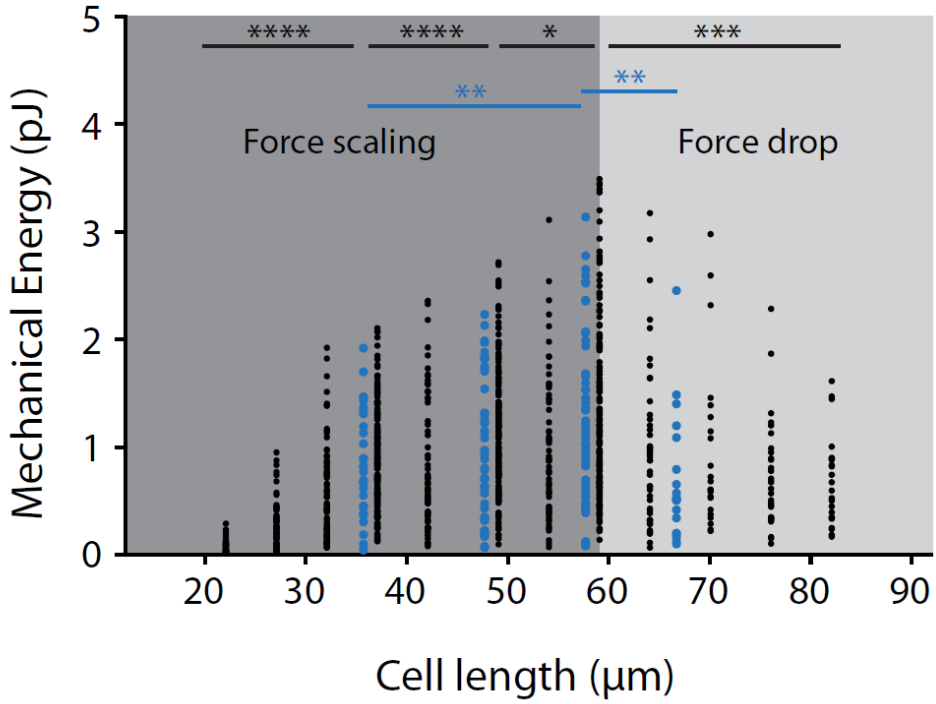

Figure 40: Force scaling in RPE1 cells

Adapted from: (Vignaud, 2013)

A: From left to right: micropattern labelled with Fibronectin-Cy3, corresponding Lifeact picture of the cell, traction map for the same cell, average traction map over many cells

B: Mechanical energy vs. cell length. Measurements performed on 35 kPa gel stiffness are represented by black dots, blue dots are used for experiments on a 9.6 kPa gel where cells show a similar force scaling trend.

It is interesting to find such large variations in both the biochemical content of cells and their ability to exert traction forces. In 2D epithelial sheets, the force landscape is highly rugged and the direction of migration is decided by the direction of maximal shear stress (Tambe et al., 2011; Trepat et al., 2009). Intracellular forces are also involved in the coordinated movement of cells required for closing gaps in epithelial sheets (P. Lee & Wolgemuth, 2011) and the emergence of leader cells on the edges of these sheets (Rausch et al., 2013) and in the directing cohesive migration in embryos (Lecaudey & Gilmour, 2006). The prediction of which cells near the border of epithelial sheets will become the leader cell is still difficult. Cytoskeletal polarization, interplay of RhoA and mechanical forces have been proposed to play important roles in the formation of leader cells (Rausch et al., 2013; Reffay et al., 2014). Modelling approaches have shown that finger like formations in an active fluid would not arise if it was homogenous (Y. Yang & Levine, 2020). The intrinsic properties of cells such as genetic expression and protein synthesis have been implicated as factors effecting the origin of a leader cell (B. Chen, Wu, Tang, Tang, & Liang, 2020). Epithelial cell extrusion, which helps to avoid crowding in epithelial sheets (Eisenhoffer et al., 2012) has been hypothesized to be influenced by the mechanical forces actin on cells (Muliyil, Krishnakumar, & Narasimha, 2011). Knowing that cell populations have such large variations in the ability to exert forces raises the question of how these variations might impact tissue level behaviors. Could the rugged force landscape,

the emergence of leader cells in epithelial sheets, and the extrusion of cells from epithelia emerge due to the differences protein levels and the resulting variation in forces exerted by cells? How do variations in force production in the cells that are part of embryos effect morphogenesis? With the knowledge of that protein levels in cells and the ratios between different components play a role in traction force variations, these questions could be answered by measuring the protein levels of cells in tissues.

8 Abbreviations

F-actin: Filamentous actin

ADF:Actin Depolymerizing Factor

ECM: Extra Cellular Matrix

PDMS: polydimethylsiloxane

SE: Strain Energy

SIM: Structured Illumination Microscopy

TFM: Traction Force Microscopy

TIRF: Total Internal Reflection

VASP: Vasodilator-stimulated phosphoprotein

WASP: Wiskott–Aldrich syndrome protein

9 Bibliography

Abercrombie, M., Heaysman, J. E. M., & Pegrum, S. M. (1971). The locomotion of fibroblasts in culture. Experimental Cell Research, 67(2), 359–367. https://doi.org/10.1016/0014-4827(71)90420-4

Alexandrova, A. Y., Arnold, K., Schaub, S., Vasiliev, J. M., Meister, J.-J., Bershadsky, A. D., & Verkhovsky, A. B. (2008). Comparative Dynamics of Retrograde Actin Flow and Focal Adhesions: Formation of Nascent Adhesions Triggers Transition from Fast to Slow Flow. PLoS ONE, 3(9), e3234. https://doi.org/10.1371/journal.pone.0003234

Aratyn-Schaus, Y., & Gardel, M. L. (2010). Transient Frictional Slip between Integrin and the ECM in Focal Adhesions under Myosin II Tension. Current Biology, 20(13), 1145–1153. https://doi.org/10.1016/j.cub.2010.05.049

Aratyn-Schaus, Y., Oakes, P. W., & Gardel, M. L. (2011). Dynamic and structural signatures of lamellar actomyosin force generation. Molecular Biology of the Cell, 22(8), 1330–1339. https://doi.org/10.1091/mbc.e10-11-0891

Austen, K., Ringer, P., Mehlich, A., Chrostek-Grashoff, A., Kluger, C., Klingner, C., … Grashoff, C. (2015). Extracellular rigidity sensing by talin isoform-specific mechanical linkages. Nature Cell Biology, 17(12), 1597–1606. https://doi.org/10.1038/ncb3268

Ayala, Y. A., Pontes, B., Hissa, B., Monteiro, A. C. M., Farina, M., Moura-Neto, V., … Nussenzveig, H. M. (2017). Effects of cytoskeletal drugs on actin cortex elasticity. Experimental Cell Research, 351(2), 173–181. https://doi.org/10.1016/j.yexcr.2016.12.016

Azatov, M., Goicoechea, S. M., Otey, C. A., & Upadhyaya, A. (2016). The actin crosslinking protein palladin modulates force generation and mechanosensitivity of tumor associated fibroblasts. Scientific Reports, 6(June), 1–12. https://doi.org/10.1038/srep28805

Bakolitsa, C., de Pereda, J. M., Bagshaw, C. R., Critchley, D. R., & Liddington, R. C. (1999). Crystal Structure of the Vinculin Tail Suggests a Pathway for Activation. Cell, 99(6), 603–613. https://doi.org/10.1016/S0092-8674(00)81549-4

Balaban, N. Q., Schwarz, U. S., Riveline, D., Goichberg, P., Tzur, G., Sabanay, I., … Geiger, B. (2001). Force and focal adhesion assembly: a close relationship studied using elastic micropatterned substrates. Nature Cell Biology, 3(5), 466–472. https://doi.org/10.1038/35074532

Beach, J. R., Shao, L., Remmert, K., Li, D., Betzig, E., & Hammer, J. A. (2014). Nonmuscle myosin II isoforms coassemble in living cells. Current Biology, 24(10), 1160–1166. https://doi.org/10.1016/j.cub.2014.03.071

Bendix, P. M., Koenderink, G. H., Cuvelier, D., Dogic, Z., Koeleman, B. N., Brieher, W. M., … Weitz, D. A. (2008). A Quantitative Analysis of Contractility in Active Cytoskeletal Protein Networks. Biophysical Journal, 94(8), 3126–3136. https://doi.org/10.1529/biophysj.107.117960

Beningo, K. A., Dembo, M., Kaverina, I., Small, J. V., & Wang, Y. (2001). Nascent Focal Adhesions Are Responsible for the Generation of Strong Propulsive Forces in Migrating Fibroblasts. The Journal of Cell Biology, 153(4), 881–888. https://doi.org/10.1083/jcb.153.4.881

Bergert, M., Erzberger, A., Desai, R. A., Aspalter, I. M., Oates, A. C., Charras, G., … Paluch, E. K. (2015). Force transmission during adhesion-independent migration. Nature Cell Biology, 17(4), 524–529. https://doi.org/10.1038/ncb3134

Bergert, M., Lendenmann, T., Zündel, M., Ehret, A. E., Panozzo, D., Richner, P., … Ferrari, A. (2016). Confocal reference free traction force microscopy. Nature Communications, 7. https://doi.org/10.1038/ncomms12814

Berginski, M. E., Vitriol, E. A., Hahn, K. M., & Gomez, S. M. (2011). High-Resolution Quantification of Focal Adhesion Spatiotemporal Dynamics in Living Cells. PLoS ONE, 6(7), e22025. https://doi.org/10.1371/journal.pone.0022025

Bernstein, B. W., & Bamburg, J. R. (1982). Tropomyosin binding to F-actin protects the F-actin from disassembly by brain actin-depolymerizing factor (ADF). Cell Motility, 2(1), 1–8. https://doi.org/10.1002/cm.970020102

Bershadsky, A. D., Balaban, N. Q., & Geiger, B. (2003). Adhesion-dependent cell mechanosensitivity. Annual Review of Cell and Developmental Biology, 19, 677–695. https://doi.org/10.1146/annurev.cellbio.19.111301.153011

Bharadwaj, M., Strohmeyer, N., Colo, G. P., Helenius, J., Beerenwinkel, N., Schiller, H. B., … Müller, D. J. (2017). αV-class integrins exert dual roles on α5β1 integrins to strengthen adhesion to fibronectin. Nature Communications, 8(1), 14348. https://doi.org/10.1038/ncomms14348

Blakely, B. L., Dumelin, C. E., Trappmann, B., McGregor, L. M., Choi, C. K., Anthony, P. C., … Chen, C. S. (2014). A DNA-based molecular probe for optically reporting cellular traction forces. Nature Methods, 11(12), 1229–1232. https://doi.org/10.1038/nmeth.3145

Blanchard, A., Ohanian, V., & Critchley, D. (1989). The structure and function of α-actinin. Journal of Muscle Research and Cell Motility, 10(4), 280–289. https://doi.org/10.1007/BF01758424

Blanchoin, L., Pollard, T. D., & Hitchcock-DeGregori, S. E. (2001). Inhibition of the Arp2/3 complex-nucleated actin polymerization and branch formation by tropomyosin. Current Biology, 11(16), 1300–1304. https://doi.org/10.1016/S0960-9822(01)00395-5

Blanchoin, L., Rajaa, B.-P., Sykes, C., & Plastino, J. (2014). Actin dynamics, architecture, and mechanics in cell motility. Physiol Rev, 94, 235–263. https://doi.org/10.1152/physrev.00018.2013

Blume, C., Benz, P. M., Walter, U., Ha, J., Kemp, B. E., & Renné, T. (2007). AMP-activated Protein Kinase Impairs Endothelial Actin Cytoskeleton Assembly by Phosphorylating Vasodilator-stimulated Phosphoprotein. Journal of Biological Chemistry, 282(7), 4601–4612. https://doi.org/10.1074/jbc.M608866200

Bonakdar, N., Gerum, R., Kuhn, M., Spörrer, M., Lippert, A., Schneider, W., … Fabry, B. (2016). Mechanical plasticity of cells. Nature Materials, 15(10), 1090–1094. https://doi.org/10.1038/nmat4689

Borgon, R. A., Vonrhein, C., Bricogne, G., Bois, P. R. J., & Izard, T. (2004). Crystal Structure of Human Vinculin. Structure, 12(7), 1189–1197. https://doi.org/10.1016/j.str.2004.05.009

Bray, D., & White, J. (1988). Cortical flow in animal cells. Science, 239(4842), 883–888. https://doi.org/10.1126/science.3277283

Bray, M. A., Sheehy, S. P., & Parker, K. K. (2008). Sarcomere alignment is regulated by myocyte shape. Cell Motility and the Cytoskeleton, 65(8), 641–651. https://doi.org/10.1002/cm.20290

Burnette, D. T., Manley, S., Sengupta, P., Sougrat, R., Davidson, M. W., Kachar, B., & Lippincott-Schwartz, J. (2011). A role for actin arcs in the leading-edge advance of migrating cells. Nature Cell Biology, 13(4), 371–382. https://doi.org/10.1038/ncb2205

Burnette, D. T., Shao, L., Ott, C., Pasapera, A. M., Fischer, R. S., Baird, M. A., … Lippincott-Schwartz, J. (2014). A contractile and counterbalancing adhesion system controls the 3D shape of crawling cells. Journal of Cell Biology, 205(1), 83–96. https://doi.org/10.1083/jcb.201311104

Burridge, K., & Chrzanowska-Wodnicka, M. (1996). Focal adhesions, contractility and signaling. Annual Review of Cell and Developmental Biology, 12(1), 463–519. https://doi.org/10.1146/annurev.cellbio.12.1.463

Burridge, K., & Feramisco, J. R. (1981). Non-muscle α-actinins are calcium-sensitive actin-binding proteins. Nature, 294(December), 565–567

Burridge, K., & Wittchen, E. S. (2013). The tension mounts: Stress fibers as force-generating mechanotransducers. Journal of Cell Biology, 200(1), 9–19. https://doi.org/10.1083/jcb.201210090

Butt, E., Abel, K., Krieger, M., Palm, D., Hoppe, V., Hoppe, J., & Walter, U. (1994). cAMP- and cGMP-dependent protein kinase phosphorylation sites of the focal adhesion vasodilator-stimulated phosphoprotein (VASP) in vitro and in intact human platelets. The Journal of Biological Chemistry, 269(20), 14509–14517. Retrieved from http://www.ncbi.nlm.nih.gov/pubmed/8182057

Califano, J. P., & Reinhart-King, C. a. (2010). Substrate Stiffness and Cell Area Predict Cellular Traction Stresses in Single Cells and Cells in Contact. Cellular and Molecular Bioengineering, 3(1), 68–75. https://doi.org/10.1007/s12195-010-0102-6

Case, L. B., Baird, M. A., Shtengel, G., Campbell, S. L., Hess, H. F., Davidson, M. W., & Waterman, C. M. (2015). Molecular mechanism of vinculin activation and nanoscale spatial organization in focal adhesions. Nature Cell Biology, 17(7), 880–892. https://doi.org/10.1038/ncb3180

Case, L. B., & Waterman, C. M. (2015). Integration of actin dynamics and cell adhesion by a three-dimensional, mechanosensitive molecular clutch. Nature Cell Biology, 17(8), 955–963. https://doi.org/10.1038/ncb3191

Chan, A. Y., Bailly, M., Zebda, N., Segall, J. E., & Condeelis, J. S. (2000). Role of Cofilin in Epidermal Growth Factor–Stimulated Actin Polymerization and Lamellipod Protrusion. Journal of Cell Biology, 148(3), 531–542. https://doi.org/10.1083/jcb.148.3.531

Chang, C. W., & Kumar, S. (2013). Vinculin tension distributions of individual stress fibers within cell-matrix adhesions. Journal of Cell Science, 126(14), 3021–3030. https://doi.org/10.1242/jcs.119032

Chang, S. S., Rape, A. D., Wong, S. A., Guo, W., & Wang, Y. (2019). Migration regulates cellular mechanical states. Molecular Biology of the Cell, 30(26), 3104–3111. https://doi.org/10.1091/mbc.E19-02-0099

Chapin, L. M., Blankman, E., Smith, M. A., Shiu, Y.-T., & Beckerle, M. C. (2012). Lateral Communication between Stress Fiber Sarcomeres Facilitates a Local Remodeling Response. Biophysical Journal, 103(10), 2082–2092. https://doi.org/10.1016/j.bpj.2012.09.038

Chaubet, L., Khadivi Heris, H., Ehrlicher, A. J., & Hendricks, A. G. (2020). Dynamic Crosslinking of the Actin Cytoskeleton Governs Cell Mechanics. Biophysical Journal, 118(3), 280a-281a. https://doi.org/10.1016/j.bpj.2019.11.1603

Chen, B., Wu, J., Tang, Y., Tang, Y., & Liang, X. (2020). What makes leader cells arise: Intrinsic properties and support from neighboring cells. Journal of Cellular Physiology, 235(12), 8983–8995. https://doi.org/10.1002/jcp.29828

Chen, Q., Nag, S., & Pollard, T. D. (2012). Formins filter modified actin subunits during processive elongation. Journal of Structural Biology, 177(1), 32–39. https://doi.org/10.1016/j.jsb.2011.10.005

Choi, C. K., Vicente-Manzanares, M., Zareno, J., Whitmore, L. A., Mogilner, A., & Horwitz, A. R. (2008). Actin and α-actinin orchestrate the assembly and maturation of nascent adhesions in a myosin II motor-independent manner. Nature Cell Biology, 10(9), 1039–1050. https://doi.org/10.1038/ncb1763

Choquet, D., Felsenfeld, D. P., Sheetz, M. P., & Carolina, N. (1997). Extracellular Matrix Rigidity Causes Strengthening of Integrin – Cytoskeleton Linkages. CELL, 88(1), 39–48. https://doi.org/10.1016/S0092-8674(00)81856-5

Chrzanowska-Wodnicka, M., & Burridge, K. (1996). Rho-stimulated contractility drives the formation of stress fibers and focal adhesions. Journal of Cell Biology, 133(6), 1403–1415. https://doi.org/10.1083/jcb.133.6.1403

Chugh, P., Clark, A. G., Smith, M. B., Cassani, D. A. D., Dierkes, K., Ragab, A., … Paluch, E. K. (2017). Actin cortex architecture regulates cell surface tension. Nature Cell Biology, 19(6), 689–697. https://doi.org/10.1038/ncb3525

Citi, S., & Kendrick-Jones, J. (1987). Regulation of non-muscle myosin structure and function. BioEssays, 7(4), 155–159. https://doi.org/10.1002/bies.950070404

Clark, A. G., Wartlick, O., Salbreux, G., & Paluch, E. K. (2014). Stresses at the Cell Surface during Animal Cell Morphogenesis. Current Biology, 24(10), R484–R494. https://doi.org/10.1016/j.cub.2014.03.059

Courtemanche, N., Pollard, T. D., & Chen, Q. (2016). Avoiding artefacts when counting polymerized actin in live cells with LifeAct fused to fluorescent proteins. Nature Cell Biology, 18(6), 676–683. https://doi.org/10.1038/ncb3351

Craig, S. W., & Pardo, J. V. (1979). Alpha-actinin localization in the junctional complex of intestinal epithelial cells. Physiological Chemistry, 80(January), 203–210.

Cramer, L. P., Siebert, M., & Mitchison, T. J. (1997). Identification of Novel Graded Polarity Actin Filament Bundles in Locomoting Heart Fibroblasts: Implications for the Generation of Motile Force. Journal of Cell Biology, 136(6), 1287–1305. https://doi.org/10.1083/jcb.136.6.1287

Critchley, D. R. (2009). Biochemical and Structural Properties of the Integrin-Associated Cytoskeletal Protein Talin. Annual Review of Biophysics, 38(1), 235–254. https://doi.org/10.1146/annurev.biophys.050708.133744

Dasbiswas, K., Hu, S., Bershadsky, A. D., & Safran, S. A. (2019). Registry Kinetics of Myosin Motor Stacks Driven by Mechanical Force-Induced Actin Turnover. Biophysical Journal, 117(5), 856–866. https://doi.org/10.1016/j.bpj.2019.07.040

Dehapiot, B., Clément, R., Alégot, H., Gazsó-Gerhát, G., Philippe, J., & Lecuit, T. (2020). Assembly of a persistent apical actin network by the formin Frl/Fmnl tunes epithelial cell deformability. Nature Cell Biology, 22(7), 791–802. https://doi.org/10.1038/s41556-020-0524-x

Del Rio, A., Perez-Jimenez, R., Liu, R., Roca-Cusachs, P., Fernandez, J. M., & Sheetz, M. P. (2009). Stretching Single Talin Rod Molecules Activates Vinculin Binding. Science, 323(5914), 638–641. https://doi.org/10.1126/science.1162912

DeMali, K. A., Barlow, C. A., & Burridge, K. (2002). Recruitment of the Arp2/3 complex to vinculin. Journal of Cell Biology, 159(5), 881–891. https://doi.org/10.1083/jcb.200206043

Dembo, M., & Wang, Y.-L. (1999). Stresses at the Cell-to-Substrate Interface during Locomotion of Fibroblasts. Biophysical Journal, 76(4), 2307–2316. https://doi.org/10.1016/S0006-3495(99)77386-8

Doss, B. L., Pan, M., Gupta, M., Grenci, G., Mège, R.-M., Lim, C. T., … Ladoux, B. (2020). Cell response to substrate rigidity is regulated by active and passive cytoskeletal stress. Proceedings of the National Academy of Sciences, 117(23), 12817–12825. https://doi.org/10.1073/pnas.1917555117

Doyle, T., & Botstein, D. (1996). Movement of yeast cortical actin cytoskeleton visualized in vivo. Proceedings of the National Academy of Sciences, 93(9), 3886–3891. https://doi.org/10.1073/pnas.93.9.3886

du Roure, O., Saez, A., Buguin, A., Austin, R. H., Chavrier, P., Silberzan, P., … Ladoux, B. (2005). Force mapping in epithelial cell migration. Proceedings of the National Academy of Sciences of the United States of America, 102(7), 2390–2395. https://doi.org/10.1073/pnas.0408482102

Dupont, S., Morsut, L., Aragona, M., Enzo, E., Giulitti, S., Cordenonsi, M., … Piccolo, S. (2011). Role of YAP/TAZ in mechanotransduction. Nature, 474(7350), 179–184. https://doi.org/10.1038/nature10137

Ehrlicher, A. J., Krishnan, R., Guo, M., Bidan, C. M., Weitz, D. A., & Pollak, M. R. (2015). Alpha-actinin binding kinetics modulate cellular dynamics and force generation. Proceedings of the National Academy of Sciences, 112(21), 6619–6624. https://doi.org/10.1073/pnas.1505652112

Eisenhoffer, G. T., Loftus, P. D., Yoshigi, M., Otsuna, H., Chien, C.-B., Morcos, P. a, & Rosenblatt, J. (2012). Crowding induces live cell extrusion to maintain homeostatic cell numbers in epithelia. Nature, 484(7395), 546–549. https://doi.org/10.1038/nature10999

Elam, W. A., Kang, H., & De La Cruz, E. M. (2013). Biophysics of actin filament severing by cofilin. FEBS Letters, 587(8), 1215–1219. https://doi.org/10.1016/j.febslet.2013.01.062

Elkhatib, N., Neu, M. B., Zensen, C., Schmoller, K. M., Louvard, D., Bausch, A. R., … Vignjevic, D. M. (2014). Fascin plays a role in stress fiber organization and focal adhesion disassembly. Current Biology, 24(13), 1492–1499. https://doi.org/10.1016/j.cub.2014.05.023

Elosegui-Artola, A., Bazellières, E., Allen, M. D., Andreu, I., Oria, R., Sunyer, R., … Roca-Cusachs, P. (2014). Rigidity sensing and adaptation through regulation of integrin types. Nature Materials, 13(6), 631–637. https://doi.org/10.1038/nmat3960

Elosegui-Artola, A., Oria, R., Chen, Y., Kosmalska, A., Pérez-González, C., Castro, N., … Roca-Cusachs, P. (2016). Mechanical regulation of a molecular clutch defines force transmission and transduction in response to matrix rigidity. Nature Cell Biology, 18(5), 540–548. https://doi.org/10.1038/ncb3336

Engler, A. J., Sen, S., Sweeney, H. L., & Discher, D. E. (2006). Matrix elasticity directs stem cell lineage specification. Cell, 126(4), 677–689. https://doi.org/10.1016/j.cell.2006.06.044

Ennomani, H., Letort, G., Guérin, C., Martiel, J.-L., Cao, W., Nédélec, F., … Blanchoin, L. (2016). Architecture and Connectivity Govern Actin Network Contractility. Current Biology, 25(4), 368–379. https://doi.org/10.1016/j.cogdev.2010.08.003

Falzone, T. T., Lenz, M., Kovar, D. R., & Gardel, M. L. (2012). Assembly kinetics determine the architecture of α-actinin crosslinked F-actin networks. Nature Communications, 3(May). https://doi.org/10.1038/ncomms1862

Fenix, A. M., Taneja, N., Buttler, C. A., Lewis, J., Van Engelenburg, S. B., Ohi, R., & Burnette, D. T. (2016). Expansion and concatenation of nonmuscle myosin IIA filaments drive cellular contractile system

formation during interphase and mitosis. Molecular Biology of the Cell, 27(9), 1465–1478. https://doi.org/10.1091/mbc.E15-10-0725

Galior, K., Liu, Y., Yehl, K., Vivek, S., & Salaita, K. (2016). Titin-Based Nanoparticle Tension Sensors Map High-Magnitude Integrin Forces within Focal Adhesions. Nano Letters, 16(1), 341–348. https://doi.org/10.1021/acs.nanolett.5b03888

Gardel, M. L., Schneider, I. C., Aratyn-Schaus, Y., & Waterman, C. M. (2010). Mechanical Integration of Actin and Adhesion Dynamics in Cell Migration. Annual Review of Cell and Developmental Biology, 26(1), 315–333. https://doi.org/10.1146/annurev.cellbio.011209.122036

Gateva, G., Tojkander, S., Koho, S., Carpen, O., & Lappalainen, P. (2014). Palladin promotes assembly of non-contractile dorsal stress fibers through VASP recruitment. Journal of Cell Science, 127(9), 1887–1898. https://doi.org/10.1242/jcs.135780

Geiger, B., Yehuda-Levenberg, S., & Bershadsky, A. D. (1995). Molecular interactions in the submembrane plaque of cell-cell and cell-matrix adhesions. Acta Anatomica. https://doi.org/10.1159/000147751

Geiger, Benjamin, Bershadsky, A., Pankov, R., & Yamada, K. M. (2001). Transmembrane crosstalk between the extracellular matrix and the cytoskeleton. Nature Reviews Molecular Cell Biology, 2(11), 793–805. https://doi.org/10.1038/35099066

Geiger, Benjamin, & Singer, S. J. (1979). The participation of α-actinin in the capping of cell membrane components. Cell, 16(1), 213–222. https://doi.org/10.1016/0092-8674(79)90202-2

Geiger, Benjamin, & Yamada, K. M. (2011). Molecular Architecture and Function of Matrix Adhesions. Cold Spring Harbor Perspectives in Biology, 3(5), a005033–a005033. https://doi.org/10.1101/cshperspect.a005033

Gerisch, G., & Weber, I. (2000). Cytokinesis without myosin II. Current Opinion in Cell Biology, 12(1), 126–132. https://doi.org/10.1016/S0955-0674(99)00066-6

Glück, U., & Ben-Ze'ev, A. (1994). Modulation of α-actinin levels affects cell motility and confers tumorigenicity on 3T3 cells. Journal of Cell Science, 107(7), 1773–1782.

Gluck, U., Kwiatkowski, D. J., & Ben-Ze'ev, A. (1993). Suppression of tumorigenicity in simian virus 40-transformed 3T3 cells transfected with alpha-actinin cDNA. Proceedings of the National Academy of Sciences, 90(2), 383–387. https://doi.org/10.1073/pnas.90.2.383

Goeckeler, Z. M., Bridgman, P. C., & Wysolmerski, R. B. (2008). Nonmuscle myosin II is responsible for maintaining endothelial cell basal tone and stress fiber integrity. American Journal of Physiology-Cell Physiology, 295(4), C994–C1006. https://doi.org/10.1152/ajpcell.00318.2008

Goffin, J. M., Pittet, P., Csucs, G., Lussi, J. W., Meister, J., & Hinz, B. (2006). Focal adhesion size controls tension-dependent recruitment of α-smooth muscle actin to stress fibers. Journal of Cell Biology, 172(2), 259–268. https://doi.org/10.1083/jcb.200506179

Gordon, W. E. (1978). Immunofluorescent and ultrastructural studies of "sarcomeric" units in stress fibers of cultured non-muscle cells. Experimental Cell Research, 117(2), 253–260. https://doi.org/10.1016/0014-4827(78)90138-6

Grashoff, C., Hoffman, B. D., Brenner, M. D., Zhou, R., Parsons, M., Yang, M. T., … Schwartz, M. A. (2010). Measuring mechanical tension across vinculin reveals regulation of focal adhesion dynamics. Nature, 466(7303), 263–266. https://doi.org/10.1038/nature09198

Green, R. A., Paluch, E., & Oegema, K. (2012). Cytokinesis in animal cells. Annual Review of Cell and Developmental Biology, 28, 29–58. https://doi.org/10.1146/annurev-cellbio-101011-155718

Gunawan, F., Gentile, A., Fukuda, R., Tsedeke, A. T., Jiménez-Amilburu, V., Ramadass, R., … Stainier, D. Y. R. (2019). Focal adhesions are essential to drive zebrafish heart valve morphogenesis. Journal of Cell Biology, 218(3), 1039–1054. https://doi.org/10.1083/jcb.201807175

Gustafsson, M. G. L. (2000). Surpassing the lateral resolution limit by a factor of two using structured illumination microscopy. Journal of Microscopy, 198(2), 82–87. https://doi.org/10.1046/j.1365-2818.2000.00710.x

Hammond, E. (2003). Comparison of hypoxia-induced replication arrest with hydroxyurea and aphidicolin-induced arrest. Mutation Research/Fundamental and Molecular Mechanisms of Mutagenesis, 532(1–2), 205–213. https://doi.org/10.1016/j.mrfmmm.2003.08.017

Harasim, M., Wunderlich, B., Peleg, O., Kröger, M., & Bausch, A. R. (2013). Direct observation of the dynamics of semiflexible polymers in shear flow. Physical Review Letters, 110(10), 1–5. https://doi.org/10.1103/PhysRevLett.110.108302

Harris, A., Wild, P., & Stopak, D. (1980). Silicone rubber substrata: a new wrinkle in the study of cell locomotion. Science, 208(4440), 177–179. https://doi.org/10.1126/science.6987736

Hartwig, J. H., Bokoch, G. M., Carpenter, C. L., Janmey, P. A., Taylor, L. A., Toker, A., & Stossel, T. P. (1995). Thrombin receptor ligation and activated rac uncap actin filament barbed ends through phosphoinositide synthesis in permeabilized human platelets. Cell, 82(4), 643–653. https://doi.org/10.1016/0092-8674(95)90036-5

Haviv, L., Gillo, D., Backouche, F., & Bernheim-Groswasser, A. (2008). A Cytoskeletal Demolition Worker: Myosin II Acts as an Actin Depolymerization Agent. Journal of Molecular Biology, 375(2), 325–330. https://doi.org/10.1016/j.jmb.2007.09.066

Hayakawa, K., Tatsumi, H., & Sokabe, M. (2011). Actin filaments function as a tension sensor by tension-dependent binding of cofilin to the filament. Journal of Cell Biology, 195(5), 721–727. https://doi.org/10.1083/jcb.201102039

Heisenberg, C. P., & Bellaïche, Y. (2013). Forces in tissue morphogenesis and patterning. Cell, 153(5). https://doi.org/10.1016/j.cell.2013.05.008

Hoffman, B. D., Grashoff, C., & Schwartz, M. A. (2011). Dynamic molecular processes mediate cellular mechanotransduction. Nature, 475(7356), 316–323. https://doi.org/10.1038/nature10316

Hoffman, L. M., Jensen, C. C., Chaturvedi, A., Yoshigi, M., & Beckerle, M. C. (2012). Stretch-induced actin remodeling requires targeting of zyxin to stress fibers and recruitment of actin regulators. Molecular Biology of the Cell, 23(10), 1846–1859. https://doi.org/10.1091/mbc.e11-12-1057

Honda, K. (2015). The biological role of actinin-4 (ACTN4) in malignant phenotypes of cancer. Cell and Bioscience, 5(1), 1–9. https://doi.org/10.1186/s13578-015-0031-0

Hotulainen, P., & Lappalainen, P. (2006). Stress fibers are generated by two distinct actin assembly mechanisms in motile cells. Journal of Cell Biology, 173(3), 383–394. https://doi.org/10.1083/jcb.200511093

Hsia, Y., Bale, J. B., Gonen, S., Shi, D., Sheffler, W., Fong, K. K., … Baker, D. (2016). Design of a hyperstable 60-subunit protein icosahedron. Nature, 535(7610), 136–139. https://doi.org/10.1038/nature18010

Hu, S., Dasbiswas, K., Guo, Z., Tee, Y. H., Thiagarajan, V., Hersen, P., … Bershadsky, A. D. (2017). Long-range self-organization of cytoskeletal myosin II filament stacks. Nature Cell Biology, 19(2), 133–141. https://doi.org/10.1038/ncb3466

Hu, S., Grobe, H., Guo, Z., Wang, Y. H., Doss, B. L., Pan, M., … Zaidel-Bar, R. (2019). Reciprocal regulation of actomyosin organization and contractility in nonmuscle cells by tropomyosins and alpha-actinins. Molecular Biology of the Cell, 30(16), 2025–2036. https://doi.org/10.1091/mbc.E19-02-0082

Huang, J., Gräter, S. V., Corbellini, F., Rinck, S., Bock, E., Kemkemer, R., … Spatz, J. P. (2009). Impact of Order and Disorder in RGD Nanopatterns on Cell Adhesion. Nano Letters, 9(3), 1111–1116. https://doi.org/10.1021/nl803548b

Huehn, A., Cao, W., Elam, W. A., Liu, X., De La Cruz, E. M., & Sindelar, C. V. (2018). The actin filament twist changes abruptly at boundaries between bare and cofilin-decorated segments. Journal of Biological Chemistry, 293(15), 5377–5383. https://doi.org/10.1074/jbc.AC118.001843

Hutter, J. L., & Bechhoefer, J. (1993). Calibration of atomic-force microscope tips. Review of Scientific Instruments, 64(7), 1868–1873. https://doi.org/10.1063/1.1143970

Huynh, J., Nishimura, N., Rana, K., Peloquin, J. M., Califano, J. P., Montague, C. R., … Reinhart-King, C. A. (2011). Age-Related Intimal Stiffening Enhances Endothelial Permeability and Leukocyte Transmigration. Science Translational Medicine, 3(112), 112ra122-112ra122. https://doi.org/10.1126/scitranslmed.3002761

Isenberg, G., Bielser, W., Meier-Ruge, W., & Remy, E. (1976). Cell surgery by laser micro-dissection: A preparative method. Journal of Microscopy, 107(1), 19–24. https://doi.org/10.1111/j.1365-2818.1976.tb02419.x

Jacinto, A., Wood, W., Woolner, S., Hiley, C., Turner, L., Wilson, C., … Martin, P. (2002). Dynamic Analysis of Actin Cable Function during Drosophila Dorsal Closure. Current Biology, 12(14), 1245–1250. https://doi.org/10.1016/S0960-9822(02)00955-7

Jannie, K. M., Ellerbroek, S. M., Zhou, D. W., Chen, S., Crompton, D. J., García, A. J., & DeMali, K. A. (2015). Vinculin-dependent actin bundling regulates cell migration and traction forces. Biochemical Journal, 465(3), 383–393. https://doi.org/10.1042/BJ20140872

Jégou, A., Carlier, M.-F., & Romet-Lemonne, G. (2013). Formin mDia1 senses and generates mechanical forces on actin filaments. Nature Communications, 4(1), 1883. https://doi.org/10.1038/ncomms2888

Jockusch, B. M., & Isenberg, G. (1981). Interaction of alpha-actinin and vinculin with actin: opposite effects on filament network formation. Proceedings of the National Academy of Sciences of the United States of America, 78(5), 3005–3009. https://doi.org/10.1073/pnas.78.5.3005

Johnson, R. P., & Craig, S. W. (1995). F-actin binding site masked by the intramolecular association of vinculin head and tail domains. Nature, 373(6511), 261–264. https://doi.org/10.1038/373261a0

Jungmann, R., Avendaño, M. S., Woehrstein, J. B., Dai, M., Shih, W. M., & Yin, P. (2014). Multiplexed 3D cellular super-resolution imaging with DNA-PAINT and Exchange-PAINT. Nature Methods, 11(3), 313–318. https://doi.org/10.1038/nmeth.2835

Jurchenko, C., & Salaita, K. S. (2015). Lighting Up the Force: Investigating Mechanisms of Mechanotransduction Using Fluorescent Tension Probes. Molecular and Cellular Biology, 35(15), 2570–2582. https://doi.org/10.1128/MCB.00195-15

Kanchanawong, P., Shtengel, G., Pasapera, A. M., Ramko, E. B., Davidson, M. W., Hess, H. F., & Waterman, C. M. (2010). Nanoscale architecture of integrin-based cell adhesions. Nature, 468(7323), 580–584. https://doi.org/10.1038/nature09621

Kassianidou, E., Brand, C. A., Schwarz, U. S., & Kumar, S. (2017). Geometry and network connectivity govern the mechanics of stress fibers. Proceedings of the National Academy of Sciences, 114(10), 2622–2627. https://doi.org/10.1073/pnas.1606649114

Kassianidou, E., & Kumar, S. (2015). A biomechanical perspective on stress fiber structure and function. Biochimica et Biophysica Acta (BBA) - Molecular Cell Research, 1853(11), 3065–3074. https://doi.org/10.1016/j.bbamcr.2015.04.006

Katoh, K., Kano, Y., Masuda, M., Onishi, H., & Fujiwara, K. (1998). Isolation and contraction of the stress fiber. Molecular Biology of the Cell, 9(7), 1919–1938. https://doi.org/10.1091/mbc.9.7.1919

Kemp, J. P., & Brieher, W. M. (2018). The actin filament bundling protein α-actinin-4 actually suppresses actin stress fibers by permitting actin turnover. Journal of Biological Chemistry, 293(37), 14520–14533. https://doi.org/10.1074/jbc.RA118.004345

Kner, P., Chhun, B. B., Griffis, E. R., Winoto, L., & Gustafsson, M. G. L. (2009). Super-resolution video microscopy of live cells by structured illumination. Nature Methods, 6(5), 339–342. https://doi.org/10.1038/nmeth.1324

Knudsen, K. A., Soler, A. P., Johnson, K. R., & Wheelock, M. J. (1995). Interaction of α-actinin with the cadherin/catenin cell-cell adhesion complex via α-catenin. Journal of Cell Biology, 130(1), 67–77. https://doi.org/10.1083/jcb.130.1.67

Koenderink, G. H., & Paluch, E. K. (2018). Architecture shapes contractility in actomyosin networks. Current Opinion in Cell Biology, 50, 79–85. https://doi.org/10.1016/j.ceb.2018.01.015

Kollimada, S. A., Khan, S., Balakrishna, S., Raju, S., Matad, S., & Ananthasuresh, G. K. (2017). A micro-mechanical compliant device for individual cell-stretching, compression, and in-situ force-measurement. In 2017 International Conference on Manipulation, Automation and Robotics at Small Scales (MARSS) (pp. 1–6). IEEE. https://doi.org/10.1109/MARSS.2017.8001943

Kollmannsberger, P., Bidan, C. M., Dunlop, J. W. C., & Fratzl, P. (2011). The physics of tissue patterning and extracellular matrix organisation: how cells join forces. Soft Matter, 7(20), 9549. https://doi.org/10.1039/c1sm05588g

Kovac, B., Teo, J. L., Mäkelä, T. P., & Vallenius, T. (2013). Assembly of non-contractile dorsal stress fibers requires α-actinin-1 and Rac1 in migrating and spreading cells. Journal of Cell Science, 126(1), 263–273. https://doi.org/10.1242/jcs.115063

Kovács, M., Tóth, J., Hetényi, C., Málnási-Csizmadia, A., & Sellers, J. R. (2004). Mechanism of blebbistatin inhibition of myosin II. The Journal of Biological Chemistry, 279(34), 35557–35563. https://doi.org/10.1074/jbc.M405319200

Kraning-Rush, C. M., Califano, J. P., & Reinhart-King, C. a. (2012). Cellular Traction Stresses Increase with Increasing Metastatic Potential. PLoS ONE, 7(2), e32572. https://doi.org/10.1371/journal.pone.0032572

Kreis, T. E., & Birchmeier, W. (1980). Stress fiber sarcomeres of fibroblasts are contractile. Cell, 22(2), 555–561. https://doi.org/10.1016/0092-8674(80)90365-7

Kulkarni, A. H., Ghosh, P., Seetharaman, A., Kondaiah, P., & Gundiah, N. (2018). Traction cytometry: Regularization in the Fourier approach and comparisons with finite element method. Soft Matter, 14(23), 4687–4695. https://doi.org/10.1039/c7sm02214j

Kumar, A., Shutova, M. S., Tanaka, K., Iwamoto, D. V., Calderwood, D. A., Svitkina, T. M., & Schwartz, M. A. (2019). Filamin A mediates isotropic distribution of applied force across the actin network. Journal of Cell Biology, 218(8), 2481–2491. https://doi.org/10.1083/jcb.201901086

Kumar, S., Maxwell, I. Z., Heisterkamp, A., Polte, T. R., Lele, T. P., Salanga, M., … Ingber, D. E. (2006). Viscoelastic retraction of single living stress fibers and its impact on cell shape, cytoskeletal organization, and extracellular matrix mechanics. Biophysical Journal, 90(10), 3762–3773. https://doi.org/10.1529/biophysj.105.071506

Kuo, J.-C., Han, X., Hsiao, C.-T., Yates III, J. R., & Waterman, C. M. (2011). Analysis of the myosin-II-responsive focal adhesion proteome reveals a role for β-Pix in negative regulation of focal adhesion maturation. Nature Cell Biology, 13(4), 383–393. https://doi.org/10.1038/ncb2216

Kurzawa, L., Vianay, B., Senger, F., Vignaud, T., Blanchoin, L., & Théry, M. (2017). Dissipation of contractile forces: the missing piece in cell mechanics. Molecular Biology of the Cell, 28(14), 1825–1832. https://doi.org/10.1091/mbc.E16-09-0672

Lan, B., Krishnan, R., Park, C. Y., Watanabe, R. A., Panganiban, R., Butler, J. P., … Fredberg, J. J. (2018). Transient stretch induces cytoskeletal fluidization through the severing action of cofilin. American Journal of Physiology-Lung Cellular and Molecular Physiology, 314(5), L799–L807. https://doi.org/10.1152/ajplung.00326.2017

Langanger, G., Moeremans, M., Daneels, G., Sobieszek, A., De Brabander, M., & De Mey, J. (1986). The molecular organization of myosin in stress fibers of cultured cells. Journal of Cell Biology, 102(1), 200–209. https://doi.org/10.1083/jcb.102.1.200

Lazarides, E., & Burridge, K. (1975). α-Actinin: Immunofluorescent localization of a muscle structural protein in nonmuscle cells. Cell, 6(3), 289–298. https://doi.org/10.1016/0092-8674(75)90180-4

Lecaudey, V., & Gilmour, D. (2006). Organizing moving groups during morphogenesis. Current Opinion in Cell Biology, 18(1), 102–107. https://doi.org/10.1016/j.ceb.2005.12.001

Lecuit, T., Lenne, P. F., & Munro, E. (2011). Force generation, transmission, and integration during cell and tissue morphogenesis. Annual Review of Cell and Developmental Biology, 27, 157–184. https://doi.org/10.1146/annurev-cellbio-100109-104027

Lee, J., Leonard, M., Oliver, T., Ishihara, A., & Jacobson, K. (1994). Traction forces generated by locomoting keratocytes. Journal of Cell Biology, 127(6), 1957–1964. https://doi.org/10.1083/jcb.127.6.1957

Lee, P., & Wolgemuth, C. W. (2011). Crawling Cells Can Close Wounds without Purse Strings or Signaling. PLoS Computational Biology, 7(3), e1002007. https://doi.org/10.1371/journal.pcbi.1002007

Lee, Stacey, Kassianidou, E., & Kumar, S. (2018). Actomyosin stress fiber subtypes have unique viscoelastic properties and roles in tension generation. Molecular Biology of the Cell, 29(16), 1992–2004. https://doi.org/10.1091/mbc.E18-02-0106

Lee, Sujin, Hong, J., & Lee, J. (2016). Cell motility regulation on a stepped micro pillar array device (SMPAD) with a discrete stiffness gradient. Soft Matter, 12(8), 2325–2333. https://doi.org/10.1039/C5SM00649J

Levayer, R., & Lecuit, T. (2012). Biomechanical regulation of contractility: Spatial control and dynamics. Trends in Cell Biology, 22(2), 61–81. https://doi.org/10.1016/j.tcb.2011.10.001

Levental, K. R., Yu, H., Kass, L., Lakins, J. N., Egeblad, M., Erler, J. T., … Weaver, V. M. (2009). Matrix Crosslinking Forces Tumor Progression by Enhancing Integrin Signaling. Cell, 139(5), 891–906. https://doi.org/10.1016/j.cell.2009.10.027

Liu, J., Wang, Y., Goh, W. I., Goh, H., Baird, M. A., Ruehland, S., … Kanchanawong, P. (2015). Talin determines the nanoscale architecture of focal adhesions. Proceedings of the National Academy of Sciences of the United States of America, 112(35), E4864–E4873. https://doi.org/10.1073/pnas.1512025112

Liu, Y., Medda, R., Liu, Z., Galior, K., Yehl, K., Spatz, J. P., … Salaita, K. (2014). Nanoparticle Tension Probes Patterned at the Nanoscale: Impact of Integrin Clustering on Force Transmission. Nano Letters, 14(10), 5539–5546. https://doi.org/10.1021/nl501912g

Livne, A., & Geiger, B. (2016). The inner workings of stress fibers – from contractile machinery to focal adhesions and back. Journal of Cell Science, 129(7), 1293–1304. https://doi.org/10.1242/jcs.180927

Lu, L., Oswald, S. J., Ngu, H., & Yin, F. C. P. (2008). Mechanical properties of actin stress fibers in living cells. Biophysical Journal, 95(12), 6060–6071. https://doi.org/10.1529/biophysj.108.133462

Machesky, L. M., & Hall, A. (1997). Role of Actin Polymerization and Adhesion to Extracellular Matrix in Rac- and Rho-induced Cytoskeletal Reorganization. Journal of Cell Biology, 138(4), 913–926. https://doi.org/10.1083/jcb.138.4.913

Maddox, A. S., & Burridge, K. (2003). RhoA is required for cortical retraction and rigidity during mitotic cell rounding. Journal of Cell Biology, 160(2), 255–265. https://doi.org/10.1083/jcb.200207130

Malmström, J., Christensen, B., Jakobsen, H. P., Lovmand, J., Foldbjerg, R., Sørensen, E. S., & Sutherland, D. S. (2010). Large Area Protein Patterning Reveals Nanoscale Control of Focal Adhesion Development. Nano Letters, 10(2), 686–694. https://doi.org/10.1021/nl903875r

Marek, L. F., Kelley, R. O., & Perdue, B. D. (1982). Organization of the cytoskeleton in square fibroblasts. Cell Motility, 2(2), 115–130. https://doi.org/10.1002/cm.970020204

Martiel, J.-L., Leal, A., Kurzawa, L., Balland, M., Wang, I., Vignaud, T., … Théry, M. (2015). Measurement of cell traction forces with ImageJ. In Methods in Cell Biology (Vol. 125, pp. 269–287). https://doi.org/10.1016/bs.mcb.2014.10.008

Martinac, B. (2004). Mechanosensitive ion channels: Molecules of mechanotransduction. Journal of Cell Science, 117(12), 2449–2460. https://doi.org/10.1242/jcs.01232

McBeath, R., Pirone, D. M., Nelson, C. M., Bhadriraju, K., & Chen, C. S. (2004). Cell Shape, Cytoskeletal Tension, and RhoA Regulate Stem Cell Lineage Commitment. Developmental Cell, 6(1), 483–495. https://doi.org/10.1016/S1534-5807(04)00075-9

Messi, Z., Bornert, A., Raynaud, F., & Verkhovsky, A. B. (2020). Traction Forces Control Cell-Edge Dynamics and Mediate Distance Sensitivity during Cell Polarization. Current Biology, 1–8. https://doi.org/10.1016/j.cub.2020.02.078

Milloud, R., Destaing, O., de Mets, R., Bourrin-Reynard, I., Oddou, C., Delon, A., … Balland, M. (2017). αvβ3 integrins negatively regulate cellular forces by phosphorylation of its distal NPXY site. Biology of the Cell, 109(3), 127–137. https://doi.org/10.1111/boc.201600041

Mitchison, T. ., & Cramer, L. . (1996). Actin-Based Cell Motility and Cell Locomotion. Cell, 84(3), 371–379. https://doi.org/10.1016/S0092-8674(00)81281-7

Mitrossilis, D., Fouchard, J., Pereira, D., Postic, F., Richert, A., Saint-Jean, M., & Asnacios, A. (2010). Real-time single-cell response to stiffness. Proceedings of the National Academy of Sciences, 107(38), 16518–16523. https://doi.org/10.1073/pnas.1007940107

Moore, J. R., Campbell, S. G., & Lehman, W. (2016). Structural determinants of muscle thin filament cooperativity. Archives of Biochemistry and Biophysics, 594, 8–17. https://doi.org/10.1016/j.abb.2016.02.016

Moore, S. W., Biais, N., & Sheetz, M. P. (2009). Traction on Immobilized Netrin-1 Is Sufficient to Reorient Axons. Science, 325(5937), 166–166. https://doi.org/10.1126/science.1173851

Muliyil, S., Krishnakumar, P., & Narasimha, M. (2011). Spatial, temporal and molecular hierarchies in the link between death, delamination and dorsal closure. Development (Cambridge, England), 138(14), 3043–3054. https://doi.org/10.1242/dev.060731

Munjal, A., & Lecuit, T. (2014). Actomyosin networks and tissue morphogenesis. Development (Cambridge), 141(9), 1789–1793. https://doi.org/10.1242/dev.091645

Murrell, M., Oakes, P. W., Lenz, M., & Gardel, M. L. (2015). Forcing cells into shape: the mechanics of actomyosin contractility. Nature Reviews Molecular Cell Biology, 16(8), 486–498. https://doi.org/10.1038/nrm4012

Murugesan, S., Hong, J., Yi, J., Li, D., Beach, J. R., Shao, L., … Hammer, J. A. (2016). Formin-generated actomyosin arcs propel T cell receptor microcluster movement at the immune synapse. Journal of Cell Biology, 215(3), 383–399. https://doi.org/10.1083/jcb.201603080

Naumanen, P., Lappalainen, P., & Hotulainen, P. (2008). Mechanisms of actin stress fibre assembly. In Journal of Microscopy (Vol. 231, pp. 446–454). https://doi.org/10.1111/j.1365-2818.2008.02057.x

Oakes, P. W., Beckham, Y., Stricker, J., & Gardel, M. L. (2012). Tension is required but not sufficient for focal adhesion maturation without a stress fiber template. The Journal of Cell Biology, 196(3), 363–374. https://doi.org/10.1083/jcb.201107042

Oliver, T, Dembo, M., & Jacobson, K. (1999). Separation of propulsive and adhesive traction stresses in locomoting keratocytes. The Journal of Cell Biology, 145(3), 589–604. https://doi.org/10.1083/jcb.145.3.589

Oliver, Tim, Jacobson, K., & Dembo, M. (1995). Traction forces in locomoting cells. Cell Motility and the Cytoskeleton, 31(3), 225–240. https://doi.org/10.1002/cm.970310306

Ono, S. (2003). Regulation of Actin Filament Dynamics by Actin Depolymerizing Factor/Cofilin and Actin-Interacting Protein 1: New Blades for Twisted Filaments †. Biochemistry, 42(46), 13363–13370. https://doi.org/10.1021/bi034600x

Ono, S., & Ono, K. (2002). Tropomyosin inhibits ADF/cofilin-dependent actin filament dynamics. Journal of Cell Biology, 156(6), 1065–1076. https://doi.org/10.1083/jcb.200110013

Otey, C. A., Vasquez, G. B., Burridge, K., & Erickson, B. W. (1993). Mapping of the α-actinin binding site within the β1 integrin cytoplasmic domain. Journal of Biological Chemistry, 268(28), 21193–21197.

Otey, C A, Pavalko, F. M., & Burridge, K. (1990). An interaction between alpha-actinin and the beta 1 integrin subunit in vitro. The Journal of Cell Biology, 111(2), 721–729. https://doi.org/10.1083/jcb.111.2.721

Otey, Carol A., & Carpen, O. (2004). α-actinin revisited: A fresh look at an old player. Cell Motility and the Cytoskeleton, 58(2), 104–111. https://doi.org/10.1002/cm.20007

Panagiotakopoulou, M., Lendenmann, T., Pramotton, F. M., Giampietro, C., Stefopoulos, G., Poulikakos, D., & Ferrari, A. (2018). Cell cycle–dependent force transmission in cancer cells. Molecular Biology of the Cell, 29(21), 2528–2539. https://doi.org/10.1091/mbc.E17-12-0726

Pasapera, A. M., Plotnikov, S. V., Fischer, R. S., Case, L. B., Egelhoff, T. T., & Waterman, C. M. (2015). Rac1-dependent phosphorylation and focal adhesion recruitment of myosin IIA regulates migration and mechanosensing. Current Biology, 25(2), 175–186. https://doi.org/10.1016/j.cub.2014.11.043

Paszek, M. J., Zahir, N., Johnson, K. R., Lakins, J. N., Rozenberg, G. I., Gefen, A., … Weaver, V. M. (2005). Tensional homeostasis and the malignant phenotype. Cancer Cell, 8(3), 241–254. https://doi.org/10.1016/j.ccr.2005.08.010

Pavalko, F. M., & Burridge, K. (1991). Disruption of the actin cytoskeleton after microinjection of proteolytic fragments of α-actinin. Journal of Cell Biology, 114(3), 481–491. https://doi.org/10.1083/jcb.114.3.481

Pellegrin, S., & Mellor, H. (2007). Actin stress fibres. Journal of Cell Science, 120(20), 3491–3499. https://doi.org/10.1242/jcs.018473

Peterson, L. J., Rajfur, Z., Maddox, A. S., Freel, C. D., Chen, Y., Edlund, M., … Burridge, K. (2004). Simultaneous Stretching and Contraction of Stress Fibers In Vivo. Molecular Biology of the Cell, 15(7), 3497–3508. https://doi.org/10.1091/mbc.e03-09-0696

Pitaval, A., Tseng, Q., Bornens, M., & Théry, M. (2010). Cell shape and contractility regulate ciliogenesis in cell cycle–arrested cells. Journal of Cell Biology, 191(2), 303–312. https://doi.org/10.1083/jcb.201004003

Plotkin, L. I., Mathov, I., Aguirre, J. I., Parfitt, A. M., Manolagas, S. C., & Bellido, T. (2005). Mechanical stimulation prevents osteocyte apoptosis: requirement of integrins, Src kinases, and ERKs. American Journal of Physiology-Cell Physiology, 289(3), C633–C643. https://doi.org/10.1152/ajpcell.00278.2004

Plotnikov, S. V., Pasapera, A. M., Sabass, B., & Waterman, C. M. (2012). Force Fluctuations within Focal Adhesions Mediate ECM-Rigidity Sensing to Guide Directed Cell Migration. Cell, 151(7), 1513–1527. https://doi.org/10.1016/j.cell.2012.11.034

Polio, S. R., Parameswaran, H., Canović, E. P., Gaut, C. M., Aksyonova, D., Stamenović, D., & Smith, M. L. (2014). Topographical control of multiple cell adhesion molecules for traction force microscopy. Integrative Biology, 6(3), 357–365. https://doi.org/10.1039/c3ib40127h

Pollard, T. D., Blanchoin, L., & Mullins, R. D. (2000). Molecular Mechanisms Controlling Actin Filament Dynamics in Nonmuscle Cells. Annual Review of Biophysics and Biomolecular Structure, 29(1), 545–576. https://doi.org/10.1146/annurev.biophys.29.1.545

Pollard, T. D., & Borisy, G. G. (2003). Cellular motility driven by assembly and disassembly of actin filaments. Cell, 112(4), 453–465. https://doi.org/10.1016/S0092-8674(03)00120-X

Poxleitner, M. K., Dawson, S. C., & Cande, W. Z. (2008). Cell Cycle Synchrony in Giardia intestinalis Cultures Achieved by Using Nocodazole and Aphidicolin. Eukaryotic Cell, 7(4), 569–574. https://doi.org/10.1128/EC.00415-07

Rahil, Z., Pedron, S., Wang, X., Ha, T., Harley, B., & Leckband, D. (2016). Nanoscale mechanics guides cellular decision making. Integrative Biology, 8(9), 929–935. https://doi.org/10.1039/C6IB00113K

Rajagopalan, J., & Saif, M. T. A. (2011). MEMS sensors and microsystems for cell mechanobiology. Journal of Micromechanics and Microengineering, 21(5). https://doi.org/10.1088/0960-1317/21/5/054002

Ramanathan, S. P., Helenius, J., Stewart, M. P., Cattin, C. J., Hyman, A. A., & Muller, D. J. (2015). Cdk1-dependent mitotic enrichment of cortical myosin II promotes cell rounding against confinement. Nature Cell Biology, 17(2), 148–159. https://doi.org/10.1038/ncb3098

Rape, A. D., Guo, W., & Wang, Y.-L. (2011). The regulation of traction force in relation to cell shape and focal adhesions. Biomaterials, 32(8), 2043–2051. https://doi.org/10.1016/j.biomaterials.2010.11.044

Rassier, D. E., MacIntosh, B. R., & Herzog, W. (1999). Length dependence of active force production in skeletal muscle. Journal of Applied Physiology, 86(5), 1445–1457. https://doi.org/10.1152/jappl.1999.86.5.1445

Rassier, Dilson E., & Pavlov, I. (2010). Contractile Characteristics of Sarcomeres Arranged in Series or Mechanically Isolated from Myofibrils. In Advances in Experimental Medicine and Biology (Vol. 682, pp. 123–140). https://doi.org/10.1007/978-1-4419-6366-6_7

Rausch, S., Das, T., Soiné, J. R., Hofmann, T. W., Boehm, C. H., Schwarz, U. S., … Spatz, J. P. (2013). Polarizing cytoskeletal tension to induce leader cell formation during collective cell migration. Biointerphases, 8(1), 36. https://doi.org/10.1186/1559-4106-8-32

Rauzi, M., Lenne, P. F., & Lecuit, T. (2010). Planar polarized actomyosin contractile flows control epithelial junction remodelling. Nature. Nature Publishing Group. https://doi.org/10.1038/nature09566

Reffay, M., Parrini, M. C., Cochet-Escartin, O., Ladoux, B., Buguin, a, Coscoy, S., … Silberzan, P. (2014). Interplay of RhoA and mechanical forces in collective cell migration driven by leader cells. Nature Cell Biology, 16(3), 217–223. https://doi.org/10.1038/ncb2917

Renkawitz, J., Schumann, K., Weber, M., Lämmermann, T., Pflicke, H., Piel, M., … Sixt, M. (2009). Adaptive force transmission in amoeboid cell migration. Nature Cell Biology, 11(12), 1438–1443. https://doi.org/10.1038/ncb1992

Reymann, A.-C. A., Boujemaa-paterski, R., Martiel, J.-L. J., Guerin, C., Cao, W., Chin, H. F., … Blanchoin, L. (2012). Actin Network Architecture Can Determine Myosin Motor Activity. Science, 336(6086), 1310–1314. https://doi.org/10.1126/science.1221708

Riveline, D., Zamir, E., Balaban, N. Q., Schwarz, U. S., Ishizaki, T., Narumiya, S., … Bershadsky, A. D. (2001). Focal Contacts as Mechanosensors : Externally Applied Local Mechanical Force Induces Growth of Focal Contacts by an mDia1-dependent and. The Journal of Cell Biology, 153(6), 1175–1185.

Roca-Cusachs, P., Conte, V., & Trepat, X. (2017). Quantifying forces in cell biology. Nature Cell Biology, 19(7), 742–751. https://doi.org/10.1038/ncb3564

Rossier, O., Octeau, V., Sibarita, J. B., Leduc, C., Tessier, B., Nair, D., … Giannone, G. (2012). Integrins β 1 and β 3 exhibit distinct dynamic nanoscale organizations inside focal adhesions. Nature Cell Biology, 14(10), 1057–1067. https://doi.org/10.1038/ncb2588

Russell, R. J., Grubbs, A. Y., Mangroo, S. P., Nakasone, S. E., Dickinson, R. B., & Lele, T. P. (2011). Sarcomere length fluctuations and flow in capillary endothelial cells. Cytoskeleton, 68(3), 150–156. https://doi.org/10.1002/cm.20501

Sabass, B., Gardel, M. L., Waterman, C. M., & Schwarz, U. S. (2008). High Resolution Traction Force Microscopy Based on Experimental and Computational Advances. Biophysical Journal, 94(1), 207–220. https://doi.org/10.1529/biophysj.107.113670

Saez, A., Ghibaudo, M., Buguin, A., Silberzan, P., & Ladoux, B. (2007). Rigidity-driven growth and migration of epithelial cells on microstructured anisotropic substrates. Proceedings of the National Academy of Sciences, 104(20), 8281–8286. https://doi.org/10.1073/pnas.0702259104

Salbreux, G., Charras, G., & Paluch, E. (2012). Actin cortex mechanics and cellular morphogenesis. Trends in Cell Biology, 22(10), 536–545. https://doi.org/10.1016/j.tcb.2012.07.001

Sandbo, N., & Dulin, N. (2011). Actin cytoskeleton in myofibroblast differentiation: Ultrastructure defining form and driving function. Translational Research, 158(4), 181–196. https://doi.org/10.1016/j.trsl.2011.05.004

Sandquist, J. C., & Means, A. R. (2008). The C-Terminal Tail Region of Nonmuscle Myosin II Directs Isoform-specific Distribution in Migrating Cells. Molecular Biology of the Cell, 19(12), 5156–5167. https://doi.org/10.1091/mbc.e08-05-0533

Sandquist, J. C., Swenson, K. I., DeMali, K. A., Burridge, K., & Means, A. R. (2006). Rho Kinase Differentially Regulates Phosphorylation of Nonmuscle Myosin II Isoforms A and B during Cell Rounding and Migration. Journal of Biological Chemistry, 281(47), 35873–35883. https://doi.org/10.1074/jbc.M605343200

Sansores-Garcia, L., Bossuyt, W., Wada, K. I., Yonemura, S., Tao, C., Sasaki, H., & Halder, G. (2011). Modulating F-actin organization induces organ growth by affecting the Hippo pathway. EMBO Journal, 30(12), 2325–2335. https://doi.org/10.1038/emboj.2011.157

Sarangi, B. R., Gupta, M., Doss, B. L., Tissot, N., Lam, F., Mège., R, … Ladoux, B. (2017). Coordination between Intra- and Extracellular Forces Regulates Focal Adhesion Dynamics. Nano Lett, 17, 17. https://doi.org/10.1021/acs.nanolett.6b04364

Schiller, H. B., & Fässler, R. (2013). Mechanosensitivity and compositional dynamics of cell–matrix adhesions. EMBO Reports, 14(6), 509–519. https://doi.org/10.1038/embor.2013.49

Sedzinski, J., Biro, M., Oswald, A., Tinevez, J.-Y., Salbreux, G., & Paluch, E. (2011). Polar actomyosin contractility destabilizes the position of the cytokinetic furrow. Nature, 476(7361), 462–466. https://doi.org/10.1038/nature10286

Senger, F., Pitaval, A., Ennomani, H., Kurzawa, L., Blanchoin, L., & Théry, M. (2019). Spatial integration of mechanical forces by α-actinin establishes actin network symmetry. Journal of Cell Science, 132(22), jcs236604. https://doi.org/10.1242/jcs.236604

Serra-Picamal, X., Conte, V., Vincent, R., Anon, E., Tambe, D. T., Bazellieres, E., … Trepat, X. (2012). Mechanical waves during tissue expansion. Nature Physics, 8(8), 628–634. https://doi.org/10.1038/nphys2355

Serrels, B., Serrels, A., Brunton, V. G., Holt, M., McLean, G. W., Gray, C. H., … Frame, M. C. (2007). Focal adhesion kinase controls actin assembly via a FERM-mediated interaction with the Arp2/3 complex. Nature Cell Biology, 9(9), 1046–1056. https://doi.org/10.1038/ncb1626

Shemesh, T., Geiger, B., Bershadsky, A. D., & Kozlov, M. M. (2005). Focal adhesions as mechanosensors: A physical mechanism. Proceedings of the National Academy of Sciences of the United States of America, 102(35), 12383–12388. https://doi.org/10.1073/pnas.0500254102

Shirai, Y. M., Tsunoyama, T. A., Hiramoto-Yamaki, N., Hirosawa, K. M., Shibata, A. C. E., Kondo, K., … Fujiwara, T. K. (2017). Cortical actin nodes: Their dynamics and recruitment of podosomal proteins as revealed by super-resolution and single-molecule microscopy. PLoS ONE (Vol. 12). https://doi.org/10.1371/journal.pone.0188778

Shutova, M. S., Spessott, W. A., Giraudo, C. G., & Svitkina, T. (2014). Endogenous species of mammalian nonmuscle myosin IIA and IIB include activated monomers and heteropolymers. Current Biology, 24(17), 1958–1968. https://doi.org/10.1016/j.cub.2014.07.070

Silver, F. H., & Siperko, L. M. (2003). Mechanosensing and Mechanochemical Transduction: How Is Mechanical Energy Sensed and Converted into Chemical Energy in an Extracellular Matrix? Critical Reviews in Biomedical Engineering. https://doi.org/10.1615/CritRevBiomedEng.v31.i4.10

Skau, C. T., & Waterman, C. M. (2015). Specification of Architecture and Function of Actin Structures by Actin Nucleation Factors. Annual Review of Biophysics, 44(1), 285–310. https://doi.org/10.1146/annurev-biophys-060414-034308

Small, J. V., Rottner, K., Kaverina, I., & Anderson, K. I. (1998). Assembling an actin cytoskeleton for cell attachment and movement. Biochimica et Biophysica Acta (BBA) - Molecular Cell Research, 1404(3), 271–281. https://doi.org/10.1016/S0167-4889(98)00080-9

Smith, M. A., Blankman, E., Gardel, M. L., Luettjohann, L., & Waterman, C. M. (2010). A Zyxin-Mediated Mechanism for Actin Stress Fiber Maintenance and Repair. Developmental Cell, 19(3), 365–376. https://doi.org/10.1016/j.devcel.2010.08.008

Sonal, Ganzinger, K. A., Vogel, S. K., Mücksch, J., Blumhardt, P., & Schwille, P. (2019). Myosin-II activity generates a dynamic steady state with continuous actin turnover in a minimal actin cortex. Journal of Cell Science, 132(4). https://doi.org/10.1242/jcs.219899

Squire, J. M., Paul, D. M., & Morris, E. P. (2017). Myosin and Actin Filaments in Muscle: Structures and Interactions. (D. A. D. Parry & J. M. Squire, Eds.), Fibrous Proteins: Structures and Mechanisms. Subcellular Biochemistry (Vol. 82). Cham: Springer International Publishing. https://doi.org/10.1007/978-3-319-49674-0

Stewart, M. P., Helenius, J., Toyoda, Y., Ramanathan, S. P., Muller, D. J., & Hyman, A. A. (2011). Hydrostatic pressure and the actomyosin cortex drive mitotic cell rounding. Nature, 469(7329), 226–230. https://doi.org/10.1038/nature09642

Stricker, J., Aratyn-Schaus, Y., Oakes, P. W., & Gardel, M. L. (2011). Spatiotemporal Constraints on the Force-Dependent Growth of Focal Adhesions. Biophysical Journal, 100(12), 2883–2893. https://doi.org/10.1016/j.bpj.2011.05.023

Stricker, J., Sabass, B., Schwarz, U. S., & Gardel, M. L. (2010). Optimization of traction force microscopy for micron-sized focal adhesions. Journal of Physics: Condensed Matter, 22(19), 194104. https://doi.org/10.1088/0953-8984/22/19/194104

Stutchbury, B., Atherton, P., Tsang, R., Wang, D.-Y., & Ballestrem, C. (2017). Distinct focal adhesion protein modules control different aspects of mechanotransduction. Journal of Cell Science, 130(9), 1612–1624. https://doi.org/10.1242/jcs.195362

Sun, Z., Tseng, H.-Y., Tan, S., Senger, F., Kurzawa, L., Dedden, D., … Fässler, R. (2016). Kank2 activates talin, reduces force transduction across integrins and induces central adhesion formation. Nature Cell Biology, 18(9), 941–953. https://doi.org/10.1038/ncb3402

Svitkina, T. M. (2018). Ultrastructure of the actin cytoskeleton. Current Opinion in Cell Biology, 54, 1–8. https://doi.org/10.1016/j.ceb.2018.02.007

Svitkina, T. M., Bulanova, E. A., Chaga, O. Y., Vignjevic, D. M., Kojima, S., Vasiliev, J. M., & Borisy, G. G. (2003). Mechanism of filopodia initiation by reorganization of a dendritic network. Journal of Cell Biology, 160(3), 409–421. https://doi.org/10.1083/jcb.200210174

Svitkina, T. M., Verkhovsky, A. B., McQuade, K. M., & Borisy, G. G. (1997). Analysis of the actin-myosin II system in fish epidermal keratocytes: Mechanism of cell body translocation. Journal of Cell Biology, 139(2), 397–415. https://doi.org/10.1083/jcb.139.2.397

Tambe, D. T., Hardin, C. C., Angelini, T. E., Rajendran, K., Park, C. Y., Serra-Picamal, X., … Trepat, X. (2011). Collective cell guidance by cooperative intercellular forces. Nature Materials, 10(6), 469–475. https://doi.org/10.1038/nmat3025

Tan, J. L., Tien, J., Pirone, D. M., Gray, D. S., Bhadriraju, K., & Chen, C. S. (2003). Cells lying on a bed of microneedles: An approach to isolate mechanical force. Proceedings of the National Academy of Sciences, 100(4), 1484–1489. https://doi.org/10.1073/pnas.0235407100

Tanner, K., Boudreau, A., Bissell, M. J., & Kumar, S. (2010). Dissecting Regional Variations in Stress Fiber Mechanics in Living Cells with Laser Nanosurgery. Biophysical Journal, 99(9), 2775–2783. https://doi.org/10.1016/j.bpj.2010.08.071

Taubenberger, A. V., Hutmacher, D. W., & Muller, D. J. (2014). Single-Cell Force Spectroscopy, an Emerging Tool to Quantify Cell Adhesion to Biomaterials. Tissue Engineering Part B: Reviews, 20(1), 40–55. https://doi.org/10.1089/ten.teb.2013.0125

Tee, Y. H., Shemesh, T., Thiagarajan, V., Hariadi, R. F., Anderson, K. L., Page, C., … Bershadsky, A. D. (2015). Cellular chirality arising from the self-organization of the actin cytoskeleton. Nature Cell Biology, 17(4), 445–457. https://doi.org/10.1038/ncb3137

Thery, M. (2010). Micropatterning as a tool to decipher cell morphogenesis and functions. Journal of Cell Science, 123(24), 4201–4213. https://doi.org/10.1242/jcs.075150

Théry, M., Pépin, A., Dressaire, E., Chen, Y., & Bornens, M. (2006). Cell distribution of stress fibres in response to the geometry of the adhesive environment. Cell Motility and the Cytoskeleton, 63(6), 341–355. https://doi.org/10.1002/cm.20126

Thievessen, I., Thompson, P. M., Berlemont, S., Plevock, K. M., Plotnikov, S. V, Zemljic-Harpf, A., … Waterman, C. M. (2013). Vinculin–actin interaction couples actin retrograde flow to focal adhesions, but is dispensable for focal adhesion growth. The Journal of Cell Biology, 202(1), 163–177. https://doi.org/10.1083/jcb.201303129

Thomas, D. B., & Lingwood, C. A. (1975). A model of cell cycle control: Effects of thymidine on synchronous cell cultures. Cell, 5(1), 37–44. https://doi.org/10.1016/0092-8674(75)90089-6

Thompson, W. R., Scott, A., Loghmani, M. T., Ward, S. R., & Warden, S. J. (2016). Understanding Mechanobiology: Physical Therapists as a Force in Mechanotherapy and Musculoskeletal Regenerative Rehabilitation. Physical Therapy, 96(4), 560–569. https://doi.org/10.2522/ptj.20150224

Tinevez, J. Y., Schulze, U., Salbreux, G., Roensch, J., Joanny, J. F., & Paluch, E. (2009). Role of cortical tension in bleb growth. Proceedings of the National Academy of Sciences of the United States of America, 106(44), 18581–18586. https://doi.org/10.1073/pnas.0903353106

Tojkander, S., Gateva, G., Husain, A., Krishnan, R., & Lappalainen, P. (2015). Generation of contractile actomyosin bundles depends on mechanosensitive actin filament assembly and disassembly. ELife, 4, 1–28. https://doi.org/10.7554/eLife.06126

Tojkander, S., Gateva, G., & Lappalainen, P. (2012). Actin stress fibers - assembly, dynamics and biological roles. Journal of Cell Science, 125(8), 1855–1864. https://doi.org/10.1242/jcs.098087

Tojkander, Sari, Gateva, G., Schevzov, G., Hotulainen, P., Naumanen, P., Martin, C., … Lappalainen, P. (2011). A Molecular Pathway for Myosin II Recruitment to Stress Fibers. Current Biology, 21(7), 539–550. https://doi.org/10.1016/j.cub.2011.03.007

Trappmann, B., Gautrot, J. E., Connelly, J. T., Strange, D. G. T., Li, Y., Oyen, M. L., … Huck, W. T. S. (2012). Extracellular-matrix tethering regulates stem-cell fate. Nature Materials, 11(7), 642–649. https://doi.org/10.1038/nmat3339

Trepat, X., Wasserman, M. R., Angelini, T. E., Millet, E., Weitz, D. a., Butler, J. P., & Fredberg, J. J. (2009). Physical forces during collective cell migration. Nature Physics, 5(6), 426–430. https://doi.org/10.1038/nphys1269

Tseng, Q., Wang, I., Duchemin-Pelletier, E., Azioune, A., Carpi, N., Gao, J., … Balland, M. (2011). A new micropatterning method of soft substrates reveals that different tumorigenic signals can promote or reduce cell contraction levels. Lab on a Chip, 11(13), 2231. https://doi.org/10.1039/c0lc00641f

Uemura, A., Nguyen, T., Steele, A. N., & Yamada, S. (2011). The LIM Domain of Zyxin Is Sufficient for Force-Induced Accumulation of Zyxin During Cell Migration. Biophysical Journal, 101(5), 1069–1075. https://doi.org/10.1016/j.bpj.2011.08.001

Uroz, M., Wistorf, S., Serra-Picamal, X., Conte, V., Sales-Pardo, M., Roca-Cusachs, P., … Trepat, X. (2018). Regulation of cell cycle progression by cell–cell and cell–matrix forces. Nature Cell Biology, 20(June), 1. https://doi.org/10.1038/s41556-018-0107-2

Vallenius, T. (2013). Actin stress fibre subtypes in mesenchymal-migrating cells. Open Biology, 3(6), 130001. https://doi.org/10.1098/rsob.130001

Verkhovsky, A. B., Svitkina, T. M., & Borisy, G. G. (1995). Myosin II filament assemblies in the active lamella of fibroblasts: Their morphogenesis and role in the formation of actin filament bundles. Journal of Cell Biology, 131(4), 989–1002. https://doi.org/10.1083/jcb.131.4.989

Vianay, B., Senger, F., Alamos, S., Anjur-Dietrich, M., Bearce, E., Cheeseman, B., … Thery, M. (2018). Variation in traction forces during cell cycle progression. Biology of the Cell, 110(4), 91–96. https://doi.org/10.1111/boc.201800006

Vicente-Manzanares, M., Ma, X., Adelstein, R. S., & Horwitz, A. R. (2009). Non-muscle myosin II takes centre stage in cell adhesion and migration. Nature Reviews Molecular Cell Biology, 10(11), 778–790. https://doi.org/10.1038/nrm2786

Vicente-Manzanares, M., Newell-Litwa, K., Bachir, A. I., Whitmore, L. A., & Horwitz, A. R. (2011). Myosin IIA/IIB restrict adhesive and protrusive signaling to generate front–back polarity in migrating cells. The Journal of Cell Biology, 193(2), 381–396. https://doi.org/10.1083/jcb.201012159

Vignaud, T. (2013). Production de forces par le cytosquelette d'actine : mécanismes et régulation par le micro-environnement. University de Grenoble.

Vignaud, T., Copos, C., Leterrier, C., Toro-Nahuelpan, M., Tseng, Q., Mahamid, J., … Kurzawa, L. (2020). Stress fibres are embedded in a contractile cortical network. Nature Materials. https://doi.org/10.1038/s41563-020-00825-z

Vignaud, T., Ennomani, H., & Théry, M. (2014). Polyacrylamide Hydrogel Micropatterning. Methods in Cell Biology, 120, 93–116. https://doi.org/10.1016/B978-0-12-417136-7.00006-9

Vogel, V., & Sheetz, M. P. (2006). Local force and geometry sensing regulate cell functions. Nature Reviews Molecular Cell Biology, 7(4), 265–275. https://doi.org/10.1038/nrm1890

Wachsstock, D. H., Schwartz, W. H., & Pollard, T. D. (1993). Affinity of alpha-actinin for actin determines the structure and mechanical properties of actin filament gels. Biophysical Journal, 65(1), 205–214. https://doi.org/10.1016/S0006-3495(93)81059-2

Wang, Y.-L., & Pelham, R. J. (1998). Preparation of a flexible, porous polyacrylamide substrate for mechanical studies of cultured cells. In Methods in Enzymology (Vol. 298, pp. 489–496). https://doi.org/10.1016/S0076-6879(98)98041-7

Watanabe, T., Hosoya, H., & Yonemura, S. (2007). Regulation of Myosin II Dynamics by Phosphorylation and Dephosphorylation of Its Light Chain in Epithelial Cells. Molecular Biology of the Cell, 18(December), 986–994. https://doi.org/10.1091/mbc.E06

Webb, D. J., Donais, K., Whitmore, L. A., Thomas, S. M., Turner, C. E., Parsons, J. T., & Horwitz, A. F. (2004). FAK–Src signalling through paxillin, ERK and MLCK regulates adhesion disassembly. Nature Cell Biology, 6(2), 154–161. https://doi.org/10.1038/ncb1094

Weber, K., & Groeschel Stewart, U. (1974). Antibody to myosin: The specific visualization of myosin containing filaments in nonmuscle cells. Proceedings of the National Academy of Sciences of the United States of America, 71(11), 4561–4564. https://doi.org/10.1073/pnas.71.11.4561

Weed, S. A., Karginov, A. V, Schafer, D. A., Weaver, A. M., Kinley, A. W., Cooper, J. A., & Parsons, J. T. (2000). Cortactin Localization to Sites of Actin Assembly in Lamellipodia Requires Interactions with F-Actin and the Arp2/3 Complex. Journal of Cell Biology, 151(1), 29–40. https://doi.org/10.1083/jcb.151.1.29

Wen, K., Rubenstein, P. A., & DeMali, K. A. (2009). Vinculin Nucleates Actin Polymerization and Modifies Actin Filament Structure. Journal of Biological Chemistry, 284(44), 30463–30473. https://doi.org/10.1074/jbc.M109.021295

Wilson, C. A., Tsuchida, M. A., Allen, G. M., Barnhart, E. L., Applegate, K. T., Yam, P. T., … Theriot, J. A. (2010). Myosin II contributes to cell-scale actin network treadmilling through network disassembly. Nature, 465(7296), 373–377. https://doi.org/10.1038/nature08994

Wong, A., Pollard, T., & Herman, I. (1983). Actin filament stress fibers in vascular endothelial cells in vivo. Science, 219(4586), 867–869. https://doi.org/10.1126/science.6681677

Wu, J.-Q. (2005). Counting Cytokinesis Proteins Globally and Locally in Fission Yeast. Science, 310(5746), 310–314. https://doi.org/10.1126/science.1113230

Wu, Z., Plotnikov, S. V, Moalim, A. Y., Waterman, C. M., & Liu, J. (2017). Two Distinct Actin Networks Mediate Traction Oscillations to Confer Focal Adhesion Mechanosensing. Biophysj, 112, 780–794. https://doi.org/10.1016/j.bpj.2016.12.035

Xia, S., Lim, Y. B., Zhang, Z., Wang, Y., Zhang, S., Lim, C. T., … Kanchanawong, P. (2019). Nanoscale Architecture of the Cortical Actin Cytoskeleton in Embryonic Stem Cells. Cell Reports, 28(5), 1251-1267.e7. https://doi.org/10.1016/j.celrep.2019.06.089

Xu, J., Wirtz, D., & Pollard, T. D. (1998). Dynamic cross-linking by α-actinin determines the mechanical properties of actin filament networks. Journal of Biological Chemistry, 273(16), 9570–9576. https://doi.org/10.1074/jbc.273.16.9570

Yamada, K. M., & Geiger, B. (1997). Molecular interactions in cell adhesion complexes. Current Opinion in Cell Biology, 9, 76–85.

Yang, J. T., Rayburn, H., & Hynes, R. O. (1995). Cell adhesion events mediated by α4 integrins are essential in placental and cardiac development. Development, 121(2), 549–560.

Yang, Y., & Levine, H. (2020). Leader-cell-driven epithelial sheet fingering. Physical Biology, 17(4), 046003. https://doi.org/10.1088/1478-3975/ab907e

Ye, N., Verma, D., Meng, F., Davidson, M. W., Suffoletto, K., & Hua, S. Z. (2014). Direct observation of α-actinin tension and recruitment at focal adhesions during contact growth. Experimental Cell Research, 327(1), 57–67. https://doi.org/10.1016/j.yexcr.2014.07.026

Yoshigi, M., Hoffman, L. M., Jensen, C. C., Yost, H. J., & Beckerle, M. C. (2005). Mechanical force mobilizes zyxin from focal adhesions to actin filaments and regulates cytoskeletal reinforcement. The Journal of Cell Biology, 171(2), 209–215. https://doi.org/10.1083/jcb.200505018

Zhang, X. F., Schaefer, A. W., Burnette, D. T., Schoonderwoert, V. T., & Forscher, P. (2003). Rho-Dependent Contractile Responses in the Neuronal Growth Cone Are Independent of Classical Peripheral Retrograde Actin Flow. Neuron, 40(5), 931–944. https://doi.org/10.1016/S0896-6273(03)00754-2

Zhang, Yanshu, Yoshida, A., Sakai, N., Uekusa, Y., Kumeta, M., & Yoshimura, S. H. (2017). In vivo dynamics of the cortical actin network revealed by fast-scanning atomic force microscopy. Microscopy, 66(4), 272–282. https://doi.org/10.1093/jmicro/dfx015

Zhang, Yun, Ge, C., Zhu, C., & Salaita, K. (2014). DNA-based digital tension probes reveal integrin forces during early cell adhesion. Nature Communications, 5(1), 5167. https://doi.org/10.1038/ncomms6167